5-2006

The Evolution from Late Miocene West Salton Detachment Faulting to Cross-Cutting Pleistocene Oblique Strike-Slip Faults in the SW Salton Trough, Southern California

Alexander N. Steely
Utah State University

THE EVOLUTION FROM LATE MIOCENE WEST SALTON DETACHMENT FAULTING TO CROSS-CUTTING PLEISTOCENE OBLIQUE STRIKE-SLIP FAULTS IN THE SW SALTON TROUGH, SOUTHERN CALIFORNIA

by

Alexander N. Steely

A thesis submitted in partial fulfillment
of the requirements for the degree

of

MASTER OF SCIENCE

in

Geology

Approved:

UTAH STATE UNIVERSITY
Logan, Utah

2006

The Evolution from Late Miocene West Salton Detachment Faulting to Cross-Cutting Pleistocene Oblique Strike-Slip Faults in the SW Salton Trough, Southern California

by

Alexander N. Steely, Master of Science

Utah State University, 2006

Major Professor: Dr. Susanne Janecke
Department: Geology

Field studies in the southwest Salton Trough between Yaqui Ridge and Borrego Mountain show that the West Salton detachment fault was active during the Pliocene and may have initiated during the latest Miocene. At Yaqui Ridge dominantly east-directed extension is recorded by slickenlines on the NW-striking detachment fault, and shows that the fault is actually a low-angle dextral oblique strike-slip fault. Crustal inheritance is responsible for the position of the fault at Yaqui Ridge, which reactivates a late Cretaceous reverse-sense mylonite zone at map scale.

Late Miocene to Pliocene basin fill deposits at Borrego Mountain display progressive unconformities, contain detritus shed from the footwall and damage zone of the West Salton detachment fault, record the growth of a large hanging wall anticline, and document the initiation and evolution of the West Salton detachment fault. The Borrego Mountain anticline is a major hanging wall growth fold that trends ~N60°W and has at least 420 m of structural relief.

The late Quaternary Sunset conglomerate is ~600 m thick, lies in angular unconformity on Pliocene basin fill, is bound on the SW by the dextral oblique Sunset fault, and coarsens upward and SW toward the fault. It is dominated by plutonic lithologies from nearby areas, contains up to 10% recycled sandstone clasts from Pliocene deposits, and was shed from the SW side of the then-active Sunset fault. Based on lithologic, stratigraphic, compositional similarities, we correlate this conglomerate to part of the ~1.1 – 0.6 Ma Ocotillo Formation.

The West Salton detachment fault was folded and deactivated at Yaqui Ridge by the dextral oblique San Felipe fault zone starting ~1.1 – 1.3 Ma. The Sunset fault is in the middle of a complex left stepover between the San Felipe fault to the NW and the Fish Creek Mountains fault to the SE. Structural analyses and mapping show that syntectonic conglomerate, the West Salton detachment fault, and footwall crystalline rocks all have similar fold geometries and record similar amounts of NE-SW shortening. The dominant SE-trending population of slip vectors on the Sunset fault is not present on the West Salton detachment fault and suggests limited or no activation of the older detachment fault by the younger fault zone.

(253 pages)

ACKNOWLEDGMENTS

I would like to thank everyone who was involved in this undertaking. Special thanks to my advisor, Susanne Janecke. Without her patient support, helpful comments, and ability to know when to push me, my thesis would not be what it is. I would like to thank Becky Dorsey and Gary Axen for help in the field, stimulating discussions, and help with the manuscripts. I would also like to acknowledge George Jefferson and the staff at Anza-Borrego State Park for free lodging and support during field work. Victoria Langenheim graciously provided gravity and magnetic figures and helpful reviews of the manuscripts.

Special thanks go out to my family for their untiring support, words of encouragement, and financial support at the end of my thesis effort. I could not have done it without you. I would like to thank all of the graduate students whom I had the extreme fortune of learning from, working with, and befriending. Their support and friendship have helped me through difficult times and made life outside of school wonderful. I would also like to thank Emily Marsh for her support and friendship towards the end of my thesis effort.

This work was funded by NSF grant #EAR-0125497 and GSA Graduate Student Research Grant # 7809-04.

Alexander Steely

CONTENTS

LIST OF TABLES

LIST OF PLATES

LIST OF FIGURES

CHAPTER 1

INTRODUCTION AND METHODS

INTRODUCTION

The Salton Trough sits across the transtensional Pacific-North America plate boundary and records the complex late Cenozoic deformation and sedimentation of this feature in southern-most California and northern Mexico. The Salton Trough is the northern extension of the Gulf of California physiographic province, a crustal depression nearly 1400 km long (Dibblee, 1954). The Salton Sea lies approximately 73 meters below sea level and the Colorado River delta currently blocks the Gulf of California from entering the Salton Trough. The San Andreas fault system bounds the north and northeast side of the basin and a ~250 km long detachment fault system with two oppositely verging segments bounds the western edge (Dibblee, 1984, 1996; Axen and Fletcher, 1998). The West Salton detachment fault is the northern segment of the fault system and accommodated top-to-the-east oblique extension (this study), whereas the Laguna Salada detachment fault is the southern segment and accommodates top-to-the-west extension (Axen, 1995; Axen and Fletcher, 1998).

The West Salton detachment fault was originally interpreted as an early to middle Miocene detachment system similar in style and age to those that bound metamorphic core complexes farther east in eastern California and western Arizona (Schultejahn, 1984; Frost et al., 1996). Parts of the fault were also interpreted as a Cretaceous low-angle normal fault system (Erskine and Wenk, 1985; George and Dokka, 1994). Recent work has shown that the West Salton detachment fault is actually a late Cenozoic detachment fault that coexisted with the early San Andreas fault system (Lough, 1993; Stinson and Gastil, 1996; Axen and Fletcher, 1998; Dorsey and Janecke, 2002; Kairouz, 2005). Contemporaneous activity on these two fault systems suggests that the extensional and dextral components of the transtensional Pacific-North American relative plate motions

may have been partitioned onto the West Salton detachment fault and the San Andreas fault, respectively (Axen and Fletcher, 1998; Dorsey and Janecke, 2002). Complete strain partitioning predicts pure dextral strike-slip on the San Andreas fault and pure dip-slip on the West Salton detachment fault. This pure dip-slip would be manifest as NE-directed slip on the detachment fault. Conversely, a simple wrench tectonic model predicts east-directed extension on east- or west-dipping normal faults that are subsidiary to the main dextral San Andreas fault.

The recent recognition of the West Salton detachment fault as a major controlling structure during the late Cenozoic in the western Salton Trough has raised many questions. The age of fault initiation, basinal response, and the kinematic and temporal relationships between the detachment fault and the San Andreas fault system are poorly known. The hanging walls of many extensional detachment faults are cut by normal faults that sole into the master fault and these systems sometimes preserve extensional folds (Wernicke, 1985, 1992; Fedo and Miller, 1992; Fowler et al., 1995; Schlishe, 1995; Janecke et al., 1998, 2003; Carney and Janecke, 2005; Steely et al., 2005a). However, many of these detachment systems formed in nearly orthogonal extensional regimes, so our study area provides a unique opportunity to observe and characterize hanging wall structures and basinal response in an oblique tectonic regime.

Starting sometime in Quaternary time, dextral strike-slip faults of the San Jacinto, San Felipe, Earthquake Valley, and Elsinore fault zones cross cut the West Salton detachment fault and dismembered the previously intact supradetachment basin and its bounding faults (Sharp, 1967, 1972; Dorsey, 2002; Kirby et al., in press; Lutz et al., in press). The San Jacinto fault zone strikes NW, is >250 km-long, and merges with the Imperial fault in the southeast and the San Andreas fault in the northwest (Sharp, 1967; Sanders, 1989). The San Felipe fault zone also strikes NW, is >160 km-long, and may merge with the Elsinore fault in the northwest and projects into the Imperial fault in the southeast. Most of the West Salton detachment fault zone has been uplifted and

exhumed between and adjacent to these faults, and only short segments continue to slip where the younger, cross-cutting dextral strike-slip faults utilize the pre-existing faults (Rogers, 1965; Sharp, 1967; Axen and Fletcher, 1998; Kairouz, 2005; Chapter 2). All of the dextral fault zones have evidence for late Pleistocene activity and some also have Holocene activity (Rockwell et al., 1990; Hull and Nicholson, 1992; Morton and Matti, 1993; Dorsey, 2002; Kirby, 2005; Lutz et al., in press).

The age and nature of the transition from slip on the West Salton detachment fault to strike-slip faulting are poorly understood in the SW Salton Trough. Most previous work has concentrated on dating the initiation of the San Jacinto fault zone (e.g. Bartholomew, 1968; Rockwell et al., 1990; Morton and Matti, 1993; Dorsey, 2002; Kirby et al., in press; Lutz et al., in review), whereas significantly less work has focused on the San Felipe fault zone. In the Peninsular Ranges, late Quaternary slip rates of ~10-12 mm/yr on the San Jacinto fault zone from paleoseismic analysis (Rockwell et al., 1990) and a total dextral offset of 24 km (Sharp, 1967) suggest an ~2.4 Ma age of fault initiation, but stratigraphic data have been interpreted to show a 1.5 to 1.2 Ma initiation along the northern part of the fault zone (e.g. Morton and Matti, 1993). The Elsinore and San Felipe faults were estimated to be active by or before ~2 Ma in the Peninsular Ranges (Magistrale and Rockwell, 1996; Hull and Nicholson, 1992). However, recent work in the Borrego Badlands (Lutz, 2005; Lutz et al., in press) and San Felipe Hills documents a major stratigraphic and structural reorganization at ~1.1 Ma in the SW Salton Trough (Kirby, 2005; Kirby et al., in press) that may signal the initiation of dextral strike-slip faults farther SE. Because these studies examined basin fill in the San Felipe-Borrego sub-basin, the ~1.1 Ma stratigraphic reorganization was linked to the basin-bounding faults with indirect methods (Lutz et al., in press; Kirby et al., in press).

This study is part of an ongoing, larger, multi-university focus in the southwest Salton Trough. Recent work in this area (Dorsey, 2002; Dorsey and Janecke, 2002; Lutz and Dorsey, 2003; Steely, 2003; Axen et al., 2004; Dorsey et al., 2004; Janecke et al.,

2004; Kirby et al., 2004a, 2004b; Steely et al., 2004a, 2004b; Dorsey, 2005; Dorsey et al., 2005; Housen et al., 2005; Janecke et al., 2005; Kairouz, 2005; Kirby, 2005; Kirby et al., 2005; Lutz, 2005; Shirvell et al., 2005; Steely et al., 2005b; Kirby et al., in press; Lutz et al., in press) has advanced our knowledge, but several key issues remain. This study seeks to 1) understand the initiation, evolution, and kinematics of the West Salton detachment fault and its supradetachment basin; and 2) better date and characterize the transition from slip on the West Salton detachment fault to slip on cross-cutting oblique strike-slip faults in the SW Salton Trough. In order to address these questions we studied the Yaqui Ridge and Borrego Mountain areas of the southwest Salton Trough and integrate our new field data and analyses with existing data and published literature. The results of this work are presented in Chapters 2 and 3 with an inclusive conclusion in Chapter 4.

METHODS

Field Methods

Detailed geological mapping was undertaken in the Borrego Mountain, Borrego Sink, Harper Canyon, Whale Peak, and Squaw Peak 7.5' USGS quadrangles. An area equivalent to about 2.5 USGS 7.5' quadrangles was mapped over approximately four months of field work and most of this mapping was conducted at 1:12,000-scale with 1:24,000-scale in areas with mostly Quaternary cover. Field maps consisted of 11"x17" prints created in ESRI ArcMap from 1 m-scale color infrared ortho-rectified aerial photographs. A rectified Digital Raster Graphic (DRG) of the 7.5' USGS topographic map was overlain on the ortho-photos and a NAD83 UTM grid overlay was created to aid in the location of field data. These maps were then printed for the entire field area at 1:12,000- and 1:24,000-scale on a color printer. 1:40,000- and 1:20,000-scale black and white stereo aerial photographs were also used for mapping. Contacts and features from these photos were transferred onto the ortho-photo prints.

Plate 1 is a compilation map of the field area. This map was created in Adobe Illustrator with a NAD83 UTM projection topographic base imported from ESRI ArcMap to match the projection of the field maps. Field data with GPS coordinates were plotted in ArcMap and exported into Ilustrator to maintain their absolute locations. The compilation map includes mostly mapping and data from my field work with lesser amounts from unpublished mapping by Susanne Janecke, Gary Axen, and Becky Dorsey. Unit descriptions and the legend are located in Plate 2.

In addition to the mapping, approximately 500 m of stratigraphic section were measured (Plate 4), 197 paleocurrent indicators were collected, and 39 clast counts in conglomeratic units were counted. Detailed sedimentologic and stratigraphic descriptions were also made in the field. Approximately 210 kinematic data, including fault orientation and slickenline trend, were collected on faults with a special emphasis on the West Salton detachment fault. Over 228 foliations and 120 stretching lineations were collected with an emphasis on the footwall of the detachment fault. Over 680 measurements of bedding help to constrain the location and geometry of folds throughout the area, and over 110 rock samples were collected. These data are included in Appendix B.

Data Analysis

Kinematic data was analyzed by binning data based on what fault it was from and then plotting the data in the *Stereonet* program by Rick Allmendinger. Once plotted, poles to fault planes and slickenlines were contoured and statistics generated. Foliation and bedding data were binned by structural or geographic domains and then plotted and contoured in Stereonet. For foliation and bedding domains that showed evidence for folding, a shortening estimate was made by approximating the domain as one large fold with the average interlimb angle.

Six geological cross sections were constructed from the compiled geologic map

(Plate 3). Five of these sections are oriented nearly perpendicular to Yaqui Ridge and the detachment fault, whereas one cross section was constructed parallel to Yaqui Ridge and connects the other five cross sections.

Approximately 20 standard 30μm thin sections were prepared for petrographic study. Twelve of these thin sections were from deformed and chloritically altered clasts of the West Butte conglomerate. The remaining thin sections are from the damage zone of the West Salton detachment fault or the Imperial Formation east of Borrego Mountain. All thin sections were analyzed and described in order to asses the likely provenance of the West Butte conglomerate.

An isopach map of basin fill thickness around Borrego Mountain was constructed to constrain the location, size, and trend of a Pliocene-age growth anticline. Thicknesses were obtained from measured sections, field descriptions, or measured from map relationships. In order to properly depict the original trend of the structure, later dextral faulting had to be removed. Therefore the isopach map uses a 2-D palinspastic reconstruction as a base (see Chapter 2 for details).

This study integrates these new data sets with a residual isostatic gravity map of data in Langenheim and Jachens (1993) augmented with new unpublished data and a filtered residual magnetic map from Vicki Langenheim. Age control is provided by magnetostratigraphy (Lutz et al., in press; Housen et al., 2005; Kirby et al., in press), and other previous work in the southwest Salton Trough.

REFERENCES

Axen, G. J., 1995, Extensional segmentation of the main Gulf escarpment, Mexico and United States. Geology, v. 23, p. 515-518.

Axen, G.J., and Fletcher, J.M., 1998, Late miocene-plesitocene extensional faulting, northern Gulf of California, Mexico and Salton Trough, California. International Geology Review, v. 40, p. 217-244.

Axen, G.J., Kairouz, M., Steely, A.N., Janecke, S.U., and Dorsey, R.J., 2004, Structural expression of low-angle normal faults developed in wrench settings: an example

from the West Salton detachment fault, southern California. Geological Society of America Abstracts with Programs, v. 36, no. 5, p. 548.

Bartholomew, M. J., 1968, Geology of the northern portion of Seventeen Palms and Font's Point quadrangles, Imperial and San Diego Counties, California. [Master Thesis]: University of Southern California, Los Angeles, 60 p.

Carney S.M., and Janecke, S. U., 2005, Excision and the original low dip of the Miocene-Pliocene Bannock detachment system, SE Idaho: Northern cousin of the Sevier Desert detachment?: Geological Society of America Bulletin, v. 117, p. 334-353.

Dibblee, T.W. Jr., 1954, Geology of the Imperial Valley Region, California, Geology of Southern California. California Division of Mines Bulletin 170, p. 21-28.

Dibblee, T.W. Jr., 1984, Stratigraphy and tectonics of the San Felipe Hills, Borrego Badlands, Superstition Hills, and vicinity, *in* Rigsby, C.A., ed., 1984, The Imperial Basin-tectonics, sedimentation, and thermal aspects. Pacific Section S.E.P.M., p. 31-44.

Dibblee, T.W. Jr.,1996, Stratigraphy and tectonics of the Vallecito-Fish Creek Mountains, Vallecito Badlands, Coyote Mountain, and Yuha Desert, southwestern Imperial basin, *in* Abbott, P.L. and Seymour, D.C., eds., 1996, Sturtzstroms and detachment faults, Anza-Borrego Desert State Park, California. South Coast Geological Society Annual Field Trip Guide Book, no. 24, p. 59-79.

Dorsey, R. J., 2002, Stratigraphic record of Pleistocene initiation and slip on the Coyote Creek fault, lower Coyote Creek, Southern California. *In:* Barth, A., ed., Contributions to Crustal Evolution of the Southwest United States: Boulder, Co. GSA Special Paper 365, p. 251-269.

Dorsey, R.J., 2005, Stratigraphy, tectonics, and basin evolution in the Anza-Borrego Desert region, *in* Jefferson, G.T. and Lindsay, L.E., eds., Fossil Treasures of Anza-Borrego Desert. Sunbelt Publications, San Diego, CA, p. 89-104.

Dorsey, R.J., and Janecke, S.U., 2002, Late Miocene to Pleistocene West Salton Detachment Fault System and Basin Evolution, Southern California: New Insights. Geological Society of America Abstracts with Programs, v. 34, no. 6, p. 248.

Dorsey, R. J., Janecke, S. U., Kirby, S., Axen, G., and Steely, A. N., 2004. Pliocene Lacustrine Transgression in the Western Salton Trough, Southern California: Implications for Regional Tectonics and Evolution of the Colorado River Delta. Geological Society of America Abstracts with Programs, v. 36, p. 317.

Dorsey, R.J., Janecke, S.U., Kirby, S.M., McDougall, K.A., and Steely, A.N., 2005,

Pliocene evolution of the lower Colorado River in the Salton Trough; tectonic controls on regional paleogeography and the regional Borrego Lake, *in* Marith C., ed., Geologic and biotic perspectives on late Cenozoic drainage history of the southwestern Great Basin and lower Colorado River region; conference abstracts. USGS Open-File Report 2005-1404, p. 13.

Erskine, B.G., and Wenk, H.R., 1985, Evidence for Late Cretaceous crustal thinning in the Santa Rosa mylonite zone, southern California. Geology, v. 13, p. 274-277.

Fedo, C.M., and Miller, J.M.F., 1992, Evolution of a Miocene half-graben basin, Colorado River extensional corridor, southeastern California: American Association of Petroleum Geologists Bulletin, v. 104, p. 481-493.

Fowler, T.K., Jr., Friedmann, S.J., Davis, G.A., and Bishop, K.M., 1995, Two-phase evolution of the Shadow Valley Basin, southeastern California: A possible record of footwall uplift during extensional detachment faulting: Basin Research, v. 7, p. 165-179.

Frost, E. G., Fattahipour, M. J., and Robinson, K. L., 1996, Neogene detachment and strike-slip faulting in the Salton Trough region and their geometric and genetic interrelationships, *in* Abbott, P. L., and Cooper, J. D., eds., Field conference guidebook and volume for the annual convention, San Diego, California, May, 1996. Bakersfield, California, Pacific Section, American Association of Petroleum Geologists, p. 263-294.

George, P. G., and Dokka, R. K., 1994, Major late Cretaceous cooling events in the eastern Peninsular Ranges, California, and their implications for Cordilleran tectonics. Geological Society of America Bulletin, v. 106, p. 903-914.

Housen, B.A., Dorsey, R.J., Janecke, S.U., and Axen, G.J., 2005, Rotation of Plio-Pleistocene sedimentary rocks in the Fish Creek Vallecito Basin, western Salton Trough, CA. EOS - Transactions of the American Geophysical Union. v. 86

Hull, A.G., and Nicholson, C., 1992, Seismotectonics of the northern Elsinore fault zone, Southern California. Bulletin of the Seismological Society of America, v. 82, no. 2, p. 800-818.

Janecke, S. U., Vandenburg, C. J., and Blankenau, J. J., 1998, Geometry, mechanisms and significance of extensional folds from examples in the Rocky Mountain Basin and Range Province, U.S.A. Journal of Structural Geology, v. 20, p. 841-856.

Janecke, S.U., Carney, S.M., Perkins, M.E., Evans, J.C., Link, P.K., Oaks, R.Q., Jr., and Nash, B.P., 2003, Late Miocene-Pliocene detachment faulting and Pliocene-Pleistocene Basin-and-Range extension inferred from dismembered rift basins of the

Salt Lake Formation, southeast Idaho, *in* Raynolds, R., and Flores, R., eds., Cenozoic Paleogeography of the Rocky Mountains: SEPM Special Publication, p. 369-406.

Janecke, S.U., Kirby, S.M., Langenheim, V.E., Housen, B., Dorsey, R.J., Crippen, R.E., Blom, R.G., 2004, Kinematics and evolution of the San Jacinto fault zone in the Salton Trough: Progress report from the San Felipe Hills area. Geological Society of America Abstracts with Programs, v. 36, no. 5, p. 317.

Janecke, S.U., Kirby, S.M., Langenheim, V., Steely, A.N., Dorsey, R.., Housen, B., and Lutz, A., 2005, High geologic slip rates on the San Jacinto fault zone in the SW Salton Trough, and possible near-surface slip defecit in sedimentary basins. Geological Society of America Abstracts with Programs, v. 37, no. 7, p. 275

Kairouz, M.E., 2005, Geology of the Whale Peak Region of the Vallecito Mountains: Emphasis on the Kinematics and Timing of the West Salton Detachment fault, Southern California [M.S. Thesis]: University of California, Los Angeles. 156 p.

Kirby, S.M., 2005, The Quaternary tectonic and structural evolution of the San Felipe Hills, California [M.S. Thesis]: Logan, Utah State University, 182 p.

Kirby, S.M., Janecke, S.U., Dorsey, R.J., and Layman, E.B., 2004a, Reorganization of the San Jacinto fault zone at 1 Ma: Evidence from syntectonic deposits in the San Felipe Hills, western Salton Trough, CA. Geological Society of America Abstracts with Programs, v. 36, no. 4, p. 37.

Kirby, S.M., Janecke, S.U., Dorsey, R.J., and Housen, B., 2004b, A 1.07 Ma change from persistent lakes to intermittent flooding and desiccation in the San Felipe Hills, Salton Trough, southern California. Geological Society of America Abstracts with Programs, v. 36, no. 5, p. 318.

Kirby, S. M., Janecke, S. U., Dorsey, R. J., Housen, B. A., McDougall, K., and Steely, A. in press, Pleistocene Brawley and Ocotillo formations: Evidence for initial strike-slip deformation along the San Felipe and San Jacinto fault zones, California: Journal of Geology. 21 p. accepted July 2006.

Langenheim, V. E., and Jachens, R. C. 1993. Isostatic residual gravity map of the Borrego Valley 1:100,000-scale quadrangle, California. U.S. Geological Survey Open-File Report 93-246, scale 1:100,000.

Lough, C. F., 1993, Structural evolution of the Vallecito Mountains, Colorado Desert and Salton Trough Geology, San Diego, California, San Diego Association of Geologists, p. 91-109.

Lutz, A.T., 2005, Tectonic controls on Pleistocene basin evolution in the central San Jacinto fault zone, southern California [M.S. thesis]: Eugene, University of Oregon, 136 p.

Lutz, A.T., and Dorsey, R.J., 2003, Stratigraphy of the Pleistocene Ocotillo Conglomerate, Borrego Badlands, southern California: Basinal response to evolution of the San Jacinto fault zone. Geological Society of America Abstracts with Programs, v. 35, no. 6, p. 248.

Lutz, A.T., Dorsey, R.J., Housen, B.A,, and Janecke, S.U., in press, Stratigraphic record of Pleistocene faulting and basin evolution in the Borrego Badlands,San Jacinto fault zone, southern California. Geological Society of America Bulletin.

Magistrale, H., and T. Rockwell, 1996. The central and southern Elsinore fault zone, southern California, Bull. Seism. Soc. Am. 86:1793-1803.

Morton, D. M., and Matti, J. C., 1993, Extension and contraction within an evolving divergent strike-slip fault complex: the San Andreas and San Jacinto fault zones at their convergence in Southern California, *in* Powell, R. E., Weldon, R. J., and Matti, J. C., eds., The San Andreas fault system: displacement, palinspastic reconstruction, and geologic evolution: Geological Society of America Memoir, v. 178, p. 217-230.

Rockwell, T., Loughman, C., Merifield, P., 1990, Late Quaternary rate of slip along the San Jacinto fault zone near Anza, Southern California. Journal of Geophysical Research, v. 95, p. 8593-8605.

Rogers, T.H., 1965, Santa Ana sheet: California Division of Mines and Geology Geologic Map of California, scale, 1:250,000.

Sanders, C. O. 1989. Fault segmentation and earthquake occurrence in the strike-slip San Jacinto fault zone, California, *in* Schwartz, D. P., Sibson, R. H., eds., Proceedings of Conference XLV; a workshop on Fault segmentation and controls of rupture initiation and termination, U. S. Geological Survey Open-File Report OF 89-0315, p. 324-349.

Schultejann, P.A., 1984, The Yaqui ridge antiform and detachment fault: Mid-Cenozoic extensional terrane west of the San Andreas fault. Tectonics, v. 3, no. 6, p. 677-691.

Sharp, R. V., 1967, San Jacinto fault zone in the Peninsular Ranges of southern California. Geological Society of America Bulletin, v. 78, p. 705-730.

Sharp, R.V., 1972, Tectonic Setting of the Salton Trough, *in* Sharp, R. V., ed., The Borrego Mountain Earthquake of April 9, 1968, USGS Professional Paper, p. 3-15.

Shirvell, C.R., Axen, G.J., and Stockli, D.F., 2005, Pliocene (U-Th)/He cooling ages from

the West Salton detachment system (WSDS), Salton Trough. Geological Society of America Abstracts with Programs, v. 37, no. 7, p. 274.

Steely, A.N., 2003, Structural geology and stratigraphy of the Borrego Mountain area, southern California: Implications for late Cenozoic tectonic evolution of the western Salton Trough. [Undergraduate thesis] Eugene, University of Oregon. 77 p.

Steely, A.N., Janecke, S.U., Dorsey, R.J., and Axen, G.J., 2004a, Evidence for late Miocene-Quaternary low-angle oblique slip faulting on the West Salton detachment fault, southern California. Geological Society of America Abstracts with Programs, v. 36, no. 4, p. 37.

Steely, A.N., Janecke, S.U., and Dorsey, R.J., 2004b, Evidence for syn-depositional folding of Imperial-age synrift deposits above the West Salton detachment fault, Borrego Mountain area, southern California. Geological Society of America Abstracts with Programs, v. 36, no. 5, p. 317.

Steely, A.N., Janecke, S.U., Long, S.P., Carney, S.M., Oaks Jr., R.Q., Langenheim, V.E., and Link, P.K., 2005a, Evolution of a late Cenozoic supradetachment basin above a flat-on-flat detachment with a folded lateral ramp, SE Idaho, *in* Pederson, J., and Dehler, C.M., eds., Geological Society of America Field Guide 6, p. 169-198.

Steely, A.N., Janecke, S.U., Axen, G.J., and Dorsey, R.J., 2005b, Pleistocene (~1 Ma) transition from West Salton detachment faulting to cross-cutting dextral strike-slip faults in the SW Salton Trough. Geological Society of America Abstracts with Programs, v. 37, no. 7, p. 274.

Stinson, A. L., and Gastil, R. G., 1996, Mid- to Late-Tertiary detachment faulting in the Pinyon Mountains, San Diego County, California: A setting for long run-out landslides in the Split Mountain Gorge area, *in* Abbott, P. L., and Seymour, D. C., eds., Sturtzstrums and Detachment Faults, Anza-Borrego Desert State Park, California, Santa Ana, California, South Coast Geological Society, p. 221-244.

Wernicke, B., 1985, Uniform-sense normal simple shear of the continental lithosphere: Can. J. Earth Sci., v. 22, p. 108-125.

CHAPTER 2

THE WEST SALTON DETACHMENT FAULT NEAR YAQUI RIDGE, SW SALTON TROUGH: THE TECTONIC EVOLUTION OF ITS FOLDED HANGING WALL, AGE, AND KINEMATICS[1]

ABSTRACT

The West Salton detachment fault has been hypothesized to accommodate the dip-slip component of oblique plate motion during late Miocene to Pliocene time in southern California adjacent to the southern San Andreas fault. The evolution of the sedimentary basin above this detachment fault, the kinematics of slip across this structure, the age of initiation and age of final slip are not well known however, and are the subject of this study. The structural style was thought to be similar to that typical of detachment faults that bound metamorphic core complexes of the Basin-and-Range province which have internally extended hanging walls and isostatically-domed detachment faults.

Geological mapping, structural analysis, and basin analysis along a portion of the detachment fault near Yaqui Ridge and extending into its hanging wall at Borrego Mountain show that the West Salton detachment fault was active during Pliocene time and may have initiated during the latest Miocene. Overall in the Salton Trough the detachment fault strikes NNW and reactivated a late Cretaceous reverse-sense mylonite zone. We show that crustal inheritance is important at Yaqui Ridge where the detachment fault reactivates the mylonite zone and strikes anomalously NW- to WNW. Slickenlines at Yaqui Ridge record dominantly east-directed extension and show that the detachment fault contains equal amounts of dip-slip and strike-slip in this area. A nearly 180° dispersal of slickenline directions when the folded SSW-dipping limb of the younger

---

[1]Coauthored by Alexander N. Steely, Susanne U. Janecke, Rebecca J. Dorsey, and Gary J. Axen.

Yaqui Ridge anticline is restored may be explained by east-directed extension during slip on the detachment fault, followed by Pleistocene flexural slip overprint on the SSW-dipping limb of the Yaqui Ridge anticline. Although there is uncertainty and complexity associated with the kinematics of the detachment fault, it differs from most detachment faults because its oblique slip produced an oblique hanging-wall growth fold, its hanging wall is not internally extended by normal faults, and the fault co-evolved with the San Andreas fault to the east.

About 3 km of basin-fill was deposited in the study area during slip on the West Salton detachment fault and all but the basal few meters and capping terrace deposits are interpreted as syntectonic deposits of the fault system. The late Miocene (?) or Pliocene Hawk Canyon formation and West Butte conglomerate provide a minimum age for initial slip on the West Salton detachment fault because they contain clasts from the footwall and damage zone of the detachment fault. We correlate these two units to marine deposits of the Imperial Group east of Borrego Mountain. Our syndetachment interpretation of the West Butte conglomerate is supported by its striking similarity to the younger Pliocene Canebrake Conglomerate which records deeper exhumation of the footwall of the West Salton detachment fault. A long run-out rockslide is interbedded with the Canebrake Conglomerate, may be ~200 km^2 in extent, and indicates the presence of significant topographic relief across the detachment fault during Pliocene time.

Instead of extending internally by normal faults, the hanging wall of the West Salton detachment fault produced at least one basement-cored anticline at Borrego Mountain. Progressive and buttress unconformities and changes in thickness of late Miocene to Pliocene basin-fill define the Borrego Mountain anticline which trends ~N60°W and has at least 420 m of structural relief on its flanks. The crest of the anticline remained fixed during deposition of the middle member of the Late Miocene – Pliocene Hawk Canyon formation through at least the Olla Formation of the Pliocene Palm Spring Group and did not migrate through the hanging wall like a typical roll-over fold. The

anticline also influenced the stratigraphic architecture of the basin-fill deposits by raising a >7 km-wide platform above sea level southwest of the anticline's crest.

INTRODUCTION

The Salton Trough lies across the transtensional Pacific-North America plate boundary and records complex late Cenozoic deformation and sedimentation in southern-most California and northern Mexico (Fig. 2-1). The Salton Trough is the northern extension of the Gulf of California physiographic province, a crustal depression nearly 1400 km long. The Salton Sea lies approximately 73 meters below sea level and the Colorado River delta currently blocks the Gulf of California from entering the Salton Trough. The San Andreas fault system bounds the north and northeast side of the basin, and a ~250 km long detachment fault system with two oppositely verging segments bounds the western edge (Fig. 2-1) (Axen and Fletcher, 1998). The West Salton detachment fault is the northern segment of the fault system (Fig. 2-2) and accommodated top-to-the-east oblique extension (this study), whereas the Laguna Salada detachment fault is the southern segment and accommodates top-to-the-west extension (Axen, 1995; Axen and Fletcher, 1998).

The West Salton detachment fault was originally interpreted as an early to middle Miocene detachment system similar in style and age to those that bound metamorphic core complexes farther east in eastern California and western Arizona (Frost et al., 1996; Schultejahn, 1984). Parts of the fault were also interpreted as a Cretaceous low-angle normal fault system (Erskine and Wenk, 1985; George and Dokka, 1994). Recent work has shown that the West Salton detachment fault is a late Cenozoic detachment fault that coexisted with the early San Andreas fault system (Lough, 1993, 1998; Stinson and Gastil, 1996; Axen and Fletcher, 1998; Dorsey and Janecke, 2002; Kairouz, 2005). Contemporaneous activity on these two fault systems suggests that the extensional and dextral components of the transtensional Pacific-North American relative plate motions

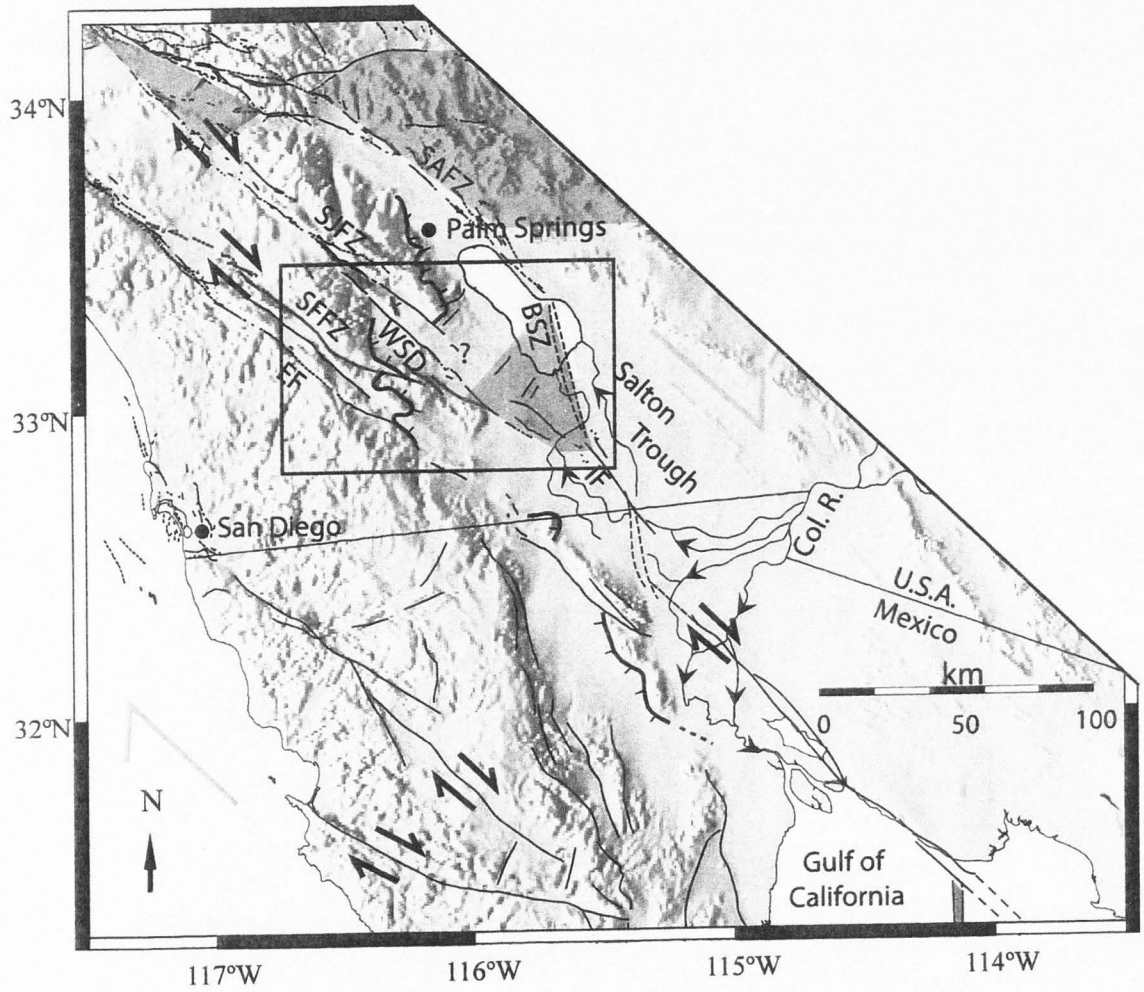

Figure 2-1. Tectonic overview of southern California and northwestern Mexico. Areas of known and inferred block rotation are shaded orange (Nicholson et al., 1985; Hudnut et al., 1989; Oskin and Stock, 2003). San Felipe fault zone (SFFZ) is in red, other strike-slip faults are in black; SAFZ-San Andreas fault zone; SJFZ-San Jacinto fault zone; IF-Imperial fault; SJFZ-San Jacinto fault zone; EF-Elsinore fault; BSZ-Brawley Seismic Zone. Oblique-slip detachment faults are in blue including the WSD-West Salton detachment fault. Fault locations are from Jennings (1977) and Axen and Fletcher (1998). Modified from Kirby et al. (in press). Box is approximate location of Figure 2-2.

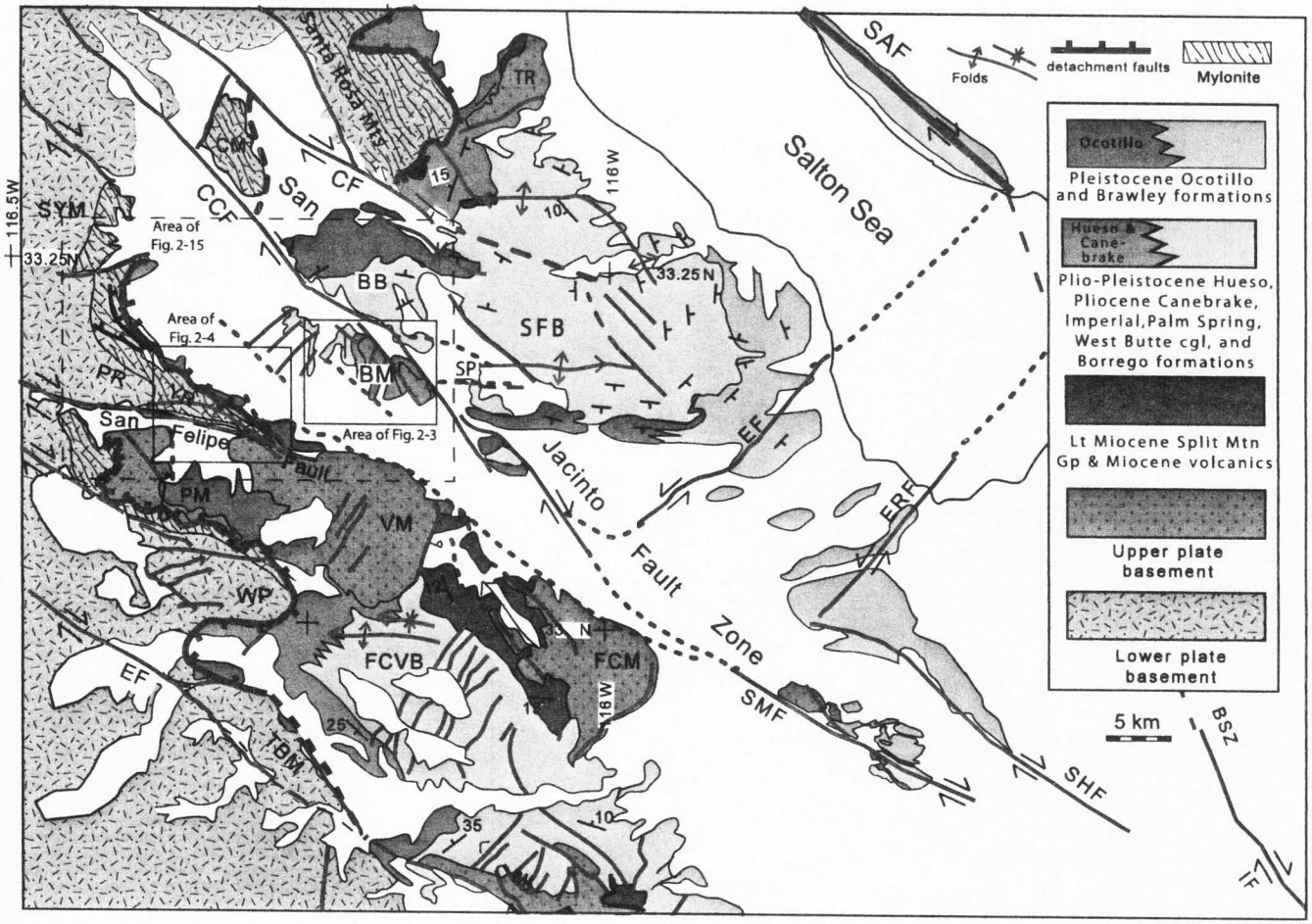
SAF
Folds
detachment faults
Mylonite
Ocotillo
Pleistocene Ocotillo and Brawley formations
Hueso & Cane-brake
Plio-Pleistocene Hueso, Pliocene Canebrake, Imperial, Palm Spring, West Butte cgl, and Borrego formations
Lt Miocene Split Mtn Gp & Miocene volcanics
Upper plate basement
Lower plate basement
5 km
Salton Sea
Santa Rosa Mts
San Jacinto Fault Zone
San Felipe Fault
Area of Fig. 2-15
Area of Fig. 2-4
Area of Fig. 2-3
116.5W
33.25N
116W
33.5N
TR
CM
CCF
CF
BB
SFB
BM
SP
PR
PM
VM
WP
FCVB
FCM
EF
TBM
SYM
SMF
SHF
BSZ
ERF

may have been partitioned onto the West Salton detachment fault and the San Andreas fault, respectively (Axen and Fletcher, 1998; Dorsey and Janecke, 2002). "Complete strain partitioning'" predicts pure dextral strike-slip on the San Andreas fault and pure dip-slip on the West Salton detachment fault (Davis and Reynolds, 1996). In this model pure dip-slip would be manifest as NE-directed slip on the detachment fault. Conversely, a simple wrench tectonic model predicts east-directed extension on east- or west-dipping normal faults that are subsidiary to the main dextral San Andreas fault.

The recent recognition of the West Salton detachment fault as a major controlling structure during the late Cenozoic in the western Salton Trough has raised many questions. The age of initial slip, the basinal response to slip on the detachment fault, and the kinematic and temporal relationships between the detachment fault and the San Andreas fault system are poorly known. The hanging walls of many extensional detachment faults are cut by normal faults that sole into the master fault and internally extend the hanging wall of these systems (Wernicke, 1985; Carney and Janecke, 2005). In addition, many detachment fault systems preserve extensional folds in the hanging wall that are subordinate to the more ubiquitous and numerous normal faults (Fedo and Miller, 1992; Fowler et al., 1995; Schlishe, 1995; Janecke et al., 1998, 2003; Carney and Janecke, 2005; Steely et al., 2005b). However, many of these detachment systems formed in nearly orthogonal extensional regimes, so our study area provides a unique opportunity to observe and characterize hanging wall structures and basinal response in an oblique tectonic regime.

This study seeks to understand the initiation, evolution, and kinematics of the West Salton detachment fault and its supradetachment basin. In order to address these questions we focus on exposures of the supradetachment basin-fill at Borrego Mountain (Fig. 2-3) westward into the mylonitic footwall of the detachment fault at Yaqui Ridge (Fig. 2-4) at the southwestern edge of the Salton Trough. We expand and update the mapping previously conducted in these areas (Dibblee, 1954, 1984; Morley, 1963;

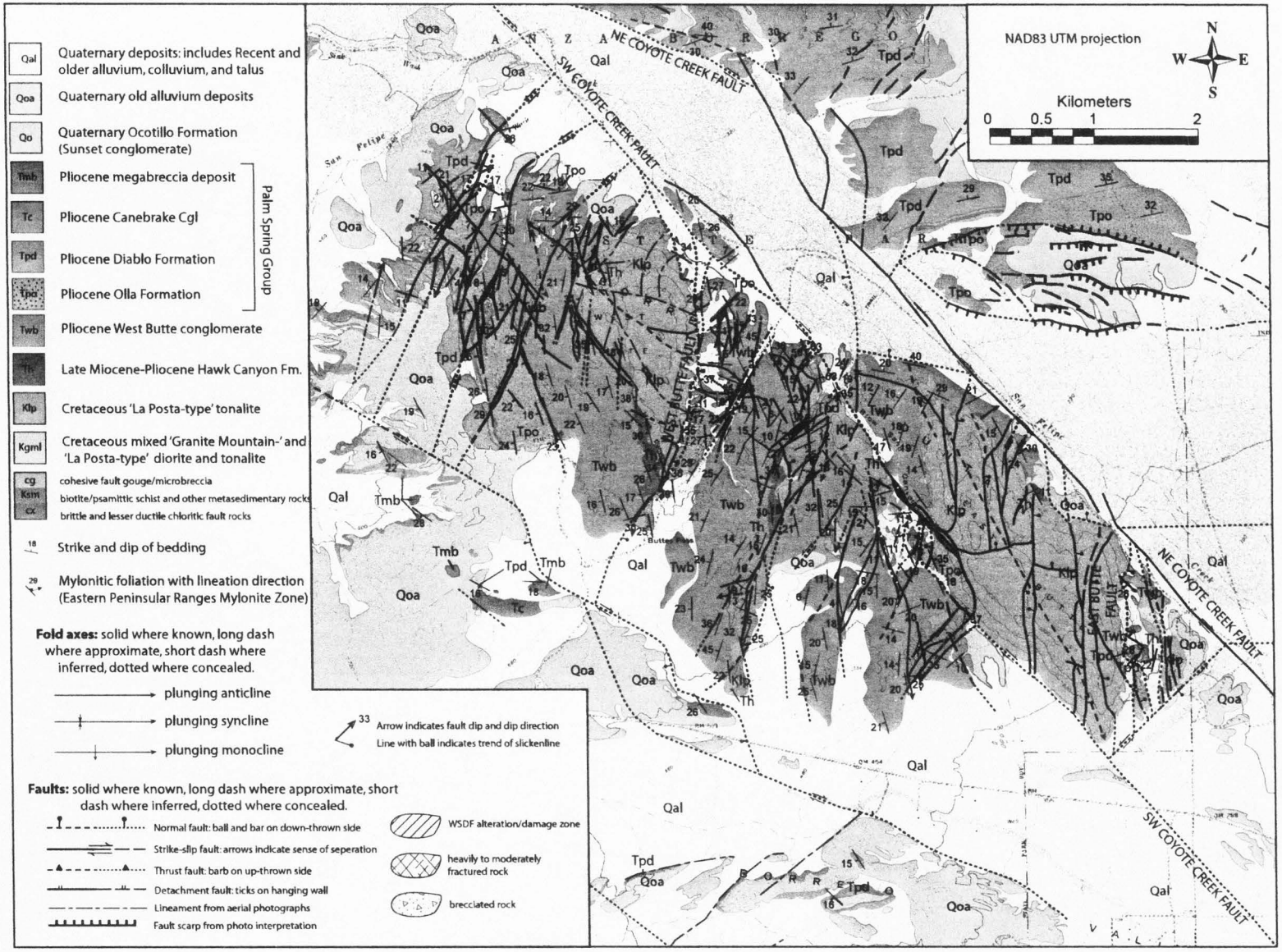

Figure 2-3. Simplified geological map of the Borrego Mountain area. Modified from Plate 1.

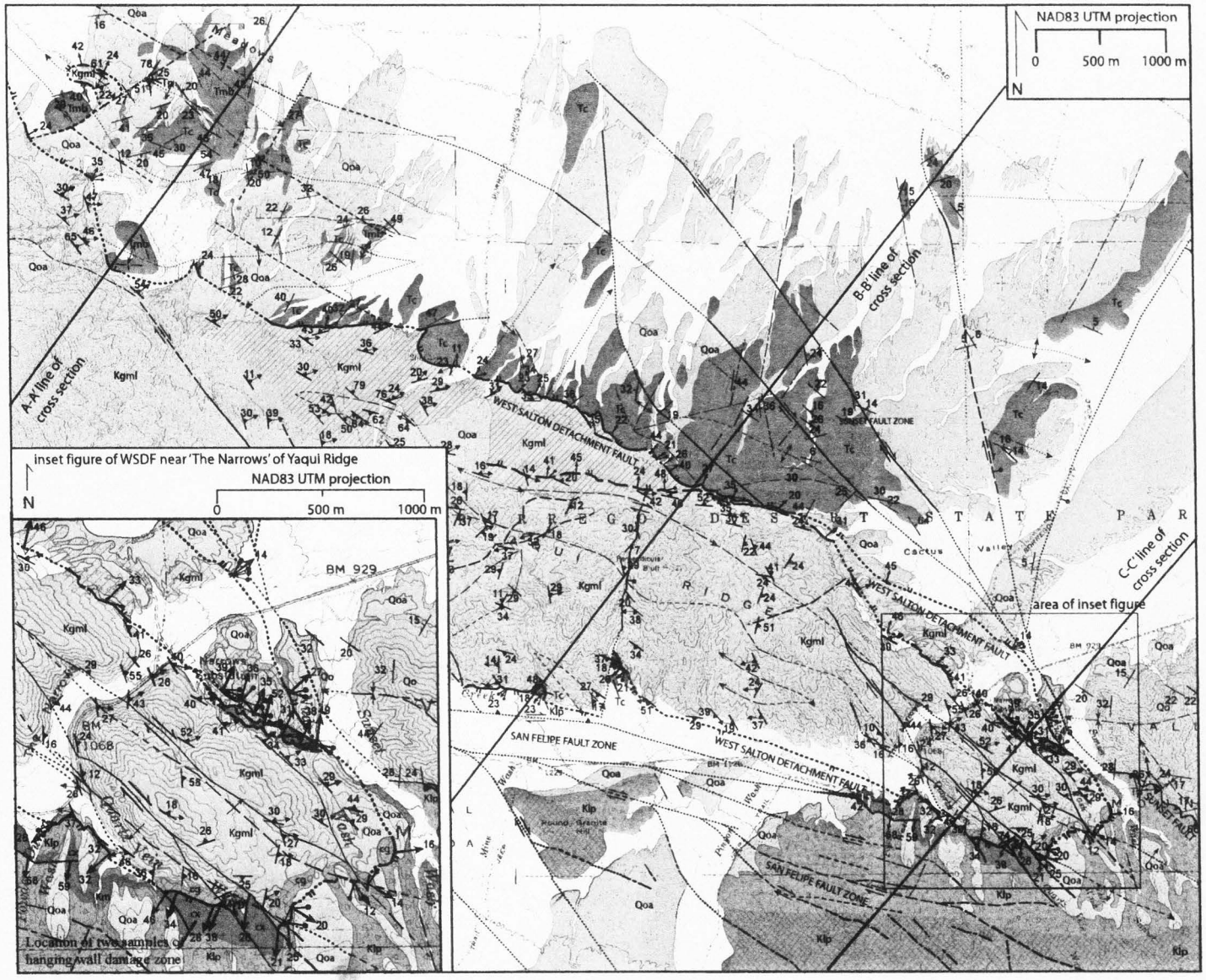

Figure 2-4. Simplified geological map of the Yaqui Ridge area. Modified from Plate 1.

Schultejahn, 1986; Lough, 1993, 1998; Herzig et al., 1995). Pleistocene faulting and folding in the Yaqui Ridge area has uplifted and exposed crystalline and sedimentary hanging wall rocks, the West Salton detachment fault and damage zone, and crystalline footwall rocks (Fig. 2-4). This area provides key kinematic data on the detachment fault.

Quaternary folding and faulting related to the San Jacinto fault zone at Borrego Mountain has uplifted and exposed the entire stratigraphic section of the supradetachment basin (Fig. 2-3). The Borrego Mountain area is the principal area where we studied the sedimentology, paleogeography, and other sedimentary relationships in the supradetachment basin. The Borrego Mountain area contains three crystalline "buttes" all separated by strands of the Coyote Creek fault of the San Jacinto fault zone (Fig. 2-3). The West Butte fault bounds the eastern edge of West Butte, has ~550 m of dip-slip displacement across it, and separates West and Middle buttes. Middle Butte is the smallest of the buttes and is bound on its NE side by a strand of the Coyote Creek fault. Map analysis shows that this butte can be restored into a small extensional stepover on the SW side of East Butte with ~1.6 km of dextral separation (Fig. 2-3). East Butte is bound on its SW and NE sides by strands of the Coyote Creek fault and on its east side by the East Butte fault. The East Butte fault is a dip-slip fault of the Coyote Creek fault zone and has ~ 400 m of displacement.

Detailed geological mapping (1:12,000- and 1:24,000-scale) in these areas was combined with sedimentologic and kinematic analyses. Approximately 500 m of stratigraphic section were measured, 197 paleocurrent indicators were measured, 39 clast counts in conglomeratic units were counted, and detailed sedimentologic and stratigraphic descriptions were made in the field. Approximately 210 kinematic measurements, including fault orientation and slickenline trend, were collected on faults with a special emphasis on the West Salton detachment fault. Over 228 foliations and 120 stretching lineations were measured with an emphasis on the footwall of the detachment fault. Over 680 measurements of bedding help to constrain the location

and geometry of folds throughout the area. Basin-fill isopach maps were constructed in addition to six geological cross sections. Twelve thin sections of clasts from the West Butte conglomerate were analyzed and compared to possible source terranes, including six thin sections from the damage zone of the West Salton detachment fault, and six thin sections from other deformed footwall rocks. A filtered gravity map based on the data from Langenheim and Jachens (1993) and augmented with new unpublished data provides additional control on locations of faults and depths to basement.

The results of this study are part of a larger, ongoing, multi-university focus in the southwest Salton Trough. Recent work in this area (Dorsey, 2002; Dorsey and Janecke, 2002; Lutz and Dorsey, 2003; Steely, 2003; Axen et al., 2004; Dorsey et al., 2004; Janecke et al., 2004; Kirby et al., 2004a, 2004b; Steely et al., 2004a, 2004b; Dorsey, 2005; Dorsey et al., 2005a, 2005b; Janecke et al., 2005; Kairouz, 2005; Kirby, 2005; Kirby et al., 2005; Lutz, 2005; Shirvell et al., 2005; Steely et al., 2005a; Kirby et al., in press; Lutz et al., in press) has advanced our knowledge in many respects, but several key issues remain. Our work is the first to directly link deposits of the late Miocene- to Pliocene-age Imperial Group with activity on the West Salton detachment fault and confirm that Pliocene-age deposits were also controlled by this structure. We show that the hanging wall was not internally extended by normal faults but was broadly deformed by a large-scale, fault-strike-parallel growth anticline that was cored by crystalline rocks. We also show that the West Salton detachment fault was a NE- to NNE-dipping low-angle oblique-slip dextral-normal fault that accommodated east-directed extension. This suggests that movement on the West Salton detachment fault contained both dextral and extensional components of the relative plate motion and is consistent with a "wrench-style" model of strain.

REGIONAL GEOLOGY

Crystalline Bedrock

Peninsular Range Batholith

The Late Cretaceous Peninsular Range batholith and older metasedimentary screens and roof pendants form the basement terrain along the western edge of the Salton Trough (Fig. 2-2) and continue south along the Baja California peninsula (Jahns, 1954; Todd et al., 1988). The plutonic rocks were emplaced between 140 and 80 Ma (Silver et al., 1979) and exhibit west-to-east variations in lithology, age, geochemistry, and structural characteristics (Todd et al., 1988; Grove et al., 2003). These variations have led many workers to divide the plutonic rocks into two major zones along a north-to northwest line that represents a significant change in age, composition, parent material and geophysical character (Gastil, 1975, 1983; Silver et al., 1979; Todd and Shaw, 1979, 1985; Clinkenbeard and Walawender, 1989; Walawender et al., 1991; Langenheim and Jachens, 2003). Western zone plutons are characterized by gabbro through mafic inclusion-rich tonalite and are 120-105 Ma (Silver et al., 1979) and syn-kinematically deformed (Todd and Shaw, 1979). Eastern zone plutons are characterized by large volume, intermediate rocks with a limited compositional range (Clinkenbeard and Walawender, 1989; Walawender et al., 1991) and are 105-89 Ma (Silver et al., 1979).

Most of the plutonic rocks in the eastern zone are part of the La Posta-type TTG (tonalite-trondhjemite-granodorite) suite (Grove et al., 2003; Todd, 2004). These plutons differ from other plutons in the eastern zone because they are voluminous (up to 1400 km^2 surface exposure), internally zoned from hornblende-biotite granodiorite in the outer zone to muscovite-biotite granodiorite in the core (Clinkenbeard and Walawender, 1989; Walawender et al., 1991), and emplaced over a relatively short time period of 96 $\pm$ 3 Ma (Grove et al., 2003). We use the term "La Posta-type" plutons when referring to these relatively mafic-poor tonalites which comprise the majority of the Vallecito and Fish Creek mountains and dominate the plutonic basement above the West Salton

detachment fault (Grove et al., 2003; Todd, 2004). In contrast, we use the term "Granite Mountain-type" plutons to refer to hornblende-biotite-to biotite-rich tonalite and quartz diorite. These more mafic plutonic rocks are exposed dominantly in the footwall of the West Salton detachment fault where they are either the more mafic margins of La Posta-type plutons, or form distinct plutons (Grove et al., 2003; Todd, 2004; Kairouz, 2005; this study).

The metasedimentary screens and roof pendants associated with the Peninsular Range batholith were pre-batholithic volcanic and sedimentary rocks of Paleozoic to mid-Cretaceous age (Gastil and Miller, 1984), and Jurassic to early-Cretaceous volcanic arc-related sedimentary rocks (Gastil et al., 1975; Silver et al., 1963, 1979; Todd et al., 1988). Carbonate- and quartz-rich metasedimentary rocks near Yaqui Ridge and the Coyote Mountains have miogeoclinal affinities and nearby plutons have $^{87}Sr/^{86}Sr$ isotopic ratios (0.706-0.708) suggesting continental basement (Gastil, 1993; Langenheim and Jachens, 2003).

Eastern Peninsular Ranges Mylonite Zone

The Eastern Peninsular Ranges mylonite zone is a mid-to late-Cretaceous west-directed reverse-sense shear zone in the Peninsular Range batholith (Simpson, 1984; Engel and Schultejahn, 1984; Todd et al., 1988; George and Dokka, 1994). The Eastern Peninsular Ranges mylonite zone deforms both the Granite Mountain and La Posta-type plutonic rocks and their associated metasedimentary rocks. Deformation fabrics are more strongly developed in biotite-rich plutons and calc-silicate metasedimentary rocks than in weakly-deformed La Posta-type plutons. This shear zone forms a ~100 km long belt of mostly ductile and lesser brittle-ductile deformation along the eastern Peninsular Ranges from Palm Springs to just south of Yaqui Ridge in the SW Salton Trough (Fig. 2-2) (Sharp, 1979; Simpson, 1984; Engel and Schultejahn, 1984; Todd et al., 1988; George and Dokka, 1994; Axen and Fletcher, 1998; Kairouz, 2005). The mylonite

zone is up to 5 km-wide, and usually about 2 km-wide (Sharp, 1979). Foliations strikes north to northwest and dips 35°-55° east to northeast (Simpson, 1984; Todd et al., 1988). The trends of stretching lineations change from approximately ENE at Yaqui Ridge (Schultejahn, 1984; this study) near the southern end of the zone to N55°E in the northern Santa Rosa Mountains (Todd et al., 1988). The fabric of the shear zone grades over short distances from non-foliated rocks into protomylonite, mylonite, and ultramylonite (Simpson, 1984; Erskine and Wenk, 1985; Todd et al., 1988).

North of our study area, fission-track cooling ages in the San Jacinto Mountains (George and Dokka, 1994) and textural, microstructural analysis, and mapping in the Santa Rosa Mountains (Erskine and Wenk, 1985) are interpreted to reflect a period of brittle, low-angle, mid-to late-Cretaceous extension spatially coincident with and younger than the Eastern Peninsular Ranges mylonite zone. These faults locally reactivate older mylonitic fabrics, and elsewhere cut across at angles 25°-30° less than the mylonite and have slickenlines parallel to stretching lineations in the mylonite (Erskine and Wenk, 1985). This extension may have been caused by collapse of an over-thickened crustal welt produced during earlier westward thrusting (George and Dokka, 1994), or early denudation caused by emplacement of the voluminous La Posta series plutons and later erosional denudation triggered by removal of lower crust and lithospheric mantle during Laramide shallow subduction (Grove et al., 2003). However, a late Cretaceous age for this brittle faulting has not been accepted in more recent analyses of the Peninsular Ranges batholith because late Cretaceous cooling is observed in both the hanging wall and footwall of the brittle faults (e.g. Axen and Fletcher, 1998; Kimbrough et al., 2001; Grove et al., 2003). The age of the brittle deformation is hard to prove without additional geochronology and syntectonic sedimentary deposits.

Regionally, the West Salton detachment fault loosely follows the Eastern Peninsular Ranges mylonite zone (Fig. 2-2) but generally dips more gently than the mylonite (Erskine and Wenk, 1985; Axen and Fletcher, 1998). This study shows that

in some areas the two fabrics are parallel. Mylonitic rocks are almost entirely confined to the footwall of the West Salton detachment fault except for localized bands at Squaw Peak (this study) and at Travertine Ridge (Janecke, unpub mapping). La Posta-type tonalite and lesser amounts of metasedimentary rocks comprise the crystalline bedrock in the hanging wall of the West Salton detachment fault and contrast with the deformed rocks of the Eastern Peninsular Ranges mylonite zone and metasedimentary rocks which occur up to 5 km structurally beneath the detachment fault.

Cenozoic Tectonics

When the Pacific plate first came into contact with North America at ~30 Ma, a transform boundary began growing along the western edge of North America as two separate triple plate junctions migrated in opposite directions (Atwater, 1970, 1989). Between ~12.5 and 6 Ma the area of the modern Gulf of California experienced a proto-gulf extensional period as a result of the southward jump of the Rivera triple junction (Nagy and Stock, 2000; Stock and Hodges, 1989; Lonsdale, 1989). As the triple junction migrated south, subduction ceased and a transform boundary was created on the western edge of Baja California (Lonsdale, 1991; Spencer and Normark, 1989). Due to oblique plate vectors, this boundary was not purely translational and included a significant component of extension (Atwater, 1970, 1989; Lonsdale, 1989). This extension may have been accommodated by oblique dextral transtension on the northwest-striking Tosco-Abrejos fault zone off the western coast and approximately NE-SW directed extension along the axis of a Miocene volcanic arc (Spencer and Normark, 1989; Nagy and Stock, 2000; Lonsdale, 1989, 1991; Umhoefer et al., 1994; Oskin and Stock, 2003). These concepts are currently being challenged by Fletcher et al. (2004) who suggest a longer period of transtension than currently accepted.

At ~6 Ma, the transtensive Pacific-North American plate boundary jumped inboard of Baja California, linking the southern San Andreas fault (the San Gabriel fault

at that time) with the Pacific and Rivera plates to the south (Oskin and Stock, 2003). This major reorganization created nearly instantaneous marine flooding along the entire length of the new plate boundary from mouth of the Gulf of California in the south, to San Gregorio Pass in the north (Winker and Kidwell, 1996; Oskin and Stock, 2003). Magnetically-lineated ocean crust has been forming since 3.58 Ma at the Alarcon Rise at the southern end of the plate boundary (DeMets, 1995). It is likely that the entire southern and middle Gulf of California is forming new oceanic crust in a complex en-echelon ocean-ridge spreading center and transform fault setting, similar to other mid-ocean ridges (Lonsdale, 1989).

Between ~6 Ma and the Pleistocene, the San Andreas and West Salton detachment faults were the major basin-controlling structures in the northern Salton Trough, and at least 5 km of basin-fill accumulated in the Salton Trough during this time (Dibblee, 1984; Winker, 1987; Kirby, 2005; Dorsey et al., 2005a). Starting in Pleistocene time, dextral strike-slip faults of the San Jacinto and San Felipe fault zones cross cut the West Salton detachment fault and dismembered the previously intact supradetachment basin (Fig. 2-2) (Axen and Fletcher, 1998; Kirby et al., in press; Lutz et al., in press; Chapter 3). The San Jacinto fault zone strikes NW and merges with the Imperial fault to the southeast and the San Andreas fault to the northwest (Figs. 2-1 and 2-2). The San Felipe fault zone strikes NW, and its strike is more westerly than the San Jacinto fault zone. The San Felipe fault zone is >160 km-long and projects towards the Elsinore fault to the northwest and the Imperial fault to the southeast (Figs. 2-1 and 2-2) (Chapter 3). Most of the West Salton detachment fault zone has been uplifted and exhumed by these faults, and only small segments of the detachment fault continue to slip where the younger, cross-cutting dextral strike-slip faults utilize the pre-existing crustal weakness (e.g. Kairouz, 2005).

WEST SALTON DETACHMENT FAULT

Footwall Rocks

Footwall and hanging wall rocks of the West Salton detachment fault are well exposed in the southwestern San Felipe-Borrego basin near Yaqui Ridge. The footwall of the West Salton detachment fault consists of a mixed zone of tonalite, diorite, granodiorite, and metasedimentary rocks that have been overprinted by the ductile reverse-sense Cretaceous Eastern Penninsular Ranges mylonite zone (Fig. 2-4) (Schultejahn, 1984; Simpson, 1985; Lough, 1993, 1998; Axen and Fletcher, 1998; this study). Plutonic protoliths range from "La Posta-type" to "Granite Mountain-type" and the more mafic Granite Mountain-type lithologies predominate in the immediate footwall of the detachment fault while La Posta-type lithologies are more common at deeper structural levels to the west along Pinyon Ridge (Grove et al., 2003). Thin, <10 m thick bands of metasedimentary rocks are exposed locally along the NE side of Yaqui Ridge near Yaqui Narrows. These rocks include medium-blue marble with light tan silicic nodules, 0.5-5 cm banded calc-silicate rocks, and 2- to150-cm thick massive metaplutonic or meta-arkose beds. Fabrics in these rocks range from thin <5 cm-wide zones of ultramylonite to non-foliated, and are typically mylonitic and have well developed ENE- to ESE-trending stretching lineations. The Eastern Peninsular Ranges mylonite zone has a foliation perpendicular thickness of ~0.5 – 1.8 km structurally beneath the West Salton detachment fault before it grades into non-foliated plutonic rocks of the eastern Peninsular Ranges batholith. The Eastern Peninsular Ranges mylonite zone also dies out along strike to the south and is only a thin protomylonite zone along the edges of Whale Peak 14 km to the south (Fig. 2-2) (Kairouz, 2005).

Foliation in the footwall of the West Salton detachment fault is folded by the Pleistocene Yaqui Ridge anticline (Chapter 3). The West Salton detachment fault generally parallels these fabrics (Figs. 2-4 and 2-5). The fault from the NE-dipping limb of the folded mylonite strikes 321° and dips 27° on average whereas the fault

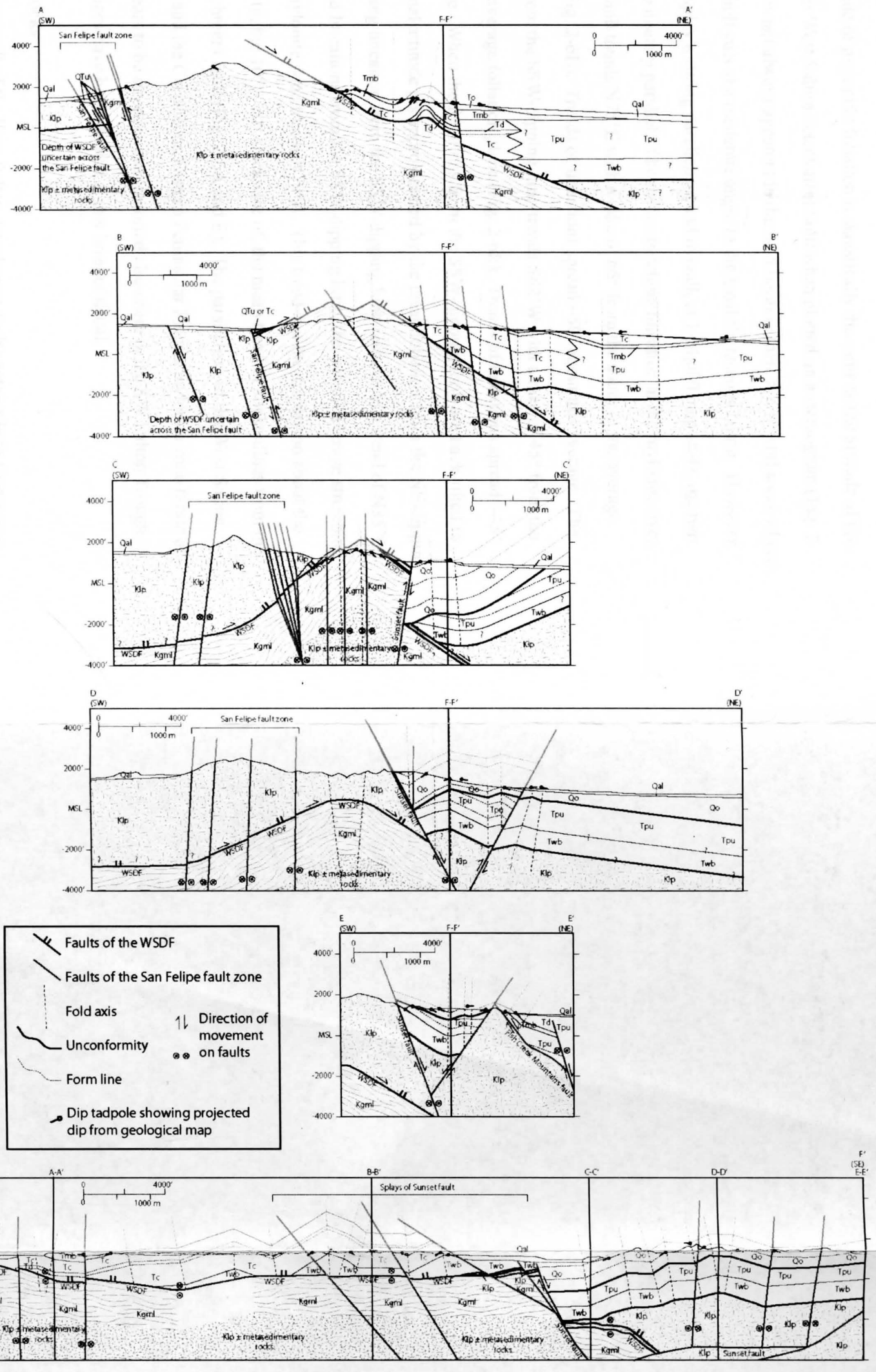

Figure 2-5. Geological cross sections across Yaqui Ridge and one section constructed parallel to Yaqui Ridge. See Figures 2-4 and 2-14 for the locations of cross section lines. Kgml, Cretaceous Granite Mountain-type diorite and granodiorite; Klp, Cretaceous La Posta-type tonalite; Qal, Quaternary alluvium; Qo, Quaternary Ocotillo Formation (Sunset Conglomerate of Steely et al., in prep); QTu, undifferentiated Quaternary-Tertiary deposits; Tc, Pliocene Canebrake Formation; Td, Pliocene Diablo Formation; Tmb, Pliocene Yaqui Ridge megabreccia; To, Pliocene Olla Formation; Tpu, Pliocene Palm Spring Group undifferentiated; Twb, Pliocene West Butte conglomerate; WSDF, West Salton detachment fault.

from the SSW-dipping limb strikes 123° and dips 25° on average (Fig. 2-6E) (n=225). The overall attitude of mylonitic foliation is statistically the same as the attitude of the structurally higher West Salton detachment fault when plotted on a stereogram (Fig. 2-6A and E). This is not always apparent in the field because there are several areas where the detachment fault cuts at a moderate angle to the local Cretaceous fabric. However, most outcrops display a strong parallelism and overall, at 1:24,000 map scale, the two fabrics are approximately parallel. The mean stretching lineation in the mylonite from the NE-dipping limb trends N75°E with a rake of 66° from the south in the average foliation plane (Fig. 2-6E). Trends of lineations spread ~50° about this average. The mean lineation from the SSW-dipping limb trends S82°W with a rake of 45° from the northwest in the average foliation plane (Fig. 2-6E). Trends of lineations spread ~45° about this average. When the foliations from the SSW-dipping limb are back-tilted to match their original attitude (as approximated by the mean foliation from the NE-dipping limb), the stretching lineation from the SSW-dipping limb restores to a trend of N85°E. Using the restored lineations from the SSW-dipping limb, the overall average stretching lineation in the mylonite zone trends N79°E. This trend and the dispersion about the mean are similar to, but 10° – 20° clockwise of, the mean trend of slickenlines from the West Salton detachment fault (Fig. 2-6A and E). The parallelism of the West Salton detachment fault and the Cretaceous Eastern Peninsular Ranges mylonite zone fabric at Yaqui Ridge appears to be stronger than reported elsewhere in the SW Salton Trough. However, few places have been studied at this level of detail.

Hanging Wall Rocks

The hanging wall of the West Salton detachment fault contains both Cretaceous crystalline basement rocks and Late Cenozoic basin-fill deposits that exhibit significant changes in lithology along the strike of the fault (Figs. 2-2, 2-3, 2-4). At the far northwest end of the study area along Church Ridge, the detachment fault cuts the Canebrake

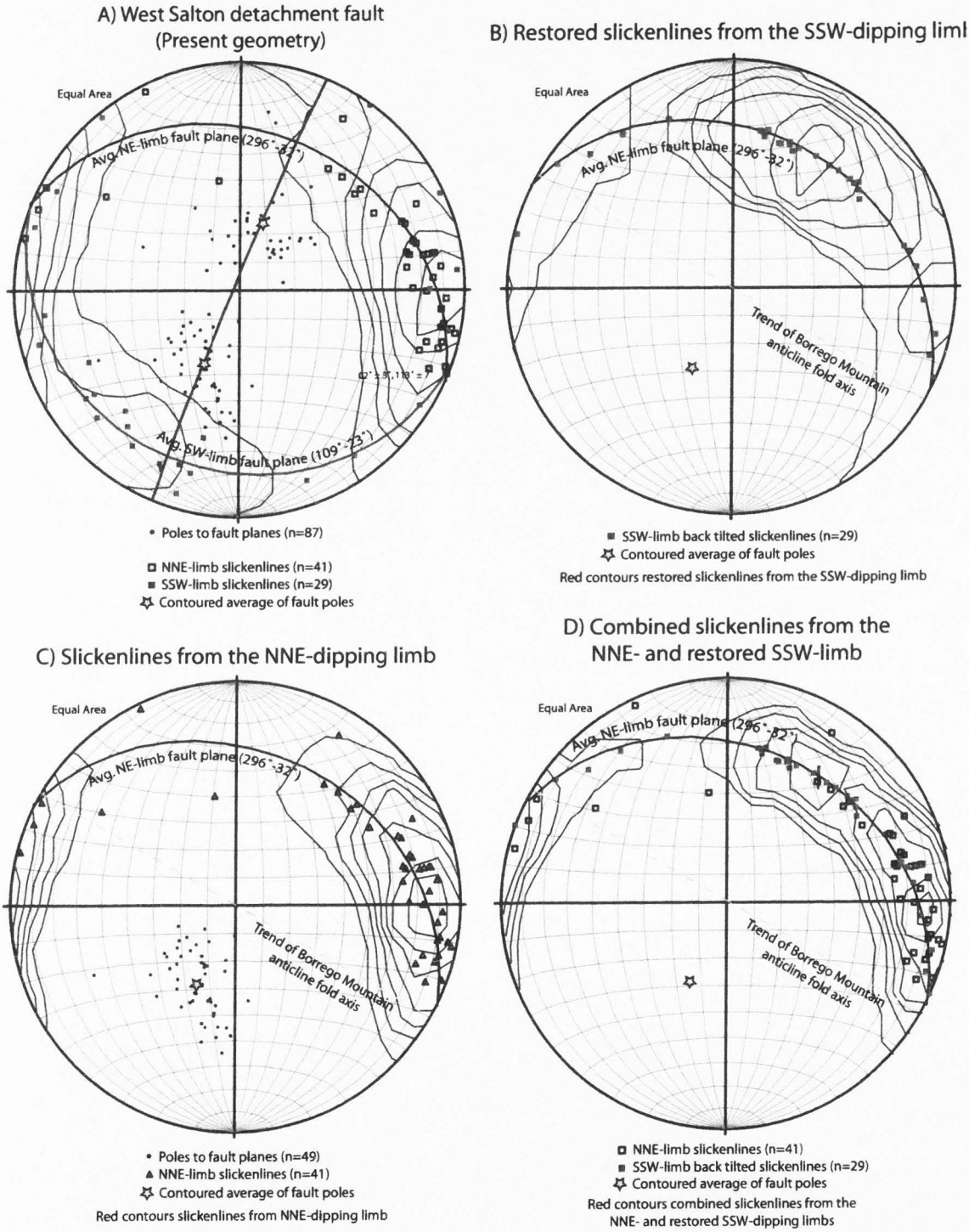

Figure 2-6. Stereograms of slickenlines on the West Salton detachment fault (WSDF). Full caption on following page.

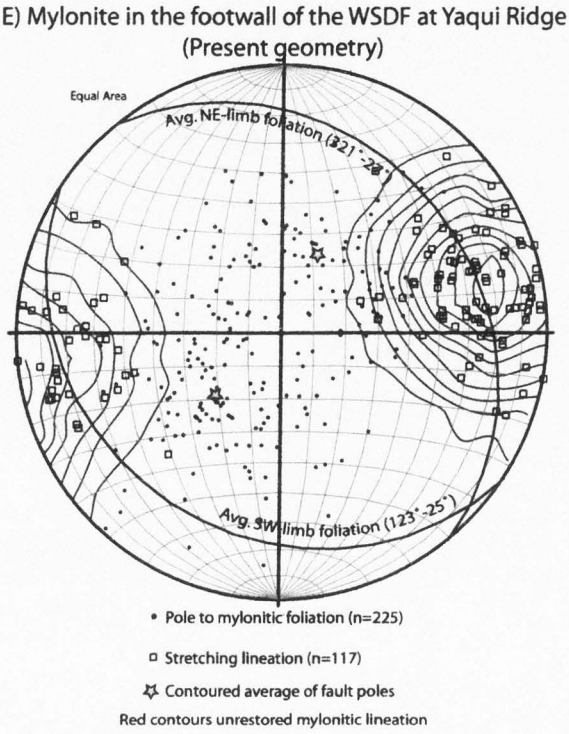

Figure 2-6. Stereograms of slickenlines on the West Salton detachment fault (WSDF) and underlying footwall mylonitic foliations. A) Present geometry of the WSDF around Yaqui Ridge. B) Contoured slickenlines on the WSDF from the SW limb of the Yaqui Ridge anticline. Slickenlines were back tilted by the amount required to restore the fault surface to the mean NNE-limb orientation. C) Contoured slickenlines on the WSDF and poles to fault surfaces from the NNE-limb of the Yaqui Ridge anticline. D) Combined and contoured NNE- and back tilted SSW-limb slickenlines on the WSDF. E) Present geometry of foliation and stretching lineations in the reverse-sense mylonite exposed in the footwall of the WSDF along Yaqui Ridge. Red contours slickenlines and stretching lineations.

Conglomerate and a megabreccia deposit, both part of the Pliocene Palm Spring Group. Along fault-strike to the southeast near Pinyon Ridge, the upper Canebrake Conglomerate and other units of the Palm Spring Group are cut by the detachment fault. Along the NE side of Yaqui Ridge near Yaqui Narrows the coarse lower Canebrake Conglomerate is cut by the detachment fault (Fig. 2-4). Basin-fill sedimentary rocks in the hanging wall of the West Salton detachment fault locally have steep cut-off angles with the fault surface and contain NE-plunging folds that do not cross the fault (Figs. 2-4 and 2-5).

The immediate hanging wall of the West Salton detachment fault changes from Palm Spring Group in the NNW to La Posta-type tonalite in the SSE along a line trending E to ENE across Yaqui Ridge (Fig. 2-4). This lateral change from La Posta-type crystalline rock to Palm Spring Group sedimentary rocks could either be a depositional contact between basin-fill and crystalline basement, or a previously unrecognized fault confined to the hanging wall of the West Salton detachment fault. Further work is needed to test these hypotheses.

Where the tonalite in the hanging wall of the detachment fault is fresh it contains large quartz grains, small biotite grains, and is part of the "La Posta-type" plutonic suite. Most crystalline rocks around Yaqui Ridge are significantly altered and brecciated or fractured by the West Salton detachment fault and adjacent dextral oblique San Felipe fault zone. Plutonic lithologies persist in the hanging wall of the detachment fault at least 14 km south of Yaqui Ridge to the northeast flank of Whale Peak (Stinson and Gastil, 1996; Kairouz, 2005). Here the Palm Spring Group again becomes the dominant rock type in the immediate hanging wall (Fig. 2-2) (Winker, 1987; Kairouz, 2005). Conglomerates mapped as Canebrake Conglomerate, and locally as Poway conglomerate, overlie the crystalline rocks along depositional contacts in this area south of the San Felipe fault zone (G. Axen, unpub. mapping).

Geometry of the West Salton Detachment Fault Zone

Along the northeast and southwest sides of Yaqui Ridge, map patterns show that the West Salton detachment fault is subdivided into three distinct segments that define the doubly plunging, NW-trending Yaqui Ridge anticline (Fig. 2-4). Mapping shows that this anticline has a box fold geometry, similarly deforms the hanging wall and footwall of the detachment fault, and was mostly or entirely created during the Pleistocene in a transpressional stepover created between strands of the dextral-oblique San Felipe fault (Chapter 3). The West Salton detachment fault is also cut by strands of the San Felipe fault in this same area. The West Salton detachment fault on the NE limb of the Yaqui Ridge anticline (Fig. 2-4) consists of up to three sub-parallel anastamosing fault strands that strike 296° and dip 32° on average (Fig. 2-6C) (n=49). The strands are up to 360 m apart or less in map view and form a fault zone up to ~500 m-wide in map view. Footwall rocks of the West Salton detachment fault are distinctly different from those in its hanging wall. In places with multiple detachment fault strands these strands only occur in footwall lithologies. The West Salton detachment fault on the SSW-dipping limb of the Yaqui Ridge anticline consists of only one strand and field measurements show that it strikes 109° and dips 23° on average (Fig. 2-6A) (n=38). However, the map trace of the detachment fault on the SSW-dipping limb of the anticline is closer to east-west. The SE-dipping section of the detachment fault at the nose of the Yaqui Ridge anticline is expressed mostly in map view as a single strand (Fig. 2-4). Direct measurements indicate a 037° strike and 16° dip (n=3).

Fault Rocks

Outcrops of the West Salton detachment fault are typically characterized by a prominent, low-angle, planar to gently undulating principal slip surface that marks a break in topography between altered and fractured mylonitic footwall rocks and altered and fractured non mylonitic hanging wall rocks (Fig. 2-7) (Schultejahn, 1984; Lough,

1993, 1998; Axen and Fletcher, 1998). This break in slope is most commonly observed where weakly cemented Pliocene sedimentary rocks are faulted against Cretaceous mylonite. The primary fault core is 0.1 to 1 cm thick cataclasite to ultracataclasite and is polished, white, tan, or yellow, and locally contains several sets of slickenlines (Fig. 2-7). Fault surface mullions are typically less than 5 cm-across and are rare. Beneath the polished fault surface, a narrow, resistant, 0.5-50 cm thick black to dark green microbreccia ledge is nearly ubiquitous (Fig. 2-7) (Schultejahn, 1984; Lough, 1993, 1998; Stinson and Gastil, 1996; Axen and Fletcher, 1998; this study). Tension fractures perpendicular to the fault plane and at high angles to slickenlines are locally common. Microstructural analysis of the microbreccia below the fault surface reveals extreme brittle grain-size comminution (Schultejahn, 1984).

Damage Zone in the Footwall

The microbreccia ledge grades downward into a zone of brown- to green-weathering, fractured to locally brecciated mylonitic rocks that persists for 5-500 m structurally beneath the fault surface (Fig. 2-7) (Schultejahn, 1984; Lough, 1993; this study). These rocks commonly have secondary chloritic alteration (Axen and Fletcher, 1998), are easily eroded, and locally erode to form 'benches' or pediments in the footwall of the fault. The degree of alteration and fracturing of these rocks decreases away from the fault surface and they grade into non-altered mylonitic rocks. Near the tip of Yaqui Ridge the damage zone in the footwall locally consists of light brown, tan, or green, well indurated and structureless groundmass with 0.1 to 4 cm blocks of mylonite or individual feldspar phenocrysts (Schultejahn, 1984; this study). This cohesive fault gouge is up to ~100 m thick and only present adjacent to and below the West Salton detachment fault (Figs. 2-4 and 2-7).

Several outcrops around Yaqui Ridge expose 0.2-30 cm thick, black, aphanitic rock that appears to have been injected or emplaced into rock surrounding the fault

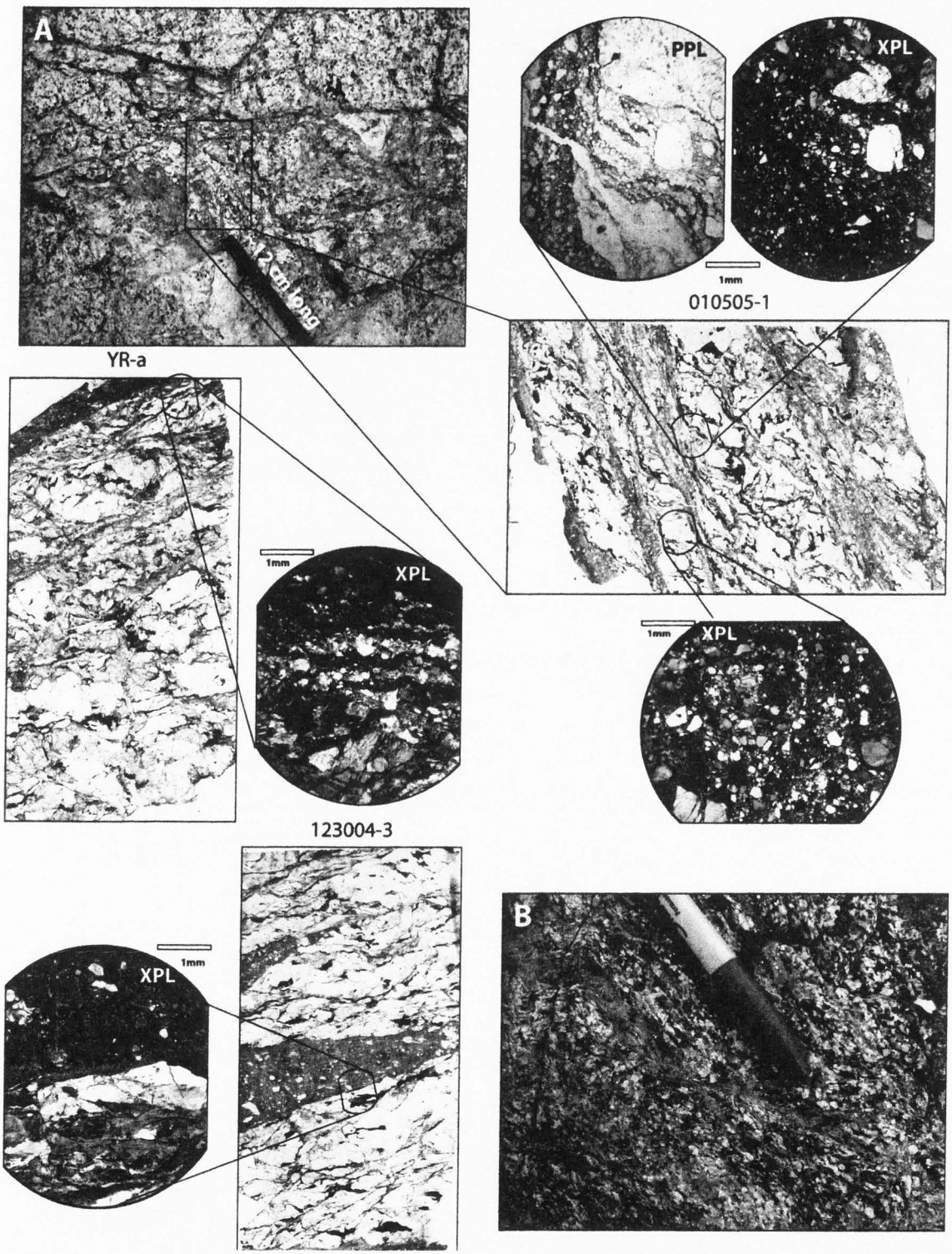
A
~2 cm long
PPL
XPL
1mm
010505-1
YR-a
1mm
XPL
1mm
XPL
123004-3
1mm
XPL
B

Figure 2-7.

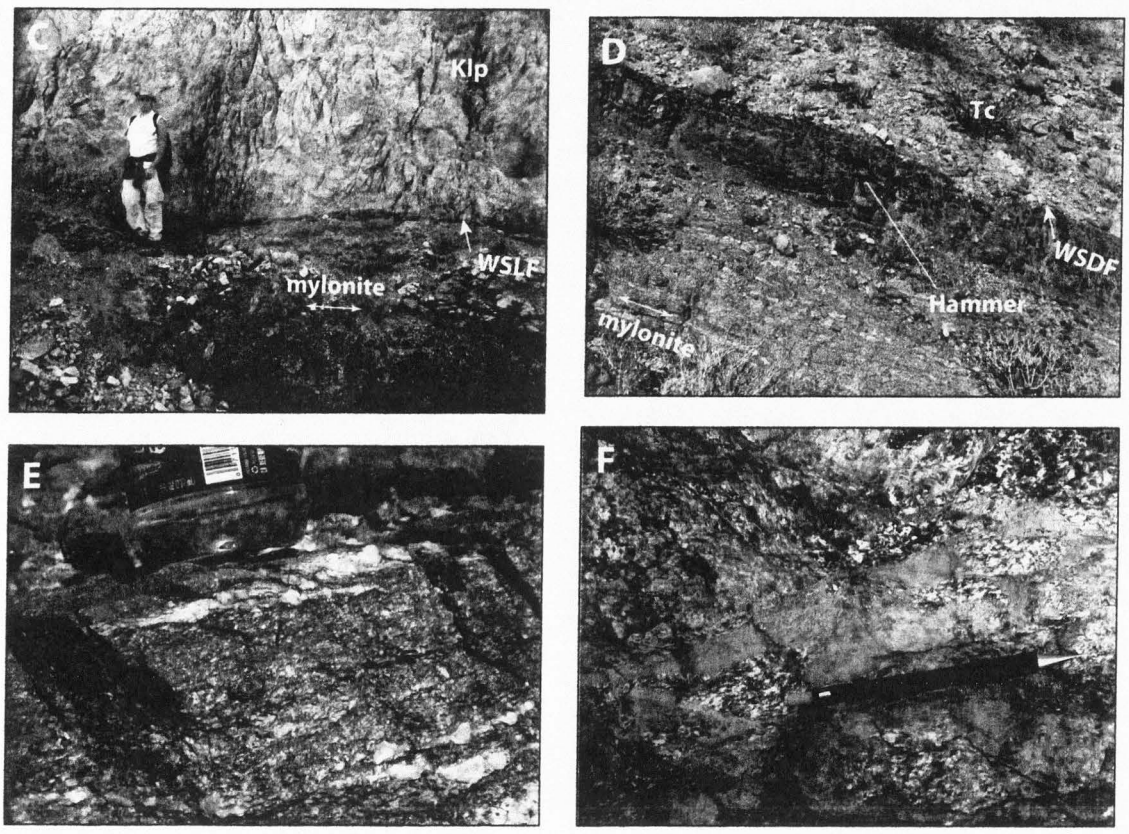

Figure 2-7, continued.

surface. These rocks were identified as pseudotachylite and $^{40}Ar/^{39}Ar$ dating yielded cooling ages as young as 2.4 Ma (Axen et al., 2004). The significance of an older 10.4 Ma ± 0.3 Ma K/Ar date from feldspar concentrates derived from the microbreccia at Yaqui Ridge (Frost and Shaquilafah, 1989) is unclear.

Damage Zone in the Hanging Wall

The damage zone in the hanging wall of the West Salton detachment fault is best developed in plutonic rocks, and less developed where sedimentary rocks are cut by the detachment fault. The damage zone developed in conglomeratic sedimentary rocks consists of fractured and locally brecciated clasts and persists for only a few meters structurally above the detachment fault. Plutonic rocks in the hanging wall of the West Salton detachment fault near Yaqui Narrows are significantly altered and display varying degrees of brecciation. From 0 to ~1000 m above the fault, plutonic rocks are bleached white to light tan, mafic minerals are absent, the rock is punky and weathers easily, and primary plutonic textures are obliterated by closely spaced faults and fractures (Fig. 2-7). These textures are a partial result of potassium metasomatism and hydrothermal alteration (Schultejahn, 1984; Lough, 1993, 1998). Locally these bleached rocks also contain an anastomosing and dendritic network of 0.05-0.5 cm-wide fractures, small faults, and small shear zones with chloritic alteration (Fig. 2-7). Near the tip of Yaqui Ridge intensely deformed and chloritically altered plutonic rocks with structural thicknesses up to 450 m thick are exposed in the hanging wall of the detachment fault directly above the highest detachment fault strand. These rocks appear to contain both brittle and ductile fabrics in hand sample but thin sections reveal dominantly brittle fabrics (Fig. 2-7).

Associated with these zones of hydrothermal alteration is a brittle deformation fabric. Hanging wall rocks are brecciated for 600-1100 m structurally above the highest fault strand of the West Salton detachment fault (Fig. 2-4). The brecciation is characterized by severe grain size reduction, crushing, obliteration of all primary rock

textures, and these rocks are typically easily eroded. The brecciation grades into a zone of intense fracturing over a short distance. The intense fracturing is up to 0.5 km thick and is characterized by slight grain size reduction and high erodability (Fig. 2-4). Above the intense fracturing is a zone of highly fractured rock up to 2 km thick. The highly fractured rocks grade into 'normal' background fracturing.

The upper surface of the intensely fractured rock defines a SE-plunging anticline that coincides with, and is likely a result of the younger Yaqui Ridge anticline. A major ridgeline curves down from the high point of Sunset Mountain and is approximately the SSE boundary between brecciated and fractured rock and intact plutonic rock. This overall pattern is slightly complicated on the south side of Yaqui Ridge by younger zones of brecciation created by SE-striking strands of the San Felipe fault zone.

Thin Sections of the Damage Zone

The West Butte conglomerate and Canebrake Conglomerate contain 14-22% brittle and semi-brittley deformed and chloritically altered plutonic rocks (see below). In order to determine the source of these clasts, we examined fault damage zones in the study area. The large amount of brittle deformation fabrics observed in thin sections of the clasts (see below) suggests that the source was in the damage zone of a major semi-brittle fault zone such as the West Salton detachment fault. No other fault zone in the area is large enough, or the correct age to supply 14-22% of material into conglomeratic basin-fill deposits.

The damage zones exposed in the footwall of any low-angle normal fault will have formed at a deeper structural level relative to the damage zone exposed in the hanging wall. Because current exposures of the footwall of the West Salton detachment fault have been exhumed from greater depth and do not reflect the fabrics exposed during deposition of the early Pliocene West Butte conglomerate, we examined thin sections of three samples from the currently exposed damage zone in the hanging wall

of the West Salton detachment fault to characterize the damage zone that was in the footwall of the West Salton detachment fault when the West Butte conglomerate was being deposited. No thin sections were analyzed from the mylonite in the footwall of the West Salton detachment fault because there are very few clasts of mylonite in basin-fill conglomerates. Therefore studying the deformation mechanisms of the footwall mylonite will not help to constrain the source area for conglomerates that were deposited during early stages of slip on the West Salton detachment fault.

Descriptions

Three standard 30 μm thin sections were made from samples collected in the damage zone in the hanging wall of the West Salton detachment fault south of Yaqui Narrows and one from the damage zone in the footwall at Agua Caliente. Samples were selected to provide examples from macroscopically brittle, brittle/ductile, and ductile fabrics. Despite a wide range of macroscopic fabrics, the thin sections revealed broadly similar deformation mechanisms ranging from brittle to lesser semi-brittle (Table 2-1). The thin section from the damage zone in the footwall near Agua Caliente displayed slightly more brittle deformation than those samples from near Yaqui Ridge. A complete record of the deformation mechanisms in each sample group are in Table 2-1 and many of these features are illustrated in Figure 2-7.

Fractured or brecciated feldspar grains with offset laminae and twins are ubiquitous to common in all samples. Quartz and micaceous minerals are also commonly fractured and quartz grains have undulose extinction that ranges from sweeping to sharp and irregular boundaries. S-C foliations without quartz recrystalization were common throughout the samples, and microfracturing was the dominant deformation mechanism. Penetrative microfracturing, brecciation, and cataclasite are also common in these samples. Margin-parallel foliation, sharp cataclasite boundaries, and brecciated clasts of cataclasite are rare. Pseudotachylite is present in two of the four samples, is up to several

Table 2-1. Summary of deformation fabrics.

	West Salton low-angle fault																									
	Hanging wall damage zone (grouped by hand sample (HS) fabric)																				**Footwall damage z**					
	Yaqui Ridge **Foliated HS** 010505-1						***Yaqui Ridge*** **Non-foliated HS** 012304-1a						***Yaqui Ridge*** YR-a, 123004-3						***Agua Caliente*** 602JPE							
Brittle to ductile deformation fabrics	Ubiquitous (>50%)	Common (15-50%)	Present (5-15%)	Rare (<5%)	Not Present		Ubiquitous (>50%	Common (15-50%	Present (5-15%)	Rare (<5%)	Not Present		Ubiquitous (>50%	Common (15-50%	Present (5-15%)	Rare (<5%)	Not Present		Ubiquitous (>50%	Common (15-50%	Present (5-15%)	Rare (<5%)	Not Present			
Cataclasite			X						X					X					X						
Ultracataclasite					X					X					X								X		
Spalled grain fragments				X						X						X					X				
Angular quartz and feldspar fragments in cataclasite or pseudotachylyte matrix	X							X						X					X						
Rounded quartz and feldspar fragments in cataclasite or pseudotachylyte matrix			X					X						X								X			
Margin-parallel foliation in cataclasite					X				X					X						X					
Brecciated clasts of cataclasite within cataclasite or pseudotachylyte					X					X							X							X	
Sharp catalasite boundaries					X					X				X					X						
Pentrative fracturing	X						X								X				X						
Microfractured quartz grains		X						X						X						X					
Microfractured feldspar grains		X					X						X							X					
Brecciation	X							X						X					X						
No grain shape preferred orientation		X						X						X					X						
S-C foliation without recrystallization	X									X						X				X					
Quartz ribbons with incipient or no recrystallization		X						X							X					X					
Undulose extinction (sharp and irregular boundaries)			X					X					X								X				
Undulose extinction (sweeping)			X					X							X					X					
Pressure solution					X						X						X							X	
Rotated grains					X						X					X						X			
Pseudotachylyte					X					X					X									X	
Spherulites					X						X			X										X	
Injection fabrics					X					X					X									X	
Aligned micaceous minerals		X					X									X						X			
Aligned and kinked micaceous minerals					X					X							X							X	
Incipient dynamic recrystallized quartz (fine-grained)				X				X						X							X				
Recrystallized quartz and subgrains in cataclasite/pseudotachylyte matrix					X			X							X								X		
Annealed fine-grained quartz in fractures				X				X							X									X	
Quartz subgrains				X				X							X								X		
Dynamic recrystallized quartz (fine-grained)					X					X					X									X	
Dynamic recrystallized quartz (medium- to large-grained)					X						X						X							X	
Weak to stong grain shape prefered orientation					X					X						X								X	
Quartz ribbons with recrystallization					X					X						X								X	
S-C foliation with recrystallization					X						X						X							X	
Ductile feldspar grains					X						X						X							X	
Other fabrics																									
Veins				X						X							X							X	
Quartz-filled veins/fractures				X							X						X							X	
Calcite-filled veins/fractures					X						X						X							X	
Chlorite-filled veins/fractures					X					X							X							X	
Hematite-filled veins/fractures					X					X							X							X	
Chloritic alteration of biotite	X							X					X							X					
Sericite growth				X					X						X									X	
Primary magmatic foliation					X			X									X							X	
Multiple cycles of fracturing/deformation	X						X						X							X					
Clay alteration					X						X						X							X	
Altered feldspar grains				X					X				X										X		
Twinned feldspar grains															X										

Table 2-1. Summary of deformation fabrics, continued.

	West Butte conglomerate clasts (grouped by similar textures)											
	>20% or thick cataclasite-pseudotachylyte 121503-2a, 011305-2b, 011305-2b, 011305-1a, 122604-1, 123104-1						<20% cataclasite 121503-2b, 113005-2b, 011305-1b, 123104-2a, 123104-2b, 010305-1					
Brittle to ductile deformation fabrics	Ubiquitous (>50%)	Common (15-50%)	Present (5-15%)	Rare (<5%)	Not Present		Ubiquitous (>50%)	Common (15-50%)	Present (5-15%)	Rare (<5%)	Not Present	
Cataclasite	X							X				
Ultracataclasite		X							X			
Spalled grain fragments			X							X		
Angular quartz and feldspar fragments in cataclasite or pseudotachylyte matrix		X						X				
Rounded quartz and feldspar fragments in cataclasite or pseudotachylyte matrix		X							X			
Margin-parallel foliation in cataclasite		X						X				
Brecciated clasts of cataclasite within cataclasite or pseudotachylyte				X						X		
Sharp catalasite boundaries	X						X					
Pentrative fracturing		X					X					
Microfractured quartz grains		X						X				
Microfractured feldspar grains		X					X					
Brecciation		X						X				
No grain shape preferred orientation		X						X				
S-C foliation without recrystallization				X						X		
Quartz ribbons with incipient or no recrystallization			X						X			
Undulose extinction (sharp and irregular boundaries)	X							X				
Undulose extinction (sweeping)		X						X				
Pressure solution				X						X		
Rotated grains				X						X		
Pseudotachylyte		X								X		
Spherulites		X							X			
Injection fabrics			X							X		
Aligned micaceous minerals			X						X			
Aligned and kinked micaceous minerals					X							X
Incipient dynamic recrystallized quartz (fine-grained)			X						X			
Recrystallized quartz and subgrains in cataclasite/pseudotachylyte matrix			X						X			
Annealed fine-grained quartz in fractures			X					X				
Quartz subgrains			X						X			
Dynamic recrystallized quartz (fine-grained)				X						X		
Dynamic recrystallized quartz (medium- to large-grained)					X					X		
Weak to stong grain shape prefered orientation				X						X		
Quartz ribbons with recrystallization					X					X		
S-C foliation with recrystallization					X							X
Ductile feldspar grains					X							X
Other fabrics												
Veins				X						X		
Quartz-filled veins/fractures			X						X			
Calcite-filled veins/fractures				X								X
Chlorite-filled veins/fractures					X					X		
Hematite-filled veins/fractures			z							X		
Chloritic alteration of biotite	X						X					
Sericite growth					X				X			
Primary magmatic foliation				X								X
Multiple cycles of fracturing/deformation	X						X					
Clay alteration					X							X
Altered feldspar grains			X				X					
Twinned feldspar grains									X			
Degree of alteration			X				X					

cm thick, and contains abundant spherulites and injection fabrics. Ultracataclasite is rare in all samples.

Semi-ductile fabrics were present to common in all thin sections. These fabrics include abundant small quartz grains with incipient dynamic recrystalization, quartz subgrains, annealed quartz in fractures, and aligned micaceous minerals. Kinked micaceous minerals were not observed, and fine- to medium-grained dynamic recrystalized quartz, weak grain shape preferred orientation, and recrystalized quartz ribbons were observed and rare. Ductile fabrics such as S-C foliations with recrystalization, strong grain shape preferred orientation, and ductile feldspar grains were absent. Multiple cycles of deformation were observed in all samples. However, there is no field or microstructural evidence to suggest systematic brittle overprinting of older semi-ductile fabrics.

Veins only occurred in two of the thin sections and contained quartz, chlorite, and hematite. Chloritic alteration of biotite was ubiquitous and relatively minor in all samples, whereas sericite growth and altered feldspar grains were common to present. Most biotite grains were unaltered.

Interpretation

Thin sections from the damage zone in the hanging wall of the West Salton detachment fault preserve brittle deformation and contain lesser but consistent incipient ductile deformation (Table 2-1 and Fig. 2-7). These semi-brittle deformation mechanisms are consistent with deformation between ~150°-200° C and below 300°-350° C (e.g. Scholz, 1988; White, 2001). Overall, these rocks have deformation fabrics consistent with formation near the brittle/ductile transition. The lack of significant vein development and rare clay alteration of feldspar grains suggests that water was not abundant in the fault zone. If the high geothermal gradients that are reported for many areas in the eastern Salton Trough today (Fuis and Kohler, 1984; Lachenbruch et al.,

1985) affected the western Salton Trough when the damage zone was forming, these semi-brittle fabrics could have developed at relatively shallow crustal levels.

Slickenlines and Distribution

The West Salton detachment fault was folded during the Pleistocene by the San Felipe fault zone to form the Yaqui Ridge anticline (Chapter 3). Therefore the present geometry and distribution of slickenlines on the fault surface does not reflect their original orientation during slip on the West Salton detachment fault. Regionally the West Salton detachment fault has a gentle E- to NE-dip throughout its length (Fig. 2-2) so the NE-dipping limb of the fault at Yaqui Ridge likely retains its original geometry. However, the West Salton detachment fault on the SSW-dipping limb differs significantly from regional trends, has been folded during the Pleistocene by strike slip faults (Chapter 3), and must be restored to its original NE dip to compare the geometry of slickenlines on that section of the fault with those preserved on the presently NE-dipping section. We restore individual fault planes, and their associated slickenlines, to match the average NE-dipping fault surface and this correction allows us to compare the distribution of slickenlines on the two sides of the Yaqui Ridge anticline.

Slickenlines from the fault on the NE limb have a contoured maximum at S89°E 15° (n=41) and 93% of the data have an asymmetric spread of 87° about this average (Fig. 2-6C). The contoured average rakes 30° from the ESE and the data range from pure dip-slip to pure strike-slip with a large population of oblique slip slickenlines. Only three of 41 slickenlines do not fall in this range. Although the dispersion of data is great, directions from the fault along the east-plunging hinge of the Yaqui Ridge anticline are just as variable as directions from the NE-dipping part of the West Salton detachment fault.

Slickenlines from the detachment fault on the restored SSW-dipping limb of the Yaqui Ridge anticline are more dispersed than slickenlines from the fault on the NE limb

and contain two contoured maxima and three population clusters of data. Two minor maxima occur at S82°E 12° (rake of 21° from the SE; n=7) and N33°E 32° (rake of 86° from the SE; n=5) (Fig. 2-6B) and are contoured as one maxima because they are near the edge of the stereogram. The main population of slickenlines (58%; n=17) trend NE with rakes of 64° from the SE to 73° from the NW and are dispersed 43° about the nearly pure dip-slip contoured average (Fig. 2-6B). When the slickenlines from the fault on the restored SSW-dipping limb are combined with those from the fault on the NE limb, data are dispersed in the entire fault plane (Fig. 2-6D). However, two maxima are still present when the data are contoured and consist of a stronger maximum at S86°E 16° (rake of 28° from the SE), and a weaker maximum at N35°E 30° (rake of 83° from the SE). These two maxima arise because the West Salton detachment fault on the northeast and south limbs have statistically distinct populations of slickenlines with little overlap, despite the large dispersion of directions on both portions of the fault.

CENOZOIC STRATIGRAPHY

Background

Late Cenozoic stratigraphy in the SW Salton Trough (Fig. 2-8) records complex interactions among geologic structures of different ages, the delta of the Colorado River, fluvial systems draining the Peninsular Ranges, and the Gulf of California. These strata are exposed in two now geographically distinct sub-basins: the San Felipe-Borrego sub-basin in the north where our study is focused (Fig. 2-2), and the more extensively studied and dated Fish Creek-Vallecito sub-basin to the south (e.g. Johnson et al., 1983; Winker and Kidwell, 1996). The Fish Creek and Vallecito mountains now separate these two sub-basins. Recent work by Winker and Kidwell (1996) elevated the Split Mountain, Imperial, and Palm Spring formations to group status, and we use their stratigraphic nomenclature herein.

A brief summary of late Miocene to early Pliocene deposits in the Fish Creek-

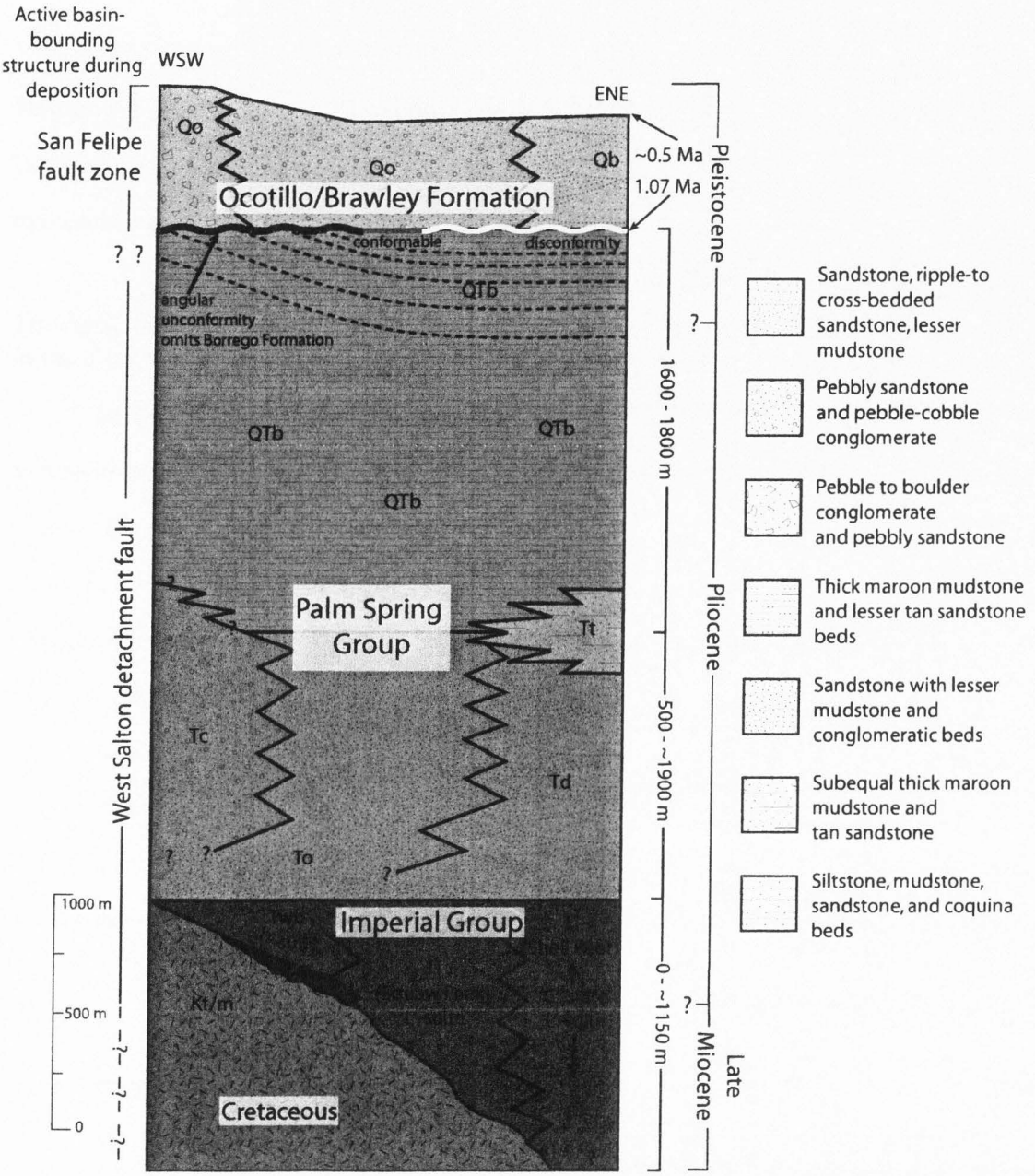

Figure 2-8. Generalized stratigraphic column for the SW Salton Trough showing laterally equivalent units, schematic thickness patterns, and active structures. Thickness of the West Butte conglomerate (Twb) and Hawk Canyon formation (Th) are from this study. Other thicknesses are shown as the average of reported thicknesses (Morley, 1963; Reitz, 1977; Dibblee, 1984; Dorsey, 2005; Lutz, 2005; Kirby, 2005). Tc-Canebrake Conglomerate; To-Olla Formation; Td-Diablo Formation; Tt-Palm Spring-Borrego transitional unit; Ti-Imperial Formation; Twb-West Butte conglomerate; Kt/m-Cretaceous plutonic rocks and local metaplutonic and metasedimentary rocks; QTb-Borrego Formation; Qo-Ocotillo Formation; Qb-Brawley Formation; Th-Hawk Canyon formation.

Vallecito basin builds a framework for understanding the stratigraphy in the western Salton Trough. No late Miocene-Pliocene-age rocks have been dated in the San Felipe-Borrego subbasin. Therefore we use lithologic and stratigraphic correlations between the two subbasins to provide age control.

The Split Mountain and Imperial Groups in the Fish Creek-Vallecito Basin

In the Fish Creek-Vallecito basin the middle Miocene (14-22 Ma) Alverson Volcanics and Miocene Red Rock Formation are the oldest Tertiary strata and overlie Cretaceous plutonic rocks (Dorsey, 2005; Dibblee, 1996, 1984; Kerr, 1984; Kerr and Kidwell, 1991; Ruisaard, 1979; Winker and Kidwell, 1996). The Red Rock Formation consists of up to 200 m of white, pink, and red braided stream and lesser eolian deposits (Kerr, 1984; Winker and Kidwell, 1996). Despite uncertainties surrounding the onset of extension in this area, the conglomeratic Elephant Trees Formation in the upper part of the Split Mountain Group is definitely a syn-rift sequence (Kerr, 1984; Winker and Kidwell, 1996; Winker and Kidwell, 2002). The Elephant Trees Formation contains locally-derived, subaerial interbedded debris flows, coarse boulder conglomerate, megabreccia, and other coarse alluvial deposits. These lithologies are consistent with rapid basin subsidence and the creation of high topography in a normal fault-bound rift-basin setting (Kerr, 1984; Kerr and Kidwell, 1991; Winker and Kidwell, 1996).

The late Miocene to Pliocene Imperial Group overlies the Split Mountain Group in the Fish Creek-Vallecito basin. It consists of a ~1.3 km thick, widespread marine unit that was deposited in 0 to ~200 m water depths (Dibblee, 1984; Winker, 1987; Kerr and Kidwell, 1991; Winker and Kidwell, 1996). At Split Mountain Gorge, the transition from the terrestrial Split Mountain Group to the Imperial Group is abrupt and contains a complex stratigraphy of megabreccia, gypsum, and marine turbidites (Dean, 1988; Jefferson and Peterson, 1998; Kerr and Kidwell, 1991; Winker and Kidwell, 1996). The

base of the Imperial Group is ~6.2 Ma in Split Mountain Gorge (Dorsey et al., 2005b). The Imperial Group displays a change in provenance from locally-derived sand at the base to Colorado River-derived upsection (Winker and Kidwell, 1996; Dorsey et al., 2005b). The first arrival of Colorado River-derived sand occurs at 5.36 ± 0.06 Ma (Dorsey et al., 2005b).

Several conglomeratic members in the Imperial Group of the Fish Creek-Vallecito basin (Stonewash, Jackson Fork, and Andrade) are locally-derived sandy conglomerate to pebble and boulder conglomerate that are localized at the basin margins, locally rest on basement paleotopography or lap across older high-angle normal faults, and contain marine fossils (Kerr, 1984; Kerr and Kidwell, 1991; Winker and Kidwell, 1996). These conglomeratic units are interpreted as deposits of narrow, rocky shorelines that were mostly submarine, with portions that may have been sub-aerial as well. These conglomerates were previously assigned to the Canebrake Conglomerate (Dibblee, 1984, 1996), but we follow the new nomenclature of Winker and Kidwell (1996) and separate Imperial-aged conglomeratic units where possible. The abrupt marine incursion, sedimentology, and high subsidence rates suggest that the Imperial Group records a major basin reorganization that is likely related to a change from slower extension on high-angle normal faults to faster extension on a regional low-angle detachment fault system (Dorsey and Janecke, 2002; Winker and Kidwell, 2002). However, direct evidence tying the Imperial-age basin-fill to activity on the detachment fault has been lacking in the Fish Creek-Vallecito basin.

The Palm Spring Group in the Fish Creek-Vallecito and San Felipe-Borrego Basins

The overlying Pliocene Palm Spring Group is lithologically similar in both sub-basins, at least 2-2.5 km thick, and consists of the laterally equivalent Diablo and Olla formations, Canebrake Conglomerate, and overlying Borrego and Hueso formations (Fig.

2-8). We summarize previous descriptions of these units and their lateral relationships from Dibblee (1954, 1984), Morley (1963), Winker (1987), Winker and Kidwell (1996), Cassiliano (1998), Kairouz (2005), and Dorsey (2005). The Diablo Formation is dominated by 'C-suite' sand that was sourced from the Colorado River (50-80% rounded quartz grains, many with hematite-coating, and recycled Cretaceous foraminfera) and records SE progradation of the sub-aerial river delta into the SW Salton Trough (Dibblee, 1984; Winker, 1987; Winker and Kidwell, 1996). The Canebrake Conglomerate consists of terrestrial pebble to boulder conglomerate and conglomeratic sandstone derived from the Peninsular Ranges (Dibblee, 1954, 1984, 1996) and is a syn-tectonic deposit derived from the footwall of the West Salton detachment fault (Axen and Fletcher, 1998; Kairouz, 2005). In contrast to the narrow belts of conglomerate preserved near the basin margins in the underlying Imperial Group of the Fish Creek-Vallecito basin (<2 km-wide; Winker and Kidwell, 1996), the Canebrake Conglomerate is much more widespread and its outcrop belt closely follows the West Salton detachment fault (Dibblee, 1984, 1996; Axen and Fletcher, 1998). The Olla Formation is the finer-grained, locally-derived equivalent of the Canebrake Conglomerate and interfingers with the Diablo Formation (Winker, 1987; Winker and Kidwell, 1996). The Olla Formation was defined as at least 20% 'L-suite' sand (>80% locally-derived grains) by Winker (1987). We revise this definition and use the criteria >50% locally-derived sand for the Olla Formation, and >50% Colorado River-derived sand for the Diablo Formation.

The Pliocene-Pleistocene lacustrine Borrego Formation overlies the Diablo Formation (Fig. 2-8) along a complexly interbedded and gradational contact in the San Felipe-Borrego sub-basin (Dibblee, 1954, 1984; Kirby, 2005; Lutz, 2005). The Borrego Formation is ~1.6-1.8 km thick in the San Felipe Hills and Borrego Badlands and consists of claystone, mudstone, and lesser sandstone (Dibblee, 1984; Kirby, 2005; Lutz, 2005). Deposits in the Borrego Formation accumulated in a freshwater to brackish lacustrine environment that experienced rare lake-level lowstands (Kirby, 2005). The

origin of the Borrego lake depocenter is poorly understood. It may have formed as a result of a now-covered structural barrier to the SE that blocked the marine waters of the Gulf of California during early deposition of the Borrego Formation (Dorsey et al., 2005a). Coarse-grained facies are rare in exposures of the Borrego Formation and locally comprise up to 50% of the beds in the uppermost ~95 m in the southern Borrego Badlands (R. Dorsey, pers. Comm., 2006).

Throughout the SW Salton Trough many exposures of conglomerate have been mapped as Canebrake Conglomerate that do not exhibit lateral relationships with the Diablo or Olla formations (e.g. Dibblee, 1954; Morley, 1963; Winker and Kidwell, 1996). Without these lateral relationships, isolated exposures of conglomerate require detailed mapping and stratigraphic analysis because they could be either younger or older than the Pliocene Canebrake Conglomerate and could potentially correlate with the Imperial Group, Borrego Formation, or the Ocotillo Formation.

The Ocotillo Formation in the San Felipe-Borrego Basin

The ~1.1 – 0.6 Ma Ocotillo Formation (Fig. 2-8) is a widespread unit of coarse-grained alluvial conglomerate, sandstone, and interbedded finer-grained lithologies up to ~600 m thick (Dibblee, 1954, 1984; Bartholomew, 1968; Lutz, 2005; Lutz et al., in press; Kirby, 2005; Kirby et al., in press; Chapter 2). It conformably overlies the Borrego Formation in the Borrego Badlands and the Ocotillo Badlands, and its base is an angular unconformity in the western San Felipe Hills (Dibblee, 1954; Kirby, 2005) and near Harper Canyon (Chapter 2). The Brawley Formation is the finer-grained, fluvial-deltaic lateral equivalent of the Ocotillo Formation (Kirby et al., in press). Several lines of evidence suggest that the conglomeratic Ocotillo Formation is the sedimentary response to the initiation of the San Felipe and San Jacinto fault zones (Kirby et al., in press; Lutz et al., in press; Chapter 2).

Previous work in the San Felipe-Borrego basin

In the San Felipe-Borrego sub-basin Dibblee (1954) was the first worker to map near Borrego Mountain and Yaqui Ridge and provided initial stratigraphic assignment of units entirely to the Palm Spring Group. The depositional base of the section is well exposed at Borrego Mountain, so it is unusual and noteworthy that there appeared to be no marine strata of the Imperial Group despite their presence 4 km to the east at Squaw Peak, and also no deposits of the older Split Mountain Group. Dibblee (1954) assigned three noncontiguous and distinctly different conglomeratic units in this area to the Canebrake Conglomerate. Morley (1963) followed Dibblee (1954) by naming the thick conglomeratic unit near Borrego Mountain Canebrake Conglomerate. He recognized a thin, discontinuous finer-grained unit beneath the main conglomerate, and Herzig et al. (1995) correlated this lower unit to either the lower part of the Palm Spring Group or the Camel's Head Formation of the Imperial Group. A late Miocene-age faunal record in this unit (Jefferson, 1999) suggested that this lower unit may correlate with the Imperial Group or older stratigraphy.

Farther to the west near the West Salton detachment fault, Schultejahn (1984) mapped both the footwall and hanging wall of the fault but her work incorrectly mapped and identified the sedimentary rocks, did not provide lithologic descriptions of sedimentary rocks, and does not have a topographic base. In light of the recent recognition of the detachment fault as a basin-controlling structure during the late Miocene through Pliocene (Axen and Fletcher, 1998), the inconsistent stratigraphic nomenclature near Borrego Mountain, and the large scale of most previous mapping, we remapped the area, revise the initial stratigraphic nomenclature, investigated the lateral relationships of the units, and document several new relationships.

Imperial Group

In the San Felipe-Borrego sub-basin, the oldest Tertiary unit exposed in the central part of the basin is the Imperial Group. It is exposed from Shell Reef west to Borrego Mountain in the core of the San Felipe anticline (Figs. 2-2 and 2-8) (Dibblee, 1984; Morley, 1963). In contrast to the Fish Creek-Vallecito basin to the south, the Imperial Group in the San Felipe-Borrego basin is dismembered by Quaternary strike-slip fault zones, outcrops are discontinuous, and there are no intact and complete sections of the Imperial Group. Three major areas expose rocks beneath the Palm Spring Group and are separated by up to ~4 km of cover and buried strands of the San Jacinto fault zone. The lithologies of these outcrops are so different that they must be discussed separately. Although our study focuses on rocks exposed around Borrego Mountain, we also examine rocks of the Imperial Group at Squaw Peak, and compile previous descriptions for the Imperial Group at Shell Reef, in order to evaluate the possibility of lateral correlations between these isolated areas.

Shell Reef Area

The Imperial Group is exposed near Shell Reef in the core of the San Felipe anticline, east of the San Felipe Hills fault, and attains a minimum thickness of ~500 m although the basal contact is not exposed here (Reitz, 1977). Up to ~1100 m of stratigraphic thickness of the Imperial Group is inferred from three deep wells in the San Felipe Hills (Dibblee, 1984). The Imperial Group near Shell Reef consists of light tan claystone and lesser amounts of tan to gray, fine- to coarse-grained sandstone, gypsiferous silty claystone, thin molluscan biostromes, and arenaceous coquina beds (Reitz, 1977; Dibblee, 1984; Kirby, 2005). The lowest exposed Imperial Group consists of well-indurated, moderately to poorly sorted, medium- to coarse-grained, subangular to rounded, massive arkosic sandstone with local mollusk fragments and discontinuous layers of siltstone and claystone (Reitz, 1977). Both 'L-suite' and 'C-suite' grains are

observed in sandstone beds, and 'C-suite' lithologies are dominant in the upper part of the section. The middle section of the Imperial Group consists of structureless to large-scale cross-bedded (up to 2 m-tall) oyster coquina beds and interbedded massive claystone that grade upward into discontinuous medium to thick, parallel bedded sandstone beds (Reitz, 1977). The upper Imperial Group consists of mostly sandstone, up to 10 m thick, thinly laminated, locally gypsiferous bentonitic claystone, and interbedded siltstone (Reitz, 1977; Kirby, 2005). There are several lithofacies in this area that are identical to those of the Mud Hills, Yuha, and Camels Head members of the Deguynos Formation of the Imperial Group exposed in the Fish Creek-Vallecito basin (Janecke and Dorsey, written comm., 2003).

The Imperial Group at Shell Reef is interpreted as a marine succession that represents coastal lagoon, littoral, barrier beach and sand bar, tidal flat marsh, and shallow neritic depositional environments (Reitz, 1977; Dibblee, 1984). The gray calcareous oyster coquina beds and other paleontologic evidence support this interpretation (Reitz, 1977; Quinn and Cronin, 1984; Powell, 1986). Corals (Durham and Allison, 1960), foraminifera (Tarbet and Holman, 1944), and gastropods (Smith, 1962) all indicate warm tropical conditions during deposition.

Squaw Peak Area

The Imperial Group is also exposed near Squaw Peak ~4 km west of Shell Reef. It grades upward into the Palm Spring Group, and is at least several hundred meters thick, but thickness estimates are hampered by many cross-cutting oblique strike-slip faults that separate the depositional base from the top of the unit. Morley (1963) reported a maximum thickness of ~890 m, but based on our mapping this appears to be an overestimate. The basal contact is a low-angle to buttress nonconformity between 'L-suite' fossiliferous to pebbly sandstone, and the underlying basement rocks that has up to 4 m of local paleorelief. The basement rocks were formerly named the Squaw Peak

schist (Morley, 1963; Dibblee, 1984) although the majority of these rocks are not schist, but rather a complexly deformed group of mylonitic granodiorite, foliated tonalite, other metaplutonic rocks, and lesser calc-silicate and quartzose metasedimentary rocks (Plate 1). Fault offsets and poor exposure around Squaw Peak preclude a detailed study of the vertical and lateral lithologic changes in the Imperial Group here.

The basal Imperial Group consists of gray 'L-suite', medium- to coarse-grained fossiliferous sandstone, pebbly sandstone and sandy pebble conglomerate. It also contains rare, thin, gray to blue sandy limestone beds with some vertical and horizontal cemented burrows up to 2-3 m long and other fossils (Quinn and Cronin, 1984; Powell, 1986). Fossiliferous sandstone beds are calcite-cemented, and commonly contain oyster casts, pelecypod shell fragments, and rare silicified wood fragments (Morley, 1963; Quinn and Cronin, 1984; Powell, 1986).

Conglomerate is rare in the Imperial Group, but is important for our correlation with the West Butte conglomerate. Several 1-3 m thick pebbly sandstone beds in the middle to upper part of the section consist of calcite-cemented medium- to coarse-grained sandstone with granules to pebbles. These coarse grained beds are interbedded with tan, brown, and green siltstone to claystone and 0.5-3 m thick oyster coquina beds. Clast lithologies in the conglomeratic beds consist dominantly of tonalite and other plutonic rocks, and locally contain up to ~25% chloritically altered plutonic rocks with brittle deformation fabrics. Although these clasts are small, they are nearly identical to the 22% of deformed and chloritically-altered clasts observed in the West Butte conglomerate near Borrego Mountain.

The Imperial Group exposed directly south of Squaw Peak consists of interbedded and variegated sandstone, siltstone and claystone, and oyster coquina beds. Sandstone beds are thin to thick bedded, fine- to coarse-grained, moderately sorted, subrounded, and have 'L-suite' compositions (Morley, 1963). Outcrops of 'C-suite' sandstone beds are rare and increase in abundance to the south and east of the outcrop belt. Claystone beds

are typically gray to yellow and green, locally gypsiferous, contain variable amounts of silt and sand, and grade laterally and vertically into siltstone and fine-grained sandstone beds (Morley, 1963). Up to 3 m thick, tan to dark gray oyster shell coquina beds are interbedded with sandstone and siltstone and grade upward into pelecypod-bearing fossiliferous sandstone beds. Locally, siltstone and fine-grained sandstone beds grade upward into coarse sandstone beneath the coquina beds and in one location a pebbly sandstone bed grades into planar bedded coarse sandstone beneath a sharp contact with the overlying coquina bed. Coquina beds locally have up to 2 m-high tabular cross stratification.

Borrego Mountain Area

Uplift at Borrego Mountain along the Coyote Creek strand of the San Jacinto fault zone exposes some of the oldest basin-fill in the San Felipe-Borrego sub-basin in non-conformable contact with basement tonalite (Fig. 2-3). In this area, two formations have been mapped beneath the Pliocene Palm Spring Group (Dibblee, 1954; Morley, 1963; Herzig et al., 1995). Based on their type locality in Hawk Canyon, the oldest formation was informally named the Hawk Canyon formation (Herzig et al., 1995) and we retain this informal nomenclature. The overlying conglomeratic unit was previously correlated with the Canebrake Conglomerate (Dibblee, 1954; Morley, 1963; Herzig et al., 1995), but we question this correlation and use the informal name West Butte conglomerate based on our proposed type section along the southwest flank of West Butte (Fig. 2-3).

Hawk Canyon formation. The Hawk Canyon formation is 0-88 m thick and consists of a lower, middle, and upper member that are exposed in five major outcrops around Borrego Mountain, including excellent exposures in Hawk Canyon and at the east end of East Butte (Fig. 2-3). The formation is depositional on Cretaceous La Posta-type tonalite with up to 4 m of local relief, and the entire formation buttresses against basement rocks along strike (Fig. 2-9A). The top of the Hawk Canyon formation is

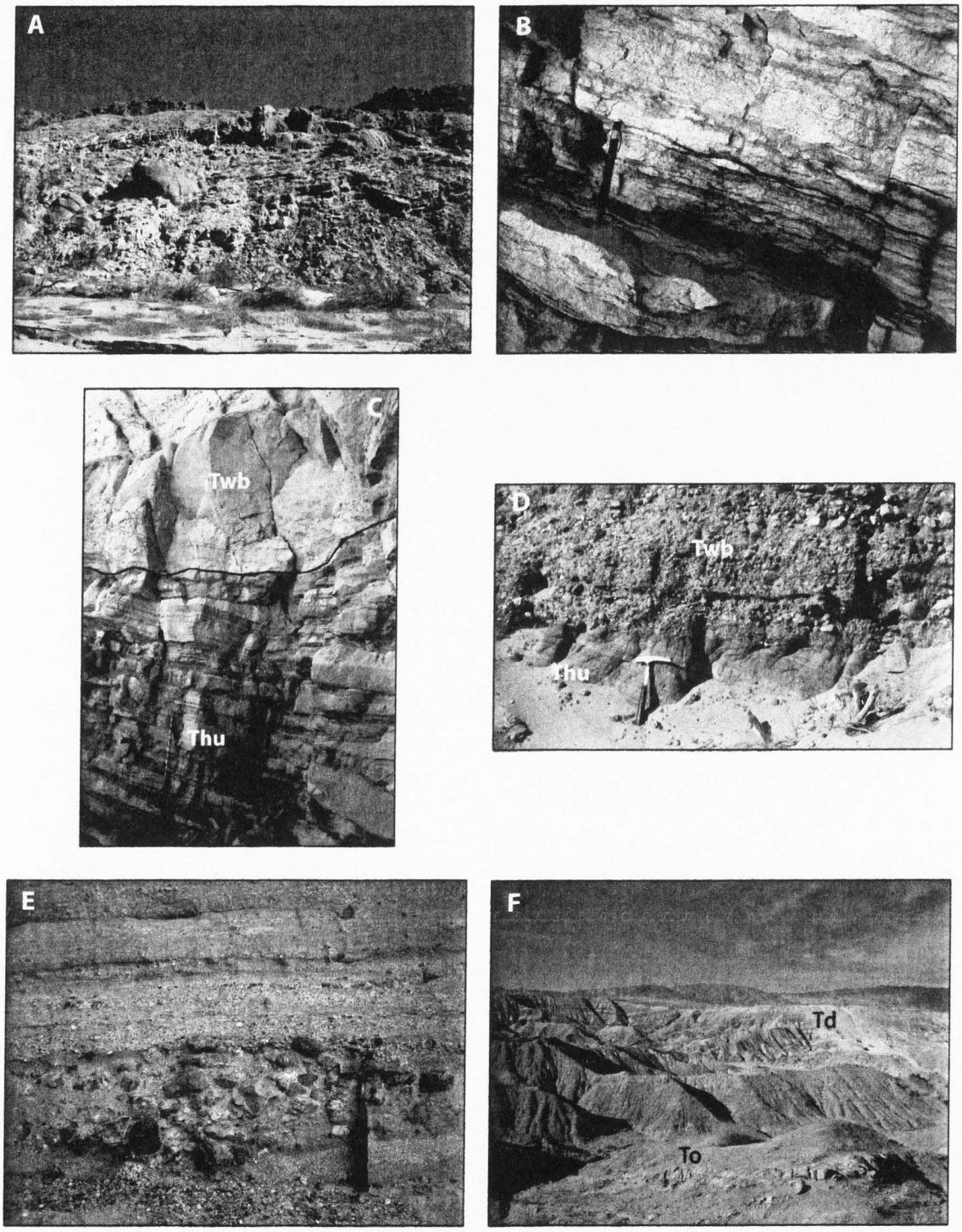

Figure 2-9.

placed beneath the first thick conglomerate bed of the West Butte conglomerate.

Description of the lower member. The lowest member of the Hawk Canyon formation is 0 to 7 m thick, coarse to sub-rounded, moderately sorted, gray to gray-green, arkosic sandstone and grus that lies nonconformably in slight depressions on basement tonalite (Plates 1 and 2). Locally, the unit has up to 2 m high buttress unconformities. Bedding is typically structureless and locally, medium to thick planar beds are poorly defined by slight grain-size segregation. Clast and grain lithologies are dominated by angular to subangular quartz and feldspar with lesser biotite. In Hawk Canyon, outsized boulders and cobbles of distinctive red and white banded pegmatites are embedded in the overlying sandstone less than 4 meters from their bedrock source and several pegmatite ridges protrude into the sandstone (Fig. 2-9A). The top of this unit is placed at a sharp contact between the relatively structureless sandstone of the lower member and well bedded to ripple cross bedded sandstone of the middle member. The lower member is exposed in most outcrops of the Hawk Canyon formation.

Description of the middle member. The middle member of the Hawk Canyon formation is 0 to 55 m thick, and fines upward from white to gray-green arkosic medium-grained sandstone into green and mottled green-red mudstone. It conformably overlies the lower member where present, and in the absence of the lower member it is depositional on basement tonalite and locally buttresses against basement rocks (Fig. 2-9A). Pebbles and cobbles of basement pegmatite are present as out-sized clasts where this unit is depositional on basement rocks. The base of the middle member is placed above the structureless sandstone of the lower member, and the top is placed above the highest green mudstone.

There are major differences in lithology and thickness between two measured sections located ~500 m apart in Hawk Canyon (Plate 4). In the northwestern section the middle member is ~13 m thick and includes ~9 m of planar bedded, moderately sorted, gray to gray-green, angular to sub-rounded arkosic sandstone overlain by ~3.5 m

of green mudstone to claystone. Thin 3-4 cm thick conglomeratic sandstone beds with tonalite pebbles are interbedded near the base of this member. Finer grained sandstone and siltstone beds commonly contain significant back-filled vertical burrow tracks. The upper part of the sandy interval locally contains 25-30 cm thick planar to low-angle cross stratified beds. Possible hummocky cross stratification is locally observed but rare. Locally, symmetrical ripples in fine to medium-grained sandstone beds are overlain by thin beds or laminae of siltstone and mudstone and display flaser bedding structures (Fig. 2-9B). These ripples have wavelengths of 5-7 cm, and rare climbing ripples show transport to the SSE when restored for local bedding tilt. Sandstone beds above these flaser-bedded intervals commonly show abundant bioturbation.

Green silty claystone to mud shale overlies the lower sandy interval along a sharp contact and contains 2-5 cm thick interbeds of fine-grained gray-green arkosic sandstone every 10-40 cm. Mudstone and claystone beds are commonly fissile and locally contain gypsum partings. Several mudstone samples were collected in Hawk Canyon and show smooth-shelled freshwater ostracodes and no marine diatoms (Kristen McDougall, written comm., 2006; William Orr, written comm., 2005). The abundance and thickness of sandstone beds increase up section to the top of this unit to become subequal to the mudstone. Most sandstone interbeds show significant burrow mottling and bioturbation.

In the other measured section, located ~500 m to the southeast the middle member is 55 m thick and the basal and middle portions of the section are lithologically similar to the northwestern section. The upper portion of the middle member contains two ~80 cm thick red pebbly sandstone beds that are lithologically identical to the upper member. These pebbly beds mark the base of a 10 m thick complexly interbedded interval consisting of 20-100 cm thick planar bedded yellow and greenish gray, medium to fine-grained arkosic sandstone, with 40-80 cm thick interbeds of yellow to mottled green and red mudstone and claystone every 80-100 cm. The sandstone beds typically have sharp bases and tops and display significant burrow mottling.

Description of the upper member. The upper member of the Hawk Canyon formation is 0 to 30 m thick and coarsens upward from interbedded red mudstone and subordinate red arkosic sandstone to dominantly sandstone and subordinate mudstone. It conformably overlies the middle member of the Hawk Canyon formation or is depositional on basement tonalite and locally buttresses against these rocks. The base of the upper member is placed above the highest green mudstone of the middle member. The top of the upper member is placed below the first thick conglomerate bed of the overlying West Butte conglomerate (Fig. 2-9C).

The contact between the Hawk Canyon formation and the overlying West Butte conglomerate varies across the Borrego Mountain area. In Hawk Canyon it is sharp and undulating with scour-and-fill geometries and a slight angular unconformity. Beds of the Hawk Canyon Formation dip more steeply southward than beds in the West Butte conglomerate across this unconformity. The contact is also an angular unconformity along the east and northeast sides of East Butte (Fig. 2-9C). However, in those locations beds of the Hawk Canyon formation dip more steeply to the north than beds of the West Butte conglomerate. At the east end of Middle Butte the upper and middle members of the Hawk Canyon formation are missing and the overlying West Butte conglomerate is concordant.

The basal 1-2 m of the upper member consists of dark red to mottled red and green, fissile, silty claystone or mud shale. This basal fine-grained interval is overlain by ~10-28 m of interbedded sandstone and mudstone that continues to the top of the unit. Sandstone beds increase in thickness upsection from 5-20 cm thick near the base to 200 cm thick near the top and are broadly lenticular for hundreds of meters, coarsen up, and locally contain 5 cm thick granule or small pebble lags at their bases. Sandstone beds are mostly planar to slightly lenticular or massive near the base and gradually become better defined and locally display trough cross bedding and low-angle cross stratification near the top. Pebble and granule composition is difficult to determine due to the small

size of clasts, but a 20 cm thick bed of rounded to sub-rounded pebble to small cobble conglomerate near the middle of this member shows tonalite, deformed and chloritically altered plutonic rocks, and assorted metamorphic clasts similar to the clast composition of the overlying West Butte conglomerate. Mudstone beds decrease thickness upsection from 20-200 cm thick near the base to 1-15 cm thick near the top.

Provenance.

Lower member: This member was derived from deep weathering of local basement with little to no transport and had significant paleotopography on basement rocks. We interpret this deposit as locally derived.

Middle member: This member contains mostly arkosic sediments with compositions that are lithologically similar to both the nearby basement rocks and the underlying lower member. Strata onlap significant paleotopography on the basement rocks, and locally contains outsized boulders of pegmatite that were derived from several meters away. We interpret this deposit as locally derived. Two conglomerate beds that have lithologies identical to conglomerate in the overlying upper member probably have a similar source (see below).

Upper member: This member has an arkosic composition and also contains several pebble to cobble conglomerate beds with chloritically and hematitically altered clasts that cannot be sourced from the local basement plutonic rocks. Because most of this unit is arkosic and buttresses against local basement rocks, the majority of the upper member is locally derived. The presence of "exotic" altered clasts in conglomerate beds strongly suggests that these conglomerate beds were derived from sources other than Borrego Mountain. The provenance of these conglomerates may be similar to the provenance of the West Butte conglomerate since the altered clasts are similar to those observed in the West Butte conglomerate.

Depositional environments.

Lower member: The poor sorting, angularity of clasts and grains, buttress to low-

angle nonconformity with basement tonalite, lack of bedding structures, composition that matches the underlying tonalite, and location in small paleodepressions suggest that the lower member of the Hawk Canyon formation was created by deep weathering of basement rocks with little or no transport. Rare imbricated clasts near the base suggest minor episodes of transport. The lower member is interpreted to be a terrestrial grus deposit that formed in-situ on crystalline basement during a time of limited sediment transport. Similar deposits are forming today on crystalline rocks in the Peninsular Ranges to the west. The sharp transition from these massive grus deposits to the bedded, better sorted and rounded, arkosic sandstone of the middle member indicates an abrupt change in the depositional environment and may be due to a disconformity between the lower and middle members of the Hawk Canyon formation.

Middle member: Symmetrical ripples in the middle member of the Hawk Canyon formation record oscillatory currents, and flaser bedding with mud drapes indicate frequent fluctuations in current energy. Abundant bioturbation in the middle member implies a shallow water depositional environment. Many of the back-filled burrows in Hawk Canyon appear similar to those in the marine Latrania Formation of the Imperial Group to the SE (Jefferson, 1999). Green gypsiferous mudstone beds in this member are lithologically similar to marine mudstone beds in the Imperial Group south of Squaw Peak. However, the lack of marine microfossils in the mudstone coupled with the presence of delicate freshwater ostracodes precludes an entirely marine interpretation of this member. Overall these data suggest that the middle member may have been deposited in a marginal marine tidal-flat to lacustrine/fluvial setting with oscillations between the two environments.

Upper member: Planar to trough cross-bedded sandstone with pebbly lag deposits and erosional bases suggest terrestrial deposition in shallow fluvial channels and bars. The composition clasts in the upper member matches the composition of clasts in the overlying West Butte conglomerate and cannot be derived from the nearby basement

tonalite despite lying depositionally on, and buttressing out along strike with these crystalline rocks. Overall, these data suggest that the upper member was deposited in a distal fluvial braided stream or distal alluvial fan environment that flowed around and accumulated sediment on basement paleohighs. The rapid upward coarsening and lack of an unconformity above the middle member suggests progradation of a distal fluvial or alluvial environment over the marginal marine or lacustrine rocks of the middle member.

Correlation and age. Recent paleontologic work in Hawk Canyon has revealed a terrestrial vertebrate taxa from the lower member that includes Canidae, Felidae, Gomphotheriidae or Mammutidae, Lamini, and Mammalia (Jefferson, 1999). While this assemblage is not age definitive, a pre-6 to 9 Ma age is preferred (Jefferson, 1999). We suggest that because the fossils were found only in the lower member and the dramatic change in depositional environments between the lower and middle members may be a disconformity, the pre-6 to 9 Ma age likely dates only the lower member of the Hawk Canyon formation. The marginal marine to lacustrine depositional environment of the middle member, gypsiferous green mudstone beds similar to those south of Squaw Peak in the Imperial Group, and locally-derived lithologies suggest that the middle member is the lateral, near-shore equivalent of the lower 'L-suite' Pliocene Imperial Group exposed 2-3 km to the east (Fig. 2-8). Because there is no unconformity between the middle and upper members of the Hawk Canyon formation and the upper member lies ~290 m beneath the Palm Spring Group (and thus cannot be equivalent to the Palm Spring Group), we suggest that the upper member is also equivalent to the upper Imperial Group farther east. Thus the upper member of the Hawk Canyon represents the arrival of the first Imperial-age fluvial or alluvial deposits in this area.

West Butte conglomerate.

Description. The West Butte conglomerate is exposed around Borrego Mountain where it varies from 0 to ~280 m thick (Figs. 2-3 and 2-8). The thickest sections occur southwest of West Butte where the type section of this unit was measured. The

West Butte conglomerate overlies the Hawk Canyon formation along a progressive unconformity. In Hawk Canyon, the West Butte conglomerate has a subtle angular unconformity to concordant contact with the upper member of the Hawk Canyon formation (Fig. 2-9C). Along the east and northeast side of East Butte, the conglomerate has an angular unconformity on the upper to middle members of the Hawk Canyon formation (Figs. 2-3 and 2-9D). Near Middle Butte, the West Butte conglomerate overlies the middle member of the Hawk Canyon formation along a disconformity. Where the Hawk Canyon formation is not present the West Butte conglomerate lies depositionally on basement tonalite (Fig. 2-3). This contact is uneven and subparallel to bedding, although locally the conglomerate buttresses against knobs of tonalite that protrude up to 5 m upsection into the unit. The West Butte conglomerate fines upward into the overlying Olla Formation of the Palm Spring Group (Figs. 2-3 and 2-8). The top of the West Butte conglomerate is placed above the last persistent >10 cm thick conglomerate bed or where sandy conglomerate becomes subordinate to coarse sandstone.

The West Butte conglomerate consists of buff, tan, and tan-red, moderately cemented, poorly to moderately sorted, rounded, interbedded pebbly sandstone, sandy conglomerate, and pebble to boulder conglomerate (Fig. 2-9D and E). Overall, the average grain size is between coarse sand and pebbles and is relatively consistent. The upper ~1/4 of the unit slightly fines upward and shows more variation in grain size as the abundance of thick conglomerate beds decreases. Sedimentary structures are dominated by planar bedding and stratification with low-angle cross stratification. Individual beds are poorly to well defined by changes in grain size and vary in thickness from ~1 cm to >2 m. Channel scours are rare in the lower 2/3 of the unit, and become more common near the top (Fig. 2-9). Trough cross bedding in sets <20 cm thick are rare.

Sandstone in the West Butte conglomerate is composed of subangular to rounded, poorly to moderately sorted, medium to granule-sized quartz, feldspar, lithic fragments,

and lesser biotite. Sandstone beds vary from ~1 to 50 cm thick and are typically less than 15 cm. The matrix of sandy conglomerate and conglomeratic sandstone beds is dominated by this lithology and these beds are also ~1 to 50 cm thick. In outcrops that are stained red or have significant hematitic alteration of larger clasts, individual biotite grains in the matrix appear fresh and unaltered.

Conglomerate beds are clast to matrix-supported, typically ~3 to 100 cm and up to 2 m thick, and vary from pebble- and granule-size through rare boulders up to 2 m in diameter. Clasts are mostly subrounded to rounded and vary from subangular to well rounded. Sedimentary structures are lacking in conglomerate beds, and locally fining upward trends are observed. Conglomerate beds typically have sharp, undulatory bottom contacts above coarse to pebbly sandstone beds. Locally, ~10 to 50 cm-deep channels are present at the base of these coarser beds. Thickness between conglomerate beds varies from ~1 to <100 cm throughout most of the unit except in the upper ~1/3 of the unit where the spacing can be upwards of 2 m between conglomerate beds.

Clast lithologies: Clast lithologies in the West Butte conglomerate consist of plutonic, metamorphic, chloritically altered and deformed plutonic rocks, and hematitically altered rocks, and do not match the lithology of the underlying crystalline bedrock. At 15 locations throughout the unit 50 clasts were identified and tabulated (Fig. 2-10). Non-chloritically altered plutonic rocks constitute 58% of the observed lithologies in the unit. Plutonic clasts are divided into La Posta-type tonalite (10%), Granite Mountain-type diorite (18%), fine- to medium-grained La Posta- or Granite Mountain-type undifferentiated (21%), and pegmatite (9%). Metamorphic rocks constitute 19% of the clast lithologies in the unit. In this category, 26% of the metamorphics are migmatite, gneiss, and lesser other metaplutonic rocks, 45% are biotite or lesser psamittic schist, and 24% are quartzose or calc-silicate metasedimentary rocks. Mylonite or proto-mylonite constitutes less than 1% of the total clast lithologies. Locations where the West Butte conglomerate is depositional on basement tonalite have identical clast lithologies to other

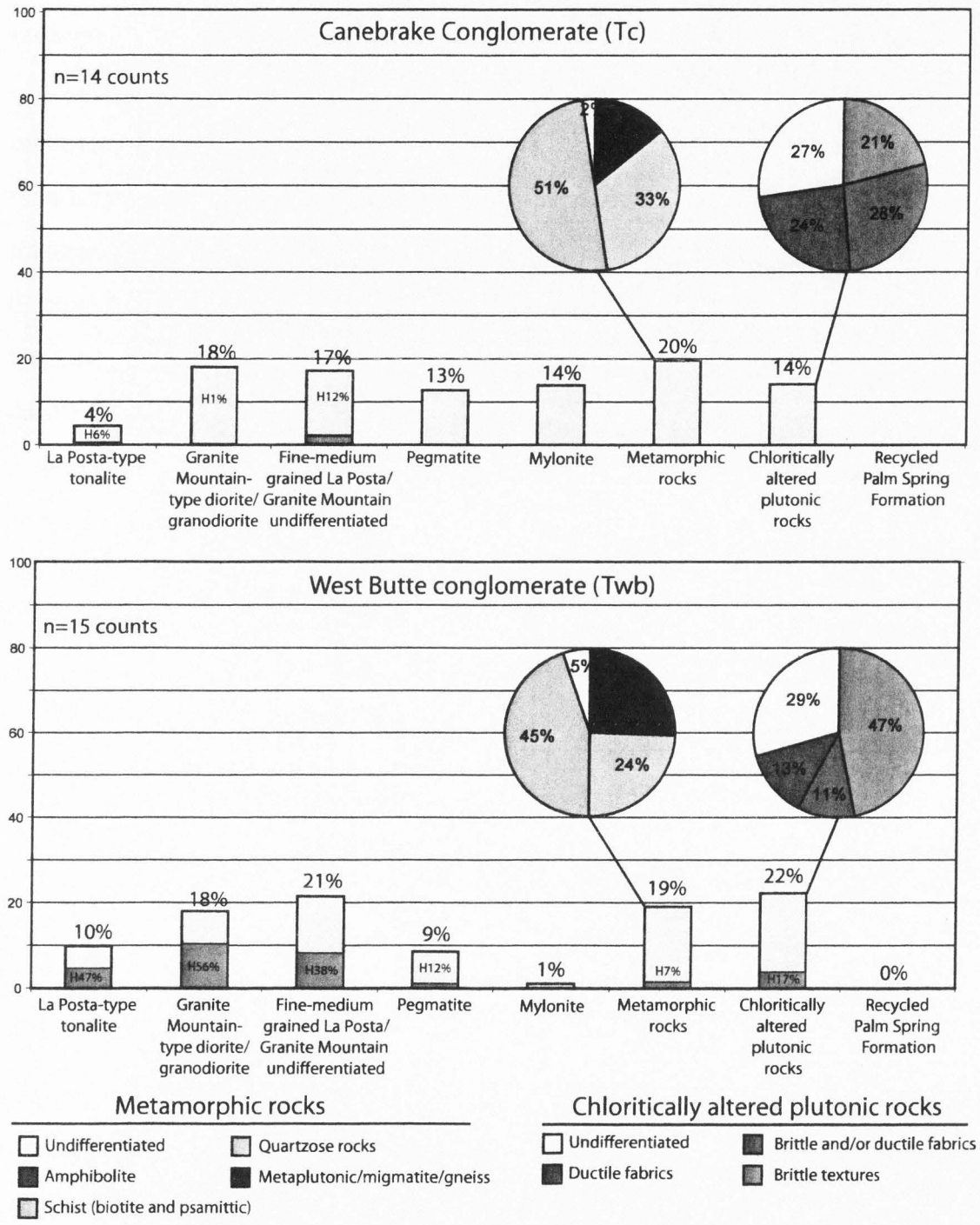

Figure 2-10. Clast counts for conglomeratic formations in the study area. Pie charts represent the percentage of different chloritic or metamorphic rocks in the binned populations. Each clast count represents 50 clasts at a single location. Clast populations are labeled with percentages (18%). Hematitically altered clasts are represented as red bars in a particular clast population and are also labeled with percentages (H12%).

outcrops.

Deformed and chloritically altered plutonic rocks (Fig. 2-11) account for 22% of the total clast lithologies in the West Butte conglomerate (Fig. 2-10). Commonly there is too much alteration to discern the lithology of the protolith, but La Posta-type lithologies may be most common. The chloritically altered clasts were subdivided by inspection in the field into those with all brittle deformation (47%), those with a majority of macroscopically ductile deformation (13%), those with both brittle and ductile deformation (11%), and those that could not be differentiated (29%). Clasts described as brittle in hand sample are pervasively brecciated or fractured, commonly have 0.5-4 cm-wide zones of aphanitic green to black cataclasite or rare pseudotachylite, fractured quartz and feldspar grains, commonly display multiple cross-cutting faults, and rarely show a macroscopic foliation (Fig. 2-11). Clasts described as ductile in hand sample display overall fabrics similar to brittle clasts but quartz grains locally form thin discontinuous ribbons, macroscopic foliation is more common, and average grain size is smaller than in brittle clasts. Clasts described as brittle and ductile display characteristics of both deformation fabrics.

Alteration: All clast lithologies in the West Butte conglomerate show some hematitic alteration (Fig. 2-9E). Clasts that have been affected by this alteration typically have much of their original biotite altered to hematite and have red matrix between grains. The alteration commonly permeates the entire clast, but some clasts only have a thin 0.5-2 cm rind of red to red-brown alteration. Some heavily altered clasts have both hematitic alteration and lesser yellow alteration that appears to affect feldspar and possibly quartz grains. Typically ~45% of plutonic lithologies are hematitically altered, whereas only ~10% of metamorphic or chloritically altered rocks have hematitic alteration (Fig. 2-10). Granite Mountain-type lithologies are most affected by the alteration (56% of the clasts), display the heaviest alteration, and these altered clasts are very brittle and crumble easily. This is probably because these rocks are especially

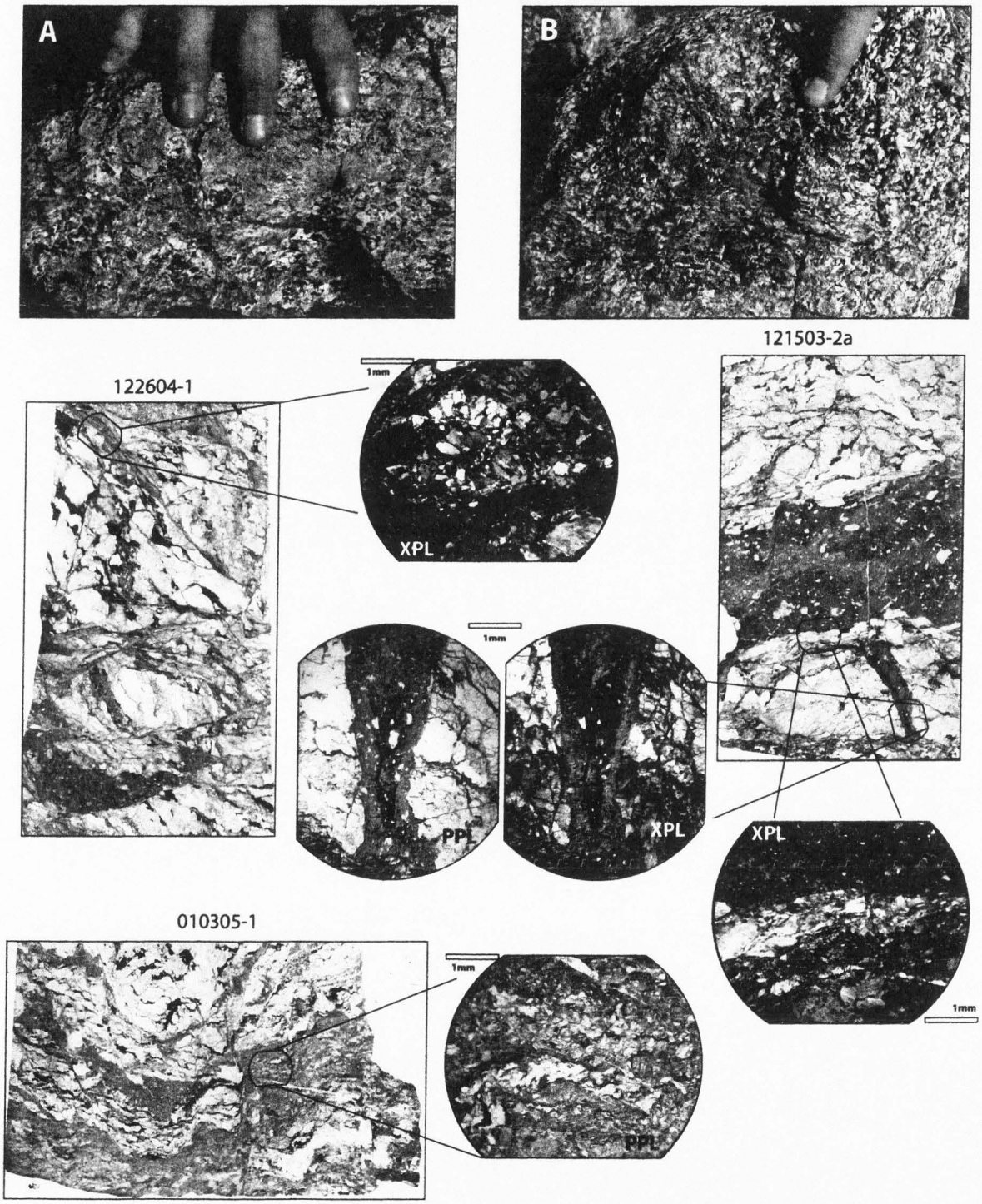
A
B
121503-2a
122604-1
1mm
XPL
1mm
PPL
XPL
XPL
1mm
010305-1
1mm
PPL

Figure 2-11.

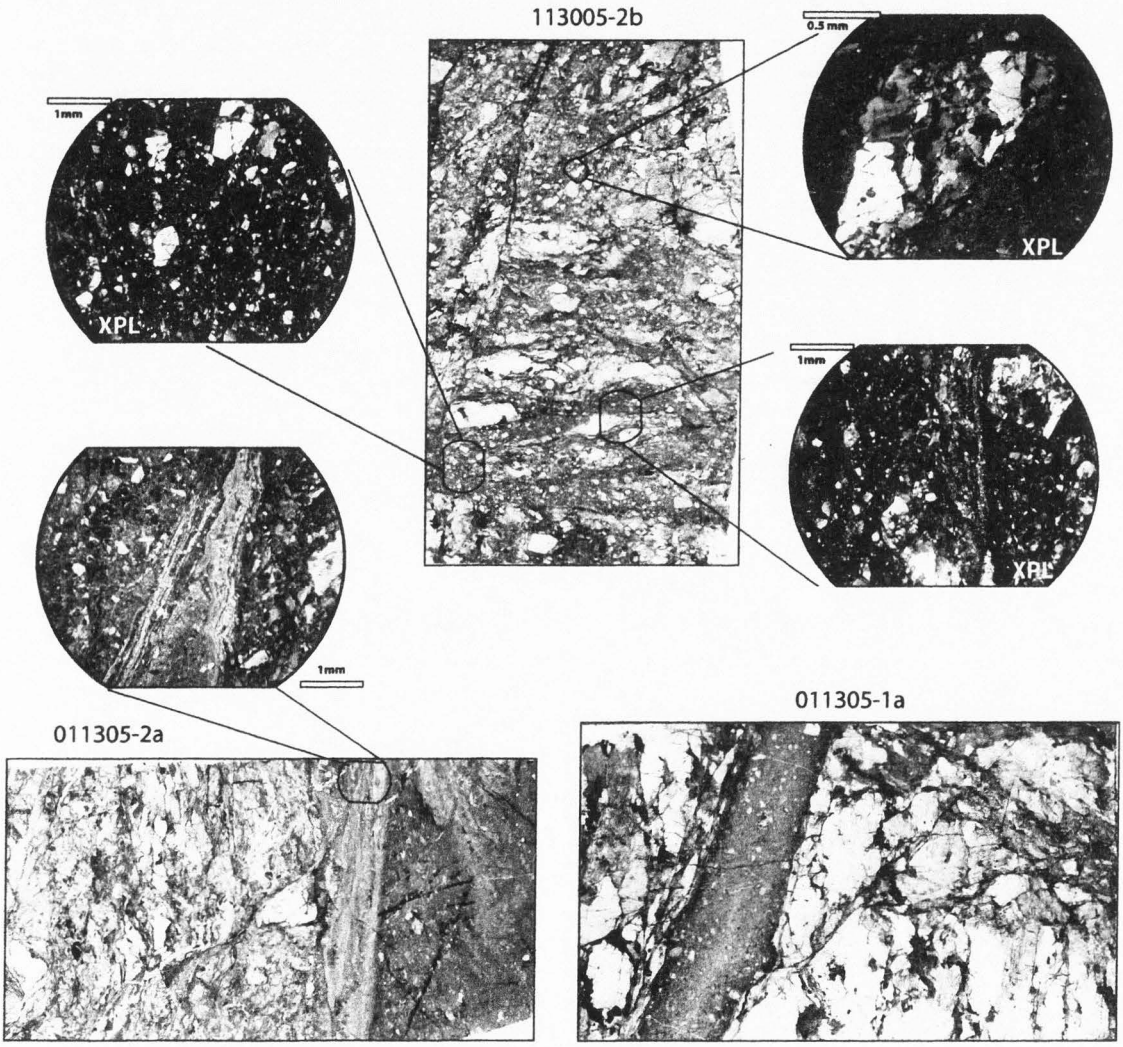

Figure 2-11, continued.

rich in biotite. The alteration of biotite in clasts contrasts with the presence of unaltered biotite grains in the sand matrix of conglomerate beds.

Paleoflow: Paleocurrents in the West Butte conglomerate were measured from clast imbrications and channel axes (Fig. 2-12). Most channel axes were bi-directional, and usually only one direction overlapped with paleotransport directions inferred from clast imbrications. Overall, paleotransport is N26°E ± 7° when measurements are corrected for bedding dip (Fig. 2-12). Data spread ~140° about this mean vector. In order to determine if there was any temporal variability of the paleoflow, paleocurrent indicators were collected at 7 stations along 280 m of measured section through this unit. There are no systematic vertical variations through the section.

Thin section description. Over 20% of clasts in the West Butte conglomerate are deformed and contain chloritic alteration. These clasts appear to have been derived from a major brittle or ductile fault zone, perhaps the the damage zone of the West Salton detachment fault or the Eastern Peninsular ranges mylonite zone. In order to investigate the source of these clasts we collected over 30 representative samples and made 12 standard 30 μm thin sections to examine the microscopic characteristics of deformation fabrics in these clasts. Clasts were selected to provide examples from brittle, brittle/ ductile, and ductile fabrics observed in hand sample. The results of these studies are summarized in Table 2-1 and many of the features are shown in Figure 2-11.

Description: Despite having variable macroscopic deformation fabrics ranging from brittle to ductile as seen in hand sample, nearly all the thin sections display similar microstructures. The thin sections were divided into two groups based on the amount of cataclasite observed. In all thin sections feldspar grains are fractured or brecciated and locally laminae and twins are offset. Quartz and mica are also commonly fractured and quartz grains have undulose extinction that ranges from sweeping to sharp and irregular boundaries. Rarely, brittley deformed quartz grains aggregate and form S-C foliations; microfracturing is the dominant observed deformation mechanism and

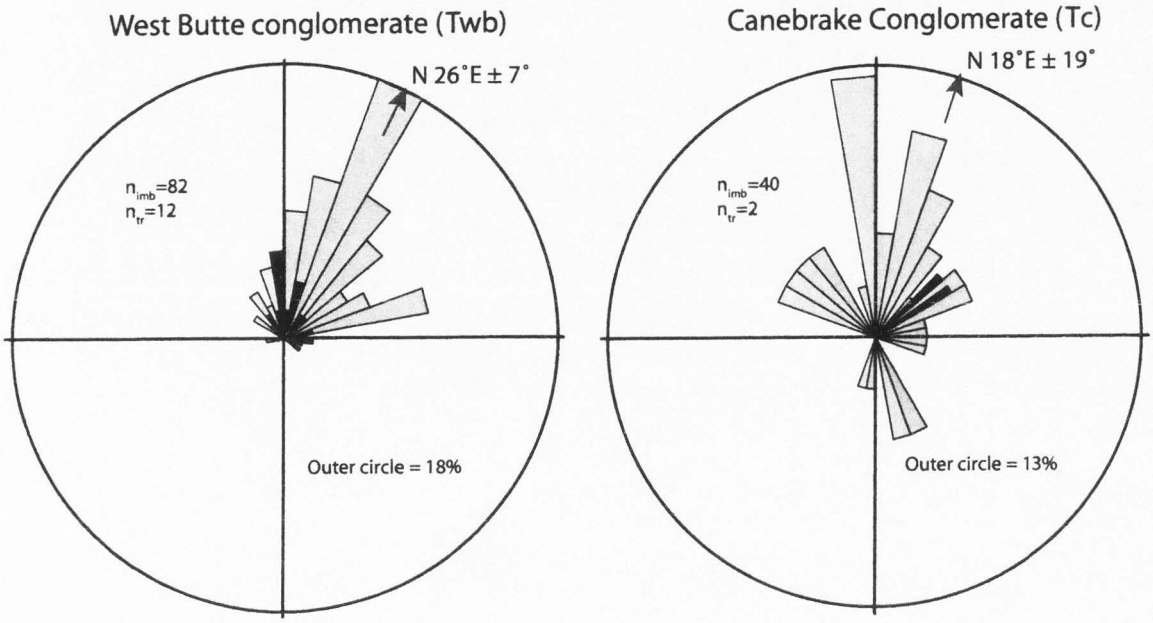

Figure 2-12. Rose diagram of paleocurrents from the Canebrake Conglomerate (Tc) and West Butte conglomerate (Twb). Light gray petals are measurements from tilt-corrected poles to clast imbrications; dark gray petals are measurements from tilt-corrected trough axes. Bi-directional trough axes are plotted in the same quadrant as the unidirectional imbrications. nimb=number of imbrications; ntr= number of trough axes. Average direction and errors given.

there is no evidence for recrystalization. Penetrative microfracturing, brecciation, and cataclasite are common to ubiquitous in these samples. Cataclasite is commonly 1-25 mm thick, dark green to black, aphanitic, and nearly isotropic with dispersed small grains of angular to rounded quartz and feldspar. Margin-parallel foliation and brecciated clasts of cataclasite dispersed in the cataclasite band are common. The boundary between cataclasite and surrounding brecciated to fractured damage zone rock is always sharp and distinct. Angular fragments of the surrounding damage zone commonly show evidence for spalling and incorporation into the cataclasite band. Ultracataclasite is common and is dark green to black and isotropic. In samples with greater than 20% cataclasite, pseudotachylite is common, and in the remaining samples it is rare. Spherulites and injection fabrics are common in the pseudotachylite which can be up to several centimeters thick.

Semi-ductile fabrics are present in all thin sections. These fabrics include small quartz grains with incipient dynamic recrystalization both in the damage zone and as grains floating in cataclasite or pseudotachylite, as well as quartz subgrains, annealed quartz in fractures, and aligned mica. Kinked mica, fine- to medium-grained dynamic recrystalized quartz, and weak grain shape preferred orientation are rare to absent. Ductile fabrics such as dynamically recrystalized quartz ribbons, S-C foliations with recrystalization, strong grain shape preferred orientation, and ductile feldspar grains are completely absent.

All of the samples display multiple cycles of deformation with 2 to 15 sets of cross-cutting features. Commonly, penetrative brecciation and microfracturing are seen to overprint pseudotachylite cutting cataclasite, which cut an earlier phase of microfracturing. A detailed study of these relationships was not performed.

Veins are rare in all thin sections, and when present, are filled with quartz and lesser calcite, chlorite, and hematite. Low levels of chloritic alteration of biotite are ubiquitous in all thin sections, but most biotite is relatively un-altered. Sericite grains are

rare and clay alteration of feldspars is not present.

Interpretation: All clasts preserve evidence for brittle deformation and evidence for lesser, but consistent incipient ductile deformation (Table 2-1 and Fig. 2-11). The semi-brittle deformation fabrics are consistent with deformation near ~200° C and below 300°-350° C (Scholz, 1988; White, 2001). The brittle and semi-brittle textures appear contemporaneous but a recent analysis of pseudotachylite-bearing mylonite shows that such textural interpretations may be in error (Sherlock et al., 2004). Overall, we interpret these rocks as being derived from a major brittle to semi-brittle fault zone in the source area of the West Butte conglomerate. Alteration is not especially common at the microscopic level despite the prevalent green altered appearance of the hand samples (Fig. 2-11). The lack of significant vein development and rare clay alteration of feldspar grains suggests that water was not abundant in the fault zone.

Provenance. The low abundance of large-grained La Posta-type tonalite clasts (10%) in the West Butte conglomerate suggests that the hanging wall of the detachment fault was a minor part of the source area. The relatively greater abundance of Granite Mountain-type plutonic (18%), fine-grained undifferentiated plutonic rocks (21%), and metamorphic rocks (19%), which constitute ~58% of the clasts, suggests that the footwall of the detachment fault was the source of most of the conglomerate clasts. Although quartzose and calc-silicate metasedimentary rocks are found in close spatial association with the Eastern Peninsular Ranges mylonite zone, the lack of identifiable mylonite clasts indicates that the Eastern Peninsular Ranges mylonite zone was either still buried during deposition of the West Butte conglomerate or the source area was entirely beyond the southern terminus of the mylonite zone. Therefore, metasedimentary clasts were likely derived from roof pendants and screens of the Cretaceous batholiths in the footwall of the detachment fault (e.g. Grove et al., 2003) instead of metasedimentary rocks in the Eastern Peninsular Ranges mylonite zone.

Of the 22% of clasts that are deformed and chloritically altered, most of these

clasts are indistinguishable from the damage zone in the hanging wall of the West Salton detachment fault (Table 2-1, Figs. 2-7 and 2-11). Samples of the Cretaceous mylonite and metaplutonic and metamorphic rocks exposed in the footwall of the detachment fault do not resemble deformed and chloritically altered clasts of the West Butte conglomerate. Mylonitic footwall rocks display strong ductile deformation textures including strong S-C mylonitic fabrics, and display no evidence for brittle deformation or chloritic alteration except in small zones where locally overprinted by the damage zone of the detachment fault or younger strike-slip faults. Thin, discontinuous, semi-brittle chloritic shear zones have been reported in the footwall of the West Salton detachment fault (Simpson, 1984; Schultejahn, 1984) and could supply similar lithologies to those observed in the West Butte conglomerate. However, the significant volume of altered clasts in the West Butte conglomerate and the scarcity of the shear zones argue against them as a major source.

We interpret the deformed and chloritic clasts as being derived from the damage zone of the West Salton detachment fault. Because the West Salton detachment fault reactivates the Cretaceous Eastern Peninsular Ranges mylonite zone along most of its length (Axen and Fletcher, 1998; this study), some of the fabrics observed in these clasts may be composite fabrics created by superposition of the late Cenozoic West Salton detachment fault onto earlier Cretaceous deformation. Although more work is needed to determine the exact age of deformation fabrics in these clasts, the spatial coincidence between these fabrics and the damage zone of the West Salton detachment fault is strong. Thus we infer that the deformed and altered clasts were eroded from the damage zone of the detachment fault regardless of whether the detachment fault produced all of the observed deformation fabrics.

The NNE-directed paleotransport direction shows that the source of these clasts was located SSW of the Borrego Mountain area and west of Whale Peak, a possible corrugation in the West Salton detachment fault. Additionally, hematitically-altered Granite Mountain-type lithologies are exposed in the footwall of the detachment

fault west of Whale Peak. Overall, we interpret the provenance for the West Butte conglomerate as an area south-southwest of Borrego Mountain that exposed an extensive brittle to semi-ductile chloritic damage zone related to the West Salton detachment fault, and a significant amount of plutonic and associated metamorphic rocks in the footwall of the detachment fault (Fig. 2-13). The La Posta-type plutonic rocks now exposed beneath the detachment fault at Whale Peak had probably not been unroofed during deposition of the West Butte conglomerate.

Depositional environment. We interpret the moderately to poorly-sorted, planar bedded to low-angle cross stratified coarse sandstone to sandy pebble conglomerate as sheet-flood deposits. Rare <20 cm-tall trough cross bedding in coarse to pebbly sandstone suggest <20 cm water depths during deposition of these finer-grained deposits. Up to 50 cm-deep channels in coarse pebble to cobble conglomerate beds, prevalence of imbricated clasts throughout the unit, and low-angle cross stratification are interpreted as minor fluvial channel fill deposits. The lack of cross bedding suggests that sediment was mostly deposited in diffuse horizontal gravel sheets. Together, these interpretations suggest that the majority of this unit was deposited in a distal alluvial fan (e.g. Rust and Koster, 1984; Collinson, 1996). Because the lithology of this unit does not significantly vary over transport-perpendicular distances of ~8 km, and there is a lack of fine-grained deposits, we further suggest that the West Butte conglomerate was deposited either in one large alluvial fan, or as part of a distal bajada.

Correlation and age. Differences in the sedimentology of basal units between Borrego Mountain and Squaw Peak created difficulty for previous workers correlating stratigraphy across the area. Our new work in these units shows that the West Butte conglomerate correlates to the late Miocene to middle Pliocene Imperial Group and does not correlate with the Canebrake Conglomerate of the Palm Spring Group (Fig. 2-8). Both the Imperial Group at Squaw Peak and the West Butte conglomerate are coarse-grained, basal arkosic sandstone and pebbly sandstone that underlie the Olla and Diablo

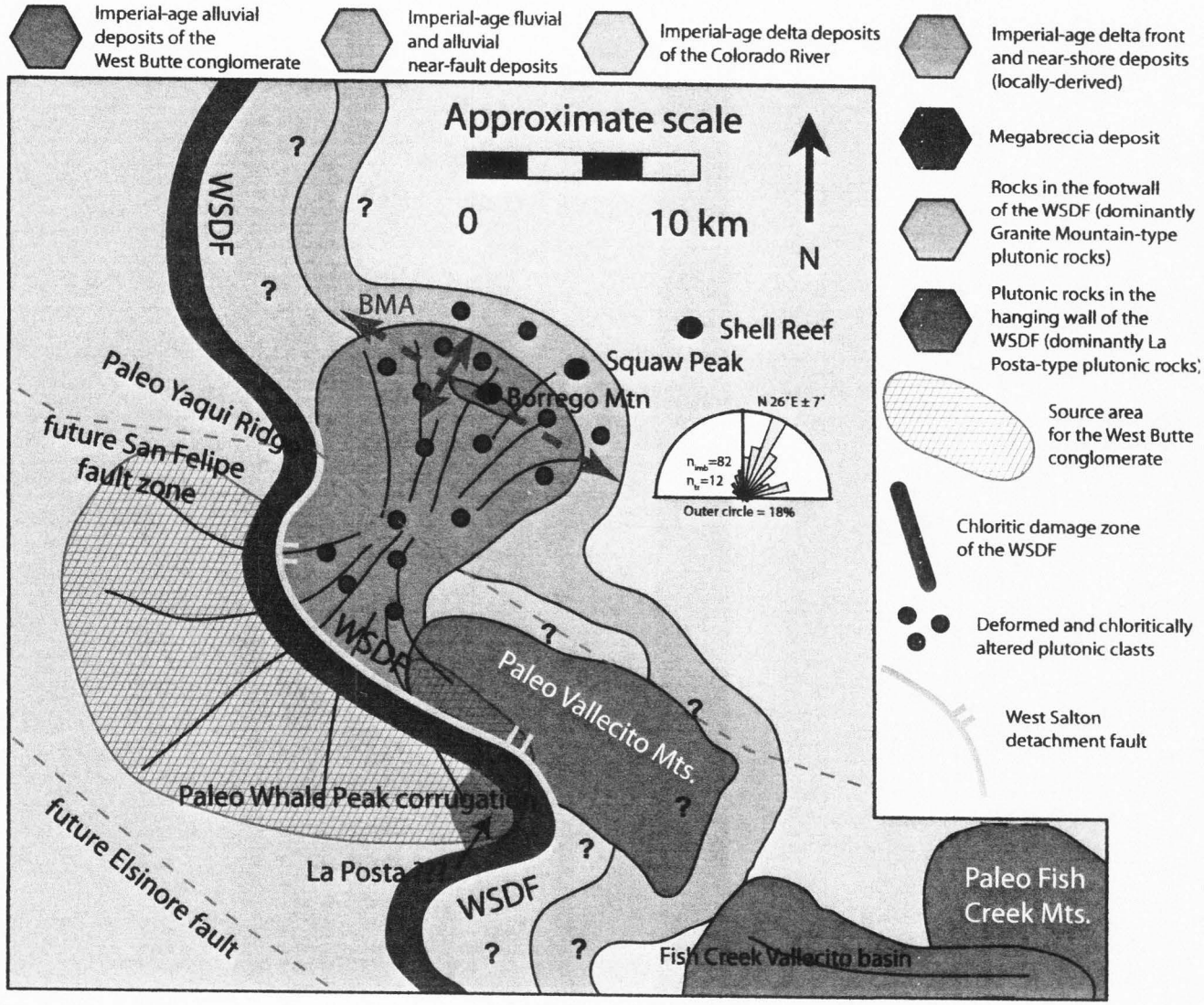
Imperial-age alluvial deposits of the West Butte conglomerate
Imperial-age fluvial and alluvial near-fault deposits
Imperial-age delta deposits of the Colorado River
Imperial-age delta front and near-shore deposits (locally-derived)
Megabreccia deposit
Rocks in the footwall of the WSDF (dominantly Granite Mountain-type plutonic rocks)
Plutonic rocks in the hanging wall of the WSDF (dominantly La Posta-type plutonic rocks)
Source area for the West Butte conglomerate
Chloritic damage zone of the WSDF
Deformed and chloritically altered plutonic clasts
West Salton detachment fault
Approximate scale
0
10 km
N
WSDF
BMA
Shell Reef
Squaw Peak
Borrego Mtn
N 26°E ± 7°
Outer circle = 18%
Paleo Yaqui Ridge
future San Felipe fault zone
Paleo Vallecito Mts.
Paleo Whale Peak corrugation
La Posta
future Elsinore fault
Paleo Fish Creek Mts.
Fish Creek Vallecito basin

Figure 2-13.

formations, rest with depositional nonconformity on Cretaceous bedrock, and onlap onto significant paleotopography. Both units also have similar provenance in conglomeratic intervals, including the distinctive deformed and chloritically altered plutonic clasts. When corrected for dextral separation on the intervening Coyote Creek fault, the finer-grained rocks at Squaw Peak lie down the paleotransport direction of the West Butte conglomerate.

We interpret these data to mean that the West Butte conglomerate correlates with the Pliocene Imperial Group at Squaw Peak, and suggest that the West Butte conglomerate is the fluvial equivalent to the marine Imperial Group (Fig. 2-13). The distal alluvial fan environment of the West Butte conglomerate is inferred to pass laterally into the near shore marine environments at Squaw Peak. A relatively narrow marine delta apparently existed between Borrego Mountain and Squaw Peak (Fig. 2-13), although no Imperial-age deposits are exposed between these two locations.

Palm Spring Group

The Palm Spring Group consists of the laterally equivalent Canebrake Conglomerate, Olla and Diablo formations, and the overlying Borrego Formation (Winker and Kidwell, 1996). In our study area the Palm Spring Group follows regional trends of changing composition and coarsening SW towards the West Salton detachment fault (Fig. 2-8) (Dibblee, 1954, 1984; Morley, 1963; Winker and Kidwell, 1996). In the Borrego Mountain area the Olla Formation overlies the West Butte conglomerate of the Imperial Group along a gradational contact and is the lowest formation of the Palm Spring Group. The Diablo Formation overlies the Olla Formation along a gradational and interbedded contact west of West Butte (Fig. 2-3) (Winker and Kidwell, 1996; this study). The Canebrake Conglomerate is exposed along the northeast side of Yaqui Ridge (Winker and Kidwell, 1996; this study), and rare outcrops show that it is locally interbedded with the Diablo and Olla formations there (Fig. 2-4). We describe and correlate a laterally

extensive megabreccia in this group that we previously unidentified. The Olla and Diablo formation are at least 670 m thick west of West Butte (Morley, 1963; Dorsey et al., 2004; this study) and possibly much thicker.

Olla Formation

Description. Around Borrego Mountain, the Olla Formation overlies the West Butte conglomerate along a gradational contact. The base is defined as the top of the last thick conglomerate bed of the West Butte conglomerate, or where sandstone is greater than 50%. The Olla Formation is up to 120 m thick near the south end of Borrego Mountain wash, and thins to ~38 m at the north end of the wash (Fig. 2-3). This lateral thickness change is accompanied by a change from tan beds where the unit is thicker, to red beds where the unit is thinner. The Olla Formation is inferred to onlap basement tonalite north of Middle Butte. This unit is overlain by the Diablo Formation along a relatively distinct boundary where thick 'C-suite' cross-bedded sandstone and thick red mudstone beds of the Diablo Formation overlie the thinner bedded 'L-suite' sandstone beds of the Olla Formation.

Where the Olla Formation is thick it consists of 'L-suite' tan, red, and yellow fine to coarse grained sandstone with rare interbeds of tan to red siltstone, mudstone, and pebble to granule sized conglomeratic sandstone (Fig. 2-9F). Sandstone is sub angular to sub rounded, moderately sorted, and composed of quartz, feldspar, lithic fragments, and lesser amounts of biotite. Beds in this unit vary from ~1-3 cm to 1-2 m thick and commonly display parallel bedding. Low-angle cross stratification is also common and trough cross stratification is rare. Locally, conglomeratic beds have up to a 20 cm-deep erosional channel at their base. In locations where the Olla Formation is thin it consists of interbedded red arkosic sandstone, granule to pebble-sized conglomeratic sandstone, and red siltstone to mudstone beds.

In the Olla Formation around Borrego Mountain and on the NE side of the Coyote

Creek fault, a 1-5 m thick prominent yellow-weathering sandstone unit is present 10-15 m beneath the contact with the Diablo Formation (Fig. 2-3). This bed is composed of both 'L-suite' and 'C-suite' coarse to fine sand grains, is planar-bedded with up to 1 m trough cross-beds, has locally developed current lineations, weathers out small 1-2 cm diameter 'C-suite' concretions, and is well cemented. This lithology is unique to this bed making it an ideal structural and stratigraphic marker. A systematic collection of paleocurrent indicators was not made in the Olla Formation.

Provenance. The Olla Formation represents fluvial deposits derived from the Peninsular Ranges southwest of the Salton Trough (Dibblee, 1984; Winker, 1987). Thickness patterns show that basement highs were completely buried near Borrego Mountain during deposition of the Olla Formation (see below). Thus, uplifted basement at the basin margin must have been the source of the <120 m thick Olla Formation. The arkosic composition of sandstone and altered clasts similar to those found in the underlying West Butte conglomerate are consistent with a source in the Peninsular Ranges that exposed both plutonic rocks and lesser brittle fault rocks. This source may be similar to that of the underlying West Butte conglomerate and probably was also located to the SSW.

Depositional environment. The conglomerate and pebbly sandstone beds in the Olla Formation contain lenticular geometry and scouring along their bases that suggest deposition in fluvial channels. The interbedded fine-grained mudstone and thin-bedded sandstone suggest deposition in standing water. These interpretations suggest that shallow fluvial channels migrated across a broad, low-gradient swampy flood plain in a meandering or anasamosing fluvial environment (e.g. Collinson, 1996; Miall, 1996). The conglomeratic channel deposits are coarser than expected for this type of environment, and could be because the fluvial system was receiving course detritus from adjacent distal alluvial fans. The change from the underlying distal alluvial fan environment of the West Butte conglomerate into the much lower-gradient environment of the Olla Formation

represents a major nonmarine transgression that continues through the Diablo Formation and into the overlying Borrego Formation.

Correlation and age. The Olla Formation was first mapped as the Palm Spring Formation by Dibblee (1954) and Morley (1963) who did not break out distinct units for 'L-suite' and 'C-suite' facies. We agree with this general assignment and use the Winker and Kidwell (1996) nomenclature of Olla Formation based on our sedimentologic descriptions. The Olla Formation is Pliocene age based on magnetostratigraphy in the Fish Creek-Vallecito basin (e.g. Johnson et al., 1983; Winker and Kidwell, 1996).

Diablo Formation

Description. The Diablo Formation is exposed southwest of the Coyote Creek fault near Borrego Mountain where it overlies the Olla Formation and is at least ~550 m thick (Fig. 2-3) (Dorsey et al., 2004). Because the top of the Diablo Formation is not preserved southwest of the Coyote Creek the ~550 m of section is only a minimum. In Harper Canyon south of Borrego Mountain, and Yaqui Meadows southwest of Borrego Mountain, a few tens of meters of Diablo Formation are exposed where neither the base nor the top are preserved, and the unit is interbedded with the Canebrake Conglomerate and Olla Formation. The base of the Diablo Formation is placed where thick 'C-suite' cross-bedded sandstone and thick red mudstone beds overlie the thinner bedded 'L-suite' sandstone beds of the Olla Formation (Fig. 2-9). The top of the Diablo Formation is not exposed in the study area, and to the north and east it consists of a complexly interbedded section of Diablo and Borrego formation-type lithologies (Kirby, 2005; Lutz, 2005).

In the study area the Diablo Formation consists of interbedded tan to yellow 'C-suite' sandstone and red claystone to siltstone (Fig. 2-9). Sandstone is fine-to medium-grained, well sorted, and medium to thick bedded. Locally, sandstone beds pinch out into mudstone layers over tens to hundreds of meters and contain concretions from 1 to 30 cm in diameter (Morley, 1963; this study). Trough cross bedding and planar bedding are the

most common sedimentary structures and many well-cemented sandstone beds display current lineations. Mudstone beds are red silty claystone to clayey siltstone, and locally contain bentonitic clay (Morley, 1963). Mudstone is medium to thick bedded (up to ~8 m thick), and is structureless to laminated.

Provenance. The Diablo Formation is defined as containing >20% rounded, hematite-coated quartz grains (Winker, 1987). These quartz grains are distinctive in the Diablo Formation in our study area and are significant because they are only dispersed by the Colorado River system and cannot be sourced from the Peninsular Ranges (Merriam and Bandy, 1965; Winker and Kidwell, 1996).

Depositional environment. The Diablo Formation is interpreted as the subaerial Colorado River delta plain (Winker, 1987; Winker and Kidwell, 1996). Abundant trough cross-stratification, thick mudstone beds, lenticular geometries, and 'C-suite' sandstone grains derived from the Colorado River (Merriam and Bandy, 1965; Winker, 1987) all support this interpretation.

Correlation and age. The Diablo Formation was first mapped as an undifferentiated deposit of the Palm Spring Formation by Dibblee (1954) and Morley (1963). Our work confirms that this unit is part of the Palm Spring Group of Winker and Kidwell (1996), and based on our sedimentological descriptions and interpretation of depositional environment, we correlate this unit with the Diablo Formation of the Palm Spring Group. The Diablo Formation was deposited between ~4.2 and 2.8 Ma in the Fish Creek-Vallecito basin (Johnson et al., 1983; Dorsey et al., 2006).

Megabreccia of Yaqui Ridge, Church Ridge, and Harper Canyon

Description. Several locations in the study area preserve a ~1-10 m thick, sheet-like deposit of brecciated plutonic and metamorphic rocks that is interbedded in strata of the Palm Spring Group. In all exposures, medium to fine-grained 'C-suite' sandstone

of the Diablo Formation is closely associated with the megabreccia deposit (Figs. 2-3 and 2-4). Near Yaqui Meadows, the deposit is thickest, overlies an interbedded section of Canebrake Conglomerate and fine-grained Diablo Formation, and is overlain by Canebrake Conglomerate. Cross sections (Fig. 2-5A and B) show that the megabreccia is located somewhere near the lower third of the Palm Spring Group, although its exact stratigraphic position is unclear because the top of the group is not exposed. At Church Ridge the deposit is interbedded with Canebrake Conglomerate and is cut by the West Salton detachment fault (Plate 1). At Harper Canyon the megabreccia overlies gritty to pebbly 'L-suite' sandstone, probably of the Olla Formation, and is directly overlain 'C-suite' sandstone of the Diablo Formation. In this location, the first 1-2 meters of 'C-suite' sandstone are bioturbated, have many carbonate-rich soils, and the section appears to be condensed relative to other exposures of the Diablo Formation. Near West Butte, the megabreccia deposit lies above a maximum of ~500 m of Diablo Formation and can be traced for ~2.5 km along strike to the north before tapering to <1 m thickness (Fig. 2-3). The megabreccia near West Butte is overlain by Diablo Formation and locally by pebbly conglomerate and 'L-suite' sandstone. Using these four outcrops, the pinch-out near West Butte, and the lack of megabreccia on the northeast side of the Coyote Creek fault, a conservative estimate of ~200 km^2 can be made for the areal extent of the megabreccia deposit (Fig. 2-14).

The megabreccia commonly consists of massively brecciated to highly fractured plutonic rock with little or no internal stratification. Grain sizes range from fine sand-sized to large boulders (up to ~6 m across) and individual grains are angular and fit together with a jigsaw fabric. Near Yaqui Meadows, severely fractured to brecciated outcrops up to ~100 square meters across locally contain pegmatites that can be traced for several meters. These features suggest translation of a large rock mass with little internal distortion.

The lithology of the megabreccia deposit is similar across the field area, consists

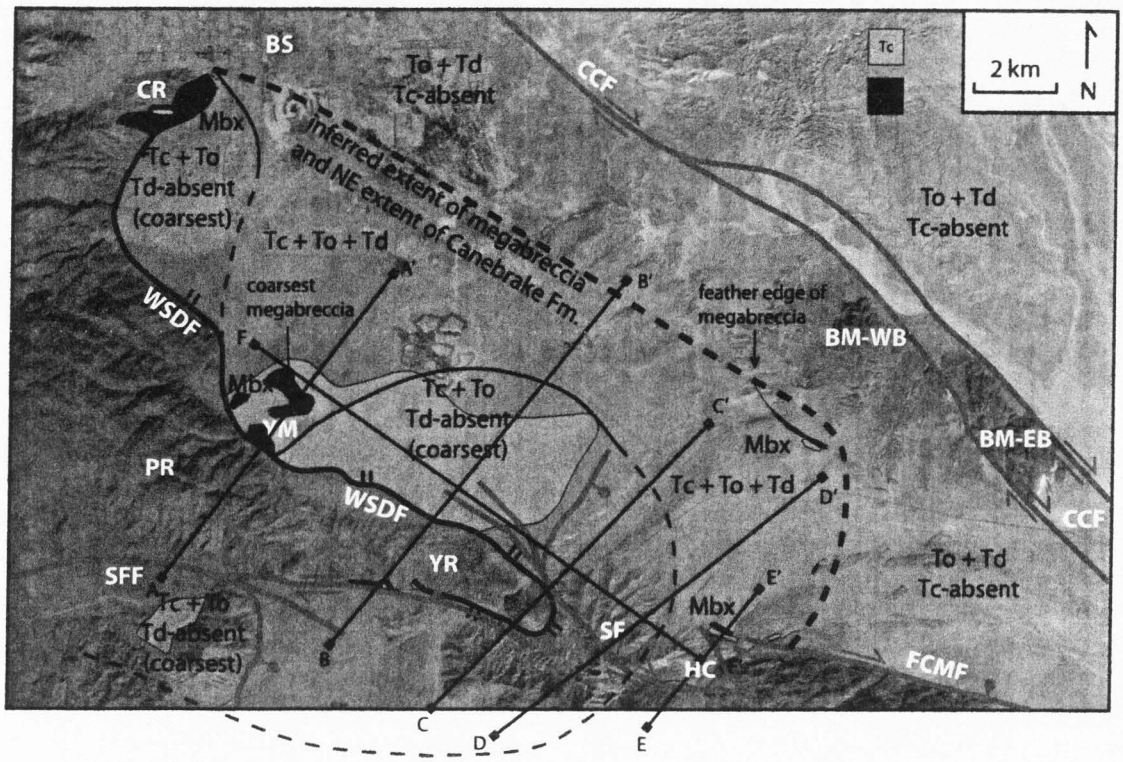

Figure 2-14. Distribution of the Canebrake Conglomerate and the aeral extent of the megabreccia interbedded in the Palm Spring Group. Base map is from a Landsat image. BM-EB-Borrego Mountain-East Butte; BM-WB-Borrego Mountain-West Butte; BS-Borrego Springs; CCF-Coyote Creek fault; CR-Church Ridge; FCMF-Fish Creek Mountains fault; HC-Harper Canyon; Mbx-megabreccia; PR-Pinyon Ridge; SF-Sunset fault; SFF-San Felipe fault; Tc-Canebrake Conglomerate; Td-Diablo Formation; To-Olla Formation; WSDF-West Salton detachment fault; YR-Yaqui Ridge.

of Granite Mountain-type plutonic rocks that show a range of deformational fabrics from undeformed to brittle to mylonitic, with significant local variations. Between ~20-70% of the lithologies at each locality consist of undeformed medium to large-grained Granite Mountain-type diorite. At Yaqui Ridge these lithologies are mixed with up to ~30% chloritically altered ultramylonite, mylonite, protomylonite, brittle shear zones, and pegmatite. At Church Ridge, the megabreccia is dominated by unaltered Granite Mountain-type diorite and contains <20% strained rocks. At Harper Canyon the megabreccia contains ~40% Granite Mountain-type diorite, ~30-50% fine-grained tonalite and diorite (not La Posta-type tonalite), and up to 10-20% pegmatite and spotted tonalite. The outcrop near West Butte displays the largest range of lithologies and consists of ~20-30% Granite Mountain-type diorite, ~20% chloritically altered brittle to ultramylonitic shear zones, ~20% chloritically altered to non altered protomylonite and mylonite, and ~20-30% 'spotted' tonalite, unaltered tonalite, minor gneiss, and schistose rocks. Nowhere does the composition of the megabreccia match either the closest crystalline rocks in the hanging wall or the closest exposures of crystalline rocks in the footwall of the West Salton detachment fault.

Provenance. The crystalline lithologies in the megabreccia are distinct and are not found in the predominantly 'La-Posta-type' tonalite hanging wall of the West Salton detachment fault. However, these lithologies are abundant in the footwall of the detachment fault southwest of Yaqui Meadows. The ductile fabrics are consistent with fabrics observed in the Eastern Peninsular Ranges mylonite zone. Therefore, we suggest that the megabreccia was derived from the footwall of the detachment fault and was transported across its trace at least 8 km NE into the basin.

Depositional mechanism. We interpret the brecciation, coarse grain sizes, textures, and sudden change of provenance in this deposit relative to the Diablo Formation to be the result of a long-runout landslide. Textures and brecciation are similar to those of the upper and lower megabreccia deposits of the Fish Creek-Vallecito basin

(Papajohn, 1980; Abbot and Rightmer, 1995; Winker and Kidwell, 1996), the 'Vallecito' megabreccia in the Palm Spring Group near Whale Peak (Hart, 1991), and the Blackhawk landslide along the northern San Bernadino Mountains (Shreve, 1994). Although the megabreccia is only exposed in four locations, it appears to thicken and coarsen toward the West Salton detachment fault and toward its likely source in the footwall of the detachment fault where the Eastern Peninsular Ranges mylonite zone is exposed.

Correlation and age. Three other megabreccias have been studied in the western Salton Trough (Papajohn, 1980; Hart, 1991; Abbot and Rightmer, 1995; Winker and Kidwell, 1996). The lower and upper megabreccias of the Imperial Group in the Fish Creek-Vallecito basin are both large run-out landslides and have similar textural characteristics to the megabreccia we describe (Papajohn, 1980; Abbot and Rightmer, 1995; Winker and Kidwell, 1996). However, neither of those deposits contain clasts similar to those in the Yaqui Ridge megabreccia, are located ~17-40 km southeast of our study area, and are interbedded in the older marine Imperial Group. The 'Vallecito' megabreccia in the Fish Creek-Vallecito basin is texturally similar to the Yaqui Ridge megabreccia and is interbedded with Canebrake and Olla formations of the Palm Spring Group (Hart, 1991; Kairouz, 2005). It is overlain by the Hueso Formation (Kairouz, 2005), a lateral equivalent of the Borrego Formation, indicating that the 'Vallecito' megabreccia is interbedded near the top of the Palm Spring Group there. The 'Vallecito' megabreccia is interpreted as a long-runout landslide shed from the footwall of the nearby West Salton detachment fault (Hart, 1991; Kairouz, 2005) and occupies a broadly similar stratigraphic position to the Yaqui Ridge megabreccia.

The interbedding of the Yaqui Ridge megabreccia with the Canebrake Conglomerate and Olla and Diablo formations shows that the megabreccia deposit is a member of the Pliocene Palm Spring Group. Because the 'Vallecito' megabreccia is located several tens of kilometers to the south and at the top of the Palm Spring Group the two units probably do not correlate.

Canebrake Conglomerate

Description. Regionally the Diablo and Olla formations pass laterally west and southwest into locally-derived coarse sandstone to cobble-boulder conglomerate of the Canebrake Conglomerate (Figs. 2-8 and 2-14) (Dibblee, 1954, 1984; Winker and Kidwell, 1996). The Canebrake Conglomerate is exposed in an 18 km-long outcrop belt along the northeast side of Yaqui Ridge where it is faulted against mylonitic plutonic rocks by the West Salton detachment fault (Fig. 2-4). Although alluvial cover obscures most of the lateral relationships between the Canebrake, Olla, and Diablo formations in the study area, several key locations display these relationships. Thin exposures of interbedded Canebrake, Olla, and Diablo formations are found in horses along the Sunset fault, and up to 15 m of Diablo Formation is interbedded in Canebrake Conglomerate near Yaqui Meadows (Fig. 2-4). Exposures up to 8 km east and northeast of the West Salton detachment fault indicate northeastward fining in the Canebrake Conglomerate. The exposures of Canebrake Conglomerate at Harper Canyon are the most eastern exposures of this unit and also the finest (Fig. 2-14). Pebbly sandstone and sandy conglomerate dominate in these outcrops. Map patterns suggest that these conglomeratic beds fine north and northeast into the Diablo Formation in Lower Borrego Valley because outcrops there are discontinuous and consistently expose Diablo Formation without any Olla Formation or Canebrake Conglomerate (Figs. 2-3 and 2-14).

Approximately 600 m thickness of Canebrake Conglomerate is measured between the oldest exposed conglomerate and the Yaqui Ridge megabreccia northeast of Yaqui Ridge using cross sections constructed parallel and perpendicular to the West Salton detachment fault (Fig. 2-5). This is a minimum thickness for the Canebrake Conglomerate near Yaqui Ridge and is similar to the ~500 m maximum thickness estimated from the map between the megabreccia and the base of the Olla Formation at Borrego Mountain. These relationships may indicate that ~500 m of Diablo Formation west and southwest of Borrego Mountain pass laterally southwestward into pebble and

boulder conglomerate of the Canebrake Conglomerate. Because thickness is difficult to estimate for the Canebrake Conglomerate and outcrops are discontinuous, we did not find any evidence for syn-deformational growth.

The Canebrake Conglomerate consists of gray to tan, poorly to moderately cemented, moderately to well sorted, rounded pebble to boulder conglomerate and poorly to moderately sorted, sub-angular to rounded pebbly sandstone. Coarse conglomerate beds are clast-supported and grain sizes range from medium sand up to ~1 m boulders. Individual conglomerate beds range in thickness from ~50 cm to >3 m thick and bedding is poorly defined. Planar bedding to low-angle cross stratification are the most common sedimentary structures in all grain sizes, and trough cross bedding is rare throughout the unit. However, because most outcrops are only a few square meters many larger-scale bedforms may be present but not well exposed. Overall, the Canebrake Conglomerate is coarser and has a greater variability of grain sizes than the West Butte conglomerate. The West Butte conglomerate also contains significantly more hematitically altered clasts than the Canebrake Conglomerate (Fig. 2-10).

Exposures of the Canebrake Conglomerate along the West Salton detachment fault near the southeast tip of Yaqui Ridge at Yaqui Narrows contain relatively few interbedded pebbly sandstone beds and are dominated by cobble to boulder conglomerate. Exposures of the unit along the detachment fault at the northwest end of Yaqui Ridge near Yaqui Meadows are dominated by pebbly sandstone beds and contain few coarse boulder beds. A cross section constructed subparallel to the West Salton detachment fault suggests that outcrops of the Canebrake Conglomerate near Yaqui Meadows may be upsection from outcrops near Yaqui Narrows (Fig. 2-5). These relationships indicate that the Canebrake Conglomerate fines northwest from Yaqui Ridge towards Yaqui Meadows, fines east towards Harper Canyon, and fines upsection.

Clast lithologies in the Canebrake Conglomerate were determined from 14 counts of 50 clasts in the outcrop belt northeast of Yaqui Ridge (Fig. 2-10). The Canebrake

Conglomerate consists of only ~4% La Posta-type tonalite, 18% Granite Mountain-type diorite and granodiorite, 17% fine-medium-grained undifferentiated plutonic rocks, and 13% pegmatitic material. The Canebrake Conglomerate also contains ~14% mylonitic plutonic rocks, 20% metamorphic rocks, and 14% chloritically altered plutonic rocks. Of the metamorphic rocks, ~51% are biotite and psamittic schist, 33% are quartzose, and 14% are undifferentiated metaplutonic, migmatite, and gneiss. The chloritically altered rocks are nearly evenly distributed between brittle, ductile, brittle ± ductile, and undifferentiated categories. Hematitic alteration is rare in clasts of the Canebrake Conglomerate (<3% of all clasts) and is only developed in the plutonic rocks (Fig. 2-10).

Paleocurrents in the Canebrake Conglomerate were measured from clast imbrications and channel axes. Most observed channel axes are bi-directional, and typically only one direction overlaps with paleotransport directions inferred from clast imbrications. Overall, mean paleotransport is N18°E ± 19° when measurements are corrected for bedding dip (Fig. 2-12). Data display an asymmetric spread of ~270° about the NNE mean vector.

Provenance. Numerous clasts of metamorphic rocks, Granite Mountain-type diorite, and mylonite all suggest that the footwall of the West Salton detachment fault was a major source of clasts for the Canebrake Conglomerate. Few clasts of La Posta-type tonalite suggest that the hanging wall of the West Salton detachment fault contributed relatively little. The presence of mylonite is important because it marks the first appearance of mylonite in basin-fill units and shows that ductile fabrics of the Eastern Peninsular Ranges mylonite zone were beginning to be exposed during late Pliocene time. The presence of brittley-deformed and chloritically-altered plutonic rocks suggests that the West Salton detachment fault damage zone was being eroded and supplied clasts into this formation. The increased amount of ductile and brittle/ductile fabrics in this clast population relative to the West Butte conglomerate suggests that deeper levels of the detachment fault's damage zone were exposed during deposition of the Canebrake

Conglomerate than during deposition of the West Butte conglomerate. The overall NNE-paleotransport direction is similar to the transport direction for the West Butte conglomerate and suggests that the source area was located south of the Yaqui Ridge area. This roughly corresponds with the source area for the West Butte conglomerate. The dramatic increase of mylonite clasts in the Canebrake Conglomerate relative to the West Butte conglomerate suggests a change in the source area, possibly due to drainage expansion or unroofing of the Eastern Peninsular Ranges mylonite zone.

Depositional environment. The moderate to poor sorting in pebble to boulder conglomerate with massive to planar stratified beds and only minor cross bedding suggests deposition by a combination of sheet floods (in the finer grained, stratified units) and debris flows (in the more matrix-rich unstratified beds). Both of these processes occur in an alluvial fan environment (e.g. Rust and Koster, 1984; Blair and McPherson, 1994). Coarse boulder-rich facies probably represent deposition in more proximal parts of the alluvial fan, and sand-rich, more stratified facies probably represent deposition in more distal parts of the fan.

Correlation and age. Although the Canebrake Conglomerate and West Butte conglomerate share many sedimentological characteristics, the Canebrake Conglomerate is up to twice as thick as the West Butte conglomerate. Additionally, there are clasts of mylonite in the Canebrake Conglomerate that are not in the West Butte conglomerate and grain size is more variable in the Canebrake Conglomerate. Also, because the West Butte conglomerate is beneath the Olla and Diablo formations, and the Canebrake Conglomerate is interbedded with the Diablo and Olla formations, we can not correlate the two units. Because of the interbedding of Canebrake Conglomerate with Pliocene Diablo and Olla formation lithologies near Yaqui Meadows and Harper Canyon, the conglomerate is roughly laterally equivalent to these formations (Fig. 2-8). We correlate the conglomerate exposed along Yaqui Ridge with the Pliocene Canebrake Conglomerate of the Palm Spring Group. Both the Canebrake Conglomerate and West

Butte conglomerate are coarse, basin-margin facies and appear to represent relatively continuous deposition in the proximal hanging wall of the West Salton detachment fault.

GROWTH FOLDING

Introduction

Folds are ubiquitous in the SW Salton Trough and most are ~1 Ma and younger (Dibblee, 1954, 1984, 1996; Lutz et al., in press; Kirby et al., in press; Chapter 3). Many of the mapped folds in the area are likely a result of Quaternary deformation related to the evolving San Felipe and San Jacinto strike-slip fault zones (Lutz, 2005; Kirby, 2005; Chapter 3). For example, the NW- to E-W-trending folds in the mylonite, the West Salton detachment fault, and Quaternary Ocotillo Formation in the Yaqui Ridge area are related to slip on the dextral-oblique San Felipe fault zone (Chapter 3).

Changes in thickness and progressive unconformities in older Pliocene-age basin-fill suggest that deformation and folding occured during deposition of these units. This older deformation was coeval with slip on the West Salton detachment fault and occurred in its hanging wall. We use subcrop and isopach maps (Fig. 2-15), and several growth cross sections (Fig. 2-16) to characterize these previously unrecognized older structures which have been overprinted by younger deformation. Up to several meters of basement paleotopography and buttress unconformities are documented in these units and can potentially affect sediment thickness. Although the overall effect of paleotopography is probably minor, we bracket thickness measurements between sedimentary units wherever possible.

To reconstruct the original trends of folds around Borrego Mountain, we use geological mapping, kinematic analyses, and cross sections to create a 2-D map-view palinspastic reconstruction (Fig. 2-15). Based on geological mapping we used a value of 1.6 km dextral separation on the SW strand of the Coyote Creek fault between East and Middle buttes of Borrego Mountain. We convert the ~550 m of dip-slip on the

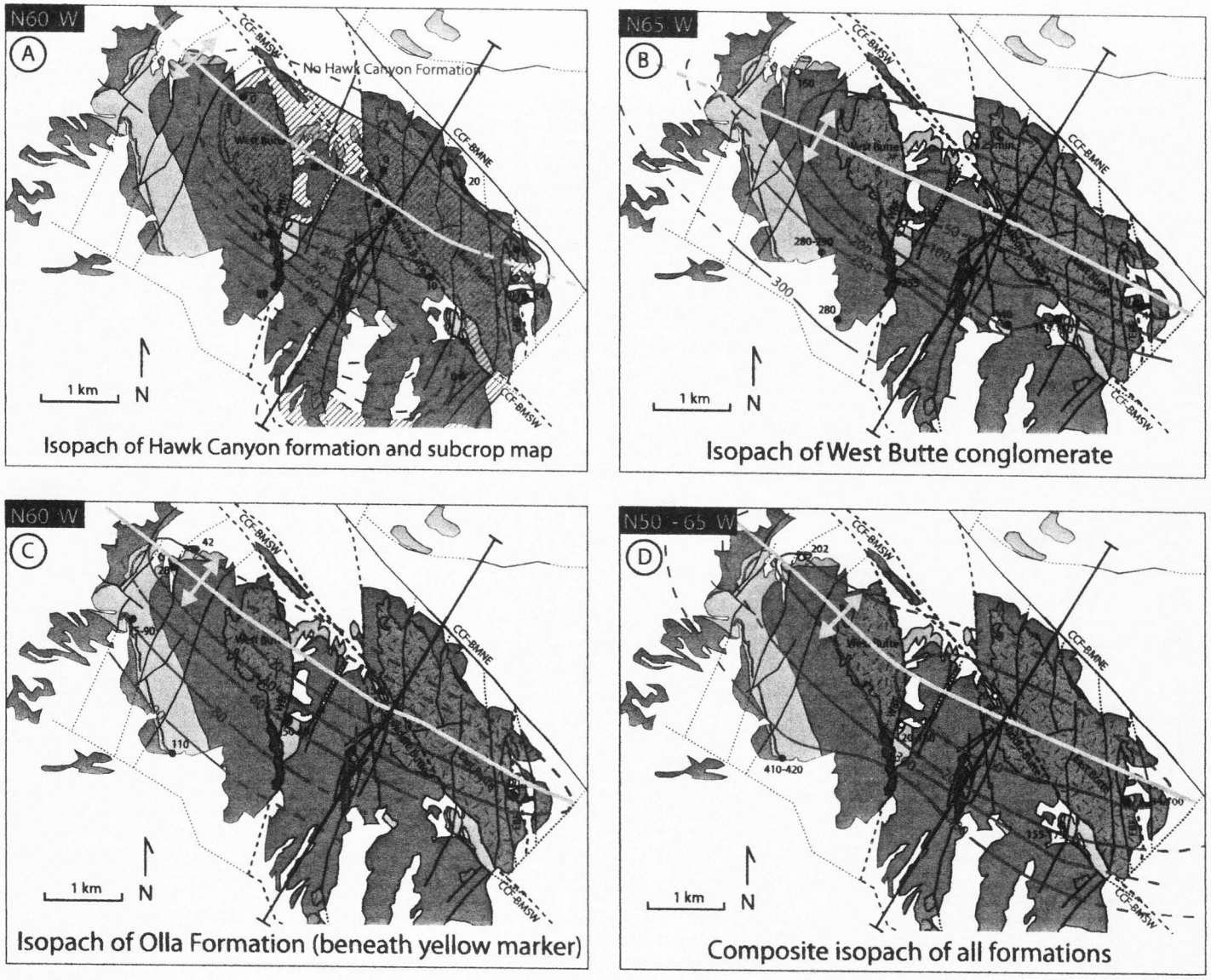
N60 W
A
No Hawk Canyon Formation
CCF-BMSW
CCF-BMNE
1 km
N
Isopach of Hawk Canyon formation and subcrop map
N65 W
B
CCF-BMSW
CCF-BMNE
150
280-290
300
280
1 km
N
Isopach of West Butte conglomerate
N60 W
C
CCF-BMSW
CCF-BMNE
42
90
110
1 km
N
Isopach of Olla Formation (beneath yellow marker)
N50 - 65 W
D
CCF-BMSW
CCF-BMNE
202
410-420
1 km
N
Composite isopach of all formations

Figure 2-15.

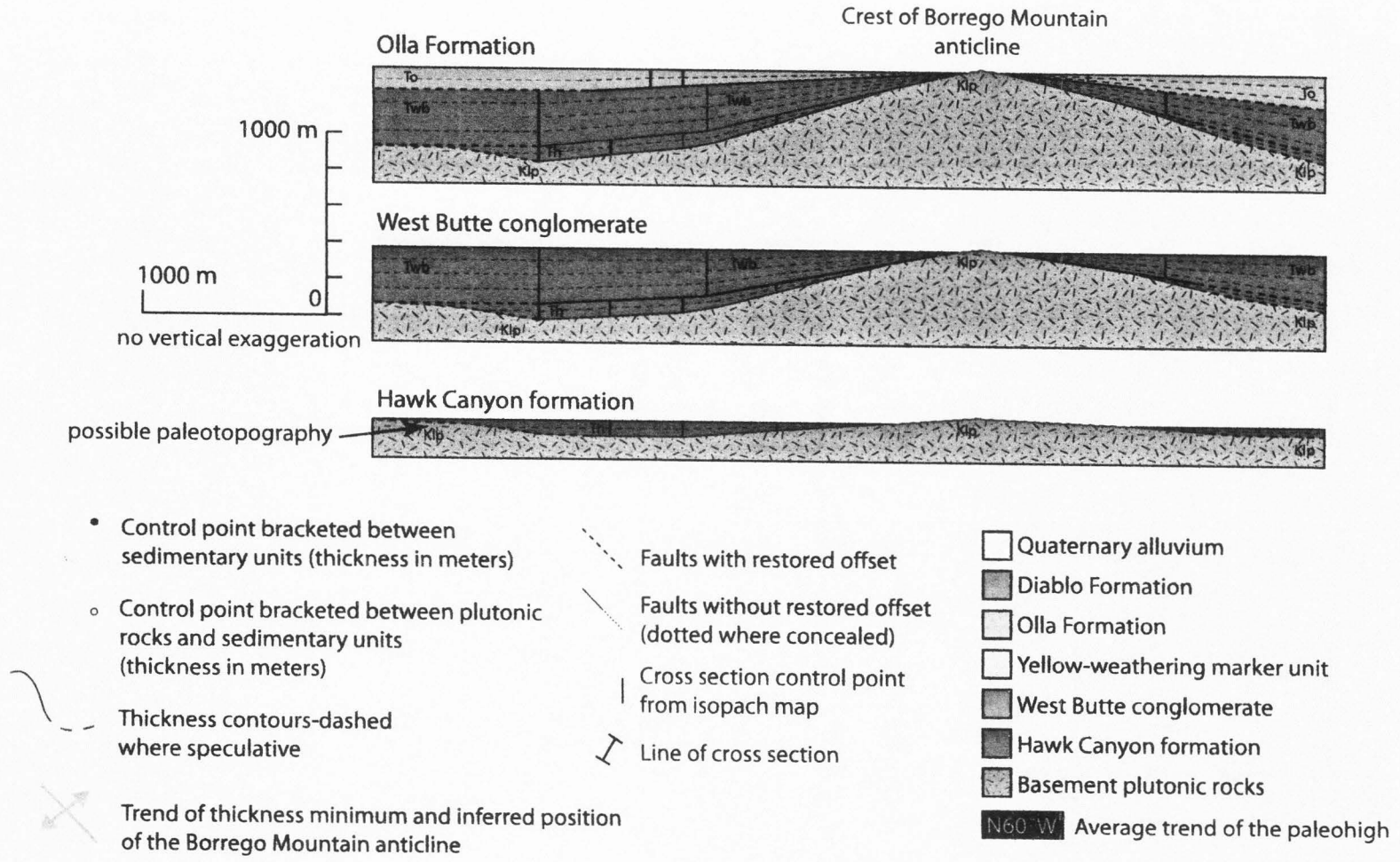

Figure 2-16. Growth cross sections at Borrego Mountain. Scale is same as Figure 2-15.

West Butte fault and ~400 m of dip-slip on the East Butte fault into 370 m and 270 m, respectively, of dextral map-view separation. Basin-fill thicknesses around Borrego Mountain were taken from measured sections (Plate 4), calculated from the map (Fig. 2-3 and Plate 1), or measured from cross sections (Plate 3), and were plotted on the restored map of the Borrego Mountain area (Fig. 2-15). Isopach maps were constructed for the Hawk Canyon formation, West Butte conglomerate, Olla Formation beneath the yellow-weathering marker bed, and all three units combined. A subcrop map of the Hawk Canyon formation was also constructed. A series of cross sections through the Borrego Mountain area were constructed for each isopach map and show the stratigraphic growth.

Thickness Patterns

Hawk Canyon formation

The subcrop map of the Hawk Canyon formation in general shows a W- to NW-trending area where the unit was not deposited or eroded off (Fig. 2-15A). An irregular lobe with no Hawk Canyon formation extends into the southern Borrego Mountain area and is difficult to interpret because of a lack of further outcrop. The isopach map of the Hawk Canyon formation is defined mostly by outcrops in Hawk Canyon and south of Middle Butte, with thicknesses ranging from 0 to 88 m. Overall thickness patterns show a ~N60°W trending paleohigh that trends through the center of the Borrego Mountain area (Fig. 2-15A). This pattern is consistent with SSE-ward thickening observed in measured sections in Hawk Canyon (Plate 4). Additionally, the sense of stratigraphic truncation beneath the West Butte conglomerate unconformity flips directions across the inferred paleohigh axis. The lack of Hawk Canyon formation south of Hawk Canyon inhibits interpretation of thickness patterns in that area. The subcrop map suggests that the underlying basement has significant erosional relief along the basement contact, because the complexity of paleohighs in this stage is not recorded in subsequent isopach maps (Fig. 2-15).

West Butte conglomerate

The isopach map of the West Butte conglomerate is constrained in 11 locations and ranges in thickness from 0 to ~290 m (Fig. 2-15B). Five of the measurements represent minimum thicknesses because they do not overlie Hawk Canyon formation and paleotopography may affect the true thickness of the unit. However, 6 measurements that show true stratigraphic thickness record ~240 m of growth so the influence of paleorelief on basement rocks is probably <40 m. Overall, the isopach shows a distinct ~N65°W trending paleohigh that trends through the Borrego Mountain area with dramatic thickening to the NE and SW (Fig. 2-15B). Although data are sparse, the gradient defined by the 250 m and 300 m contours is significantly less steep than all other gradients in this unit.

Olla Formation

Thicknesses for this isopach map are measured from the base of the Olla Formation to the base of the prominent yellow-weathering sandstone bed, constrained in 8 locations, and range from 0 to ~110 m thick. Seven of these locations are bracketed by sedimentary units and are not influenced by basement paleotopography. The trend of this paleohigh is well constrained by data points and trends ~N60°W through the Borrego Mountain area (Fig. 2-15C). The northeast side of the paleohigh is poorly constrained, but the significant thickness of Olla Formation across the Coyote Creek fault (Plate 1) suggests a similar or even steeper thickening across the NE flank of the paleohigh.

Composite isopach

This isopach map is a composite of the Hawk Canyon formation, West Butte conglomerate, and Olla Formation isopach maps (Fig. 2-15D). Total stratigraphic thicknesses are constrained in 7 locations and range from 0 to ~420 m. Only three of these locations contain all three formations. The map was constructed using the 7

measurements as control points and adding the isopach maps from the three separate formations. Although the trend of the paleohigh is less well constrained on the composite isopach map than it is on individual isopach maps, its N50°-65°W trend is consistent with individual unit isopach trends (Fig. 2-15).

Interpretation

All of the isopach maps consistently reveal a NW-trending paleohigh that we interpret as a Pliocene-age growth anticline, herein called the Borrego Mountain anticline (Fig. 2-16). This structure was active during deposition of the middle member of the Hawk Canyon formation, continued growing at least through deposition of the Olla Formation, and significantly affected the thickness of these units (Fig. 2-16). The Borrego Mountain anticline may have also been active during deposition of the Diablo Formation, but thickness patterns are difficult to interpret because a full section of Diablo Formation is not present NW of Borrego Mountain. In this area southwest of the Coyote Creek fault, the top of the Diablo Formation is covered, eroded, or faulted out.

The trend of the Borrego Mountain anticline varies from ~N50°W to N65°W, and the location of the anticlinal crest remained fixed during deposition of all three formations (Fig. 2-15). The composite isopach map shows that the Borrego Mountain anticline has a structural relief of ~420 m and is ~3.5 – 4 km-wide (Figs. 2-15 and 2-16). Although the NE side of the anticline is poorly constrained, the amplitude is at least 200 m and may be similar in magnitude to the SSW-dipping limb. The Borrego Mountain anticline is at least 7 km long according to the isopach maps (Fig. 2-15). A ~7 km-long, NW-trending gravity ridge may reflect the subsurface continuation of the structure northwest of Borrego Mountain (Fig. 2-17). There is no evidence for a SE continuation of the anticline in lower Borrego Valley on the gravity field (Fig. 2-17). Overall, these data show that the Borrego Mountain anticline is at least 7 km-long and may be up to 14 km-long.

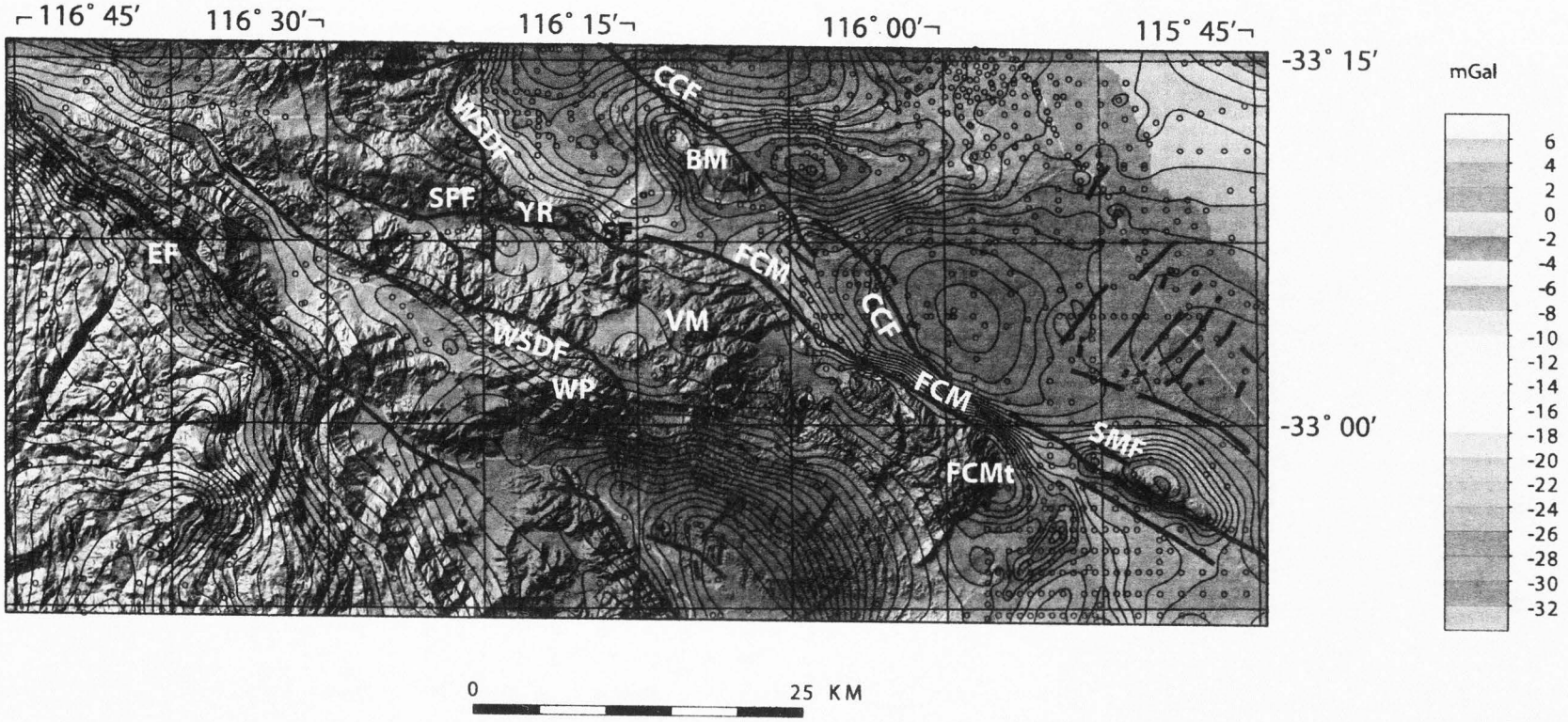

Figure 2-17. Filtered residual Bouger gravity anomaly in the SW Salton Trough. Some major faults are marked in red. Note the NW-trending gravity high near Borrego Mountain. This may be the subsurface expression of the basement-cored Borrego Mountain anticline. Also note that the gravity high does not continue SE of the Borrego Mountain area. BM-Borrego Mountain; CCF-Coyote Creek Fault; EF-Elisnore Fault; FCM-Fish Creek Mountain Fault; FCMt-Fish Creek Mountains; SFF-San Felipe Fault; SF-Sunset Fault; VM-Vallecito Mountains; YR-Yaqui Ridge. Figure provided courtesy of V. Langenheim.

DISCUSSION

Timing of Faulting and Basin-fill Deposits

We interpret the West Butte conglomerate as a late Miocene or early Pliocene basin margin deposit shed from the newly forming footwall of the West Salton detach,ent fault that is correlative with the Imperial Group (Fig. 2-13). This age assignment and lateral correlation are based on: 1) the similar stratigraphic position of the West Butte conglomerate and deposits of the Imperial Group deposits east of Borrego Mountain, 2) the presence of distinctive deformed and chloritically altered plutonic clasts in rare conglomerate beds at Squaw Peak that match the ubiquitous deformed and altered clasts in the West Butte conglomerate; 3) west-to-east lateral changes and decrease in grain size from pebbly sandstone and conglomerate at Borrego Mountain to locally-derived sandstone at Squaw Peak, to locally- and Colorado River-derived sandstone and mudstone in the Shell Reef area. Overall, the facies and grain size variations in the Tertiary section record late Miocene to early Pliocene progradation during deposition of the Imperial Group. This progradation was followed by a large transgression from Pliocene to early Pleistocene time during deposition of the Palm Spring Group (Fig. 2-8).

Five lines of evidence show that the West Salton detachment fault was active during deposition of the Hawk Canyon formation and West Butte conglomerate: 1) The Hawk Canyon formation and thick West Butte conglomerate are the first evidence in this area for creation of accommodation space in the hanging wall of the detachment fault. Local paleotopography around Borrego Mountain was submerged and buried, first beneath locally-derived sediment, then beneath voluminous sediment shed from the SSW. 2) The West Butte conglomerate shows a progressive unconformity across a persistent NW-trending basement-cored anticline. This anticline continued to be active during deposition of the syntectonic Olla Formation, and possibly also during deposition of the Diablo Formation. Because these units are clearly synkinematic to slip on the West Salton detachment fault (e.g. Axen and Fletcher, 1998; Kairouz, 2005; this study),

the growth of this anticline overlaps with the main phase of activity on the detachment fault and therefore documents deformation in the hanging wall during fault slip. 3) The composition of clasts in the West Butte conglomerate require a source in the footwall and damage zone of the West Salton detachment fault where no Cretaceous mylonite was exposed. 4) Paleocurrents in the West Butte conglomerate show a source to the SSW of Borrego Mountain, consistent with a location in the footwall of the West Salton detachment fault. 5) The West Butte conglomerate is very similar to the overlying and distinctly younger Canebrake Conglomerate of the Palm Spring Group. We confirm that the Canebrake Conglomerate is a syntectonic deposit of the West Salton detachment fault as suggested by Axen and Fletcher (1998).

Twenty to twenty five percent of clasts in the West Butte conglomerate are deformed and chloritically altered plutonic rocks (Fig. 2-11). These clasts suggest that the source area contained an extensive brittle to semi-brittle fault zone to provide such a large fraction of the clasts in this unit. Microscopic and macroscopic examination of these clasts, and samples from the damage zone in the hanging wall of the West Salton detachment fault, show that the clasts and the damage zone contain nearly identical deformation fabrics (Fig. 2-7). The semi-brittle textures in the clasts and the damage zone of the West Salton detachment fault indicate temperatures less than 300°-350° C during deformation (e.g. Scholz, 1988; White, 2001) and may have been ~200° C. Geologic constraints using the Eocene Poway conglomerate preserved in the footwall of the detachment fault indicate that the hanging wall of the West Salton detachment fault at Yaqui Ridge was buried less than ~1-2 km when deposition of the West Butte conglomerate began. At these depths it is implausible for the newly formed West Salton detachment fault to produce and expose the semi-brittle and incipient recrystallized quartz, undulose extinction, and pseudotachylite that we observe in clasts of the West Butte conglomerate. These deformation mechanisms indicate temperatures much higher than predicted along the detachment fault unless we infer very high geothermal gradients.

Three possibilities could explain the presence of semi-brittle fabrics in the now-eroded damage zone of the detachment fault that was exposed during deposition of the West Butte conglomerate. One explanation is that the West Salton detachment fault may have reactivated the inferred up-dip, semi-brittle extension of the Eastern Peninsular Ranges mylonite zone at Yaqui Ridge. This would imply that the West Salton detachment fault parallels the Eastern Peninsular Ranges mylonite zone at all structural levels in the Yaqui Ridge area. At shallow structural levels, represented by the hanging wall of the detachment fault and the clasts in the West Butte conglomerate, the semi-brittle segment of the Eastern Peninsular Ranges mylonite zone guided the younger, entirely brittle detachment fault and at deeper structural levels, the detachment overprinted purely ductile fabrics. However, field examination of semi-brittle deformation fabrics in the hanging wall of the detachment fault near Yaqui Ridge does not show any evidence for multiple cycles of deformation as predicted by this model.

A second explanation is that the West Salton detachment fault experienced an older period of activity with enough slip to expose the semi-brittle damage zone of the fault. In this model the deformed and altered clasts in the West Butte conglomerate were derived from the damage zone create during this older slip history. Our sedimentologic data in the San Felipe-Borrego sub-basin suggest a late Miocene – Pliocene creation of accommodation space, and recent thermochronologic data from the Yaqui Ridge area show that the onset of rapid cooling and exhumation also began between 4 – 8 Ma (Shirvell et al., 2005). The thermochronologic data allow a period of early slip on the detachment fault starting near ~12 Ma (Shirvell et al., 2005). Therefore it is not possible to rule out this explanation at this time.

A third explanation is that geothermal gradients high enough to create semi-brittle deformation fabrics at 1-2 km depths existed in the western Salton Trough during the late Miocene – Pliocene. Geothermal gradients as high as 200° C/km have been reported in the modern central Salton Trough (Lachenbruch et al., 1985). However, this third

possibility seems unlikely because the extensive hydrothermal alteration we would expect from such high geothermal gradients is not observed.

Our work shows that the West Butte conglomerate and the younger Canebrake Conglomerate of the Palm Spring Group share many lithologic and sedimentologic similarities despite the younger age of the Canebrake Conglomerate. The main sedimentologic differences between the two units are their thicknesses (Canebrake Conglomerate is at least twice as thick as the West Butte conglomerate), the greater variability in grain size of the Canebrake Conglomerate, and evidence for unroofing and exhumation of structurally deeper, more ductile parts of the footwall in the younger Canebrake Conglomerate. The unroofing sequence is evident by the first appearance of mylonite clasts (14%) in the Canebrake Conglomerate, and the greater proportion of deformed and chloritically altered plutonic rocks that show evidence for ductile deformation. We interpret the greater average grain size in the Canebrake Conglomerate as a result of its proximity to the West Salton detachment fault.

The composition and provenance of the Canebrake Conglomerate indicate a footwall source area, northward paleoflow, and the coarse conglomeratic nature of the unit show it is a syntectonic unit. The presence of an extensive footwall-derived megabreccia interbedded in the Palm Spring Group stratigraphically near the Canebrake Conglomerate suggest that creation of steep basin-margin topography in the footwall of the detachment fault continued during deposition of the Pliocene Palm Spring Group. The Yaqui Ridge megabreccia is interbedded high in the Diablo Formation and our provenance data show that it was derived from the footwall of the West Salton detachment fault. The outer limits of the preserved megabreccia coincide well with the farthest extent of the Canebrake Conglomerate (Fig. 2-14). If our correlation of the megabreccia across a 25 km by 8 km area is correct (~200 km^2), it represents a long run-out landslide that may be much larger than the well known Fish Creek and Split Mountain sturtzstroms, with 11 km and >5.4 km runout distances, respectively (Kerr and

Abbott, 1996; Rightmer and Abbott, 1996). Other smaller megabreccias interbedded in the Palm Spring Group have been noted previously east at Whale Peak (Hart, 1991; Kairouz, 2005), and in the SE Santa Rosa mountains (Pettinga, unpub mapping).

Geometry and Kinematics of the West Salton Detachment Fault

Analysis of map relationships and stereograms show that at Yaqui Ridge the brittle West Salton detachment fault has a strong inheritance and at map scale reactivates the older ductile Cretaceous Eastern Peninsular Ranges mylonite zone. The brittle detachment fault plane and ductile mylonite are generally parallel on both sides of the Yaqui Ridge anticline. Stretching lineations in the mylonite on the north limb of the Yaqui Ridge anticline average approximately 10 – 20° counterclockwise of the largest population of slickenlines on the detachment fault (Figs. 2-4 and 2-6). The similarities between foliation planes and fault planes is best explained by brittle reactivation of weaknesses along the pre-existing foliation planes, a process known as crustal inheritance (e.g. Beacon et al., 2001; Tavarnelli et al., 2001; Gray and Gregory, 2003).

The similarity of trends between stretching lineations in the mylonite and slickenlines on the brittle detachment fault is more difficult to explain. This similarity is seen in metamorphic core complexes and typically results from extreme extensional denudation, juxtaposing brittle hanging wall rocks on ductiley-deformed footwall rocks (e.g. Cemen et al., 2001; Davis et al., 2004). In these settings, both the brittle fault and ductile fabrics are extension-related; the ductile rocks form at depth early and are exhumed and overprinted by later brittle deformation. Because fabrics of the Eastern Peninsular Ranges mylonite zone are thrust-related and up to 90 Ma older than the extensional brittle fabrics of the West Salton detachment fault, the similar lineation and slickenline directions are not related to the same deformation episode. Corrugations in the Cretaceous mylonitic fabric may have controlled the extension direction during

younger reactivation, or the similar orientation of mylonitic lineation and brittle fault striae may be coincidental.

Because fault striae on the West Salton detachment fault at Yaqui Ridge have complicated patterns and exhibit nearly any orientation in the fault plane, they are difficult to interpret. There is a significant difference in the orientation of slickenlines between fault exposures on the present day SSW-dipping limb and the NNE-dipping limb of the Yaqui Ridge anticline, when the SSW-dipping limb is restored to its original NE dip (Fig. 2-6D). The fault on the SSW-dipping limb has a major concentration of slickenlines centered around a dip-slip orientation (trends ~NE when restored). This average is mostly absent from the fault on the NE limb, and only 17% of slickenlines from the fault on the NE limb overlap with part of the high-raking population of slickenlines from the fault on the restored SSW-dipping limb. The second major population of slickenlines from the fault on the SSW-dipping limb overlaps with the strong east-trending average from the fault on the NE limb.

There are several possible explanations for the increased proportion of dip-slip slickenlines on the detachment fault from the SSW-dipping limb of the Yaqui Ridge anticline compared to the detachment fault on the NE-dipping limb. Previous explanations all suggested that the detachment fault experienced early NE-directed slip followed by a change to ENE- and E-directed slip (Axen et al., 2004; Steely et al., 2004a). The formation of the Yaqui Ridge anticline was suggested to occur during slip on the detachment fault and deactivate the SSW-dipping limb (Axen et al., 2004). In this model, folding was followed by continued slip on the NE limb of the detachment fault with either a slow rotation of the slip vectors from NE to ESE, or an immediate change to E-directed slip with significant scatter (Axen et al., 2004; Steely et al., 2004a). Recent work (Chapter 3) shows that the antiformal geometry of Yaqui Ridge is actually the result of Pleistocene folding in an oblique contractional stepover between strands of the San Felipe fault and post dates slip on the detachment fault. Therefore we must investigate

new mechanisms for the formation of these slickenline patterns.

Prior to folding of the Yaqui Ridge anticline, the detachment fault and its mylonitic footwall probably had a NE to ENE dip similar to regional trends. The formation of a NW-trending antiform with SSW and NNE-dipping limbs from originally NE-dipping structural elements requires monoclinal folding that reoriented the now SSW-dipping limb to a much higher degree than the NE-dipping limb (Chapter 3). During folding, this model predicts that flexural slip perpendicular to the fold axis will occur along planes of weakness such as the West Salton detachment fault (Fig. 2-18).

We suggest that the different slickenline patterns from the detachment fault on opposing limbs of the Yaqui Ridge anticline were produced during flexural slip between the hanging wall and footwall of the West Salton detachment fault when it was folded into the Yaqui Ridge anticline (Fig. 2-18). The higher proportion of dip-slip slickenlines from the fault on the SSW-dipping limb of the Yaqui Rige anticline are approximately perpendicular to the trend of the anticline (Fig. 2-6B) and therefore the correct orientation for flexural slip. We suggest that the slickenlines produced during flexural slip overprinted slickenlines produced during slip on the detachment fault and biased observations of the older slip history on the fault from the SSW-dipping limb. The greater reorientation of the fault on the SSW-dipping limb compared to the fault on the NE-dipping limb may explain the greater proportion of "flexural" dip-slip slickenlines on the fault from the SSW-dipping limb.

Once we remove the slickenlines that may have been produced by flexural slip, the distribution of slickenlines from the detachment fault on the NE and SSW-dipping limbs of the Yaqui Ridge anticline is very similar. Both limbs record dominantly east-directed extension with an average rake of ~25° – 30° from the SE (Fig. 2-6D). Although the slickenlines are dispersed over 120° about this mean, the majority of the data are clustered within ~50° of the mean direction. We interpret these data as recording dominantly east-directed extension on the West Salton detachment fault at Yaqui Ridge

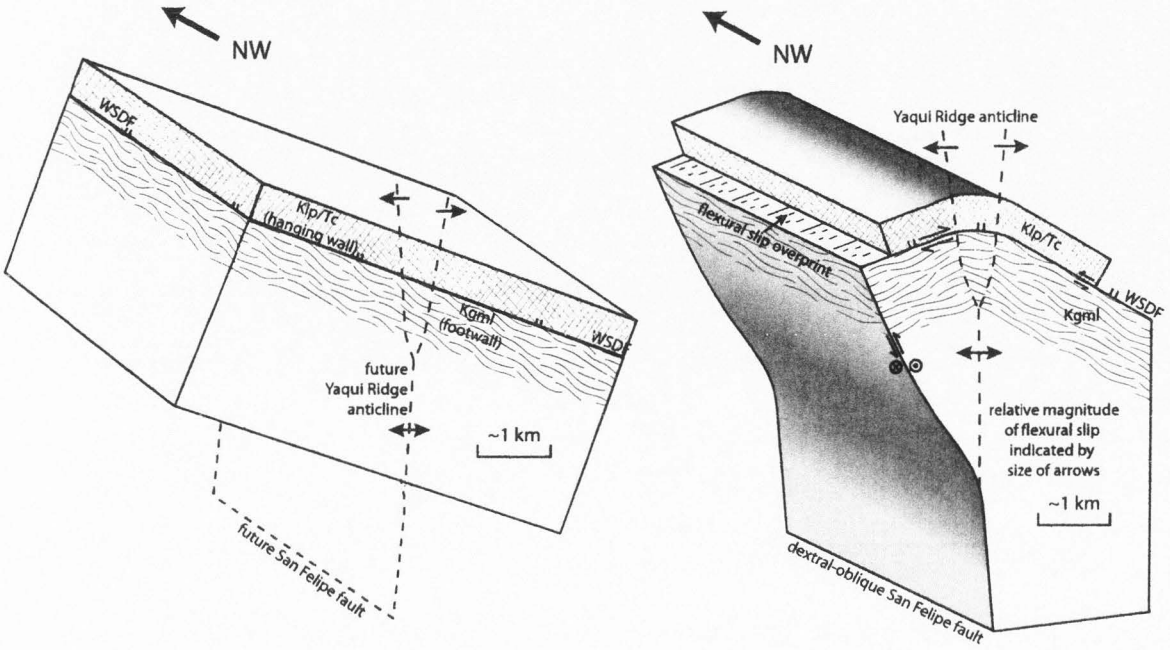

Figure 2-18. Schematic diagram showing the formation of slickenlines due to flexural slip between the hanging wall and footwall of the West Salton detachment fault during younger folding. Kgml-Cretaceous Granite Mountain-type diorite and granodiorite with a mylonitic fabric; Klp-Cretaceous La Posta-type tonalite; Tc-Pliocene Canebrake Conglomerate; WSDF-West Salton detachment fault.

with significant scatter about this average (Fig. 2-19).

At least three mechanisms could explain the scatter of slickenline orientations about an E-directed maximum on the West Salton detachment fault, and represent three end members of a complex spectrum. Vertical axis rotation of the hanging wall and footwall together, either clockwise or counter clockwise, with a constant direction of extension predicts a 'fanning' of slickenline orientations over time in the first model. In this model, early formed slickenlines would be progressively rotated and overprinted by younger slickenlines. If clockwise vertical axis rotation of rocks occurred, the detachment fault would now strike more clockwise than its original orientation before rotation began. Because the West Salton detachment fault at Yaqui Ridge already strikes WNW, restoring clockwise rotations would make the fault nearly perpendicular to regional trends. Therefore significant clockwise vertical axis rotation of the hanging wall and footwall seems unlikely in this area. The current strike of the detachment fault at Yaqui Ridge is slightly counterclockwise of regional trends and is consistent with some counterclockwise rotation. However, most other documented rotations in the area are clockwise (e.g. Johnson et al., 1983) and current data in the area are equivocal.

Changes in the direction of extension through time, without vertical axis rotation of rocks, also predict a "fanning" of slickenline orientations over time in the second model. In this model, early formed slickenlines would be overprinted by younger slickenlines that record a different direction of extension. The lack of cross-cutting slickenlines makes this model difficult to evaluate. Cross-cutting slickenlines may have formed but are no longer, or rarely preserved, or there may be no systematic changes in the direction of extension. Further work may help to eliminate or support this model.

Our third model, and preferred interpretation, requires no vertical axis rotations or changes in the direction of extension, but instead suggests that the dispersion of slickenline directions may be characteristic of low-angle oblique-slip faults. Therefore we suggest that the West Salton detachment fault experienced E-directed extension

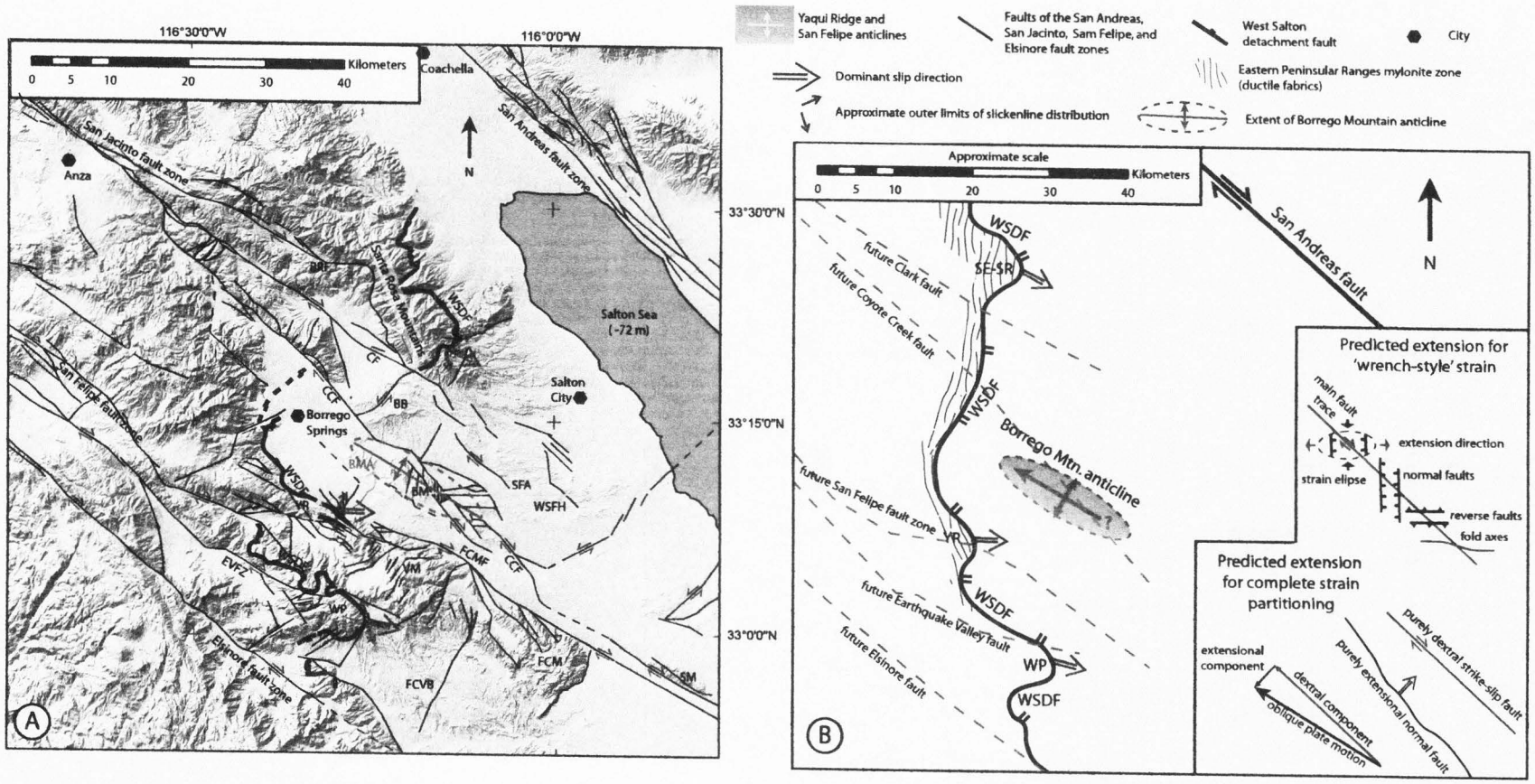
116°30'0"W
116°0'0"W
Kilometers
0 5 10 20 30 40
Coachella
Anza
San Jacinto fault zone
San Andreas fault zone
N
Salton Sea (-72 m)
Salton City
Borrego Springs
San Felipe fault zone
Santa Rosa Mountains
WSDF
CF
CCF
BB
BMA
BM
SFA
WSFH
FCMF
VM
EVFZ
WP
FCVB
FCM
SM
Elsinore fault zone
A
33°30'0"N
33°15'0"N
33°0'0"N
Yaqui Ridge and San Felipe anticlines
Faults of the San Andreas, San Jacinto, Sam Felipe, and Elsinore fault zones
West Salton detachment fault
City
Dominant slip direction
Eastern Peninsular Ranges mylonite zone (ductile fabrics)
Approximate outer limits of slickenline distribution
Extent of Borrego Mountain anticline
Approximate scale
Kilometers
0 5 10 20 30 40
WSDF
SE-SR
future Clark fault
future Coyote Creek fault
San Andreas fault
N
Borrego Mtn. anticline
future San Felipe fault zone
WP
future Earthquake Valley fault
future Elsinore fault
B
Predicted extension for 'wrench-style' strain
main fault trace
strain ellipse
extension direction
normal faults
reverse faults
fold axes
Predicted extension for complete strain partitioning
extensional component
dextral component
oblique plate motion
purely extensional normal fault
purely dextral strike-slip fault

Figure 2-19.

throughout its history and did not have a significant period of NE- or ESE-directed extension. Attitudes of slickenlines on low-angle normal faults are infrequently reported, although slickenline data from the Laguna Salada detachment fault ~80-150 km to the south show up to 90° of scatter about the average extension direction (Axen, 1995). Our data from the West Salton detachment fault at Yaqui Ridge, Whale Peak (Kairouz, 2005), the SE Santa Rosa segment of the detachment fault (Janecke, unpublished mapping) (Fig. 2-19), and data from Axen (1995) and Huerta and Rodgers (1996) all show that slickenlines on low-angle normal faults can be highly variable and that individual measurements often do not represent the overall slip direction. Structural studies along a low-angle strike-slip fault suggest that a near uniaxial strain field may produce this high dispersion of slickenline orientations (Huerta and Rodgers, 1996).

The West Salton detachment fault and San Andreas fault overlapped in activity and these two faults were suggested to partition the transtensional plate boundary strain (Axen and Fletcher, 1998). One implication of this hypothesis is that pure strike-slip occurred on the San Andreas fault while orthogonal NE-directed extension occurred on the West Salton detachment fault. Although our data confirm that the West Salton detachment fault was contemporaneous with the San Andreas fault, our data also show that the West Salton detachment fault at Yaqui Ridge is a low-angle dextral oblique-slip fault with dominantly E-directed extension (Fig. 2-6D), and is not a 'typical' detachment fault with top-to-the-NE dip-slip extension. East-west extension on north-striking normal faults is predicted by a "wrench-style" strain field along the San Andreas fault (Davis and Reynolds, 1996) (Fig. 2-19). We suggest that the West Salton detachment fault at Yaqui Ridge would have been a north-striking normal fault but instead was guided by and reactivated the Cretaceous mylonite zone. Therefore, east-directed extension occurred as predicted in the wrench model, and because of crustal inheritance the detachment fault has a WNW strike instead of a north strike at Yaqui Ridge, and the slip vectors were oblique to the strike of the fault in that location (Fig. 2-19). Recent work to the

north along the SE Santa Rosa segment of the West Salton detachment fault (Janecke, unpublished mapping), and to the south near Whale Peak (Kairouz, 2005) shows complicated patterns of slip with a strong ENE to ESE component. These slip directions are also consistent with a "wrench-style" model and together with our data at Yaqui Ridge suggest that complete strain partitioning did not occur along most of the West Salton detachment fault.

Growth Folding in the Hanging Wall of the West Salton Detachment Fault

Changes in thickness of basin-fill units and progressive unconformities at Borrego Mountain record growth of a large anticline in the hanging wall of the West Salton detachment fault during slip. The Borrego Mountain anticline was active during deposition of the middle member of the Hawk Canyon formation through the Olla Formation of the Palm Spring Group and possibly during deposition of the Diablo Formation (Fig. 2-15). The anticline has a trend of ~300° and created at least 420 m of structural relief across its flanks (Fig. 2-15). Basin-fill isopach maps show that the structure did not shift position during its evolution and was a full anticline, not just a monocline.

The spatial distribution of different facies in the Imperial Group in the San Felipe-Borrego subbasin reflect the influence of the Borrego Mountain anticline (Fig. 2-13). After palinspastic restoration of ~1.5-4 km on the Coyote Creek fault, the marine Imperial Group at Squaw Peak is separated from the fluvial West Butte conglomerate by ~ 2 km. Assuming that these rocks are correlative based on similar lithologies and stratigraphic positions, the ~2 km-wide abrupt change from fluvial to marine environments marks a narrow marine shoreline. The close spatial association of the northeast-dipping limb of the Borrego Mountain anticline and the shoreline is probably a result of the size and relief of the growth fold and suggests that the fold influenced the

paleogeography and stratigraphic architecture of the basin (Fig. 2-13).

The origin of the Borrego Mountain anticline is unclear. The trend of the anticline is similar to the strike of the detachment fault on the northeast side of Yaqui Ridge where the majority of slickenlines trend east. These data show that the Borrego Mountain anticline parallels the strike of the detachment fault, and is significantly oblique to the extension direction. Simple roll-over folds that form above normal faults are commonly monoclines and parallel the controlling fault during pure dip-slip (e.g. Janecke et al., 1998). Full anticlines can develop in these settings where ramp-flat geometries exist along the fault plane (Janecke et al., 1998), and as the hanging wall moves over these irregularities the axis of the anticline will migrate through the hanging wall toward the basin-bounding fault. Our data show that the Borrego Mountain anticline is significantly oblique to the slip direction and cannot be a simple roll-over monocline. The static location of the fold axis through time suggests that ramp-flat geometries also cannot explain its formation. Analogue modeling shows that transtensional folds rotate through time from alignment with the infinitesimal strain axis into parallelism with the finite stretching axis and extension direction (Venkat-Ramani and Tikoff, 2004). Because the WNW-trending Borrego Mountain anticline does not parallel the east-directed extension recorded on the West Salton detachment fault it is unlikely to have formed in this manner. Although its formation is poorly understood, it most likely formed as an originally E-W trending wrench fold that has since rotated into its present NW-trend.

CONCLUSIONS

We use geological mapping and structural and basin analyses to show that the West Salton detachment fault was active during the Pliocene in the western Salton Trough near Yaqui Ridge and may have initiated during the latest Miocene. Regionally the West Salton detachment fault strikes NNW, but at Yaqui Ridge it strikes anomolously NW to WNW. We show that crustal inheritance is important and that the West Salton

detachment fault reactivates the late Cretaceous reverse-sense Eastern Peninsular Ranges mylonite zone at map-scale. Slickenlines are dispersed nearly 180° in the detachment fault plane when the fault on the SSW-dipping limb of the younger Yaqui Ridge anticline is restored to its original NE dip. This observation is best explained by: 1) dominantly east-directed extension during slip on the detachment fault with significant dispersion of data about this mean; followed by 2) flexural slip between the hanging wall and footwall of the detachment fault during folding of the Pleistocene Yaqui Ridge anticline. The east-directed extension during slip on the detachment fault at Yaqui Ridge shows that in that location the fault is actually a low-angle dextral oblique-slip fault. The 50° – 90° dispersion about an east-directed average may be characteristic of the West Salton detachment fault throughout its length.

Dominantly east-directed extension is not predicted by complete strain partitioning between the West Salton detachment fault and the contemporaneous San Andreas fault. However, east directed extension on north-striking normal faults is predicted by a "wrench-style" model of structures along a NW-striking strike-slip fault (e.g. Christie-Blick and Biddle, 1985; Davis and Reynolds, 1996). We suggest that the West Salton detachment fault at Yaqui Ridge would have formed as a north-striking normal fault, but instead reactivated older, weaker fabrics that still permitted east-directed extension. Although there are complex patterns of slickenlines on the West Salton detachment fault, it is clearly not a simple detachment fault because its oblique slip produced an oblique hanging wall growth fold, its hanging wall is not internally extended by normal faults that sole into the detachment fault, and it co-evolved with the San Andreas fault to the east.

The Hawk Canyon formation is the basal deposit at Borrego Mountain and correlates with late Miocene-Pliocene marine deposits of the Imperial Group to the east near Squaw Peak and Shell Reef. The Pliocene West Butte conglomerate is a fluvial braid plain deposit that contains clasts of brittley to semi-brittley deformed and chloritically

altered fault rocks that were eroded from the damage zone of the West Salton detachment fault to the south of Borrego Mountain. We correlate the West Butte conglomerate to 'L-suite' marine rocks of the Pliocene Imperial Group east of Borrego Mountain. The West Butte conglomerate is >300 m thick and ties basin-fill deposits to activity on the West Salton detachment fault. The distinctly younger Canebrake Conglomerate of the Palm Spring Group is strikingly similar to the West Butte conglomerate in clast composition, source area, and depositional environment, and records deeper exhumation of the footwall of the West Salton detachment fault. The associated Yaqui Ridge megabreccia is a long run-out rockslide interbedded in the Palm Spring Group, may be ~200 km^2 in extent, and is the largest recorded megabreccia deposit in the SW Salton Trough. The conglomeratic deposits and the megabreccia document activity on the West Salton detachment fault and the creation of steep topography in the footwall of the detachment fault.

The late Miocene to Pliocene basin-fill deposits contain progressive unconformities, significant thickness changes, and record the growth of a large hanging wall growth fold. The Borrego Mountain anticline formed as a result of slip on the detachment fault, trends ~N60°W, and has at least 420 m of structural relief. The anticline was active from deposition of the middle member of the Hawk Canyon formation through at least the Olla Formation of the Palm Spring Group. The crest of the anticline remained fixed throughout deposition of these units and the northeast flank of the fold coincides with a narrow marine shoreline during deposition of the Pliocene Imperial Group. The Borrego Mountain anticline is not a simple roll-over monocline above a normal fault and ramp-flat geometries along the West Salton detachment fault also cannot explain its existence. Although its formation is poorly understood it most likely formed as an E-W-tending wrench fold and has since been rotated to its current NW-trend.

REFERENCES

Atwater, T., 1970, Implications of plate tectonics for the Cenozoic evolution of western North America. Geological Society of America Bulletin, v. 81, p. 3513-3536.

Atwater, T., 1989, Plate Tectonic history of the northeast Pacific and western North America, in Winterer, E.L., Hussong, D.M., and Decker, R.W., eds., The Eastern Pacific Ocean and Hawaii: Boulder, Colorado, Geological Society of America, The Geology of North America, v. N, p. 21-72.

Axen, G. J., 1995, Extensional segmentation of the main Gulf escarpment, Mexico and United States. Geology, v. 23, p. 515-518.

Axen, G.J., and Fletcher, J.M., 1998, Late Miocene-Pleistocene extensional faulting, northern Gulf of California, Mexico and Salton Trough, California. International Geology Review, v. 40, p. 217-244.

Axen, G.J., Kairouz, M., Steely, A.N., Janecke, S.U., and Dorsey, R.J., 2004, Structural expression of low-angle normal faults developed in wrench settings: an example from the West Salton detachment fault, southern California. Geological Society of America Abstracts with Programs, v. 36, no. 5, p. 548.

Beacom, L.E., Holdsworth, R.E., McCaffrey, K.J., and Anderson, T.B., 2001, A quantitative study of the influence of pre-existing compositional and fabric heterogeneities upon fracture-zone development during basement reactivation. In Holdsworth, R.E., Strachan, R.A., Magloughlin, J.F., Knipe, R.J., (eds.), The nature and tectonic significance of fault zone weakening. Geological Society of London Special Publication 186, p. 195-211.

Blair, T.C., and McPherson, J. G., 1994, Alluvial fans and their natural distinction from rivers based on morphology, hydraulic processes, sedimentary processes, and facies assemblages: Journal of Sedimentary Research, v. 64, no. 3, p. 450-489.

Carney S.M., and Janecke, S. U., 2005, Excision and the original low dip of the Miocene-Pliocene Bannock detachment system, SE Idaho: Northern cousin of the Sevier Desert detachment?: Geological Society of America Bulletin, v. 117, p. 334-353.

Cassiliano, M.L., 1998, Stratigraphic patterns and depositional environments in the Huesos Member (new lithostratigraphic unit) of the Palm Spring Formation of Southern California. Rocky Mountain Geology, v. 32, no. 2, p. 133-157.

Cemen, I., Isik, V., Tekeli, O., and Seytoglu, G., 2001, Extension parallel folding in northern Menderes Massif, western Turkey. Geological Society of America Abstracts with Programs, v. 33, no. 6, p. 151.

Christie-Blick, N., and Biddle, K.T., 1985, Deformation and basin formation along strike-slip faults, *in* Biddle, K.T., and Christie-Blick, N., eds., Strike-slip deformation, basin formation, and sedimentation. SEPM Special Publication 37, p. 1-34.

Clinkenbeard, J.P., and Walawender, M.J., 1989, Mineralology of the La Posta pluton: Implications for the origin of zoned plutons in the eastern Peninsular Ranges batholith, southern and Baja California. American Mineralogist, v. 74, p. 1258-1269.

Collinson, J.D., 1996, Alluvial sediments, *in* Reading, H. G., ed., Sedimentary Environments: Processes, Facies and Stratigraphy: London, Blackwell Science, p. 37-82.

Davis, G.A., and Reynolds, S.J., 1996, Strucutural Geology of Rocks and Regions. John Wiley and Sons, Inc.

Davis, G.H., Constentius, K.N., Dickinson, W.R., Rodriguez E.P., and Cox, L.J., 2004, Fault and fault-rock characteristics associated with Cenozoic extension and core-complex evolution in the Catalina-Rincon region, southeastern Arizona. Geological Society of America Bulletin, v. 116, no. 1-2, p. 128-141.

Dean, M.A., 1988, Genesis, mineralogy, and stratigraphy of the Neogene Fish Creek Gypsum, southwestern Salton Trough, California. [M.S. thesis]: San Diego State University, CA, 150 p.

DeMets, C., 1995, A reappraisal of seafloor spreading lineations in the Gulf of California: Implications for the transfer of Baja California to the Pacific plate and estimated of Pacific-North America motion. Geophysical Research Letters, v. 22, no. 4, p. 3545-3548.

Dibblee, T.W. Jr., 1954, Geology of the Imperial Valley Region, California, Geology of Southern California. California Division of Mines Bulletin 170, p. 21-28.

Dibblee, T.W. Jr., 1984, Stratigraphy and tectonics of the San Felipe Hills, Borrego Badlands, Superstition Hills, and vicinity. In: Rigsby, C.A., (ed.), 1984, The Imperial Basin-tectonics, sedimentation, and thermal aspects. Pacific Section S.E.P.M., p. 31-44.

Dibblee, T.W. Jr.,1996, Stratigraphy and tectonics of the Vallecito-Fish Creek Mountains, Vallecito Badlands, Coyote Mountain, and Yuha Desert, southwestern Imperial basin, *in* Abbott, P.L. and Seymour, D.C., eds., 1996, Sturtzstroms and detachment faults, Anza-Borrego Desert State Park, California. South Coast Geological Society Annual Field Trip Guide Book, no. 24, p. 59-79.

Dorsey, R. J., 2002, Stratigraphic record of Pleistocene initiation and slip on the

Coyote Creek fault, lower Coyote Creek, Southern California. *In:* Barth, A., ed., Contributions to Crustal Evolution of the Southwest United States: Boulder, Co. GSA Special Paper 365, p. 251-269.

Dorsey, R.J., 2005, Stratigraphy, tectonics, and basin evolution in the Anza-Borrego Desert region, *in* Jefferson, G.T. and Lindsay, L.E., eds., Fossil Treasures of Anza-Borrego Desert. Sunbelt Publications, San Diego, CA, p. 89-104.

Dorsey, R.J., and Janecke, S.U., 2002, Late Miocene to Pleistocene West Salton Detachment Fault System and Basin Evolution, Southern California: New Insights. Geological Society of America Abstracts with Programs, v. 34, no. 6, p. 248.

Dorsey, R. J., Janecke, S. U., Kirby, S., Axen, G., and Steely, A. N., 2004. Pliocene Lacustrine Transgression in the Western Salton Trough, Southern California: Implications for Regional Tectonics and Evolution of the Colorado River Delta. Geological Society of America Abstracts with Programs, v. 36, p. 317.

Dorsey, R.J., Janecke, S.U., Kirby, S.M., McDougall, K.A., and Steely, A.N., 2005a, Pliocene evolution of the lower Colorado River in the Salton Trough; tectonic controls on regional paleogeography and the regional Borrego Lake, *in* Marith C., ed., Geologic and biotic perspectives on late Cenozoic drainage history of the southwestern Great Basin and lower Colorado River region; conference abstracts. USGS Open-File Report 2005-1404, p. 13.

Dorsey, R.J., Fluette, A., McDougall, K., Housen, B.A., and Janecke, S.U., 2005b, Terminal Miocene arrival of Colorado River sand in the Salton Trough, Southern California: Implications for initiation of the lower Colorado River drainage. Geological Society of America Abstracts with Programs, v. 37, no. 7, p. 109.

Dorsey, R. J., Fluette, A. L., Housen, B. A., McDougall, K. A., Janecke, S. U., Axen, G. J., Shirvell, C., 2006, Chronology of Late Miocene to Early Pliocene Sedimentation at Split Mt. Gorge, Western Salton Trough: Implications for Development of the Pacific-North America Plate: Abstracts for NSF MARGINS program, Workshop on Rupturing of Continental Lithosphere. Ensenada Mexico, January 9-13. http://rcl-cortez.wustl.edu/Workshop_Abstracts.pdf p. 23-24

Durham, J.W., and Allison, E.C., 1960, The geologic history of Baja California and its marine faunas, *in* Geologic history, Pt. 1, of Symposium, the Biostratigraphy of Baja California and adjacent seas. Systematic Zoology, v. 9, p. 47-91.

Engel, A.E.J., and Schultejann, P.A., 1984, Late Mesozoic and Cenozoic tectonic history of south central California. Tectonics, v. 3, p. 659-675.

Erskine, B.G., and Wenk, H.R., 1985, Evidence for Late Cretaceous crustal thinning in

the Santa Rosa mylonite zone, southern California. Geology, v. 13, p. 274-277.

Fedo, C.M., and Miller, J.M.F., 1992, Evolution of a Miocene half-graben basin, Colorado River extensional corridor, southeastern California: American Association of Petroleum Geologists Bulletin, v. 104, p. 481-493.

Fletcher, J.M., Martin-Atienza, B., Axen, G.J., Gonzalez, A., Hollbrook, W.S., Kent, G., Lizzarralde, D., Harding, A., and Umhoefer, P., 2004, Relative magnitudes of seafloor spreading and continental rifting across the Gulf of California: An example of orogen-scale strain compatibility. Geological Society of America Abstracts with Programs, v. 36, no. 5, p. 317.

Fowler, T.K., Jr., Friedmann, S.J., Davis, G.A., and Bishop, K.M., 1995, Two-phase evolution of the Shadow Valley Basin, southeastern California: A possible record of footwall uplift during extensional detachment faulting: Basin Research, v. 7, p. 165-179.

Friedmann, S. J, and Burbank, D. W., 1995, Rift basin and supradetachment basins: intracontinental extensional end-members; Basin Research, v. 7, p. 109-127.

Friedmann, S. J., Davis, G. A., and Fowler, T. K., 1996, Geometry, paleodrainage, and geologic rates from the Miocene Shadow Valley supradetachment basin, eastern Mojave Desert, California., *in* Beratan, K. K., ed., Reconstructing the History of Basin and Range Extension Using Sedimentology and Stratigraphy, Geological Society of America Special Paper 303, p. 85-106.

Frost, E.G., and Shafiqullah, M., 1989, Pre-San Andreas opening of the Salton Trough as an extensional basin: K-Ar ages on regional detachment faults along the western margin of the Salton Trough. Geological Society of America Abstracts with Programs, v. 21, no. 5, p. 81.

Frost, E. G., Fattahipour, M. J., and Robinson, K. L., 1996, Neogene detachment and strike-slip faulting in the Salton Trough region and their geometric and genetic interrelationships, *in* Abbott, P. L., and Cooper, J. D., eds., Field conference guidebook and volume for the annual convention, San Diego, California, May, 1996. Bakersfield, California, Pacific Section, American Association of Petroleum Geologists, p. 263-294.

Fuis, G.S., and Kohler, W.M., 1984, Crustal structure and tectonics of the Imperial Valley region, California, *in* Rigsby, C.A., ed., The Imperial basin-Tectonics, sedimentation, and thermal aspects: Pacific Section, S.E.P.M., p. 1-13.

Gastil, R.G., 1975, Plutonic zones in the Peninsular Ranges of southern California and northern Baja California: Geology, v. 3, p. 361-363.

Gastil, R.G., 1983, Mesozoic and Cenozoic granitic rocks of southern California and western Mexico: Boulder, Colorado, Geological Society of America Memoir 159, p. 265-275.

Gastil, R.G., 1993, Prebatholithic history of peninsular California, in Gastil, R.G., and Miller, R.H., eds., The prebatholithic stratigraphy of peninsular California: Boulder, Colorado, Geological Society of America Special Paper 279, p. 145-156.

Gastil, R.G., Phillips, R.P., and Allison, E.C., 1975, Reconaissance geology of the state of Baja California. Geological Society of America Memoir, v. 140, p. 170.

Gastil, R.G., and Miller, R.H., 1984, Prebatholithic paleogeography of peninsular California and adjacent Mexico, *in* Frizzell, A., Jr., ed., Geology of Baja California peninsula: Los Angeles, California, Society of Economic Paleontologists and Mineralogists Pacific Section, v. 39, p. 9-16.

Gastil, G., Kimbrough, J., Shimizu, M., Tainosho, Y., and Gunn, S., 1991, Plutons of the eastern Peninsular Ranges, southern California, USA and Baja California, Mexico, *in* Walawender, M.J., and Hanan, B.B., eds., Geological excursions in southern California. Guidebook 1991 Annual Meeting Geological Society of America, San Diego, California, p. 319-331.

George, P. G., and Dokka, R. K., 1994, Major late Cretaceous cooling events in the eastern Peninsular Ranges, California, and their implications for Cordilleran tectonics. Geological Society of America Bulletin, v. 106, p. 903-914.

Gray, D.R., and Gregory, R.T., 2003, Fault geometry as evidence for inversion of a former rift basin in the eastern Lachlan Orogen. Australian Journal of Earth Sciences, v. 50, no. 4, p. 513-523.

Grove, M., Lovera, O., and Harrison, M., 2003, Late Cretaceous cooling of the east-central Peninsular Ranges batholith (33N): Relationship to La Posta pluton emplacement, Laramide shallow subduction, and forearc sedimentation, in Scott, J.E., Scott, P.R., Fletcher, J.M., Girty, G.H., Kimbrough, D.L., and Martin-Barajas, A, (eds), Tectonic evolution of northwestern Mexico and Southwestern USA, Geological Society of America Special Paper 374, p. 355-379.

Hart, M.W., 1991, Landslides in the Peninsular Ranges, southern California, *in* Walawender, M.J., and Hanan, B.B., eds., Geological excursions in southern California. Guidebook 1991 Annual Meeting Geological Society of America, San Diego, California, p. 297-312.

Herzig, C., Carrasco, A., Schar, T., Murray, G., Rightmer, D., Lawerence, J., Milton, Q.,

Wirths, T., 1995, Neogene stratigraphy of the Borrego Mountain area, Anza-Borrego Desert State Park, California, *in* Remeika, P., and Sturz, A., eds., Paleontology and geology of the western Salton Trough detachment, Anza-Borrego Desert State Park, California. Field trip guidebook and volume for the 1995 San Diego Assoc. of Geologist's field trip to Anza-Borrego Desert State Park. Volume 1, p. 133-136.

Hudnut, K. W., Seeber, L., Pacheco, J., Armbruster, J. G., Sykes, L. R., Bond, G. C., Kominz, M. A., 1989, Cross faults and block rotation in Southern California; earthquake triggering and strain distribution, Yearbook Lamont –Doherty Geological Observatory of Columbia University, p. 44-49.

Huerta, A.D., and Rodgers, D.W., 1996, Kinematic and dynamic analysis of a low-angle strike-slip fault: the Lake Creek fault of south-central Idaho. Journal of Structural Geology, v. 18, no. 5, p. 585-593.

Jahns, R.H., 1954, Geology of southern California. California Division of Mines and Geology Bulletin, v. 170, no. 1-2, pp. 878.

Janecke, S. U., McIntosh, W., and Good, S., 1999, Testing models of rift basins; structure and stratigraphy of an Eocene-Oligocene supradetachment basin, Muddy Creek half graben, southwest Montana. Basin Research, v. 11, p. 143-165.

Janecke, S. U., Vandenburg, C. J., and Blankenau, J. J., 1998, Geometry, mechanisms and significance of extensional folds from examples in the Rocky Mountain Basin and Range Province, U.S.A. Journal of Structural Geology, v. 20, p. 841-856.

Janecke, S.U., Carney, S.M., Perkins, M.E., Evans, J.C., Link, P.K., Oaks, R.Q., Jr., and Nash, B.P., 2003, Late Miocene-Pliocene detachment faulting and Pliocene-Pleistocene Basin-and-Range extension inferred from dismembered rift basins of the Salt Lake Formation, southeast Idaho, *in* Raynolds, R., and Flores, R., eds., Cenozoic Paleogeography of the Rocky Mountains: SEPM Special Publication, p. 369-406.

Janecke, S.U., Kirby, S.M., Langenheim, V.E., Housen, B., Dorsey, R.J., Crippen, R.E., Blom, R.G., 2004, Kinematics and evolution of the San Jacinto fault zone in the Salton Trough: Progress report from the San Felipe Hills area. Geological Society of America Abstracts with Programs, v. 36, no. 5, p. 317.

Janecke, S.U., Kirby, S.M., Langenheim, V., Steely, A.N., Dorsey, R., Housen, B., and Lutz, A., 2005, High geologic slip rates on the San Jacinto fault zone in the SW Salton Trough, and possible near-surface slip defecit in sedimentary basins. Geological Society of America Abstracts with Programs, v. 37, no. 7, p. 275

Jefferson, G.T., 1999, A late Miocene terrestrial vertebrate assemblage from Anza-Borrego Desert State Park, *in* Reynolds, R.E., ed., The 1999 Desert Research

Symposium Abstracts, San Bernardino County Museum Association Quarterly v. 46, no. 3. p. 109-111.

Jefferson, G.T, and Peterson, D., 1998, Hydrothermal origin of the Fish Creek Gypsum, Imperial County, southern California, in Lindsay, L., and Hample, W.G., eds.,

Jennings, C.W., 1977, Geologic map of California. California Division of Mines and Geology, Sacramento, CA.

Johnson, no.M., Officer, C.B., Opdyke, no.D., Woodard, G.D., Zeitler, P.K., and Lindsay, E.H., 1983, rates of late Cenozoic tectonism in the Vallecito-Fish Creek basin, western Imperial Valley, California. Geology, v. 11, p. 664-667.

Kairouz, M.E., 2005, Geology of the Whale Peak Region of the Vallecito Mountains: Emphasis on the Kinematics and Timing of the West Salton Detachment fault, Southern California, [M.S. Thesis]: University of California, Los Angeles. 156 p.

Kerr, D.R., 1984, Early Neogene continental sedimentation in the Vallecito and Fish Creek mountains, western Salton Trough, California. Sedimentary Geology, v. 38, p. 217-246.

Kerr, D.R., and Kidwell, S.M., 1991, Late Cenozoic sedimentation and tectonics, western Salton Trough, California, *in* Walawender, M.J., and Hanan, B.B., eds., Geological excursions in southern California. Guidebook 1991 Annual Meeting Geological Society of America, San Diego, California, p. 397-416b.

Kerr, D.R. and P.L. Abbott, 1996. Miocene suberial sturzstrom deposits, Split Mountain, Anza-Borrego Desert State Park, *in* Abbott, P., and Seymour, D., eds., Sturzstroms and Detachment Faults Anza-Borrego Desert State Park California: South Coast Geological Society Annual Field Trip Guide Book v. 24, p. 149-163.

Kimbrough, D.L., Smith, D.P., Mahoney, J.B., Moore, T.E., Grove, M., Gastil, R.G., Ortega-Rivera, A., 2001, Forearc-basin sedimentary response to rapid Late Cretaceous batholithemplacement in the Peninsular Ranges of Southern and Baja California, Geology, v. 29, p. 491-494.

Kirby, S.M., 2005, The Quaternary tectonic and structural evolution of the San Felipe Hills, California, [M.S. Thesis]: Logan, Utah State University, 182 p.

Kirby, S.M., Janecke, S.U., Dorsey, R.J., and Layman, E.B., 2004a, Reorganization of the San Jacinto fault zone at 1 Ma: Evidence from syntectonic deposits in the San Felipe Hills, western Salton Trough, CA. Geological Society of America Abstracts with Programs, v. 36, no. 4, p. 37.

Kirby, S.M., Janecke, S.U., Dorsey, R.J., and Housen, B., 2004b, A 1.07 Ma change from persistent lakes to intermittent flooding and desiccation in the San Felipe Hills, Salton Trough, southern California. Geological Society of America Abstracts with Programs, v. 36, no. 5, p. 318.

Kirby, S. M., Janecke, S. U., Dorsey, R. J., Housen, B. A., McDougall, K., and Steely, A. in press, Pleistocene Brawley and Ocotillo formations: Evidence for initial strike-slip deformation along the San Felipe and San Jacinto fault zones, California: Journal of Geology. 21 p. accepted July 2006.

Lachenbruch, A.H., Sass, J.H., and Galanis, S.P., 1985, Heat flow in southernmost California and the origin of the Salton Trough. Journal of Geophysical Research, v. 90, no. B8, p. 6709-6736.

Langenheim, V. E., and Jachens, R. C. 1993. Isostatic residual gravity map of the Borrego Valley 1:100,000-scale quadrangle, California. U.S. Geological Survey Open-File Report 93-246, scale 1:100,000.

Langenheim, V.E., and Jachens, R.C., 2003, Crustal Structure of the Peninsular Ranges Batholith from Magnetic Data: Implications for Gulf of California Rifting: Geophysical Research Letters, v. 30, no. 11, 1597, doi:10.1029/2003GL017159.

Lonsdale, P., 1989, Geology and tectonic history of the Gulf of California, in Winterer, E.L., Hussong, D.M., and Decker, R.W., eds., The Eastern Pacific Ocean and Hawaii: Boulder, Colorado, Geological Society of America, The Geology of North America, v. N, p. 499-520.

Lonsdale, P., 1991, Structural patterns of the Pacific floor offshore of Peninsular California, *in* Dauphin, J.P., and Simoneit, B.T., eds., The Gulf and peninsular provinces of the Californias. Tulsa, OK, Amer. Assoc. Petrol. Geol. Memoir, v. 47, p. 87-125.

Lough, C. F., 1993, Structural evolution of the Vallecito Mountains, Colorado Desert and Salton Trough Geology, San Diego, California, San Diego Association of Geologists, p. 91-109.

Lough, C. F., 1998, Detachment faulting around Borrego Valley, *in* Lindsay, L., and Hample, W.G., eds., Geology and geothermal resources of the Imperial and Mexicali Valleys: San Diego Association of Geologists, San Diego, California, p. 40-51.

Lutz, A.T., 2005, Tectonic controls on Pleistocene basin evolution in the central San Jacinto fault zone, southern California, [M.S. thesis]: Eugene, University of Oregon, 136 p.

Lutz, A.T., and Dorsey, R.J., 2003, Stratigraphy of the Pleistocene Ocotillo Conglomerate, Borrego Badlands, southern California: Basinal response to evolution of the San Jacinto fault zone. Geological Society of America Abstracts with Programs, v. 35, No. 6, p. 248.

Lutz, A.T., Dorsey, R.J., Housen, B.A,, and Janecke, S.U., in press, Stratigraphic record of Pleistocene faulting and basin evolution in the Borrego Badlands,San Jacinto fault zone, southern California. Geological Society of America Bulletin.

Mancktelow, N.S., and Pavlis, T.L., 1994, Fold-fault relationships in low-angle detachment systems. Tectonics, v. 13, no. 2, p. 668-685.

Morton, D. M., and Matti, J. C., 1993, Extension and contraction in an evolving divergent strike-slip fault complex: the San Andreas and San Jacinto fault zones at their convergence in Southern California, *in* Powell, R. E., Weldon, R. J., and Matti, J. C., eds., The San Andreas fault system: displacement, palinspastic reconstruction, and geologic evolution: Geological Society of America Memoir, v. 178, p. 217-230.

Merriam, R., and Bandy, O. L., 1965, Source of upper Cenozoic sediments in the Colorado delta region. Journal of Sedimentary Petrology, v. 35, p. 911-916.

Miall, A.D., 1996, The geology of fluvial deposits: Sedimentary facies, basin analysis, and petroleum geology: Berlin, Springer-Verlag, 582 p.

Morley, E. R., 1963, Geology of the Borrego Mountain Quadrangle and the western portion of the Shell Reef Quadrangle, San Diego County, California, [M.S. Thesis]: University of Southern California, Los Angeles, California, 138 p.

Nagy, E.A., and Stock, J.M., 2000, Structural controls on the continent-ocean transition in the northern Gulf of California. Journal of Geophysical Research, v. 105, no. B7, p. 16251-16269.

Nicholson, C., Williams, P., Seeber, L., and Sykes, L.R., 1985, Seismicity and fault kinematics along the Brawley seismic zone and adjacent regions. EOS, Transactions, American Geophysical Union. 66. v. 46, p. 953.

Oskin, M., and Stock, J., 2003, Marine incursion synchronous with plate-boundary localization in the Gulf of California: Geology, v. 1, p. 23-26.

Pappajohn, S., 1980, Description of Neogene marine section at Split Mountain, easternmost San Diego County, California, [MS Thesis]: San Diego State University 72 p.

Powell, C.L., II, 1986, Stratigraphy and bivalve molluscan paleontology of the Neogene

Imperial Formation in Riverside County, California, [M.S. Thesis]: California State University, San Jose, 275 p.

Quinn, H.A., and Cronin, T.M., 1984, Micro-paleontology and depositional environments of the Imperial and Palm Spring Formations, Imperial Valley, California, *in* Rigsby, C.A., ed., Imperial Basin, Tectonics, Sedimentation and Thermal Aspects: Society of Economic Paleontologists and Mineralogists v. 40, p. 71-85.

Reitz, D. T., 1977, Geology of the western and central San Felipe Hills, northwestern Imperial County, California, [MS thesis]: University of Southern California, Los Angeles, California, 155 p.

Rightmer, D.A., and Abbott, P.L., 1996, The Pliocene Fish Creek sturzstrom, Anza-Borrego Desert State Park, southern California, *in* Abbott, P. L., and Seymour, D. C., eds., Sturzstroms and Detachment Faults, Anza-Borrego Desert State Park, California. South Coast Geological Society Annual Field Trip Guide Book, no. 24, p. 165-184.

Ruisaard, C.I. 1979. Stratigraphy of the Miocene Alverson Formation, Imperial County, California, [MS Thesis]: San Diego State University, California 125 p.

Rust, B.R., and Koster, E.H., 1984, Coarse alluvial deposits, *in* Walker, R. G., ed., Facies Models: Toronto, Geological Society of Canada.

Schlische, R.W., 1995, Geometry and origin of fault-related folds in extensional settings. AAPG Bulletin, v. 79, p. 1661-1678.

Scholz, C.H., 1988, The brittle-plastic transition and the depth of seismic faulting. International Journal of Earth Science, V. 77, no. 1, p. 319-328.

Schultejahn, P.A., 1984, The Yaqui ridge antiform and detachment fault: Mid-Cenozoic extensional terrane west of the San Andreas fault. Tectonics, v. 3, no. 6, p. 677-691.

Sharp, R. V., 1967, San Jacinto fault zone in the Peninsular Ranges of southern California. Geological Society of America Bulletin, v. 78, p. 705-730.

Sharp, R.V., 1979, Some characteristics of the eastern Peninsular Ranges mylonite zone, in Proc. Conf. VIII: Analysis of actual fault zones in bedrock. United State Geological Survey Open File Report 79-1239, p. 258-267.

Sherlock, S.C., Watts, L.M., Holdsworth, R.E., and Roberts, D., 2004, Dating fault reactivation by Ar/Ar lasterprobe: and alternative view of apparently cogenetic mylonite-pseudotachylite assemblages. Journal of the Geological Society, v. 161, no. 3, p. 335-338.

Shirvell, C.R., Axen, G.J., and Stockli, D.F., 2005, Pliocene (U-Th)/He cooling ages from the West Salton detachment system (WSDS), Salton Trough. Geological Society of America Abstracts with Programs, v. 37, no. 7, p. 274.

Shreve, R.L., 1994, The Blackhawk landslide, southwestern San Bernardino County, California, *in* Murbach, D., and Baldwin, J., eds., Annual Field Trip Guidebook, South Coast Geological Society, v. 22, p. 432-438.

Silver, L.T., Taylor, H.P., and Chappell, B., 1979, Some petrological, geochemical, and geochronological observations of the Peninsular Ranges batholith near the international border of the U.S.A. and Mexico, *in* Abbott, P.L., and Todd, V.R., eds., Mesozoic crystalliune rocks – Peninsular Ranges batholith and pegmatites, Point Sal Ophiolite. Guidebook of the Geological Society of America Annual Meeting, San Diego State University, San Diego, CA, p. 177-231

Simpson, C., 1984, Borrego Springs-Santa Rosa mylonite zone: A Late Cretaceous west-directed thrust in southern California. Geology, v. 12, p. 8-11.

Smith, D.D., 1962, Geology of the northeast quarter of the Carrizo Mountain quadrangle, California. M.A. Thesis, University of Southern California, Los Angeles. 89 pp.

Spencer, J.E., and Normark, W.R., 1979, Tosco-Abreojos fault zone: A Neogene transform plate boundary in the Pacific margin of southern Baja California, Mexico. Geology, v. 7, p. 554-557.

Steely, A.N., 2003, Structural geology and stratigraphy of the Borrego Mountain area, southern California: Implications for late Cenozoic tectonic evolution of the western Salton Trough, [Undergraduate thesis]: Eugene, University of Oregon, 77 p.

Steely, A.N., Janecke, S.U., Dorsey, R.J., and Axen, G.J., 2004a, Evidence for late Miocene-Quaternary low-angle oblique slip faulting on the West Salton detachment fault, southern California. Geological Society of America Abstracts with Programs, v. 36, no. 4, p. 37.

Steely, A.N., Janecke, S.U., and Dorsey, R.J., 2004b, Evidence for syn-depositional folding of Imperial-age synrift deposits above the West Salton detachment fault, Borrego Mountain area, southern California. Geological Society of America Abstracts with Programs, v. 36, no. 5, p. 317.

Steely, A.N., Janecke, S.U., Axen, G.J., and Dorsey, R.J., 2005a, Pleistocene (~1 Ma) transition from West Salton detachment faulting to cross-cutting dextral strike-slip faults in the SW Salton Trough. Geological Society of America Abstracts with Programs, v. 37, no. 7, p. 274.

Steely, A.N., Janecke, S.U., Long, S.P., Carney, S.M., Oaks Jr., R.Q., Langenheim, V.E., and Link, P.K., 2005b, Evolution of a late Cenozoic supradetachment basin above a flat-on-flat detachment with a folded lateral ramp, SE Idaho, *in* Pederson, J., and Dehler, C.M., *eds*., Geological Society of America Field Guide 6, p. 169-198.

Stinson, A. L., and Gastil, R. G., 1996, Mid- to Late-Tertiary detachment faulting in the Pinyon Mountains, San Diego County, California: A setting for long run-out landslides in the Split Mountain Gorge area, *in* Abbott, P. L., and Seymour, D. C., eds., Sturtzstrums and Detachment Faults, Anza-Borrego Desert State Park, California, Santa Ana, California, South Coast Geological Society, p. 221-244.

Stock, J.M., and Hodges, K.V., 1989, Pre-Pliocene extension around the Gulf of California and the transfer of Baja California to the Pacific plate. Tectonics, v. 8, p. 99-115.

Tarbet, L.A., and Holman, W.H., 1944, Stratigraphy and micropaleontology of the west side of the Imperial Valley, California. American Association of Petroleum Geology Abstracts, v. 28, p. 1781-1782.

Tavarnelli, E., Decandia, F.A., Renda, P., Tramutoli, M., Gueguen, E., and Alberti, M., 2001, Repeated reactivation in the Apennine-Maghrebide system, Italy; a possible example of fault-zone weakening? *in* Holdsworth, R.E., Strachan, R.A., Magloughlin, J.F., Knipe, R.J., eds., The nature and tectonic significance of fault zone weakening. Geological Society of London Special Publication 186, p. 273-286.

Todd, V.R., 2004, Preliminary Geologic Map of the El Cajon 30' x 60' Quadrangle, Southern California. California Division of Mines and Geology Open-File Report 2004-1361.

Todd, V.R., and Shaw, S.E., 1979, Structural, metamorphic and intrusive framework of the Peninsular Ranges batholith in southern San Diego County, California, *in* Abbott, P.L., and Todd, V.R., eds., Mesozoic crystalliune rocks – Peninsular Ranges batholith and pegmatites, Point Sal Ophiolite. Guidebook of the Geological Society of America Annual Meeting, San Diego State University, San Diego, CA, p. 177-231.

Todd, V.R., and Shaw, S.E., 1985, S-type granitoid suites in the Peninsular Ranges batholith, southern California. Geology, v. 13, p. 231-233.

Todd, V. R., Erskine, B. G., and Morton, D. M., 1988, Metamorphic and tectonic evolution of the northern Peninsular Ranges Batholith, southern California, *in* Ernst, W. G., ed., Metamorphism and Crustal Evolution of the Western United States; Rubey Volume VII, Englewood Cliffs, New Jersey, Prentice Hall, p. 894-937.

Umhoefer, P.J., Dorsey, R.J., and Renne, P., 1994, Tectonics of the Pliocene Loreto Basin,

Baja California, and evolution of the Gulf of California. Geology, v. 22, no. 7, p. 649-652.

Venkat-Ramani, M., and Tikoff, B. 2002, Physical models of transtensional folding. Geology, v. 30, no. 6, p. 523-526.

Walawender, M.J., Girty, G.H., Lombardi, M.R., Kimbrough, D., Girty, M.S., and Anderson, C., 1991, A synthesis of recent work in the Peninsular Ranges batholith, *in* Walawender, M.J., and Hanan, B.B., eds., Geological excursions in southern California. Guidebook 1991 Annual Meeting Geological Society of America, San Diego, California, p. 297-312.

Wernicke, B., 1985, Uniform-sense normal simple shear of the continental lithosphere: Canadian Journal of Earth Science., v. 22, p. 108-125.

White, S., 2001, Textural and microstructural evidence for semi-brittle flow in natural fault rocks with varied mica contents. International Journal of Earth Sciences, v. 90, no. 1, p. 14-27.

Winker, C.D. 1987. Neogene stratigraphy of the Fish Creek - Vallecito section, southern California: implications for early history of the northern Gulf of California and Colorado delta, [Ph.D. dissertation]: Tucson, University of Arizona, 494 p.

Winker, C.D., and Kidwell, S.M., 1996, Stratigraphy of a marine rift basin: Neogene of the western Salton Trough, California, *in* Abbott, P.L., and Cooper, J.D., eds., Field conference guidebook and volume for the annual convention, San Diego, California, May, 1996, Bakersfield, California, Pacific Section. American Association of Petroleum Geologists, p. 295-336.

Winker, C. D., and Kidwell, S. M., 2002, Stratigraphic evidence for ages of different extensional styles in the Salton Trough, Southern California. Geological Society of America Abstracts with Programs, v. 34, no. 6, p. 83-84.

CHAPTER 3

PLEISTOCENE REORGANIZATION OF PLATE-BOUNDARY FAULT SYSTEMS, SW SALTON TROUGH

ABSTRACT

During Quaternary time subsidiary faults of the southern San Andreas fault system changed their location, structural style and kinematics, and this major reorganization produced new sub-basins in the Salton Sea area of southern California. We use structural and stratigraphic analyses along the SW margin of the Salton Trough to document folding and deactivation of the late Miocene to Pliocene West Salton detachment fault by the dextral oblique San Felipe fault zone starting ~1.1 Ma. The San Felipe fault zone consists of three principal faults (from west to east these strands are the San Felipe fault, Sunset fault, and the Fish Creek Mountains fault), and has four structural segment boundaries at bends and steps in the main traces, and at branch points of subsidiary faults. The San Felipe fault strand has about ~5 km of dextral separation on northeast-dipping markers due to both dextral and north-side-up slip

We examined a transpressional part of the San Felipe fault zone to test our hypothesis that the fault zone consists of three left-stepping en-echelon fault segments. These three faults bound two folded domains in the Narrows segment boundary. The Sunset conglomerate, the older West Salton detachment fault, and its footwall crystalline rocks are all folded about WNW- trending and fewer E-W and NE-trending folds, and each domain records about 9-12% NE-SW shortening. We interpret the similar geometries of these folds as resulting from the transfer of strain across two contractional stepovers in the fault zone. The stepovers produced mostly fault-parallel folds and

---

[1]Coauthored by Alexander N. Steely, Susanne U. Janecke, Gary J. Axen, Rebecca J. Dorsey, and Victoria Langenheim.

represent a strain-partitioned contractional step.

The ~10.8 km long Sunset fault is in the middle of the Narrows segment boundary at the east end of an ~15 km long restraining bend of the San Felipe fault. The Sunset fault is steep to moderately dipping, changes dip direction over short strike distances, and has mostly strike-slip and sparse purely dip-slip slickenlines. We estimate less than ~2.5 km of right slip on the Sunset fault because the provenance of syntectonic conglomerate matches rocks currently SW of the fault, and because the Sunset fault is a short fault that changes NW-ward into a radial fan of small-offset faults..

Evidence for Pleistocene initiation of the San Felipe fault zone is preserved in deformed syntectonic conglomerate exposed NE of the Sunset fault. Slip through the Narrows stepover uplifted poorly sorted angular boulder conglomerate to pebbly coarse sandstone, informally named the Sunset conglomerate. The Sunset conglomerate is ~600 m thick and lies in angular unconformity on the Pliocene Diablo and Olla formations. The conglomerate is bounded on the SW by the Sunset fault, and coarsens upward and SW toward the fault. It is dominated by plutonic lithologies from nearby areas, contains up to 10% recycled sandstone clasts from the Diablo Formation, was deposited by NE-flowing alluvial fans, and was shed from the SW side of the then-active Sunset fault. Based on lithologic, stratigraphic, and compositional similarities, we correlate this conglomerate to part of the Ocotillo Formation. Clasts of recycled sandstone record erosion of older basin fill that once covered the Vallecito and Fish Creek mountains. This uplift may have initiated as a fault propagation fold above the growing San Felipe fault zone when the fault zone formed ~1.1 – 1.3 Ma. After the fault reached the surface, the obliquity of the fault zone created accommodation space for the Sunset conglomerate and later uplifted and exhumed these syntectonic conglomerates.

Altogether these data show that the Sunset and Fish Creek Mountains faults initiated in the dextral San Felipe fault zone ~1.1 – 1.3 Ma and activity continued into the latest Pleistocene. The West Salton detachment fault was replaced by the San Felipe fault

zone as the new basin-bounding structure during this major, region-wide reorganization of faults along the North American plate boundary. Most of the folding in the fault zone occurred after ~0.6 Ma, and former basinal areas have been uplifted since the middle Pleistocene. This second kinematic and structural change is coeval with increasing contraction across the San Jacinto fault zone after ~0.6 Ma and may represent a second structural adjustment along the plate boundary. The San Felipe fault zone is still active and two of its structural segments ruptured in the latest Pleistocene or Holocene.

INTRODUCTION

Rocks and structures in the Salton Trough contain a record of complex late Cenozoic deformation and sedimentation related to the evolution of the transtensional Pacific-North America plate boundary in southernmost California and northern Mexico (Fig. 3-1) (Dibblee, 1954; Atwater, 1970; Crowell, 1981; Axen and Fletcher, 1998; Chapter 2). The Salton Trough is the northern extension of the Gulf of California physiographic province, a crustal depression nearly 1400 km long that ends near the Salton Sea approximately 73 meters below sea level (Dibblee, 1984). The Colorado River delta currently blocks the Sea of Cortez from entering the Salton Trough. The San Andreas fault bounds the north and northeast side of the basin and a ~250 km long zone of low-angle detachment faults with both ENE and west dips bounds the western edge (Fig. 3-1) (Axen and Fletcher, 1998). The West Salton detachment fault is the northern-most low-angle fault system and accommodated top-to-the-east oblique extension, whereas low-angle faults in the Laguna Salada area are at the southern end of the zone and accommodate top-to-the-west extension (Axen and Fletcher, 1998). During the Pliocene the West Salton detachment fault coexisted with the southern San Andreas fault and together were the major controlling structures in the Salton Trough (Axen and Fletcher, 1998; Chapter 2).

Starting in the Pleistocene, dextral strike-slip faults of the San Jacinto, San

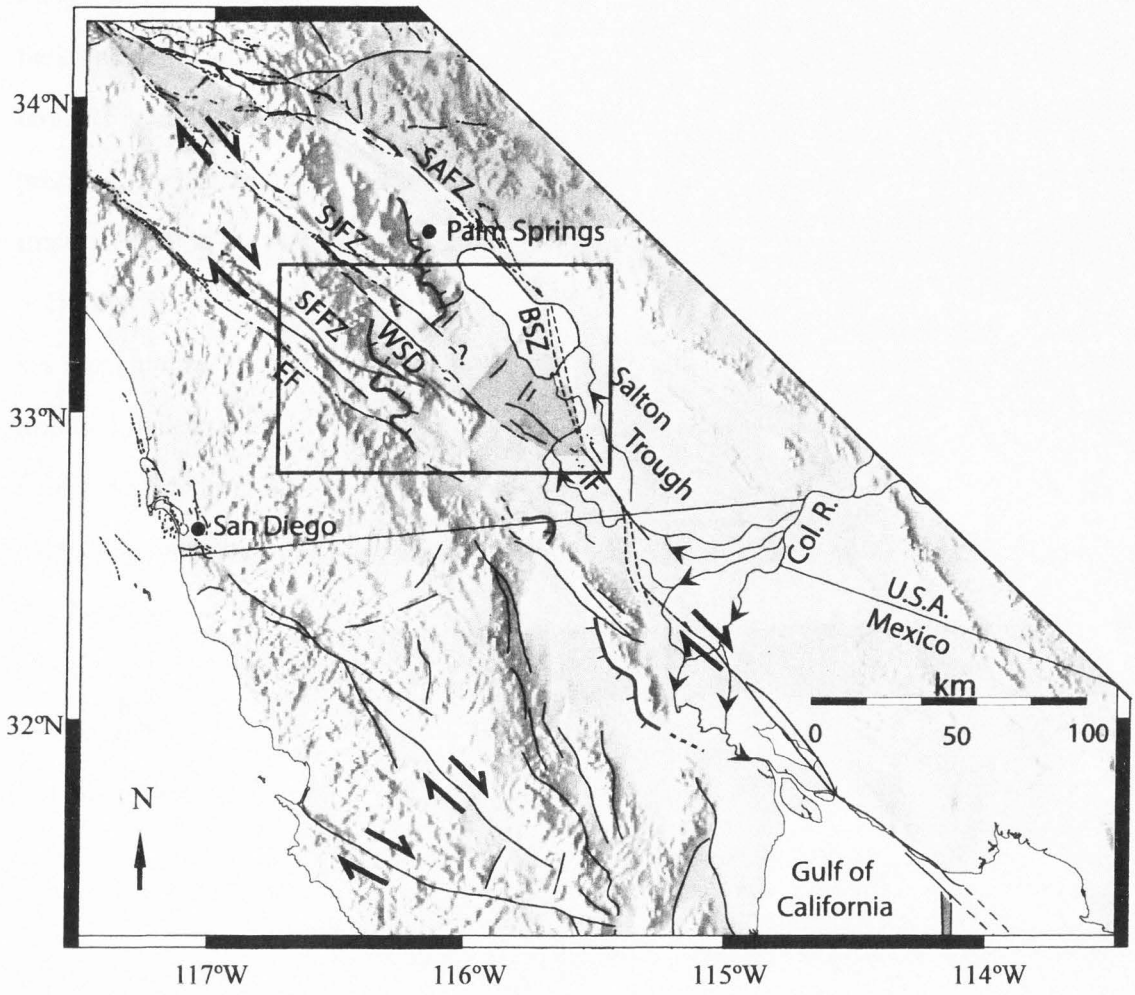

Figure 3-1. Tectonic overview of southern California and northwestern Mexico. Areas of known and inferred block rotation are shaded orange (Nicholson et al., 1985; Hudnut et al., 1989; Oskin and Stock, 2003). San Felipe fault zone (SFFZ) is in red, other strike-slip faults are in black; SAFZ-San Andreas fault zone; SJFZ-San Jacinto fault zone; IF-Imperial fault; SJFZ-San Jacinto fault zone; EF-Elsinore fault; BSZ-Brawley Seismic Zone. Oblique-slip detachment faults are in blue including the WSD-West Salton detachment fault. Fault locations are from Jennings (1977) and Axen and Fletcher (1998). Modified from Kirby et al. (in press). Box is approximate location of Figure 3-2.

Felipe, Earthquake Valley, and Elsinore fault zones cross cut the West Salton detachment fault and dismembered the previously intact supradetachment basin and its bounding faults (Fig. 3-2) (Sharp, 1967, 1972; Dorsey, 2002; Kirby et al., in press; Lutz et al., in press). The San Jacinto fault zone strikes NW, is >250 km long, and merges with the Imperial fault in the southeast and the San Andreas fault in the northwest (Figs. 3-1 and 3-2) (Sharp, 1967; Sanders, 1989). The San Felipe fault zone also strikes NW, is >160 km long, and may merge with the Elsinore fault in the northwest and projects into the Imperial fault in the southeast (Figs. 3-1 and 3-2). Most of the West Salton detachment fault zone has been uplifted and exhumed between and adjacent to these faults, and only short segments continue to slip where the younger, cross-cutting dextral strike-slip faults utilize the pre-existing faults (Rogers, 1965; Sharp, 1967; Axen and Fletcher, 1998; Kairouz, 2005; Chapter 2). All of the dextral fault zones have evidence for late Pleistocene activity and some also have Holocene activity (Rockwell et al., 1990; Hull and Nicholson, 1992; Morton and Matti, 1993; Dorsey, 2002; Kirby, 2005; Lutz et al., in press).

The age and nature of the transition from slip on the West Salton detachment fault to strike-slip faulting are poorly understood in the SW Salton Trough. Many previous studies have addressed the initiation and slip rates of the San Jacinto fault zone (e.g. Bartholomew, 1968; Rockwell et al., 1990; Morton and Matti, 1993; Dorsey, 2002; Kirby et al., in press; Lutz et al., in press), whereas significantly less work has focused on the San Felipe fault zone. In the Peninsular Ranges, late Quaternary slip rates of ~10-12 mm/yr on the San Jacinto fault zone from paleoseismic analysis (Rockwell et al., 1990) and a total dextral offset of 24 km (Sharp, 1967) suggest an ~2.4 Ma age of fault initiation, but stratigraphic data have been interpreted to show a 1.5 to 1.2 Ma initiation along the northern part of the fault zone (e.g. Morton and Matti, 1993). The Elsinore and San Felipe faults were estimated to be active by or before ~2 Ma in the Peninsular Ranges (Hull and Nicholson, 1992; Magistrale and Rockwell, 1996). However, recent work

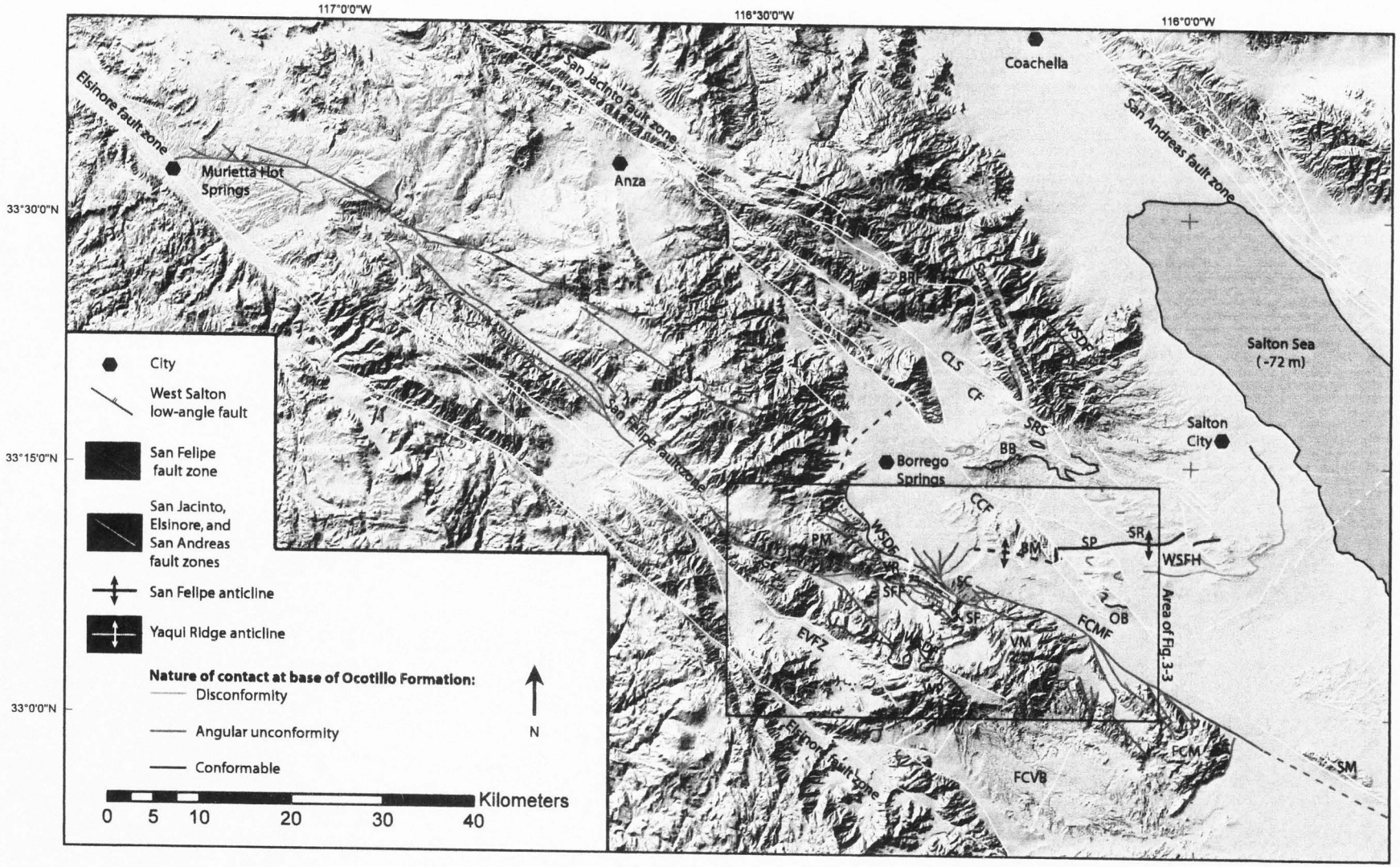
117°0'0"W
116°30'0"W
116°0'0"W
33°30'0"N
33°15'0"N
33°0'0"N
Elsinore fault zone
San Jacinto fault zone
San Andreas fault zone
Murietta Hot Springs
Anza
Coachella
Salton Sea (-72 m)
Salton City
Borrego Springs
San Felipe fault zone
City
West Salton low-angle fault
San Felipe fault zone
San Jacinto, Elsinore, and San Andreas fault zones
San Felipe anticline
Yaqui Ridge anticline
Nature of contact at base of Ocotillo Formation:
Disconformity
Angular unconformity
Conformable
N
Kilometers
0 5 10 20 30 40
BR
CLS
CF
SRS
BB
CCF
PM
WSDF
SR
SFF
SC
SF
EVFZ
BM
SP
WSFH
OB
FCMF
VM
Area of Fig. 3-3
FCM
FCVB
SM

Figure 3-2.

in the Borrego Badlands (Lutz, 2005; Lutz et al., in press) and San Felipe Hills (Kirby, 2005; Kirby et al., in press) documents a major stratigraphic and structural reorganization at ~1.1 Ma in the SW Salton Trough that may signal the initiation of dextral strike-slip faults farther SE. Because these studies examined basin fill in the San Felipe-Borrego sub-basin, the ~1.1 Ma stratigraphic reorganization was linked to the basin-bounding faults with indirect methods (Kirby et al., in press; Lutz et al., in press).

To better date and characterize the transition from slip on the West Salton detachment fault to slip on cross-cutting oblique strike-slip faults in the SW Salton Trough, we examine exposures near Yaqui Ridge at the southwestern edge of the San Felipe-Borrego sub-basin. Geological mapping over an area of ~2.5 USGS 7.5' quadrangles was undertaken at scales of 1:12,000 and 1:24,000 in the Borrego Mountain, Borrego Sink, Harper Canyon, Whale Peak, and Squaw Peak 7.5' USGS quadrangles. Sedimentologic and kinematic analyses were performed in this area and six geological cross sections were constructed. A filtered gravity map based on the data from Langenheim and Jachens (1993) and augmented with new unpublished data, and a filtered residual magnetic map provide additional control on locations of faults and depths to basement. This study integrates these new data sets with magnetostratigraphy (Housen et al., 2005; Kirby et al., in press; Lutz, et al., in press) and other previous work in the SW Salton Trough to document several basin-bounding oblique strike-slip faults that cut, deactivated, and folded the West Salton detachment fault during deposition of the syn-tectonic Ocotillo Formation.

PRE-QUATERNARY ROCK UNITS

Crystalline Bedrock

Peninsular Range Batholith

The Late Cretaceous Peninsular Range batholith and older metasedimentary screens and floor rocks form the basement terrane along the western edge of the Salton

Trough and continue south along the Baja California peninsula (Jahns, 1954; Todd et al., 1988). The plutonic rocks were emplaced between 140 and 80 Ma (Silver et al., 1979) and exhibit west-to-east variations in lithology, geochemistry, and geophysical and structural characteristics (Todd et al., 1988; Langenheim and Jachens, 2003). Eastern zone plutonic rocks of the La Posta-type TTG (tonalite-trondhjemite-granodorite) suite comprise the majority of the Vallecito and Fish Creek mountains and are the dominant rock type in the hanging wall of the West Salton detachment fault (Grove et al., 2003).

Eastern Peninsular Ranges Mylonite Zone

The Eastern Peninsular Ranges mylonite zone is a mid-to late-Cretaceous west-directed reverse-sense shear zone in the Peninsular Range batholith that forms a ~100 km long belt of ductile and brittle-ductile deformation along the eastern Peninsular Ranges from Palm Springs to Whale Peak in the SW Salton Trough (Fig. 3-3) (Sharp, 1979; Simpson, 1984; Engel and Schultejahn, 1984; Todd et al., 1988; George and Dokka, 1994; Axen and Fletcher, 1998; Kairouz, 2005). Foliation generally strikes north to northwest and dips 35°-55° east to northeast (Simpson, 1984; Todd et al., 1988). The trends of stretching lineation change from ~N85°E near Yaqui Ridge (Chapter 2) at the south end of the zone to N55°E in the northern Santa Rosa Mountains (Todd et al., 1988). The West Salton detachment fault loosely follows the Eastern Peninsular Ranges mylonite zone and dips more gently in some areas (Fig. 3-3) (Axen and Fletcher, 1998; Chapter 2.).

Cenozoic Stratigraphy

Winker and Kidwell (1996) elevated several long-standing stratigraphic formations in the SW Salton Trough to group status and we follow the nomenclature of these workers herein. Strata in the San Felipe-Borrego sub-basin consist of the Late Miocene (?) to Pliocene Imperial Group, Pliocene Palm Spring Group, Plio-Pleistocene

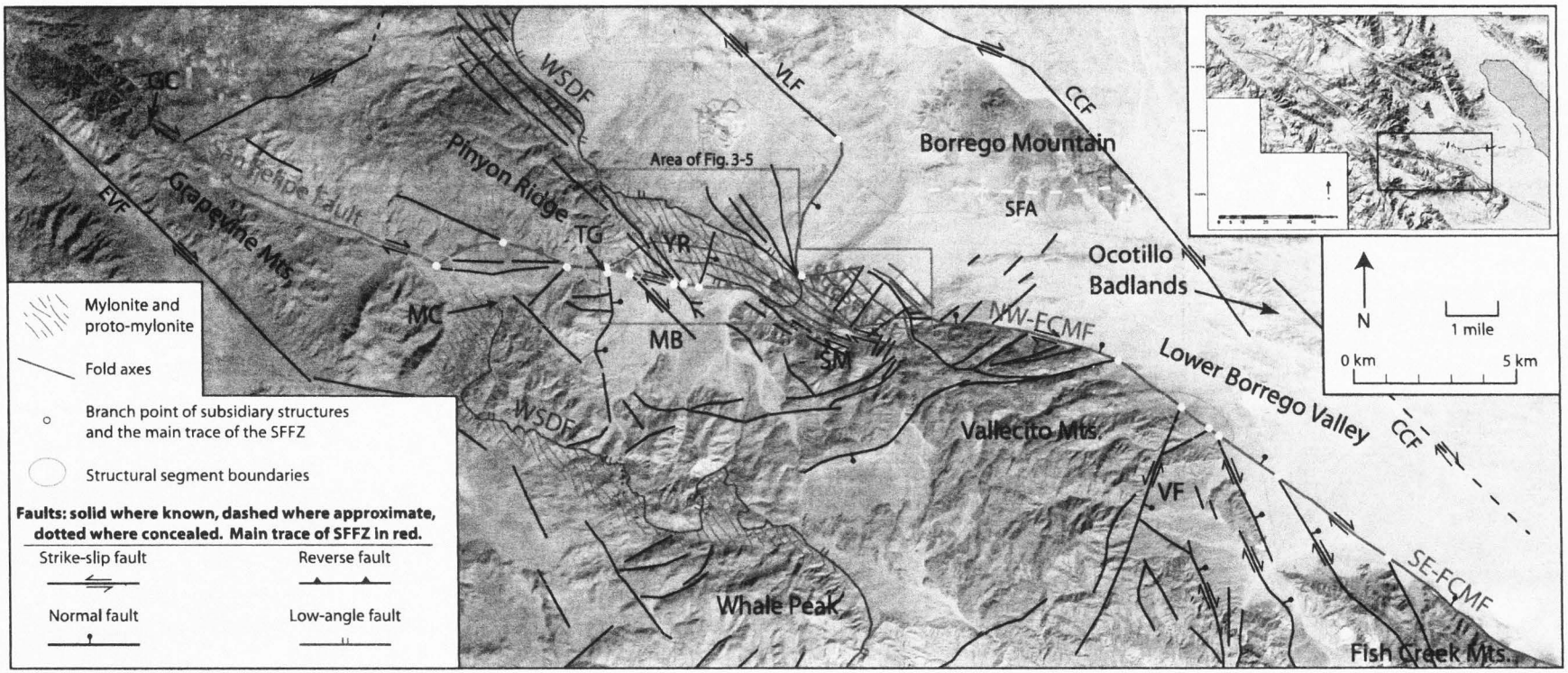

Figure 3-3. The central portion of the San Felipe fault zone near Yaqui Ridge. Notice the overall contractional left bend in the fault zone from the SE Fish Creek Mountain fault to the San Felipe fault. CCF-Coyote Creek fault; EVF-Earthquake Valley fault; MC-Mine Canyon; NW-FCMF-Northwest Fish Creek Mountain fault; SE-FCMF-Southeast Fish Creek Mountain fault; SFA-San Felipe anticline; GC-Grapevine Canyon; MB-Mescal Bajada; SM-Sunset Mountain; VLF-'Veggie-line' fault; VF-Vallecito fault; WSDF-West Salton detachment fault; YR-Yaqui Ridge.

Borrego Formation, and Quaternary Ocotillo and Brawley formations and have an aggregate thickness of ~5.4 km (Fig. 3-4) (Dibblee, 1954, 1984, 1996; Morley, 1963; Reitz, 1977; Dorsey, 2005; Lutz, 2005; Kirby, 2005). The late Cenozoic basin fill was deposited during east-directed dextral-oblique extension on the E- to NE-dipping West Salton detachment fault and records complex interactions among geologic structures of different ages, the Colorado River delta system, fluvial systems draining off the Peninsular Ranges, and the Gulf of California seaway (Winker and Kidwell, 1996, 2002; Axen and Fletcher, 1998; Dorsey and Janecke, 2002; Dorsey et al., 2005; Chapter 2). The early to middle Pleistocene Ocotillo Formation and its finer-grained lateral equivalent, the Brawley Formation, overlie these older basin fill deposits conformably or along an angular unconformity to laterally equivalent disconformity (Fig. 3-2 and 3-4) (Dibblee, 1984; Lutz, et al. in press; Kirby et al., in press).

Imperial Group

The Imperial Group records the first marine incursion into the Salton Trough and consists of submarine delta deposits of the Colorado River (Dean, 1988; Kerr, 1984; Kerr and Kidwell, 1991; Winker and Kidwell, 1996) and locally-derived subaerial fluvial conglomerate (Fig. 3-4) (Chapter 2). The base of the Imperial Group in the San Felipe-Borrego sub-basin is exposed at Borrego Mountain, where it consists of the Late Miocene (?) to Pliocene marine to fluvial Hawk Canyon formation and Pliocene fluvial West Butte conglomerate (Herzig et al., 1995; Chapter 2). The West Butte conglomerate becomes finer-grained laterally east and north and may be the fluvial equivalent of locally-derived marine grit, sandstone, coquina, and rare conglomerate near Squaw Peak, and may also correlate with sandy to muddy marine Colorado River delta deposits farther east near Shell Reef (Fig. 3-4) (Chapter 2). The West Butte conglomerate contains conspicuous chloritically and hematitically altered clasts that were exposed in the damage zone of the West Salton detachment fault. The conglomerate is up to ~300 m thick and was folded

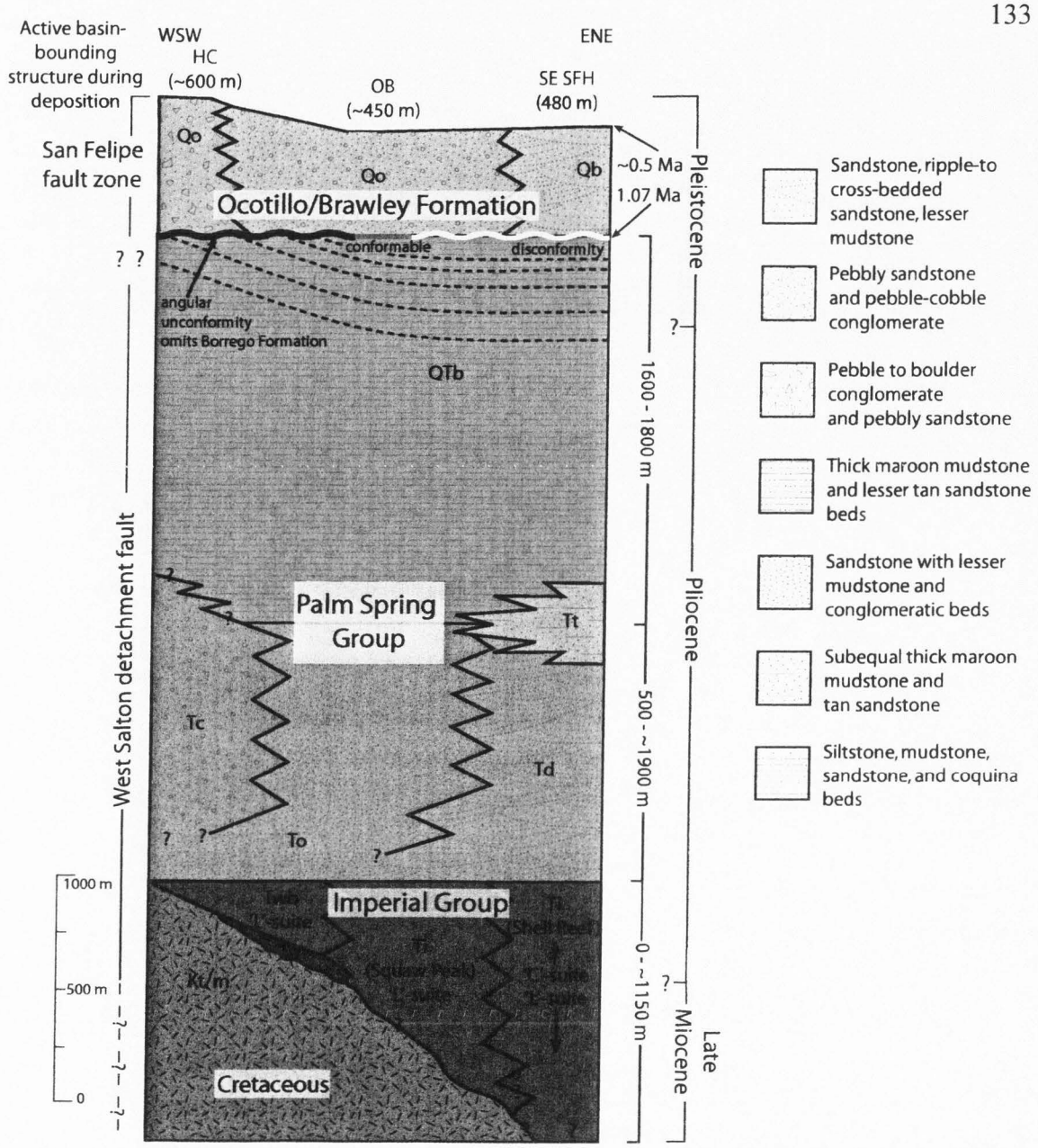

Figure 3-4. Generalized stratigraphic column for the SW Salton Trough showing laterally equivalent units, schematic thickness patterns, and active structures. Thicknesses of the Ocotillo/Brawley formation are from this study at Harper Canyon (HC), and Kirby et al., (in review) at Ocotillo Badlands (OB) and southeast San Felipe Hills (SE SFH). Other thicknesses are shown as the average of reported thicknesses (Morley, 1963; Reitz, 1977; Dibblee, 1984; Dorsey, 2005; Lutz, 2005; Kirby, 2005). Tc-Canebrake Conglomerate; To-Olla Formation; Td-Diablo Formation; Tt-Palm Spring-Borrego transitional unit; Ti-Imperial Formation; Twb-West Butte conglomerate; Kt/m-Cretaceous plutonic rocks and local metaplutonic and metasedimentary rocks; QTb-Borrego Formation; Qo-Ocotillo Formation; Qb-Brawley Formation; Th-Hawk Canyon formation.

syn-depositionally during slip on the West Salton detachment fault (Chapter 2).

Palm Spring Group

Diablo Formation, Olla Formation, and Canebrake Conglomerate. The Plio-Pleistocene Palm Spring Group conformably overlies the Imperial Group and consists of the laterally equivalent Diablo Formation, Olla Formation, Caenbrake Conglomerate, and the overlying lacustrine Borrego Formation (Fig. 3-4) (Dibblee, 1984, 1996; Winker and Kidwell, 1996; Axen and Fletcher, 1998). Sandstone in the Diablo Formation is typically tan to yellow-orange and consists of >50% distinctive, rounded hematite-coated quartz grains derived from the Colorado River ('C'-suite) (Winker, 1987; Winker and Kidwell, 1996). Northwest of Borrego Mountain the Diablo Formation is >500 m thick (Dorsey et al., 2004), overlies the Olla Formation (Chapter 2), and is the subaerial fluvial-deltaic deposit of the SE-flowing Colorado River delta (Winker and Kidwell, 1986, 1996; Dorsey et al., 2005). The Olla Formation is 0-110 m thick and is also a sandy and muddy fluvial deposit, and is dominated by locally derived (Peninsular Ranges plutons) sandstone grains ('L'-suite) and represents stream systems flowing from the Peninsular Ranges (Chapter 2). The Diablo and Olla formations pass laterally SW into locally-derived coarse sandstone to cobble-boulder conglomerate of the Canebrake Conglomerate near Yaqui Meadows. There the Canebrake Conglomerate is faulted against Cretaceous mylonitic rocks along the West Salton detachment fault.

Borrego Formation. The lacustrine Borrego Formation overlies the Diablo Formation along a complexly interbedded and gradational contact in the San Felipe-Borrego sub-basin (Fig. 3-4) (Dibblee, 1954, 1984; Kirby, 2005). The Borrego Formation is ~1.6 – 1.8 km thick in the San Felipe Hills and Borrego Badlands and consists of claystone, mudstone, and lesser sandstone (Dibblee, 1984; Kirby, 2005). The Borrego Formation accumulated in a perennial freshwater to brackish lacustrine environment that experienced rare lake-level low stands (Kirby et al., in press). The sill

of the Borrego lake depocenter is traditionally interpreted as the delta of the Colorado River (Dibblee, 1954) but may have been a now-buried structural barrier that blocked the northward incursion of marine waters of the Gulf of California (Dorsey et al., 2005). Coarse pebbly sandstone is rare in most exposures of the Borrego Formation but becomes common (up to ~ 50%) in the western Borrego Badlands where it is interbedded with lacustrine mudstone and claystone of the upper Borrego Formation. There, sandy pebble conglomerate in the upper ~95 meters of the Borrego Formation contains clasts of well cemented sandstone reworked from the underlying Diablo and Olla Formations.

Hueso Formation. In the Fish Creek-Vallecito basin south of our study area, the Borrego Formation is absent and the Hueso Formation is the chronological equivalent. The Hueso Formation is ~0.9 – 1.3 km thick, overlies the Diablo and Olla formations, and is laterally equivalent to the upper part of the Canebrake Conglomerate (Winker, 1987; Winker and Kidwell, 1996; Kairouz, 2005). The Hueso Formation is coarser than the Borrego Formation in grain size, is locally-derived, and contains very little detritus from the Colorado River. Near Whale Peak, deposits of the Canebrake Conglomerate that correlate with the upper part of the Hueso Formation are cut by the West Salton detachment fault and provide the first direct evidence for activity on the detachment fault during the latest Pliocene and early Pleistocene (Kariouz, 2005).

The paleogeographic transition from the Fish Creek-Vallecito basin to the San Felipe-Borrego basin during deposition of the Borrego and Hueso formations is poorly understood because the uplifted and eroded Vallecito and Fish Creek mountains now separate the two basins (e.g. Dorsey et al., 2005; Kirby et al., in press). Our study area near Harper Canyon is one of the few locations that lie between these two basins and should expose rocks of the appropriate age. However, the Borrego and Hueso formations are absent between the Diablo Formation and the much younger Sunset conglomerate of the Ocotillo Formation. The absence of this stratigraphic interval is important for paleogeographic reconstructions and constraining the evolution of the San Felipe fault

zone. The reason for its absence may lie along a complex spectrum with two end members: 1) The area was a paleohigh during deposition of the Borrego and Hueso formations and accumulated little to no sediment of either formation, or, 2) The full thickness of Borrego Formation (1.8 km), or the Hueso Formation (1.3 km) accumulated. Because current data is equivocal we use these two end members in our later analyses.

QUATERNARY STRATIGRAPHY

Ocotillo and Brawley Formations

The Ocotillo Formation is a widespread unit of coarse-grained alluvial sandstone, conglomerate, and interbedded finer-grained lithologies (Fig. 3-4) (Bartholomew, 1968; Dibblee, 1984; Kirby, 2005; Lutz et al., in press). Its basal contact with the Borrego Formation changes laterally in the Borrego Badlands from a slight disconformity in the west to a conformable contact in the east (Lutz et al., in press). It is also a slight disconformity in the eastern San Felipe Hills that changes to an angular unconformity across the crest of the San Felipe anticline in the western San Felipe Hills (Fig. 3-2) (Dibblee, 1954, 1984; Kirby et al., in press). The Brawley Formation is the finer-grained, fluvial-deltaic lateral equivalent of the Ocotillo Formation (Kirby, 2005). The Ocotillo Formation is up to ~450 m thick in the Ocotillo Badlands (Kirby, 2005), ~500 m in the Borrego Badlands (Lutz et al., in press), and the Ocotillo and Brawley formations are 480 m thick in the eastern San Felipe Hills (Fig. 3-4) (Kirby, 2005).

The age of the Ocotillo and Brawley formations is ~1.1- to 0.5-0.6 Ma based on new magnetostratigraphy in the Borrego Badlands (Lutz, 2005; Lutz et al., in press) and San Felipe Hills (Kirby, 2005; Kirby et al., in press). In the Borrego Badlands, the base of the Ocotillo Formation is ~1.05 Ma and the base of the overlying Font's Point sandstone is ~0.6 Ma (Lutz et al., in press). In the San Felipe Hills 18 km SE of the Borrego Badlands, the disconformable base of the laterally equivalent Brawley Formation is ~1.057 Ma old and the top of the exposed section is 0.5-0.6 Ma-old (Kirby, 2005).

The nearly-synchronous progradation of coarse-grained deposits over the finer lacustrine Borrego Formation suggests a major reorganization of the basin-bounding structures that may be due to initiation or reorganization of early dextral strike-slip faults on the NE flank of the Fish Creek Mountains (Kirby, 2005) and creation of new faults in the San Jacinto fault zone (Lutz et al., in press). Data from the Borrego Badlands show that the Clark lake and Santa Rosa segments of the Clark fault were active by ~1 Ma (Lutz et al., in press). The widespread and abrupt end of deposition of the Ocotillo and Brawley formations at ~0.5-0.6 Ma in the San Felipe-Borrego sub-basin reflects a second major structural reorganization related to changes in the geometry and kinematics of the San Jacinto fault zone (Kirby, 2005; Lutz et al., in press).

Exposures of the Ocotillo Formation in the San Felipe-Borrego basin are located around the Borrego Badlands, the western and southern San Felipe Hills, and the Ocotillo Badlands. We will show that an ~5.8 km long by 2.6 km wide outcrop belt of conglomerate along the northern flank of the Vallecito Mountains, which was previously correlated to the Canebrake Conglomerate of the Palm Spring Group (Dibblee, 1984; Winker and Kidwell, 1996), is actually a proximal part of the Ocotillo Formation. Because this outcrop is not contiguous with other outcrops of the Ocotillo Formation, we informally name this unit the Sunset conglomerate of the Ocotillo Formation and use this coarse-grained basin-margin facies to locate and infer the age of the active basin-bounding fault system.

Sunset Conglomerate

Description. The Sunset conglomerate is exposed NE of the Sunset fault for 5.7 km from Harper Canyon in the east to Yaqui Narrows in the west, and up to 2.6 km NE of the Sunset fault (Fig. 3-5). The Sunset conglomerate has been exhumed due to uplift in the San Felipe fault zone and is the only exposure of this unit near the fault zone. The NW-striking oblique dextral Sunset fault and subsidiary dextral faults place Sunset

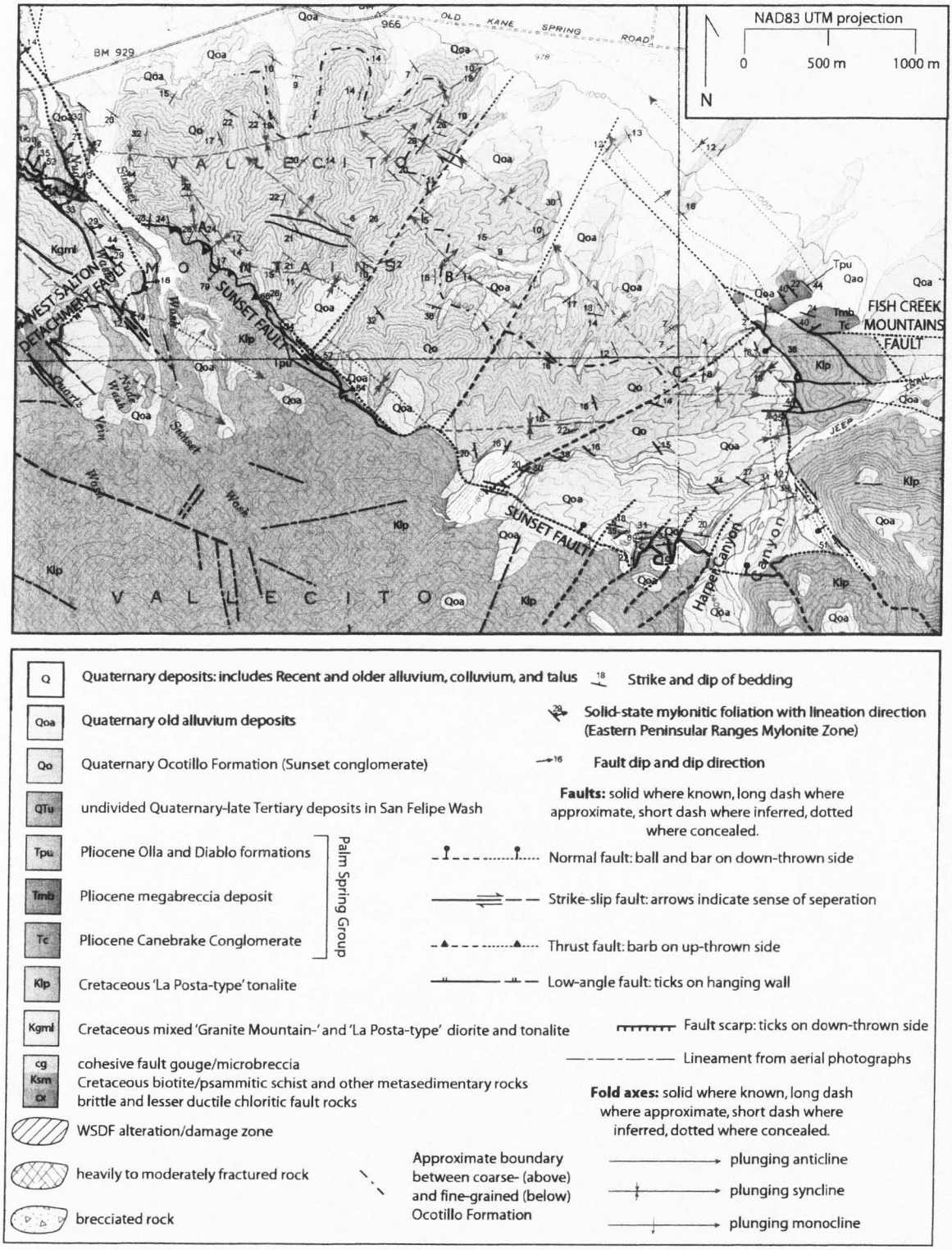

Figure 3-5. Simplified geological map of the folded Sunset conglomerate and bounding structures. Figure 3-6 slightly overlaps the western edge of this map. Modified from Plate 1.

conglomerate, and locally exposed underlying Pliocene Palm Spring Group, against Cretaceous La Posta-type tonalite. The Sunset conglomerate lies along slight angular unconformity on a narrow belt of Canebrake, Olla, and Diablo formations of the Palm Spring Group near Harper Canyon where the intervening Borrego Formation was either never deposited or was eroded away before the Sunset conglomerate was deposited. At this location the Palm Spring Group dips 10°-15° more steeply north than the overlying Sunset conglomerate (Fig. 3-5). Elsewhere, the base of the conglomerate is not exposed. The Sunset conglomerate is at least 600 m thick based on map estimates and geological cross sections (Figs. 3-5 and 2-5). Lateral equivalents of the Sunset conglomerate are inferred to exist in the subsurface to the east, northeast of the Fish Creek Mountains fault, and were inferred to have been eroded from the north side of Yaqui Ridge.

The Sunset conglomerate consists of light gray to gray-tan, moderately to poorly consolidated, poorly sorted coarse to pebbly sandstone, pebble-cobble conglomerate, and angular to sub-rounded boulder to cobble conglomerate. Overall this unit coarsens upsection from pebbly conglomeratic sandstone near the base to angular to rounded boulder conglomerate near the top. It also coarsens laterally SW toward the Sunset fault where grain size changes from coarse sandstone ~2 km NE of the fault to angular boulder conglomerate along the fault in the SW. Deposits proximal to the Sunset fault are dominated by light gray, coarse sandy matrix- to clast-supported, angular to sub-angular, cobble to boulder conglomerate with boulders up to 4 m in diameter (Fig. 3-6). Poorly defined bedding in proximal deposits is typically characterized by 0.5 – 2 m thick interbedded coarser and finer conglomerate beds which locally contain outsized clasts. Outsized clasts are typically small to large boulders. Proximal deposits contain <20-30% sand whereas distal deposits typically contain >50% sand.

Distal exposures of the Sunset conglomerate are characterized by poorly to moderately bedded, 1 – 50 cm thick, poorly sorted, angular to rounded, planar to low-angle trough cross-stratified coarse to pebbly sandstone and lesser pebble to cobble

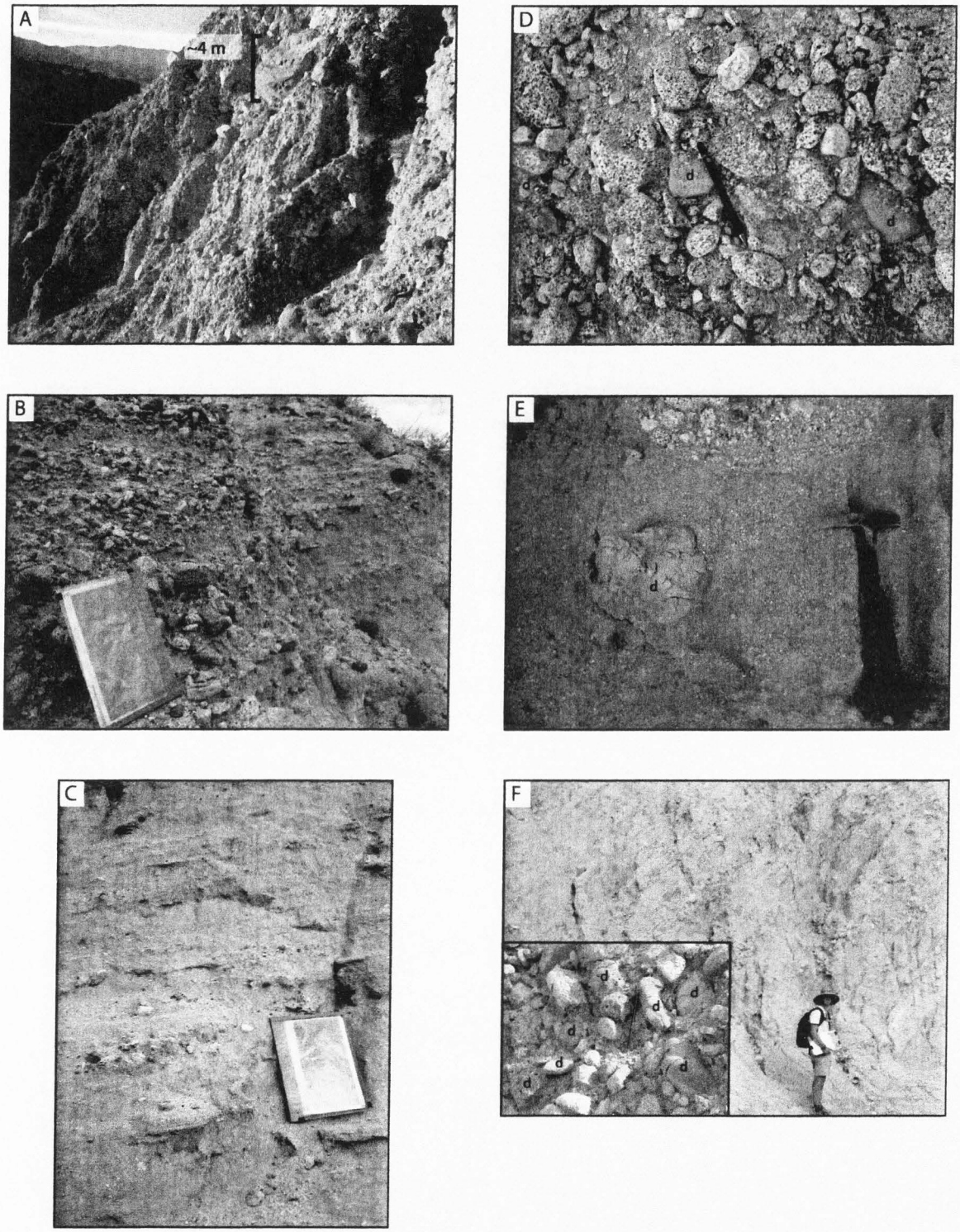

Figure 3-6.

conglomerate (Fig. 3-6). Overall, distal exposures are more tan than exposures proximal to the Sunset fault and, although not extensively studied, contain 10-30% pink hematite-coated rounded quartz sand grains. Distal conglomerate beds are typically 10-50 cm thick, poorly sorted, sandy matrix- to clast-supported pebble to cobble conglomerate, commonly contain imbricated clasts, and locally have 0.25 – 1 m erosive channel fills (Fig. 3-6). Deposits between the Sunset fault and distal exposures contain characteristics of both proximal and distal lithologies (Fig. 3-6).

Imbricated clasts (n=58) and trough axes (n=3) show overall N57°E ± 12° paleotransport when corrected for bedding tilt (Fig. 3-8). Paleocurrent directions spread 120° about the average direction. This NE-directed paleoflow is approximately perpendicular to the N25°W – N55°W strike of the Sunset fault (Figs. 3-8 and 3-5).

Clast lithologies in the Sunset conglomerate are dominated by La Posta-type tonalite and associated plutonic rocks (85%), and lesser metamorphic rocks (8%) and deformed and chloritically altered plutonic rocks (3%) (Figs. 3-9 and 3-6d). An average 4% of all clasts are distinctive light tan to tan-pink recycled sandstone clasts (Figs. 3-9 and 3-6). These sandstone clasts contain pink hematite-coated rounded quartz grains, are locally present throughout the Sunset conglomerate, may account for up to 10% of the clasts at a single location, and are more obvious in pebbly beds. The presence of these recycled sandstone clasts has significant paleogeographic implications.

Depositional environment. We interpret the poorly sorted, matrix-supported, pebble to angular boulder conglomerate with outsized clasts near the Sunset fault as debris-flow deposits. These beds fine laterally NE into planar and trough cross-bedded coarse sandstone to pebbly conglomerate that we interpret as dominantly gravelly sheet-flood deposits with some conglomerate-filled stream channels. The lateral continuity of these facies and the paleoflow indicators suggest deposition in the upper and middle part of a NE-flowing alluvial fan.

Provenance and recycling. La Posta-type tonalite clasts, which dominate the

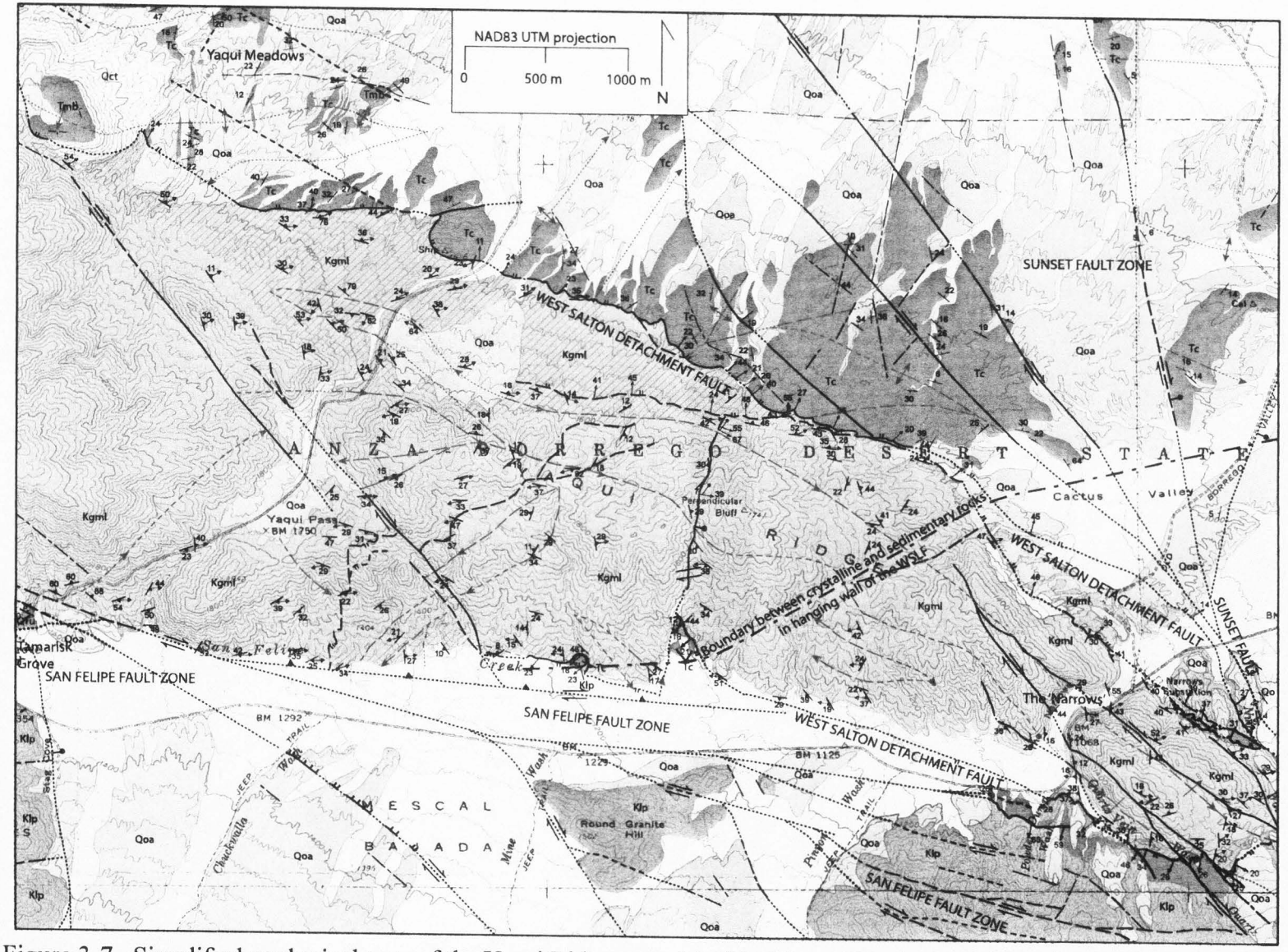

Figure 3-7. Simplified geological map of the Yaqui Ridge area. Modified from Plate 1. Key is same as Figure 3-5.

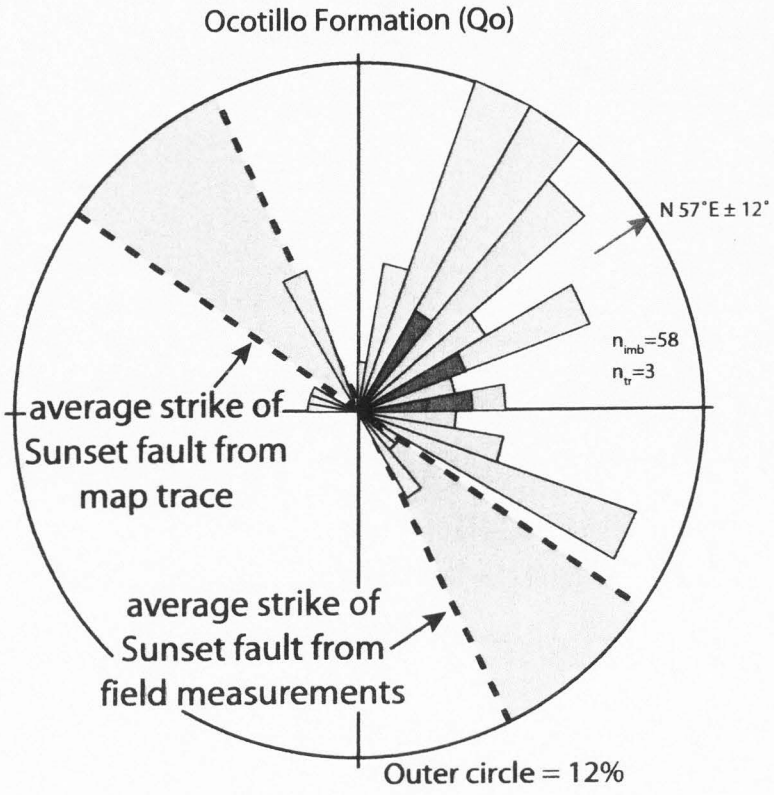

Figure 3-8. Rose diagram of paleocurrents from the Ocotillo Formation (Sunset conglomerate). Light gray petals are measurements from tilt-corrected poles to clast imbrications; dark gray petals are measurements from tilt-corrected trough axes. Bi-directional trough axes are plotted in the same quadrant as the unidirectional imbrications. nimb=number of imbrications; ntr= number of trough axes.

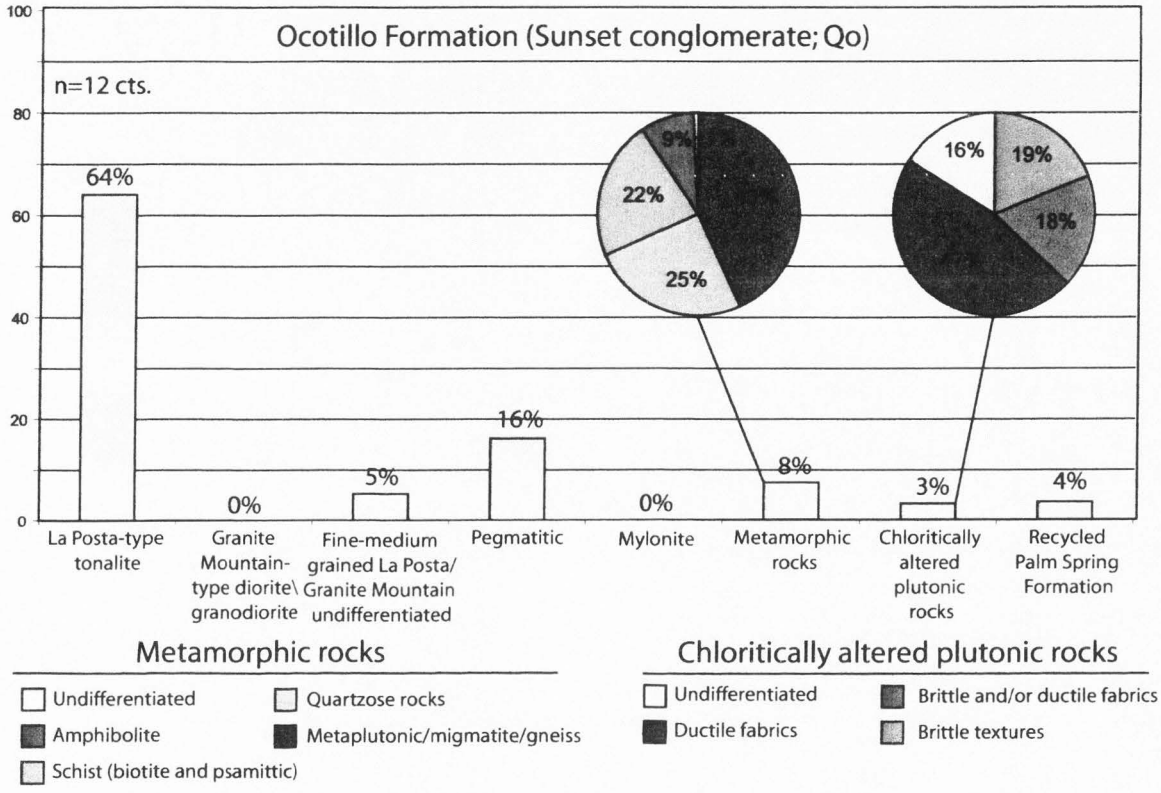

Figure 3-9. Clast count for the Ocotillo Formation (Sunset conglomerate). Pie charts represent the percentage of different chloritic or metamorphic rocks within the binned populations. Each clast count represents 50 clasts at a single location. Clast populations are labeled with percentages (18%).

Sunset conglomerate (64%), are identical to plutonic rocks on the SW side of the Sunset fault (Figs. 3-5, 3-7, and 3-9). These La Posta-type plutonic rocks are only located south and southeast of a poorly understood boundary with the Canebrake Conglomerate in the hanging wall of the West Salton detachment fault (Fig. 3-7). Diorite, granodiorite, and mylonitic rocks in the footwall of the West Salton detachment fault are exposed along Yaqui Ridge <500 m farther west but do not occur as clasts in the Sunset conglomerate (Figs. 3-7 and 3-9). Distinctive tan-pink sandstone clasts in the Sunset conglomerate are present in the Ocotillo Formation throughout the SW Salton Trough (Fig. 3-6), and also are found in sandy pebble conglomerate in the upper ~95 meters of proximal Borrego Formation in the western Borrego Badlands. Hematite-coated rounded quartz grains are diagnostic of sand from the Colorado River (Merriam and Bandy, 1965) and are especially abundant in the deltaic sandstone of the Diablo Formation of the Pliocene Palm Spring Group (Winker, 1987; Winker and Kidwell, 1996). The upper Imperial Group and Borrego Formation contain lesser amounts of these sandstone lithologies (Reitz, 1977; Dibblee, 1984; Kirby, 2005). The presence of this distinctive lithology as clasts in the Sunset conglomerate (4%, and up to 10% at a single location) records recycling of older basin-fill sediments in the source area of the younger Sunset conglomerate. We interpret the hematite-coated rounded quartz grains in distal sandstone of the Sunset conglomerate as Colorado River sand grains recycled from older basin fill. The change in color from gray-colored proximal deposits to tan-colored distal deposits is likely due to a reduction in average grain size, which consequentially preserves a larger fraction of the finer hematitically-stained quartz grains in the finer-grained deposits. Because the Diablo Formation of the Palm Spring Group contains the most Colorado River-derived sand grains of any unit in the SW Salton Trough, and no shells from the Imperial Group or mudstone clasts from the Borrego Formation were observed in recycled clasts in the Sunset conglomerate, the Diablo Formation is most likely the source of the tan recycled sandstone clasts and sand grains.

Metamorphic and chloritically altered rocks are also found as clasts in the Sunset conglomerate (11%). These lithologies cannot be derived from the large body of La Posta-type plutonic rocks SW of the Sunset fault. The underlying Canebrake Conglomerate of the Pliocene Palm Spring Group contains ~34% of these metamorphic and chloritically altered rocks. Although these lithologies are also present in the footwall of the detachment fault farther to the west and could be derived from there, the angular unconformity between the Sunset conglomerate and the Canebrake Conglomerate suggests that the Canebrake Conglomerates is the more likely source for these clasts.

Correlation and age. Based on the similar stratigraphic position, thickness, basal contact, grain size, depositional environments, paleoflow, composition, and recycled Diablo sandstone clasts, we interpret the Sunset conglomerate as a proximal part of the Ocotillo Formation (Fig. 3-4). The Sunset conglomerate overlies the Palm Spring Group along an angular unconformity so it must be younger than the Palm Spring Group. This relationship rules out correlation with the Canebrake Conglomerate and West Butte conglomerate. The Ocotillo Formation rests conformably on the Borrego Formation in the Borrego and Ocotillo badlands and is disconformable in the eastern San Felipe Hills (Fig. 3-2) (Dibblee, 1984; Brown et al., 1991; Lutz et al., in press; Kirby et al., in press). The disconformity changes laterally westward into an angular unconformity in the western San Felipe Hills (Fig. 3-2). In locations with angular unconformities, the Ocotillo Formation overlies north- or south-dipping Borrego Formation and Palm Spring and Imperial group strata. The Sunset conglomerate overlies north-dipping Palm Spring Group along a possibly major unconformity with a slight angular discordance. The ~600 m thickness of the Sunset conglomerate is similar to, but somewhat thicker than the Ocotillo Formation in the Borrego Badlands (~500 m; Lutz et al., in press), Ocotillo Badlands (450 m), and the eastern San Felipe Hills (480 m) (Kirby, 2005).

Regionally, the Ocotillo Formation commonly contains sand- to pebble-sized grains, sheet flood deposits, and represents deposition in medial to distal alluvial fan

environments. The laterally equivalent Brawley Formation represents deposition in distal fluvial, fluvial deltaic, and lacustrine environments (Kirby et al., in press). The two formations are interpreted as syn-tectonic deposits related to slip on dextral strike-slip faults SW and N of the San Felipe-Borrego sub-basin (Lutz et al., in press; Kirby et al., in press). The Sunset conglomerate is dominated by pebble- to cobble-sized grains, contains both sheet flood and debris-flow deposits, represents deposition in proximal to medial alluvial fan environments, and is a syn-tectonic deposit related to slip on the oblique-dextral Sunset fault.

Paleocurrents in the Ocotillo Formation are spatially variable in the SW Salton Trough and are generally E- to NE-directed except where influenced by syn-depositional folds and fault blocks (Lutz et al., in press; Kirby et al., in press). In the Borrego Badlands, clasts were shed to the SW across the then-active Clark fault, and toward the NE across the Coyote Creek fault (Lutz et al., in press). In the San Felipe Hills and Ocotillo Badlands E- to NE-paleotransport is recorded (Kirby et al., in press). Sediment dispersal in the Ocotillo Badlands is slightly clockwise from that in the San Felipe Hills and may have been affected by the E-trending San Felipe anticline just to the north. The Ocotillo Formation in the Borrego Badlands thickens NNE-ward (Lutz et al., in press), and Kirby et al. (in press) document SW-ward coarsening toward the Fish Creek Mountains fault. The Sunset conglomerate also has NE-directed paleotransport and coarsens southwest towards a dextral oblique fault, the Sunset fault. The greater thickness of the Sunset conglomerate compared to the Ocotillo Formation to the NE and E in the San Felipe Hills and Ocotillo Badlands is consistent with overall SW-ward thickening toward bounding faults.

The Ocotillo Formation is dominated by clasts derived from the Peninsular Ranges plutonic and metamorphic rocks that vary with the geology exposed in local highlands (Bartholomew, 1968; Dibblee, 1984; Kirby, 2005; Lutz et al., in press). A lesser but significant population of clasts and matrix sand grains in the Ocotillo

Formation are recycled from older basin fill of the Palm Spring Group (Fig. 3-6) (Kirby, 2005; Lutz et al., in press). These distinctive recycled Diablo Formation clasts and grains are also present in the Sunset conglomerate but not in other conglomerates of the SW Salton Trough. Although the Sunset conglomerate contains a few metamorphic clasts similar to those in the Canebrake Conglomerate, a possible reason for correlation (e.g. Dibblee, 1984; Winker and Kidwell, 1996), recycled clasts of the laterally equivalent Diablo Formation argue against this age correlation.

Together these data show that the Sunset conglomerate is most likely the proximal lateral equivalent to the ~1.1 – 0.6 Ma Ocotillo and Brawley formations (Fig. 3-4). The lithologic correlation between the Sunset conglomerate and the Ocotillo Formation is strong. However, the angular unconformity and absence of Borrego Formation beneath the Sunset conglomerate may potentially affect the age assigned to the oldest Sunset conglomerate. Interpreting the age of the oldest Sunset conglomerate is highly dependant upon why the Borrego Formation is missing beneath the angular unconformity at Harper Canyon. If the lower Sunset conglomerate correlates with the upper Borrego Formation in the Borrego Badlands, as suggested by similar clast lithologies, it suggests that the oldest Sunset conglomerate is older than the oldest Ocotillo Formation to the north. However, if up to 1.8 km of Borrego Formation was eroded from the Harper Canyon area before deposition of the Sunset conglomerate, it would suggest that the Sunset conglomerate and upper Borrego Formation are not equivalent and that the oldest Sunset conglomerate is equivalent to or younger than the Ocotillo Formation in the Borrego Badlands. If deposition of the Ocotillo Formation in the Borrego Badlands records the erosion of the Borrego Formation near Harper Canyon, it would suggest that the oldest Sunset conglomerate is younger than the oldest Ocotillo Formation there.

Because we know little about the amount of Borrego (or Hueso) Formation deposited at Harper Canyon, we cannot assign absolute age ranges for the oldest deposits of the Sunset conglomerate. Since the entire Ocotillo Formation was deposited basin-

wide in only ~0.5 m.y., the Sunset conglomerate is probably not more than ~0.2 Ma younger or older than other outcrops of the Ocotillo Formation. Therefore we suggest that the age of the oldest Sunset conglomerate is probably ~1.1 Ma and recognize that the basal deposits may be slightly younger or older than basal deposits of the Ocotillo Formation elsewhere in the San Felipe-Borrego sub-basin.

Paleogeography. Paleoflow perpendicular to the Sunset fault, lateral coarsening toward the fault, decrease in rounding toward the fault, and an angular unconformity at the base of the unit all suggest that the Sunset conglomerate is a syn-tectonic NE-directed alluvial fan deposit shed from the SW side of the then active Sunset fault. Because the Sunset conglomerate is correlative with the Ocotillo Formation, the ~1.1 Ma base of the unit dates a period of major activity on the Sunset fault of the San Felipe fault zone. The nearby Fish Creek Mountains fault is also part of the San Felipe fault zone and initiated at this time (Kirby et al., in press).

We interpret the presence of recycled sandstone clasts, which account for at least 4% of the conglomerate, and up to 11% more (metamorphic and chloritically altered clasts possibly recycled from the Canebrake Conglomerate) in the Sunset conglomerate, as recording uplift and erosion of older basin fill SW of the Sunset fault during deposition of the Sunset conglomerate. The distinctive recycled sandstone clasts are not present in older conglomeratic units in the study area or region (e.g. Chapter 2) except for the upper ~95 m of the Borrego Formation. We interpret their sudden appearance in these units as dating erosion of the Palm Spring Group in uplifted highlands (Fig. 3-10). The persistence of recycled clasts throughout the thickness of the unit suggests that erosion of these highland source areas continued throughout deposition of the Sunset conglomerate. Paleocurrents and stratigraphic analysis in the Ocotillo Formation along the southern edge of the SW Salton Trough show that there was not a single point source for these recycled clasts, but rather a long, relatively continuous plutonic-cored uplift coincident with the Vallecito and Fish Creek mountains (Fig. 3-10) (Kirby et al., in press).

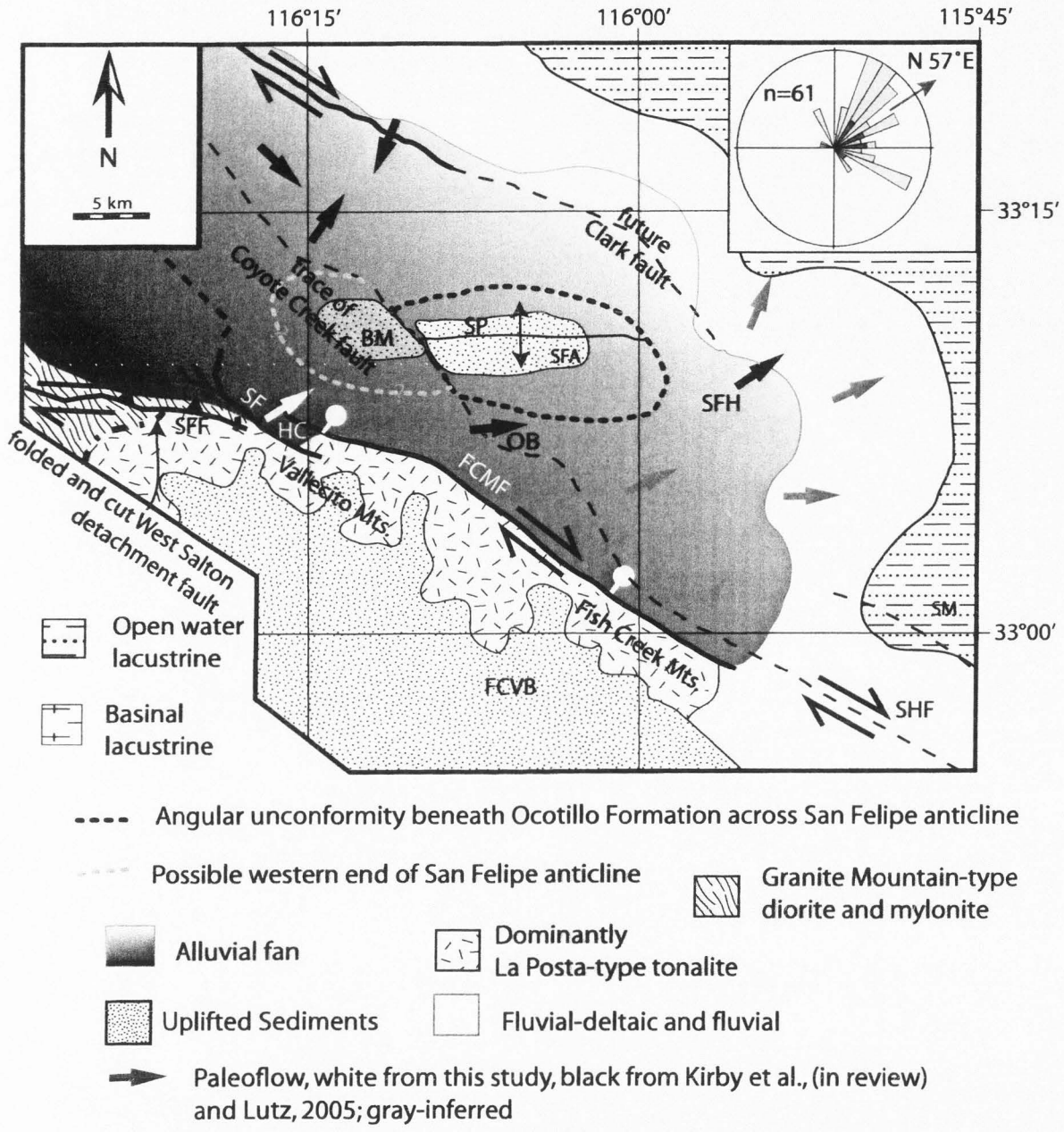

Figure 3-10. Paleogeography during deposition of the Ocotillo and Brawley formations just after 1 Ma. HC-Harper Canyon; SFA-San Felipe anticline; OB-Ocotillo Badlands; SFH-San Felipe Hills; SP-Squaw Peak; SFF-San Felipe fault; SF-Sunset fault; SHF-Superstition Hills fault; FCMF-Fish Creek Mountains fault; FCVB-Fish Creek-Vallecito basin; BM-Borrego Mountain; SM-Superstition Mountains; SRM-Southern Santa Rosa Mountains. Rose diagram shows paleoflow from the Sunset conglomerate unit of the Ocotillo Formation near Harper Canyon. Lighter shades represent finer grain size. Modified from Kirby et al. (in press).

Recycled sandstone clasts in the upper Borrego Formation may be the first record of this uplift and we use sedimentation rates to estimate the age of their appearance. Although the rate of sediment accumulation in the upper Borrego Formation is unknown, it is likely less than that of the lower Ocotillo Formation (1.4 - 3.9 mm/yr) (Lutz et al., in press; Kirby et al., in press). A range of about 0.5 to 2 mm/yr may be reasonable. Using that range and the age of the basal Ocotillo Formation in the Borrego Badlands, the oldest recycled clasts might be bracketed between about 1.1 and 1.3 Ma.

The Sunset conglomerate is a syntectonic deposit that we interpret as a result of slip on the Sunset fault of the San Felipe fault zone. We suggest that this fault zone uplifted older basin-fill deposits in fault blocks prior to and during deposition of the Sunset conglomerate (Fig. 3-10). Since the Vallecito Mountains were clearly the source area for the Sunset conglomerate (this study) and now expose mostly plutonic lithologies (Lough, 1993; Stinson and Gastil, 1996; Kairouz, 2005; Axen, unpublished mapping), the deposits of the Palm Spring Group that once covered the plutonic mountain core have been fully stripped by erosion.

STRUCTURAL GEOLOGY

We examine the geometry and segment boundaries of the San Felipe fault zone and we show that there are three major en-echelon fault segments at the east end of a major transpressive bend in the San Felipe fault zone. Folds in this stepover zone are typically either fault parallel or wrench folds and each type has a distinct spatial distribution. Our analysis shows that the West Salton detachment fault and Sunset conglomerate were folded by the San Felipe fault zone and that this younger fault zone deactivated the detachment fault. We also identify three additional structural segment boundaries on the San Felipe and Fish Creek Mountains faults.

San Felipe Fault Zone

The San Felipe fault zone is a >160 km long dextral to oblique dextral strike slip fault zone, strikes NW to WNW, and consists of anastomosing and branching fault strands. The fault zone projects toward the Murietta Hot Springs and northern Elsinore faults near Temecula and approaches the southern San Jacinto fault zone near Superstition Mountain but linkages are currently unproven (Figs. 3-2 and 3-3). Compared to the Elsinore and San Jacinto fault zones, the San Felipe fault zone is poorly characterized and incompletely mapped. Strands of the fault zone were first described by Dibblee (1954, 1984) and Rogers (1965) in the SW Salton Trough as a set of several strike-slip faults that bound the south side of Yaqui Ridge and the north side of the Vallecito and Fish Creek mountains.

The fault zone has an overall sigmoidal map pattern with N55°W-striking faults along Grapevine Canyon and the NE side of the Fish Creek and Vallecito mountains (Fig. 3-3). These segments are connected by a central ~15 km long zone of transpressive E-W-striking faults south of Pinyon and Yaqui ridges. In this central part of the fault zone we have identified structural segments at the tips of major folds, bends in the fault, left and right steps, branch points in the fault zone, and major changes in the structural style adjacent to the fault zone (Fig. 3-3). Our study focuses on the eastern half of the central transpressive segment of the San Felipe fault zone. This segment is exposed from ~5 km west of Tamarisk Grove to the Harper Canyon area and the Fish Creek Mountains in the SE (Figs. 3-3, 3-5, and 3-7).

Based on prior nomenclature and studies (e.g. Dibblee, 1984, 1996) we use the name San Felipe fault zone to refer to the entire collection of fault strands from Grapevine Canyon in the NW to the front of the Fish Creek Mountains in the SE. We restrict the name San Felipe fault to the portion of the entire fault zone that is south of Yaqui and Pinyon Ridges and extends NW into Grapevine Canyon after Dibblee (1984, 1996). We apply the new name of Sunset fault and the Fish Creek Mountains fault to

strands of the fault zone NE and E of Yaqui Ridge as described below.

Three left-stepping en-echelon fault strands comprise a major structural boundary at the east end of central transpressive segment of the San Felipe fault zone (Fig. 3-3). From NW to SE these are the San Felipe fault, Sunset fault, and Fish Creek Mountains fault (Figs. 3-3, 3-5, and 3-7). These three faults step left and bound two distinct contractional stepovers between them. The older West Salton detachment fault is folded in the stepover between the San Felipe and Sunset faults, and is cut by subsidiary small-offset strands of these two faults (Fig. 3-7). We discuss the characteristics of each of these faults below and their segment boundaries.

The age of the San Felipe fault zone is incompletely known and may vary along its length. Poor exposure and/or significant alluvial cover obscure the fault for much of its length NW and SE of the Yaqui and Pinyon Ridge area and hamper efforts to date the initiation of the fault. Magistrale and Rockwell (1996) suggested that most of the San Felipe fault zone was active from ~2.0 Ma to 0.9 Ma. Our new mapping and analysis of the San Felipe fault zone in the Yaqui and Pinyon ridge areas indicate a younger inception of this fault and activity into the late Pleistocene or Holocene.

San Felipe Fault

The San Felipe fault is the most northwestern fault of the San Felipe fault zone in our study area. The fault is >28 km long, and strikes E-W near Sunset Mountain to N50°W at the western edge of the study area (Fig. 3-3). It is vertical to nearly horizontal in rare outcrops and flattens near the surface west of Tamarisk Grove. Dibblee (1954, 1984, 1996) first identified this fault and mapped it as continuous with the Fish Creek Mountains fault. Our mapping shows multiple strands and no connection with the Fish Creek Mountains fault at the surface. To the northwest the San Felipe fault strikes ~N55°W in Grapevine Canyon and may consist of two major strands in that area.

We define two structural segments along the transpressive part of the San Felipe

fault: the Pinyon Ridge segment in the west and the Mescal Bajada segment in the east. The boundary between these two segments near Tamarisk Grove is characterized by a slight left bend, the branch point of an E-dipping normal fault south of the fault zone, and the existence of a major bedrock-cored anticline on Yaqui Ridge north of the Mescal Bajada segment (Figs. 3-3 and 3-7). Faults of the San Felipe fault zone are exposed west of Tamarisk Grove, east of Pinyon Wash in plutonic rocks, and are elsewhere concealed beneath Quaternary alluvium (Figs. 3-3 and 3-7). The San Felipe fault juxtaposes different plutonic lithologies along its length in the study area except for local narrow belts of late Pleistocene (?)-age sedimentary rocks caught up in the fault zone west of Tamarisk Grove (Plate 1).

The gravity signature along these two segments of the San Felipe fault is subdued and at most consists of a NW-trending 2 mGal gradient that extends from the western edge of the study area to near the tip of Yaqui Ridge at Yaqui Narrows (Fig. 3-11). The smaller gradient across the fault zone compared with other faults of the SW Salton trough (e.g. Fish Creek Mountains or Coyote Creek faults) is a result of faulting plutonic rocks of similar densities. The aeromagnetic map shows a prominent WNW-trending, ~3 km wide, 22 km long magnetic low on the NE side of the fault zone (Fig. 3-12).

In the structural segment boundary near Tamarisk Grove along the Borrego Springs Road, locally-derived bedded mudstone, siltstone, and sandstone coarsen up-section over ~15 m into pebble to cobble conglomerate that is overlain by a 5 m thick poorly sorted, angular boulder rock avalanche or debris flow deposit (QTu of Fig. 3-7). These sedimentary rocks are confined to a 300 m wide, ~1.5 km long belt along the San Felipe fault (Plate 1). Faults of the San Felipe fault zone disrupt the sedimentary beds (Plate 1) (Wagner, 1996). Because these rocks are part of a small outcrop belt and isolated from other sedimentary rocks in the area, it was not possible to correlate them with other stratigraphy in the SW Salton Trough. However, their poor consolidation and local provenance suggests that they are probably no older than late Pleistocene. Two

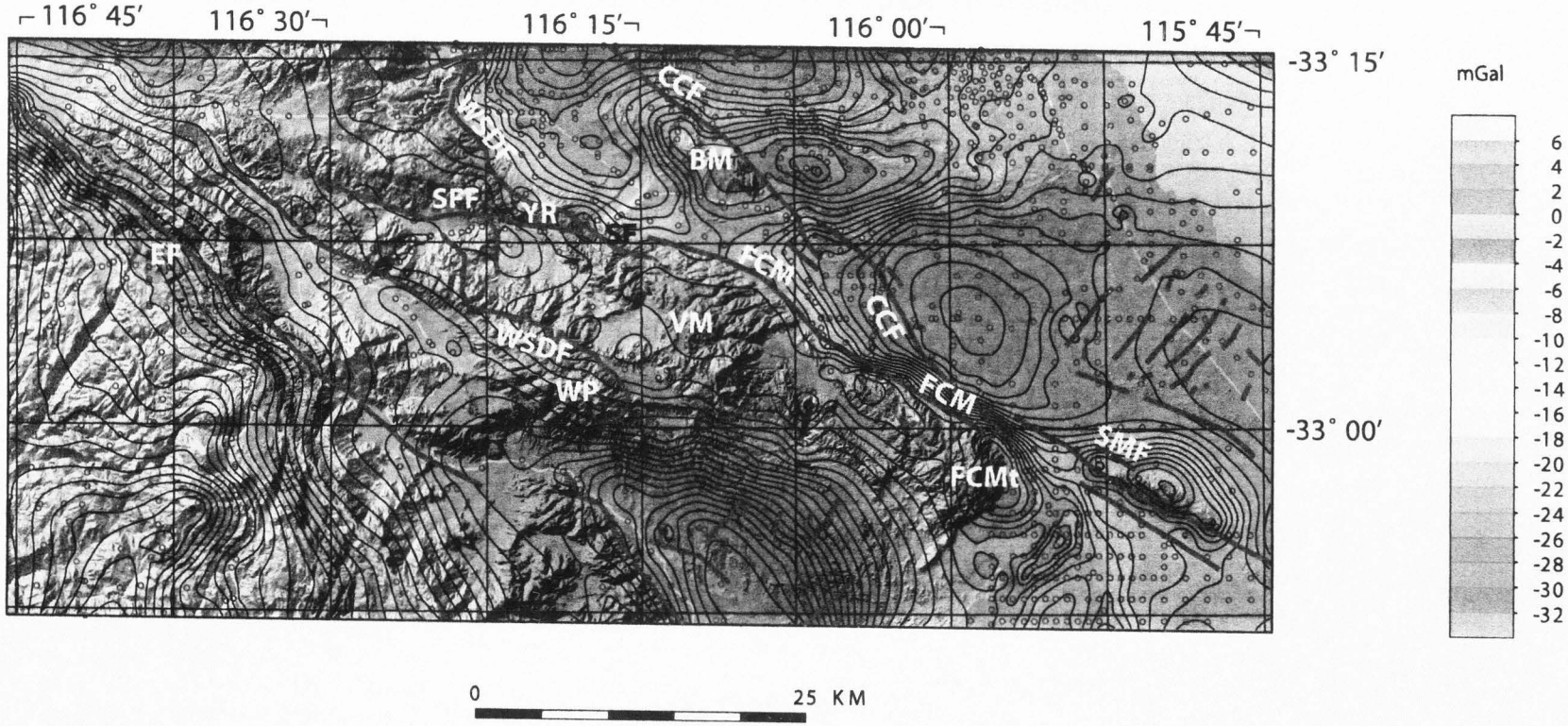

Figure 3-11. Filtered residual Bouger gravity anomaly in the SW Salton Trough. Some major faults are marked in red. Note the strong NW-SE trending alignment of gravity gradients especially along younger dextral faults. BM-Borrego Mountain; CCF-Coyote Creek Fault; EF-Elisnore Fault; FCM-Fish Creek Mountain Fault; FCMt-Fish Creek Mountains; SFF-San Felipe Fault; SF-Sunset Fault; VM-Vallecito Mountains; YR-Yaqui Ridge. Figure provided courtesy of V. Langenheim.

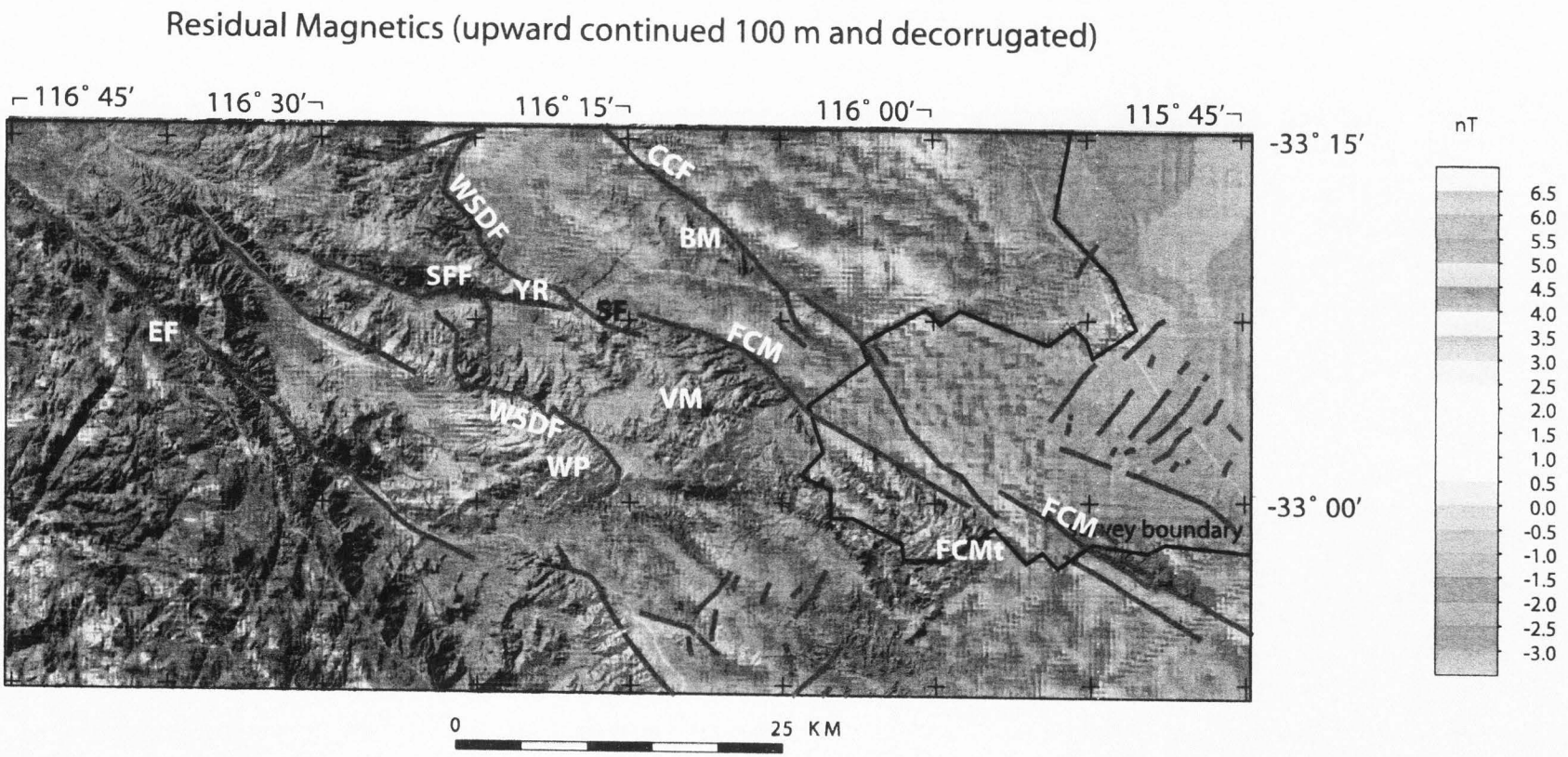

Figure 3-12. Residual magnetic anomaly map of the SW Salton Trough. Major crystalline rock outcrops and some major faults are marked with light red outlines. Note the strong spatial association between younger dextral faults and high magnetic anomalies. Figure provided courtesy of V. Langenheim. See Figure 3-10 for abbreviations.

other outcrops of conglomerate and sandstone on the south side of Yaqui Ridge may also be this age.

Pinyon Ridge segment of the San Felipe fault. The Pinyon Ridge segment of the San Felipe fault strikes about E-W overall but contains faults with NE to WNW strikes and define a concave south map pattern (Fig. 3-3 and Plate 1). This segment persists for ~5.5 km from the segment boundary at Tamarisk Grove to the right bend at the boundary with the Grapevine Canyon segment of the San Felipe fault. Although alluvial fans shed south into the San Felipe Creek drainage from Pinyon Ridge cover much of the fault along this segment in the study area, several good exposures of fault surfaces west of Tamarisk Grove can be correlated with prominent lineaments on air photos. Three-point solutions in exposures of the fault in crystalline rocks and a fault exposure in late Pleistocene sediment show that this segment is steeply north-dipping, and locally shallows to nearly horizontal dips near the surface. No slickenlines were found along this segment of the fault.

There are significant differences in the lithology exposed north and south of the San Felipe fault (Fig. 2-5). In general the northern side of the fault is composed of relatively fine-grained La Posta-type plutonic rocks with a weak foliation. These plutonic rocks grade north and northeast into mylonitic Granite Mountain-type plutonic lithologies and rare pods of metasedimentary rocks appear to be localized near this contact (G. Axen and S. Janecke, unpub. mapping). The mylonite zone projects over the top of Pinyon Ridge and is exposed in a thin fault slice along the fault zone. The south side of the fault contains a much more diverse assemblage of rock types. Near Sentanac Canyon, metasedimentary and metaplutonic rocks dominate and grade eastward into mylonite and protomylonite in the footwall of the West Salton detachment fault (G. Axen, unpublished mapping). The hanging wall of the detachment fault includes a significant amount of metasedimentary rocks, especially biotitic and quartzose lithologies, and an extensive exposure of brecciated coarse-grained La Posta-type plutonic rocks.

The base of the mylonite zone and trace of the West Salton detachment fault may show ~5 km of right lateral separation, but incomplete mapping and irregularities in the distribution of the mylonite and detachment fault hamper efforts to define a precise separation (Fig. 3-3). Although dextral slip estimates along this segment of the fault zone are hampered by a lack of steeply-dipping marker units, a minimum of ~1800 m of vertical offset and north dips on the fault show a significant reverse component.

The Pinyon Ridge segment of the San Felipe fault preserves discontinuous fault scarps along a significant fraction of its many subparallel and anastamosing fault traces (S. Janecke, unpub.mapping). Most of these traces have short fault scarps with up to 3-5 m of throw in surficial deposits of different ages. The scarps are most numerous and best developed in the highest and oldest pediments and Quaternary deposits, and some inset pediments and alluvial fan deposits preserve faint scarps, vegetation alignments, and steps in the landscape at high angles to fluvial channels. One stream cut through a scarp shows that within a few meters of the Earth's surface the San Felipe fault flattens and thrusts Quaternary gravel southward over a pediment surface. A fault strand ~400 m farther north has a similar cross-sectional geometry but carries different crystalline rocks in its footwall and hanging wall and has at least 1.25 km of N-side up displacement (Fig. 2-5). Some topographic steps along the fault that may be fault scarps are even higher in places and mostly indicate north-side up displacements. The history of faulting is complex, however, because some of the highest pediment gravels lap across the fault zone in the Tamarisk Grove segment boundary.

The presence of several branch points of subsidiary structures along the San Felipe fault suggests that the Tamarisk Grove area may be a structural segment boundary (Fig. 3-3). The main strands of the fault zone extend through the boundary with slight changes in strike. East of the boundary the fault trace is buried and to the west the fault zone is actively being exhumed and preserves late Pleistocene of Holocene fault scarps. A major east-dipping normal fault, a major NE-trending anticline, and a NW-striking

dextral fault all merge with the fault zone at the segment boundary.

Mescal Bajada segment of the San Felipe fault. The Mescal Bajada segment of the San Felipe fault is a ~9 km long complex zone at the east end of the transpressional part of the San Felipe fault (Figs. 3-3 and 3-7). Exposure is generally poor along this segment except for outcrops in the segment boundary north of Tamarisk Grove and distributed faulting at the east end. Many NW-striking subsidiary faults in Quaternary sediments and Cretaceous bedrock were identified on aerial photographs (Fig. 3-7). Our mapping shows that this segment consists of several sub-parallel en-echelon and branching NW-striking faults that crop out in plutonic rocks of Yaqui Ridge, the Quaternary alluvium of Mescal Bajada, and plutonic rocks of Round Granite Hill and Sunset Mountain (Fig. 3-5). Although the main strands of the San Felipe fault are buried along San Felipe Wash, its position and E-W trend is well defined by bedrock exposures north and south of the wash.

Main strand. The inferred main trace of the Mescal Bajada segment strikes between E-W and SE and is buried beneath the active channel of San Felipe Wash where no scarps are preserved (Figs. 3-7 and 2-5). Outcrops of the fault near Tamarisk Grove show that it dips steeply to nearly vertical northward. Plutonic rocks next to the fault are brecciated for up to several tens of meters from the fault surface and may be heavily fractured for hundreds of meters. Locally, plutonic rocks are bleached white and have a chalky, punky texture for several meters around fault strands.

Displacement estimates across the entire Mescal Bajada segment are difficult because of the distributed nature of faults and a lack of steeply-dipping offset markers. The West Salton detachment fault dips ~20° SW in its westernmost exposure on the south side of Yaqui Ridge (Fig. 3-7). The detachment fault crops out east of Plum Canyon ~5 km west of its last outcrop south of Yaqui Ridge (Fig. 3-3), although the detachment fault may be overturned in its closest exposures to the San Felipe fault (G. Axen, unpublished mapping). The roughly 5 km of right separation is the result of both dextral and vertical

displacements and may overestimate the true dextral offset.

Subsidiary structures. Subsidiary structures of the Mescal Bajada segment consist of steeply dipping, NW-striking dextral oblique faults and moderately-east-dipping, north-striking normal faults (Figs. 3-3 and 3-7). An en-echelon set of NW-striking faults cuts obliquely across Yaqui Ridge near Yaqui Pass. At its southeastern end the fault set branches from the main strand of the San Felipe fault near the midpoint of the Mescal Bajada segment and has an up to 10 m wide brecciated damage zone along its length. Near this branch point the fault offsets the damage zone of the West Salton detachment fault <100 m (Fig. 3-7). To the northwest the fault does not cut the West Salton detachment fault but instead makes a left bend and parallels Pinyon Ridge in the footwall of the detachment fault (Fig. 3-7).

Near Yaqui Narrows, 70°-90° NE- and SW-dipping, NW-striking faults cut the West Salton detachment fault and its footwall and hanging wall rocks (Figs. 3-5 and 3-7). These faults are less than 3.5 km long, have nearly horizontal striae, and dextrally offset the West Salton detachment fault with <200 m of seperation. The faults cannot be traced more than 2.5 km NW of Yaqui Narrows in the footwall of the West Salton detachment fault, and to the SE they fault brecciated plutonic rock in the hanging wall of the West Salton detachment fault. The breccia zones associated with the steeply-dipping, NW-striking San Felipe fault zone are similar to the hanging wall damage zone created by the West Salton detachment fault. It is difficult to distinguish strands of the San Felipe fault from the background brecciation associated with the detachment fault. However, steep, linear brecciated zones can be traced in the hanging wall of the detachment fault on air photos from known fault strands in the WNW to Harper Canyon in the ESE and likely represent the continuation of fault strands (Fig. 3-3). These faults step left between the Sunset fault and San Felipe fault and are part of the large segment boundary at the east end of the Mescal Bajada segment (Figs. 3-3, 3-5, and 3-7).

A north-striking, east-dipping normal fault in this segment is located along the

western edge of Mescal Bajada and another is located at Yaqui Ridge. The fault along the western edge of Mescal Bajada is inferred from scarps that cut alluvial fan deposits and defines the western edge of a small shallow sedimentary basin beneath Mescal Bajada (Fig. 3-7) with a 2.5 mGal gravity gradient across the fault (Fig. 3-11). To the north the normal fault is inferred to merge with the main strand of the San Felipe fault at the segment boundary.

The sinistral normal fault at Yaqui Ridge that passes near Perpendicular Bluff is 1.8 km long, strikes NNE, dips moderately to steeply east (Fig. 3-7), and has slickenlines that rake from 25° to 35°N (n=3). To the north the fault cannot be traced across the West Salton detachment fault and may lose displacement in that direction. Alternatively it may transfer some displacement and reactivate a portion of the detachment fault on the north side of Yaqui Ridge. At its southern end, the fault cuts the SW-dipping West Salton detachment fault and branches from the San Felipe fault near the middle of the Mescal Bajada segment. Approximately 500 m of sinistral separation is measured across this normal fault near its branch point with the San Felipe fault (Fig. 3-7). Both faults are covered by alluvium and it is clear that the E-dipping normal fault does not continue south into Round Granite Hill.

The divergent splays of the San Felipe fault south of the main strand preserve evidence for late Pleistocene surface rupture. Discontinuous < 2m NE-side down scarps, 65 – 225 m long, are preserved on older alluvial fan deposits along one SE-trending dextral splay of the San Felipe fault (Fig. 3-7). This strand splays from the main fault zone at the segment boundary, strikes ~N50°W, and persists at least 2.5 km to the SE (Fig. 3-3). The east-dipping normal fault on the west edge of Mescal Bajada also preserves short scarps in surficial deposits. The WSW edge of Round Granite Hill is a fault line scarp and may be a bedrock tectonic scarp associated with a small 340° – 325° striking dextral fault that splays from the buried trace of the main San Felipe fault. Although the alluvial surfaces that are cut by these scarps are not dated, they are probably

not older than late Pleistocene, and may be Holocene in age.

Segment boundary at Yaqui Narrows. The east end of the Mescal Bajada segment is a major complex segment boundary between the San Felipe fault to the west and the Fish Creek Mountains fault to the east (Fig. 3-3). The Sunset fault is a smaller intermediary fault strand between the two much larger faults. Both the main trace and subsidiary structures of the Mescal Bajada segment of the San Felipe fault die out to the southeast and do not merge with the Sunset or Fish Creek Mountains faults, and neither subsidiary faults nor the main trace of the Sunset fault merge with the San Felipe fault. Therefore the boundary between the San Felipe and Fish Creek Mountans faults is an ~8 km long, ~3 km wide transpressional left stepover. In this stepover zone the San Felipe and Sunset faults bound folded Cretaceous mylonite and the folded Sunset conglomerate (Fig. 3-3 and 3-7).

Sunset Fault

Main strand. A newly-identified NW-striking fault is located between the San Felipe fault to the west and the Fish Creek Mountains fault to the east-southeast (Figs. 3-3, 3-5, and 3-7). The fault is named the Sunset fault for exposures in Sunset Wash, and it is also exposed in Harper Canyon to the SE (Fig. 3-5). Structural and kinematic data were collected in several locations, although much of the fault is either covered by alluvium or is poorly exposed. Throughout most of its length the Sunset fault places the ~1.0 ± 0.1 Ma- to 0.6 Ma Sunset conglomerate of the Ocotillo Formation and the uppermost underlying Canebrake, Diablo, and Olla formations of the Palm Spring Group against plutonic La Posta-type tonalite (Fig. 3-5). Locally, thin belts of moderately- to steeply-dipping fault-bound slivers of Palm Spring Group crop out along the fault. Northwest of San Felipe Wash the main strand of the Sunset fault becomes an inferred buried N- to NE-striking normal fault and a set of smaller faults that cut and uplift the Canebrake Conglomerate (Figs. 3-3 and 3-7). Along most of its length, plutonic

rocks SW of the fault are brecciated for 0.5 – 5 m from the fault surface and are locally bleached white and have a chalky texture. Fracturing is locally well developed up to several hundred meters from the fault surface.

The Sunset fault zone persists for ~10.8 km from near Harper Canyon northwest to near Borrego Springs Road and changes northwestward from a ~5.7 km long single strand to several moderate to small magnitude normal to dextral faults with northwest to northeast strikes (Figs. 3-3, 3-5, and 3-7). The Sunset fault zone parallels the San Felipe fault for ~7.5 km and is 1-3 km farther NE.

The Sunset fault could either merge laterally and at depth with the West Salton detachment fault or cut the detachment fault and become an 4 km wide by 5 km long horsetail splay NE of Yaqui Ridge and include one ESE-dipping normal fault with <1.5 km of throw (Fig. 2-5). We prefer the second interpretation because small-offset strike-slip faults of the San Felipe fault zone (sensu latu) cut the West Salton detachment fault near the tip of Yaqui Ridge and show that dextral faults cut the detachment fault instead of reactivating it. At its southeastern end the Sunset fault is cut by a small, unnamed steeply to moderately SW-dipping, northwest-striking fault (Fig. 3-7) and parallels the Fish Creek Mountains fault for at least 2.5 km (Fig. 3-3). The boundary between the Sunset fault and the Fish Creek Mountains fault is a faulted transpressional left stepover in which the two faults bound complexly folded Quaternary Sunset conglomerate of the Ocotillo Formation (Figs. 3-3 and 3-5).

East of San Felipe Wash (The Narrows) the map trace of the Sunset fault trends N55°W ± 10° and three point solutions from along the length of the fault show that it changes dip and dip-direction along strike. In Sunset Wash the fault dips steeply SW, near Harper Canyon the fault dips moderately to steeply NE, and about halfway between it is vertical (Fig. 3-5). Measurements from primary fault surfaces (n=12) show a set of N20°W ± 12° striking, 70° – 85° dipping surfaces and a set of N50°W striking, ~70° – 90° dipping faults (Fig. 3-13a). Slickenlines measured from fault surface striae (n=17)

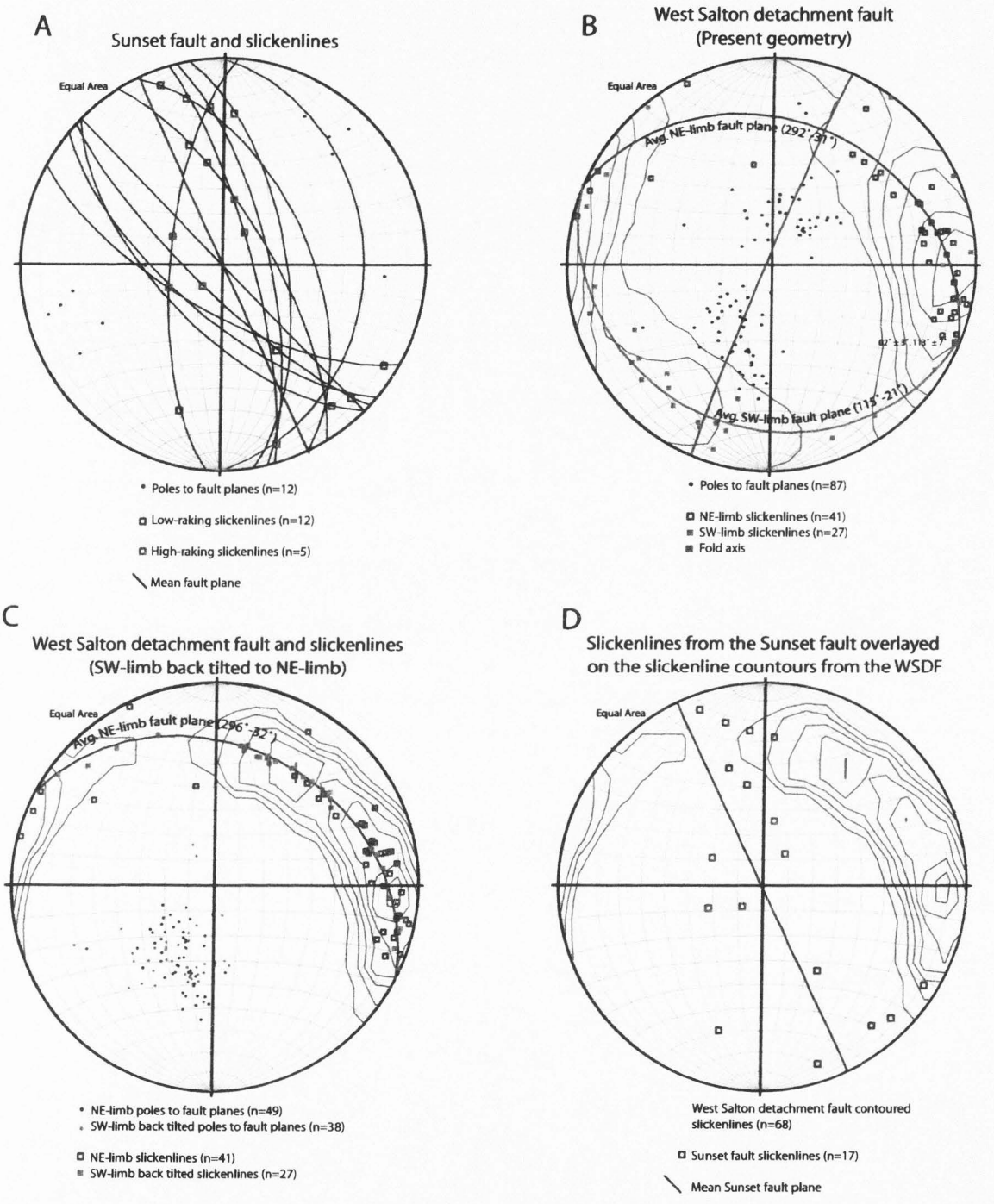
A
Sunset fault and slickenlines
Equal Area
• Poles to fault planes (n=12)
Low-raking slickenlines (n=12)
High-raking slickenlines (n=5)
Mean fault plane
B
West Salton detachment fault
(Present geometry)
Equal Area
Avg. NE-limb fault plane (292°, 32°)
Avg. SW-limb fault plane (115°, 21°)
• Poles to fault planes (n=87)
NE-limb slickenlines (n=41)
SW-limb slickenlines (n=27)
Fold axis
C
West Salton detachment fault and slickenlines
(SW-limb back tilted to NE-limb)
Equal Area
Avg. NE-limb fault plane (296°, 32°)
• NE-limb poles to fault planes (n=49)
SW-limb back tilted poles to fault planes (n=38)
NE-limb slickenlines (n=41)
SW-limb back tilted slickenlines (n=27)
D
Slickenlines from the Sunset fault overlayed
on the slickenline countours from the WSDF
Equal Area
West Salton detachment fault contoured
slickenlines (n=68)
Sunset fault slickenlines (n=17)
Mean Sunset fault plane

Figure 3-13.

are also scattered and ~70% have rakes <45° with average trends of NNW to SE (Fig. 3-13a). The remaining 30% of data are nearly pure dip-slip vectors. These data show that the Sunset fault has complex slip patterns and is mostly a NE-side down reverse or normal oblique strike-slip fault. The slip vectors measured on the Sunset fault, although small in number, are not recorded by any major slickenline population on the nearby West Salton detachment fault (Fig. 3-13a – c) and overlap with <6-7% of slickenlines on the detachment fault (Fig. 3-13d).

Geophysical character of the Sunset fault. The gravity gradient across the Sunset fault is subdued (Fig. 3-11) and there are few data in the vicinity of the fault. Because the fault juxtaposes at least 600 m of sedimentary rocks against plutonic rocks a large gravity gradient would be expected. However, because the Sunset conglomerate is composed dominantly of plutonic rocks derived from the SW side of the fault the density of sedimentary rocks may be similar to the density of the brecciated plutonic rocks across the fault. Two other factors may also contribute to the weak gravity gradient. Cross sections show that the West Salton detachment fault is located at shallow depths beneath the Sunset conglomerate where the detachment fault has truncated the low density basin fill (Fig. 2-5). Furthermore, because the folded West Salton detachment fault at Yaqui Ridge projects beneath the Vallecito Mountains (Fig. 2-5) it may produce complicated gravity signals in that area.

The filtered residual magnetic map shows that the trace of the Sunset fault follows a very weak NW-trending magnetic gradient (Fig. 3-12). This gradient continues along Yaqui Ridge several kilometers NW of San Felipe Wash, then appears to merge with a stronger ESE-trending magnetic high along the north side of the San Felipe fault. To the southeast, the magnetic gradient disappears near Harper Canyon where the Sunset fault is cut and the gradient reappears near the topographic front of the Fish Creek Mountains (Fig. 3-12).

Displacement across the Sunset fault. A lack of displaced steeply-dipping

markers prevents an accurate offset measurement across the Sunset fault. Therefore we use the thickness of the Sunset conglomerate and kinematic data to provide an estimate of the amount of slip across the fault. The Sunset conglomerate is ~600 m thick and was deposited during slip on the Sunset fault. If the thickness of the conglomerate records the amount of accommodation space produced as a result of the vertical component of slip on the fault, and we generalize the Sunset fault as a near-90°-dipping fault, we can use the average ~30° rake of slickenlines (Fig. 3-13a) to calculate the amount of dextral slip required to produce 600 m of vertical offset. This calculation yields a minimum estimate of ~1.2 km of dextral offset across the Sunset fault.

Further constraints on the amount of slip can be made from the provenance, grain size, and paleocurrents of the Sunset conglomerate. Provenance studies show that ~64% of clasts in the conglomerate were derived from La Posta-type plutonic rocks in the hanging wall of the West Salton detachment fault. The lack of mylonite clasts in the Sunset conglomerate suggests that the source area must have been in the hanging wall of the detachment fault. The tonalite clasts are up to 4 m diameter angular boulders near the fault zone (Fig. 3-6) and require that the Sunset conglomerate was located close to the tonalite source area during deposition. La Posta-type plutonic rocks have a unique spatial distribution in this area and only crops out south of a poorly understood ENE-trending boundary (Fig. 3-7). North of this boundary Canebrake Conglomerate of the Palm Spring Group is the only lithology in the hanging wall of the West Salton detachment fault (Fig. 3-7). Using this unique distribution, clast lithologies in the Sunset conglomerate, coarse grain size of the Sunset conglomerate near the Sunset fault, and fault-perpendicular paleocurrents, the Sunset conglomerate could not have been located north of the La Posta-Canebrake boundary during deposition. This limits slip to less than ~2.5 km of dextral separation.

Fish Creek Mountains Fault

The Fish Creek Mountains fault was first mapped by Dibblee (1954, 1984) as the southeastern continuation of the San Felipe fault. Our mapping and analysis show that the Fish Creek Mountains fault is a separate fault at the east end of a faulted transpressional stepover (Fig. 3-3). Although the Fish Creek Mountains fault is only exposed near Harper Canyon (Fig. 3-5), the steep, up to 0.8 km high, 32 km long topographic escarpment along the northeast edge of the Vallecito and Fish Creek mountains coincides with major NE-side-down gradients in the gravity field and approximately marks the location of the fault (Figs. 3-3 and 3-11). The Fish Creek Mountains fault strikes N60°W over a distance of >55 km (Fig. 3-2) based on escarpments and gravity gradients, and juxtaposes late Cenozoic basin fill in Lower Borrego Valley against plutonic and metamorphic rocks of the Vallecito and Fish Creek mountains. To the southeast the fault projects toward the Superstition Mountain fault (Fig. 3-2), and to the northwest it parallels the Sunset fault for at least 2.5 km and terminates NW of Harper Canyon (Fig. 3-3). Because the fault is buried beneath the alluvium of Lower Borrego Valley, most inferences about the geometry and position of this fault are based on topography, gravity, and magnetic data.

Based on differences observed in the gravity anomaly, the trend of topographic escarpments, and convergence of several subsidiary faults southwest of the Fish Creek Mountains fault, we divide the fault into two major structural segments (Fig. 3-3). Both of these segments have gravity gradients that trend NW and indicate steep to gentle northeast fault dips. We define the structural segment boundary at the northeast corner of the Vallecito Mountains on the basis of: 1) an ~25° right bend in the gravity contours, 2) a change in the trend and character of topography; 3) a dramatic southeastward increase in the gravity gradient NE-ward across the fault; 4) a clustering of branch points with divergent cross faults on the southwest side of the fault, and: 5) the intersection between

the ENE-striking Vallecito fault and the Fish Creek Mountains fault. Subsidiary faults with strikes ~20° clockwise of the main SE Fish Creek Mountains fault crop out south of the main strand in the Fish Creek Mountains (Dibblee, 1954, 1984) and project NW into the segment boundary zone.

NW segment of Fish Creek Mountains fault. The northeastern edge of the Vallecito Mountains, a NW-trending gravity gradient, and several small fault exposures define the NW segment of the Fish Creek Mountains fault. The NW segment has an 11.5 km long, N70°W trending gently curving topographic escarpment (Figs. 3-2 and 3-3). This escarpment coincides with a gravity saddle on the north side of the fault (Fig. 3-11). The gravity gradient across the fault increases in magnitude southeastward along the fault. A subtle positive magnetic anomaly coincides with the northwest segment for most of its trace and diverges northwestward at the WNW end of the segment. The divergent magnetic anomaly projects toward the Veggie-line fault (Fig. 3-3).

Although the fault is buried along most of its length, several exposures near Harper Canyon show 2-3 sub-parallel NW-striking, moderately NE-dipping faults, and several E-W-striking, steeply dipping faults (Figs. 3-3 and 3-5). Anomalous strikes and dips in the Sunset conglomerate suggest that the Fish Creek Mountains fault persists at least 2 km northwest of the plutonic rocks at Harper Canyon and cuts Cenozoic basin fill. Overall, we interpret these data as an 11.5 km long, ~N70°W striking, steeply to moderately NNE-dipping fault that overlaps for 2.5 km with the Sunset fault at its northwest end. We interpret the northwestward decrease in the gravity gradient across the fault and divergent fault strands near Harper Canyon as a horsetail splay and northwestward decrease in displacement toward the NW terminus of the Fish Creek Mountains fault (Figs. 3-3 and 3-5).

Displacement on the NW segment of the FCM fault is difficult to estimate from surficial geology because of no exposures in the hanging wall and the dominance of plutonic rocks in the footwall. Because no plutonic rocks crop out in Lower Borrego

Valley and no sedimentary rocks are preserved in the central and northern Vallecito Mountains we can use the 0.7 km height of the mountains as a minimum constraint on the vertical component of slip along this segment.

SE segment of the Fish Creek Mountains fault. The steep and sharply curving northeastern edge of the Fish Creek Mountains and a prominent NW-trending gravity step show that the SE segment of the Fish Creek Mountain fault is at the mountain front (Figs. 3-2, 3-3, and 3-11). The topographic escarpment of the Fish Creek Mountains trends N55°W for at least 37 km and lies 1-2 km southwest of the active trace of the Coyote Creek strand of the San Jacinto fault zone (Fig. 3-2). To the southeast both the SE segment of the Fish Creek Mountains fault and the Coyote Creek fault project into the Superstition Mountain fault. North of the Fish Creek Mountains the gravity gradient tightens and trends NW for ~22 km to the segment boundary (Fig. 3-11). Southeast of the Fish Creek Mountains a gravity saddle exists between the Fish Creek Mountains and Superstition Mountain and the location of the gravity low switches from the NE to the SW side of the Fish Creek Mountains fault. We interpret these data as an >37 km long, ~N55°W striking, steeply to moderately NE-dipping fault along the NE side of the Fish Creek Mountains.

Age of the SE Fish Creek Mountains fault. Paleogeographic reconstructions, paleocurrents, and sedimentologic data from the ~1.1- to 0.6 Ma Ocotillo and Brawley formations in the San Felipe Hills document a W- to NW-trending plutonic-cored uplift coincident with the modern Fish Creek and southeastern Vallecito mountains that supplied recycled Diablo Formation clasts to the Ocotillo Formation (Kirby et al., in press). These workers suggest that activity on the Fish Creek Mountains fault created this uplift and that the fault likely initiated around ~1.1 Ma (Kirby, 2005). Although no scarps are present along the FCM fault, the Holocene shoreline of Lake Cahuilla coincides with the southern Fish Creek Mountain front, suggesting that subsidence continued until late Quaternary time.

Folds in and near the San Felipe Fault Zone

Folds deform all of the Cenozoic sedimentary rocks and some of the crystalline rocks in the study area (Fig. 3-3). The directions and magnitudes of shortening vary tremendously across the area so we analyzed this deformation in each of five structural domains (Fig. 3-14). We use stereonet analyses, map patterns, and shortening estimates from cross sections and average interlimb angles to show that three of the fold domains are strikingly similar to each other (West Salton detachment fault, Yaqui Ridge footwall, and Harper Canyon domains) and differ from the remaining two domains (Yaqui Meadows northeast and southeast domains). We use cross-cutting relationships and the age of the Sunset conglomerate to constrain the age of folding to middle Pleistocene to Recent time in the stepover zones.

Folded Rocks and Structures in Stepovers of the San Felipe Fault Zone

The footwall of the West Salton detachment fault at Yaqui Ridge. This domain is located north of the Mescal segment of the San Felipe fault in the footwall of the West Salton detachment fault along Yaqui Ridge (Fig. 3-14). In this domain, the footwall of the West Salton detachment fault consists of foliated to mylonitic plutonic rocks of the Eastern Peninsular Ranges mylonite zone and local lozenges of metasedimentary rocks (Fig. 3-7). Foliations in these rocks define NW, NE, and E-W-trending folds (Figs. 3-7 and 3-14).

Map analysis of folds shows that there are two major fold trends; WNW-trending with fewer E-W-trending and NE-trending folds (Fig. 3-7). At the SE-tip of Yaqui Ridge, two monoclines define an anticlinal box fold with hinges 300-600 m apart. These two major monoclines define the crest of the footwall, generally parallel the West Salton detachment fault on the north flank of Yaqui Ridge, and are 0.25 – 1 km SSW of the fault (Fig. 3-7). The monoclines persist ~2 km NW-ward from the tip of Yaqui Ridge

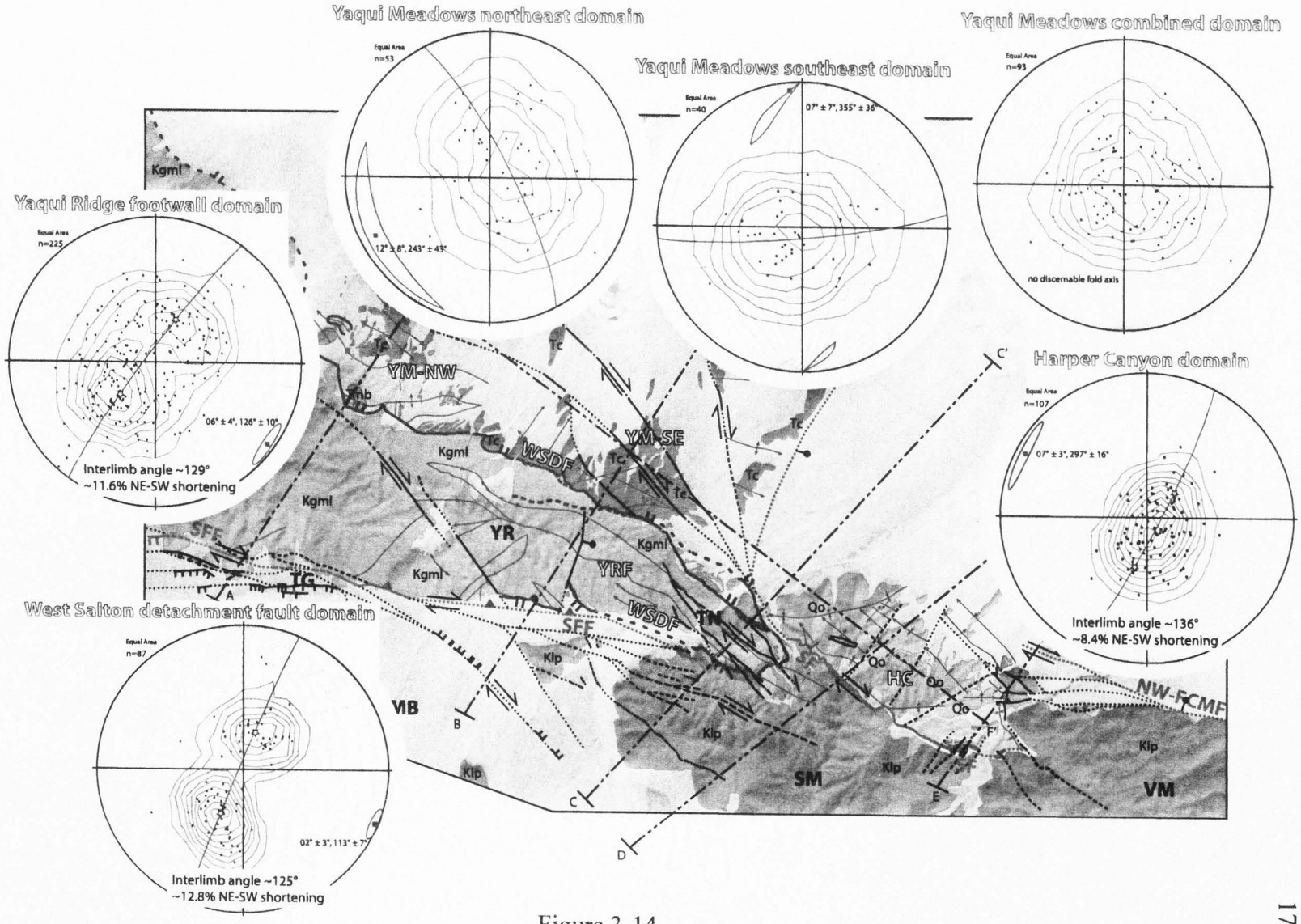
Yaqui Meadows northeast domain
Equal Area
n=53
12° ± 8°, 243° ± 43°
Yaqui Meadows southeast domain
Equal Area
n=40
07° ± 7°, 355° ± 36°
Yaqui Meadows combined domain
Equal Area
n=93
no discernable fold axis
Yaqui Ridge footwall domain
Equal Area
n=225
06° ± 4°, 126° ± 10°
Interlimb angle ~129°
~11.6% NE-SW shortening
Harper Canyon domain
Equal Area
n=107
07° ± 3°, 297° ± 16°
Interlimb angle ~136°
~8.4% NE-SW shortening
West Salton detachment fault domain
Equal Area
n=87
02° ± 3°, 113° ± 7°
Interlimb angle ~125°
~12.8% NE-SW shortening
Kgml
Tc
YM-NW
YM-SE
WSDF
YR
YRF
SFF
Klp
TH
HC
SM
VM
VIB
NW-FCMF
Qo
A
A'
B
C
C'
D
E
F
F'

Figure 3-14.

where they change into anticlines and several smaller scale synclines merge with and link the major anticlines. NE and SW-plunging folds are localized SW of the monoclinal and anticlinal pair of folds, especially in the west, where NE, E, and SW-plunging folds become the dominant set of folds. One of the dominant NW-trending anticlines dies out in the NW whereas the other major NW-trending anticline changes orientation and may be continuous with the NE-plunging anticline that intersects the San Felipe fault zone at the Tamarisk Grove segment boundary. The overall trace of the southern monocline-anticline has a strong concave south map trace and connects the segment boundary at Tamarisk Grove with the boundary near Harper Canyon (Figs. 3-5, 3-7, and 3-14).

Stereonet analysis of 225 foliation measurements shows that ESE-plunging folds dominate this domain (Fig. 3-14). Folds in this domain plunge 06° ± 4°, and trend 126° ± 10°. The dominant ESE plunge of the folds is probably due to the original easterly dip of the Cretaceous fabrics. The NE- and E-trending folds are not evident in the stereonet analysis in part because fewer attitudes were collected in the southwest. Although data are scattered, an interlimb angle of 129° is measured from the contoured center of the average fold limbs (Fig. 3-14). If this interlimb angle is used to construct a single fold, it represents ~11.6% NE-SW shortening across the fold (Table 3-1). The lack of a distinct marker unit in the mylonite precludes a cross section analysis of shortening.

The West Salton detachment fault. We analyzed the geometry of the West Salton detachment fault throughout its exposure along the NE and S sides of Yaqui Ridge. Overall, the West Salton detachment fault has a NW-trending anticlinal geometry at Yaqui Ridge (Figs. 3-5, 3-7, and 3-14). At the SE tip of Yaqui Ridge a NE-dipping limb, SE-dipping limb, and SW-dipping limb define an ESE-plunging anticline (Figs. 3-5 and 3-7). This box fold is coincident with the box fold defined by the foliations in the structurally underlying footwall. The ESE plunge is likely inherited from the original ENE dip of the West Salton detachment fault. Further analysis of the folded West Salton detachment fault is difficult because fault exposures are parallel to the dominant ESE-

Table 3-1. Fold domain characteristics for domains inside and outside of transpressional stepovers. Note the similarities between the Yaqui Ridge footwall, West Salton lowangle fault, and Harper Canyon domains, all of which are bound between strands of the San Felipe fault zone. Shortening estimates in parentheses for the Harper Canyon domain include 3.7% NE-SW shortening as recorded by the 15° angular unconformity below the Sunset conglomerate.

Domain	Fold axis trend and plunge	Interlimb angle	NE-SW shortening from IL angle	NE-SW shortening from cross section analysis
Yaqui Ridge footwall mylonite	126° ± 10°, 06° ± 4°	~129°	~11.6%	N/A
West Salton low-angle fault	113° ± 7°, 02° ± 3°	~125°	~12.8%	~11.4 – 14.0%
Harper Canyon (Sunset conglomerate)	297° ± 16° 07° ± 3°	~136°	~8.4% (~12.1%)	~7 – 8.3% (~10.7 – 12.0%)
Yaqui Meadows NE	243° ± 43° 12° ± 8°	N/A	N/A	N/A
Yaqui Meadows SW	355° ± 36° 07° ± 7°	N/A	N/A	N/A
Yaqui Meadows combined	No fold axis	N/A	N/A	N/A

plunging fold axes for most of the length of the West Salton detachment fault. Therefore it is not possible to determine whether the closely spaced folds in the footwall of the West Salton detachment fault also deform the fault. However, two cross sections drawn perpendicular to the trend of Yaqui Ridge show that the West Salton detachment fault has a fold geometry that is very similar to that of the underlying footwall rocks (Fig. 2-5).

Stereonet analysis of 87 fault plane measurements show that the West Salton detachment fault is folded into an anticlinal geometry and has two well defined limbs (Fig. 3-14). These two limbs define a 02° ± 3° plunging, 113° ± 7° trending fold axis. A slight spread in the data from the NE limb of the West Salton detachment fault defines a second 22° ± 2° plunging, 077° ± 21° trending anticlinal axis that is not apparent in the data from the SW limb. An interlimb angle of 125° is measured from the overage orientation of the north and south limbs of Yaqui Ridge. If this interlimb angle is used to construct a single fold, it represents ~12.8% NE-SW shortening across Yaqui Ridge. Analysis of two cross sections show that the West Salton detachment fault has minimum of ~11.4 – 14.0% NE-SW shortening across Yaqui Ridge (Fig. 2-5; Table 3-1).

Sedimentary rocks near Harper Canyon. The Harper Canyon domain involves Pliocene to Quaternary sedimentary rocks exposed in the hanging wall of the West Salton detachment fault between Yaqui Narrows and Harper Canyon (Figs. 3-5 and 3-14). Map analysis shows that folds in the Sunset conglomerate only deform sedimentary rocks and are composed of two fold orientations; a dominant set of NW-plunging folds in the central part of the domain, and a pair of E-W-trending synclines at the north and south ends of the domain (Fig. 3-5). Overall, NW-plunging folds are parallel to the dextral oblique strike-slip faults that bound the domain and have a left-stepping central anticline in each of three fault blocks bounded by NE-striking left lateral faults (Fig. 3-5). Together the folds transform a 1.7 km wide SW-dipping homocline in the north into a 1.25 km wide NE-dipping homocline in the south. An angular unconformity at the base of the Sunset conglomerate and the syntectonic character of the unit suggest that some

of the shortening may have occurred before and possibly during deposition of the Sunset conglomerate. This angular unconformity translates into ~3 – 4% NE-SW shortening (Table 3-1). This is consistent with the somewhat smaller strains in this domain relative to those measured in the footwall of the West Salton detachment fault and the fault itself. However, most of the folding post-dates deposition of the Sunset conglomerate.

Strike and dip measurements for the stereonet analysis are mostly from the Quaternary Sunset conglomerate (n=100) with a few measurements from the thin belt of underlying Pliocene Palm Spring Group (n=7). Measurements from fault-bound slivers of Palm Spring Group or from Palm Spring Group that is not overlain by Sunset conglomerate were not included. Stereonet analysis of 107 bedding orientations show an overall 07° ± 3° plunging, 297° ± 16° trending cylindrical fold axis with significant scatter (Fig. 3-14). An interlimb angle of 136° is estimated from the data and represents ~8.4% NE-SW shortening. Cross section analysis of the Sunset conglomerate in this domain shows a minimum of ~7-8.3% NE-SW shortening (Fig. 2-5; Table 3-1). The WNW plunge of the folds is due to NW-ward tilting in the hanging wall of the normal fault at the east edge of the horsetail fault zone (Fig. 3-14 and 2-5).

Folded Sedimentary Rocks Outside the San Felipe Fault Zone:

The NW and SE Yaqui Meadows domains. This domain analyzes Canebrake Conglomerate of the Pliocene Palm Spring Group in the hanging wall of the West Salton detachment fault along the NE side of Yaqui and Pinyon ridges (Fig. 3-14). The Canebrake Conglomerate can be divided into two separate domains, the northwest and southeast Yaqui Meadows domains because of differences in fold geometries. The two domains lie on either side of the NW-trending Borrego Springs Road. Both domains are bound on the SW by the West Salton detachment fault which faults the Canebrake Conglomerate against mylonitic rocks (Figs. 3-7 and 3-14). These rocks are not in

the two stepovers of the San Felipe fault zone and are cut by the horsetail splay at the NW end of the Sunset fault. Quaternary alluvium surrounds the domains along their remaining boundaries.

The NW Yaqui Meadows domain contains mostly W plunging folds. The SE domain also preserves E-W-trending folds and also has at least three NNE-plunging folds at a high angle to the West Salton detachment fault (Figs. 3-7 and 3-14). The detachment fault appears to cut across these folds and is not folded about NNE axes. Strike and dip analysis of the NW Yaqui Meadows domain (n=53) shows significant scatter with an average 12° ± 8° plunging, 243° ± 43° trending fold axis (Fig. 3-14). Analysis of the SE Yaqui Meadows domain (n=39) also shows significant scatter with an average 07° ± 7° plunging, 355° ± 36° trending fold axis (Fig. 3-14). When combined, these data yield significant scatter with no discernible fold axis (Fig. 3-14). The significant scatter of bedding poles in the strike and dip analysis likely results from the superposition of two to three fold sets in each domain. The lack of any discernible fold axis when the data from the NW and SE domains are probably reflects sampling of perpendicular fold sets.

DISCUSSION

Age of the Sunset Fault

The age of the Sunset fault is constrained by the Sunset conglomerate which was deposited syn-kinematic to slip on the fault. The oldest deposits of this syntectonic unit are ~1.1 Ma and show that the Sunset fault existed by that time. Some amount of uplift and erosion prior to the ~1.1 Ma base of the Sunset conglomerate is required by the absence of Borrego Formation and a 15° angular unconformity at the base of the conglomerate. The angular unconformity and possible missing stratigraphy may have been created by a fault-tip propagation anticline above the nascent and growing Sunset fault of the San Felipe fault zone (e.g. Gawthorpe et al., 1997; Sharp et al., 2000). A fault propagation fold above a normal fault would uplift the footwall in early stages of

development and be similar to a fault propagation fold above a reverse fault (Gawthorpe et al., 1997). Once the fault tip of a propagating normal fault reaches the surface, accommodation space is created on the down-thrown side of the fault and deposition begins (Gawthorpe et al., 1997). Although the San Felipe fault zone is predominantly a strike-slip fault it has significant reverse and normal components. A fault propagation fold can explain the uplift and erosion of Plio-Pleistocene basin fill from the Vallecito Mountains before deposition of the Sunset conglomerate, the north dip of the basal unconformity, and the north dip of older basin-fill deposits beneath the angular unconformity when it is restored to horizontal.

The length of time represented by the angular unconformity at the base of the Sunset conglomerate greatly depends upon how much Borrego or Huseo Formation was originally present and could significantly affect the age of the Sunset fault. Based on estimated uplift rates of 2 – 10 mm/yr and complete erosion of the maximum 1.3 – 1.8 km thick section of Huseo or Borrego Formation respectively, between ~0.1 – 0.9 m.y. may have been required to erode these formation before deposition of the Sunset conglomerate began. However, if little to no Borrego or Huseo Formation was deposited, the angular unconformity could have formed by slight tilting and little erosion in a much shorter period of time.

Overall, these data suggest that the Sunset fault was active by the base of the Sunset conglomerate at ~1.1 Ma and may have initiated slightly earlier. Depending on the thickness of the Borrego o Hueso Formation deposited near Harper Canyon, the initiation of the Sunset fault can be bracketed between ~2.0 and 1.1 Ma. The sudden appearance of recycled sandstone clasts in the upper Borrego Formation between ~1.1 and 1.3 Ma may signal the first uplift along the Sunset fault of the San Felipe fault zone. Therefore, our preferred interpretation is that the Sunset fault initiated sometime between ~1.1 and 1.3 Ma, but also acknowledge that it may be as old as ~2.0 Ma. A fault-tip propagation fold may have been the surface expression of the fault during early stages of

slip, and it most likely had ruptured to the surface by ~1.1 Ma

Interpretation and Timing of Folding

The San Felipe fault zone bounds the Yaqui Ridge footwall, West Salton detachment fault, and Harper Canyon structural domains (Fig. 3-14). Folds in these three domains have similar dominant WNW and secondary ENE to E-W fold trends and record similar amounts of NE-SW shortening (Fig. 3-14; Table 3-1). The Yaqui Meadows fold domains are north of the San Felipe fault zone and have distinctly different fold geometries than the other domains (Fig. 3-14; Table 3-1). These relationships suggest a common origin for the folds in the Yaqui Ridge footwall, West Salton detachment fault, and Harper Canyon domains that differs from the one in the two Yaqui Meadows domains. Steeper dips there, including southwest dips probably developed during slip on the West Salton detachment fault. Because three left-stepping dextral oblique faults of the San Felipe fault zone bound the three similar domains, we suggest that folds were the result of strain transfer across the two left stepovers in the fault zone. These two contractional stepovers provide a soft link between the Mescal Bajada segment of the San Felipe fault, the Sunset fault, and the NW segment of the Fish Creek Mountains fault.

The errors associated with our strain estimates are probably large enough that the estimates are statistically similar. However, the strains appear to be consistently less in the Harper Canyon domain (Table 3-1). These differences could be a result of a period of pre-Sunset conglomerate folding recorded in the crystalline rocks. The ~15° angular unconformity at the base of the Sunset conglomerate records ~3.7% NE-SW shortening prior to deposition of the syntectonic conglomerate. When this earlier phase of deformation is included in the shortening estimates for the Sunset conglomerate the discrepancy between the conglomerate domain and the crystalline rock domains vanishes (Table 3-1). We suggest that this preliminary, small-magnitude folding event (less than 25% of the entire NE-SW shortening), may have been related to early movements

and associated folding of the nascent San Felipe fault zone and probably represents a relatively minor component of the total strain recorded in the fold domains. However, we recognize that the age of postulated early folding is only constrained to sometime between deposition of the Pliocene Palm Spring Group and deposition of the Quaternary Sunset conglomerate and may not be related to the San Felipe fault zone.

Although a small amount of pre-Sunset folding is our preferred explanation for the differences in shortening estimates, three other options may also explain the discrepancy: 1) less strain being transferred across the stepover that bounds the Harper Canyon domain than across the stepover that bounds the Yaqui Ridge footwall and West Salton detachment fault domains, 2) syn-depositional folding that is not captured in our analysis, or; 3) similar amounts of deformation in each domain but more N-S shortening and less NE-SW shortening in the Harper Canyon domain than in the other two domains. It is possible that several of these processes contributed to the shortening differences, but current data are equivocal.

The inferred ~1.1 Ma- to 0.6 Ma age of the Sunset conglomerate and cross-cutting relationships provide constraints on the timing of folding. Because the majority of folds in the Harper Canyon domain deform the Sunset conglomerate, the folds must post-date the end of conglomerate deposition at ~0.6 Ma. Evidence for syn-depositional folding is equivocal and further mapping is needed to address this possibility. The angular unconformity beneath the Sunset conglomerate records slight north- to northeast-ward tilting prior to deposition which may suggest that nascent folds began forming prior to or around ~1.1 Ma.

Because the Yaqui Ridge footwall, West Salton detachment fault, and Harper Canyon domains have similar fold geometries (Table 3-1) and were formed by the same set of bounding structures, we suggest that most folds in the Yaqui Ridge footwall and West Salton detachment fault domains also post-date ~0.6 Ma. The post ~0.6 Ma age of folding in the San Felipe fault zone shows that the Yaqui Ridge anticline was formed

entirely during Quaternary time and is neither a primary corrugation of the West Salton detachment fault nor an anticline that formed during principal slip on the detachment fault. The age of folding is similar to the ~0.6 Ma onset of closely-spaced folding in the San Felipe Hills and Borrego Badlands (Kirby, 2005; Lutz et al., in press). These events are interpreted as the result of a structural reorganization in the San Jacinto fault zone (Kirby, 2005; Lutz et al., in press) and together with folding in the Sunset conglomerate suggest a major basin-wide tectonic reorganization at ~0.5 - 0.6 Ma.

Geometry of Stepovers along the San Felipe Fault Zone

The geometries of folds in the two stepovers along the dextral-oblique San Felipe, Sunset, and Fish Creek Mountains faults are unusual for contractional stepovers along strike-slip faults (e.g., Christie-Blick and Biddle, 1985; Sylvester, 1988). In the San Felipe fault zone, WNW-trending folds are dominant and are often parallel and close to bounding strike-slip faults (Fig. 3-14). E-W- to NE-trending folds are subsidiary to, and are often located adjacent to the WNW-trending folds at the boundaries of strongly folded or homoclinal domains (Fig. 3-14). We interpret the WNW-trending fold set as fault-strike-parallel transpressional folds resulting from strain partitioning of fault-perpendicular shortening near the bounding dextral-oblique strike-slip faults. The subsidiary E-W-trending folds are interpreted as wrench folds that form perpendicular to the maximum finite compressive stress in many strike-slip systems (e.g., Christie-Blick and Biddle, 1985; Sylvester, 1988). The presence of a few NE-trending folds is difficult to interpret.

We believe that fold geometries found in stepovers of the San Felipe fault zone represent a unique, previously unrecognized type of stepover. Typically, folds in contractional strike-slip fault stepovers are dominated by wrench folds and a few strain-partitioned, fault-parallel folds. The Ocotillo Badlands preserve a well known example of this geometry in a ~2 km wide contractional stepover between NW-striking dextral strike-

slip faults of the Coyote Creek fault (Brown et al., 1991). The Ocotillo Badlands fault-bound domain shows two fold geometries; dominant E-W trending folds located between the two bounding faults and subordinate NW-trending folds parallel to sub-parallel with bounding strike-slip faults that are localized in a few hundred meters of the dextral faults.

Each of the three main faults of the San Felipe fault zone have significant oblique components of slip and the overall left stepping geometry from the San Felipe fault to the Fish Creek Mountains fault is contractional. We suggest that the dominance of WNW-trending strain-partitioned folds in stepovers of the San Felipe fault zone is a consequence of the obliquity of slip vectors on the bounding faults and the contractional geometry of the San Felipe fault south of Yaqui Ridge. This geometry is best described as an oblique strain-partitioned stepover and is very different from the wrench-dominated stepovers of many strike-slip fault zones.

Deactivation of the West Salton Detachment Fault

The West Salton detachment fault was the active, basin-bounding structure during the Late Miocene through Plio-Pleistocene in the SW Salton Trough (Axen and Fletcher, 1998; Kairouz, 2005; Chapter 2). Subsidiary strands of the Sunset fault and Mescal Bajada segment of the San Felipe fault cut the West Salton detachment fault near Yaqui Ridge (Figs. 3-5 and 3-7) where the detachment fault is now folded in a contractional stepover between the San Felipe and Sunset faults (Figs. 3-7 and 3-14). Different populations of slip vectors on the detachment fault and the Sunset fault and the cross-cutting relationships indicate that the detachment fault was deactivated by initiation of the Sunset fault at ~1.1 Ma. These data argue against an alternate interpretation in which the Sunset and Fish Creek Mountains faults sole into the West Salton detachment fault and represent oblique-slip faults that internally extend the supradetachment basin. Our data suggest that most of the folding of the detachment fault (at least ~75%) occured after ~0.6 Ma.

The transition from West Salton detachment faulting to oblique strike-slip faulting near Yaqui Ridge likely occurred in <1 m.y., and probably have occurred much faster. Near Whale Peak the West Salton detachment fault cuts deposits that correlate to the upper one-third of the Hueso Formation age (Kairouz, 2005). The Hueso Formation is ~0.9 Ma at its top, and ~2.8 Ma at its base (Johnson et al., 1983) so the detachment fault at Whale Peak may have been active until ~1.5 Ma. Although this age is an estimate, it suggests that the West Salton detachment fault was probably active until the Sunset fault and San Felipe fault zone initiated. Even if the two fault systems coexisted until 0.6 Ma when the West Salton detachment fault was folded at Yaqui Ridge the transition occurred over less than a million years.

Differing Ages for the NW San Felipe Fault and SE Fish Creek Mountains Fault

Our data constrain the initiation of the Sunset fault and the Fish Creek Mountains fault to ~1.1 - 1.3 Ma. The San Felipe fault west of Yaqui Ridge could have a pre-1.1 Ma history. The Pinyon Ridge segment of the San Felipe fault, and segments farther northwest, may have had an earlier history if the E-dipping normal fault in Mescal Bajada transferred displacements southward to the West Salton detachment fault on the north side of Whale Peak, as unpublished mapping suggests (G. Axen). However, this southward transfer of strain to the southern West Salton detachment fault along Whale Peak might also have been coeval with slip through the contractional stepovers near Yaqui Narrows. Further work in the Mescal Bajada area, and farther NW along the San Felipe fault zone, may elucidate the age of the fault zone west of Yaqui Ridge.

The larger gravity gradient across the SE Fish Creek Mountains fault suggests that a deeper sedimentary basin is preserved in its hanging wall and may therefore be an older fault (Fig. 3-11). This deeper basin may be the result of: 1) an earlier phase of slip on this fault that did not occur on the NW segment, 2) a dramatic along-strike strain gradient

between the NW and SE segments, or: 3) more total slip across the SE segment due to possibly merging strands of other faults in the area.

CONCLUSIONS

Geological mapping coupled with structural and stratigraphic analyses show two structural and basin reorganizations in the SW Salton Trough in the late Pleistocene. The older event likely started between ~1.1 - 1.3 Ma and records the abrupt (<1 m.y.) transition from activity on the West Salton detachment fault to cross-cutting dextral strike-slip faults of the San Felipe fault zone. The ~1.1 – 0.6 Ma coarse-grained Sunset conglomerate of the Ocotillo Formation was deposited during this transition. The younger event began ~0.6 Ma and records significant folding of the West Salton detachment fault, its crystalline footwall rocks, and the Sunset conglomerate. We suggest that this is a result of a change in the kinematics of the San Felipe fault zone, similar to the ~0.6 Ma onset of closely-spaced folding along the San Jacinto fault zone (Kirby et al., in press; Lutz et al., in press).

The Sunset conglomerate consists of angular boulder conglomerate to conglomeratic coarse sandstone, was deposited by NE-directed alluvial fans, coarsens up and toward the bounding Sunset fault, and contains recycled sandstone clasts from older basin fill. The appearance of recycled clasts in the Ocotillo Formation throughout the SW Salton Trough records uplift and striping of older basin fill from the paleo-Vallecito and Fish Creek mountains. This uplift may have stripped up to 1.8 km of the Borrego Formation from these highlands before deposition of the Sunset conglomerate. The uplift may have been created by a fault-tip propagation fold during early stages of slip on the San Felipe fault zone. After the fault reached the surface, obliquity across the fault created accommodation space for the Sunset conglomerate and continued uplifting the mountain ranges.

The San Felipe fault zone is a major dextral oblique fault zone in southern

California that initiated in the early Pleistocene. It may have accumulated up to 5 km of right slip, and continues to be active. It strikes NW along most of its >160 km length and consists of relatively continuous fault strands. Near Yaqui Ridge the fault zone has an anomalous ~15 km long E-W-striking restraining bend and consists of the left-stepping, en-echelon, San Felipe, Sunset, and Fish Creek Mountains faults.

The San Felipe fault is divided into three structural segments south of Pinyon and Yaqui Ridges. The Grapevine Canyon segment is farthest west and strikes NW and appears to be a pure strike slip faults whereas the Pinyon Ridge and Mescal Bajada segments strike ~E-W and have significant reverse slip and north-south shortening. The boundary between the Pinyon Ridge and Mescal Bajada segments coincides with branch points of subsidiary normal and dextral faults and the SW tip of the basement-cored Yaqui Ridge anticline.

The oblique dextral Sunset fault is part of a complex, kinematically-linked left stepover between the San Felipe and Fish Creek Mountains faults, has less than ~2.5 km of slip, and was active during deposition of the ~1.1 Ma- 0.6 Ma Sunset conglomerate of the Ocotillo Formation. The San Felipe and Sunset faults cut the West Salton detachment fault near Yaqui Ridge. Kinematic analysis of slickenlines on the Sunset fault and West Salton detachment fault shows little to no overlap in slip vectors. The different populations of slip vectors and cross-cutting relationships show that the ~1.1 - 1.3 Ma initiation of the Sunset fault most likely dates the deactivation of the West Salton detachment fault. This transition occurred in <1 m.y., and may have occurred in as little as 0.2 – 0.4 m.y., although contemporaneous activity on both fault systems before ~0.6 Ma cannot be ruled out.

The West Salton detachment fault at Yaqui Ridge and the crystalline rocks in its footwall were folded in the stepover between the Mescal Bajada segment of the San Felipe fault and the Sunset fault. The Quaternary Sunset conglomerate is folded between the Sunset fault and the NW segment of the Fish Creek Mountains fault. NE-

side up components of slip on the reverse-dextral San Felipe fault, and NE-side down components of slip on the normal-dextral Fish Creek Mountains fault expose the two stepovers. Each domain records ~11-14% NE-SW shortening and has largely WNW-trending and fewer E-W and NE-trending folds. These are interpreted as WNW-trending strain-partitioned transpressional folds in the center of each stepover zone and E-W- to NE-trending wrench folds in more peripheral positions. These fold geometries are unlike those of most contractional stepovers and are likely a result of the obliquity of the bounding San Felipe fault zone. Folding in these stepovers probably began when their bounding faults initiated and mostly postdates the end of Sunset conglomerate deposition at ~0.6 Ma. Some folding may be recorded in syn-depositional folds, but current data are equivocal. Overall, this shows that the San Felipe fault zone experienced a significant period of activity after ~0.6 Ma similar to the San Jacinto fault zone (Kirby et al., in press; Lutz et al., in press).

The San Felipe Fault zone in the SW Salton Trough is a young fault zone as shown by its ~1.1 - 1.3 Ma initiation and continued deformation after ~0.6 Ma. Late Pleistocene or Holocene scarps on the main strands of the Pinyon Ridge segment, and on subsidiary faults of the Mescal Bajada segment suggest that the fault may be capable of generating future large earthquakes. The West Salton detachment fault was replaced as the major basin-bounding structure by this structure during a major region-wide reorganization of faults along the North American plate boundary.

REFERENCES

Atwater, T., 1970, Implications of plate tectonics for the Cenozoic evolution of western North America. Geol. Soc. Amer. Bull., v. 81, p. 3513-3536.

Axen, G.J., and Fletcher, J.M., 1998, Late Miocene-Pleistocene extensional faulting, northern Gulf of California, Mexico and Salton Trough, California. International Geology Review, v. 40, p. 217-244.

Bartholomew, M. J., 1968, Geology of the northern portion of Seventeen Palms and Font's Point quadrangles, Imperial and San Diego Counties, California, [MS Thesis]: University of Southern California, Los Angeles, 60 p.

Brown, no. N., Fuller, M. D., and Sibson, R. H., 1991, Paleomagnetism of the Ocotillo Badlands, southern California, and implications for slip transfer through an antidilational fault jog. Earth and Planetary Science Letters, v. 102, p. 277-288.

Christie-Blick, no., and Biddle, K.T., 1985, Deformation and basin formation along strike-slip faults, *in* Biddle, K.T., and Christie-Blick, no., eds., Strike-slip deformation, basin formation, and sedimentation. SEPM Special Publication 37, p. 1-34.

Crowell, J.C., 1981, An outline of the tectonic history of southeastern California, *in* Ernst, W.G., ed., The geotectonic development of California. Rubey Vol. I: Englewood Cliffs, NJ, Prentice-Hall, p. 582-500.

Dean, M.A., 1988, Genesis, mineralogy, and stratigraphy of the Neogene Fish Creek Gypsum, southwestern Salton Trough, California, [M.S. thesis]: San Diego State University, CA, 150 p.

Dibblee, T.W. Jr., 1954, Geology of the Imperial Valley Region, California, Geology of Southern California. California Division of Mines Bulletin 170, p. 21-28.

Dibblee, T.W. Jr., 1984, Stratigraphy and tectonics of the San Felipe Hills, Borrego Badlands, Superstition Hills, and vicinity, *in* Rigsby, C.A., ed., 1984, The Imperial Basin-tectonics, sedimentation, and thermal aspects. Pacific Section S.E.P.M., p. 31-44.

Dibblee, T.W. Jr.,1996, Stratigraphy and tectonics of the Vallecito-Fish Creek Mountains, Vallecito Badlands, Coyote Mountain, and Yuha Desert, southwestern Imperial basin, *in* Abbott, P.L. and Seymour, D.C., eds., 1996, Sturtzstroms and detachment faults, Anza-Borrego Desert State Park, California. South Coast Geological Society Annual Field Trip Guide Book, no. 24, p. 59-79.

Dorsey, R. J., 2002, Stratigraphic record of Pleistocene initiation and slip on the Coyote Creek fault, lower Coyote Creek, Southern California, *in* Barth, A., ed., Contributions to Crustal Evolution of the Southwest United States: Boulder, Co. GSA Special Paper 365, p. 251-269.

Dorsey, R.J., 2005, Stratigraphy, tectonics, and basin evolution in the Anza-Borrego Desert region, *in* Jefferson, G.T., and Lindsay, L.E. eds., Fossil Treasures of Anza-Borrego Desert. Sunbelt Publications, San Diego, CA, p. 89-104.

Dorsey, R.J. and Janecke, S.U., 2002, Late Miocene to Pleistocene West Salton Detachment Fault System and Basin Evolution, Southern California: New Insights. Geological Society of America Abstracts with Programs, v. 34, no. 6, p. 248.

Dorsey, R. J.; Janecke, S. U.; Kirby, S.; Axen, G.; and Steely, A. N. 2004. Pliocene Lacustrine Transgression in the Western Salton Trough, Southern California: Implications for Regional Tectonics and Evolution of the Colorado River Delta. Geological Society of America Abstracts with Programs 36:317.

Dorsey, R.J., Janecke, S.U., Kirby, S.M., McDougall, K.A., and Steely, A.N., 2005, Pliocene evolution of the lower Colorado River in the Salton Trough; tectonic controls on regional paleogeography and the regional Borrego Lake. *In:* Marith C., *ed.,* Geologic and biotic perspectives on late Cenozoic drainage history of the southwestern Great Basin and lower Colorado River region; conference abstracts. USGS Open-File Report 2005-1404, p. 13.

Engel, A.E.J., and Schultejann, P.A., 1984, Late Mesozoic and Cenozoic tectonic history of south central California. Tectonics, v. 3, p. 659-675.

Gawthorpe, R. L., Sharp, I., Underhill, J., Gupta, S., 1997, Linked sequence stratigraphic and structural evolution of propagating normal faults. Geology, v. 25, p. 695-798.

George, P. G., and Dokka, R. K., 1994, Major late Cretaceous cooling events in the eastern Peninsular Ranges, California, and their implications for Cordilleran tectonics. Geological Society of America Bulletin, v. 106, p. 903-914.

Grove, M., Lovera, O., and Harrison, M., 2003, Late Cretaceous cooling of the east-central Peninsular Ranges batholith (33N): Relationship to La Posta pluton emplacement, Laramide shallow subduction, and forearc sedimentation, *in* Scott, J.E., Scott, P.R., Fletcher, J.M., Girty, G.H., Kimbrough, D.L., and Martin-Barajas, A, (eds), Tectonic evolution of northwestern Mexico and Southwestern USA, Geological Society of America Special Paper 374, p. 355-379.

Herzig, C., Carrasco, A., Schar, T., Murray, G., Rightmer, D., Lawrence, J., Milton, Q., Wirths, T., 1995, Neogene stratigraphy of the Borrego Mountain area, Anza-Borrego Desert State Park, California, *in* Remeika, P., and Sturz, A., eds., Paleontology and geology of the western Salton Trough detachment, Anza-Borrego Desert State Park, California. Field trip guidebook and volume for the 1995 San Diego Assoc. of Geologist's field trip to Anza-Borrego Desert State Park. Volume 1, p. 133-136.

Housen, B.A., Dorsey, R.J., Janecke, S.U., and Axen, G.J., 2005, Rotation of Plio-Pleistocene sedimentary rocks in the Fish Creek Vallecito Basin, western Salton Trough, CA. EOS - Transactions of the American Geophysical Union. v. 86

Hull, A.G., and Nicholson, C., 1992, Seismotectonics of the northern Elsinore fault zone, Southern California. Bulletin of the Seismological Society of America, v. 82, no. 2, p. 800-818.

Hudnut, K. W., Seeber, L., Pacheco, J., Armbruster, J. G., Sykes, L. R., Bond, G. C., and Kominz, M. A., 1989, Cross faults and block rotation in Southern California; earthquake triggering and strain distribution, Yearbook Lamont –Doherty Geological Observatory of Columbia University, p. 44-49.

Jahns, R.H., 1954, Geology of southern California. California Division of Mines and Geology Bulletin, v. 170, no. 1-2, pp. 878.

Janecke, S.U., Kirby, S.M., Langenheim, V., Steely, A.N., Dorsey, R.., Housen, B., and Lutz, A., 2005, High geologic slip rates on the San Jacinto fault zone in the SW Salton Trough, and possible near-surface slip defecit in sedimentary basins. Geological Society of America Abstracts with Programs, Vol. 37, No. 7, p. 275

Jennings, C.W., 1977, Geologic map of California. California Division of Mines and Geology, Sacramento, CA.

Johnson, no.M., Officer, C.B., Opdyke, no.D., Woodard, G.D., Zeitler, P.K., and Lindsay, E.H., 1983, rates of late Cenozoic tectonism in the Vallecito-Fish Creek basin, western Imperial Valley, California. Geology, v. 11, p. 664-667.

Kairouz, M.E., 2005, Geology of the Whale Peak Region of the Vallecito Mountains: Emphasis on the Kinematics and Timing of the West Salton Detachment fault, Southern California, [M.S. Thesis]: University of California, Los Angeles. 156 p.

Kerr, D.R., 1984, Early Neogene continental sedimentation in the Vallecito and Fish Creek mountains, western Salton Trough, California. Sedimentary Geology, v. 38, p. 217-246.

Kerr, D.R., and Kidwell, S.M., 1991, Late Cenozoic sedimentation and tectonics, western Salton Trough, California. *In*: Walawender, M.J., and Hanan, B.B., (eds.), Geological excursions in southern California. Guidebook 1991 Annual Meeting Geological Society of America, San Diego, California, p. 397-416b.

Kennedy, M.P., and Morton, D.M., 2003, Preliminary geologic map of the Murrieta 7.5' quadrangle, Riverside County, California. USGS Open File Report 03-189.

Kirby, S.M., 2005, The Quaternary tectonic and structural evolution of the San Felipe Hills, California, [M.S. Thesis]: Logan, Utah State University, 182 p.

Kirby, S. M., Janecke, S. U., Dorsey, R. J., Housen, B. A., McDougall, K., and Steely, A. in press, Pleistocene Brawley and Ocotillo formations: Evidence for initial strike-slip deformation along the San Felipe and San Jacinto fault zones, California: Journal of Geology. 21 p. accepted July 2006.

Langenheim, V. E., and Jachens, R. C. 1993. Isostatic residual gravity map of the Borrego Valley 1:100,000-scale quadrangle, California. U.S. Geological Survey Open-File Report 93-246, scale 1:100,000.

Lough, C. F., 1993, Structural evolution of the Vallecito Mountains, Colorado Desert and Salton Trough Geology, San Diego, California, San Diego Association of Geologists, p. 91-109.

Lutz, A.T., 2005, Tectonic controls on Pleistocene basin evolution in the central San Jacinto fault zone, southern California, [M.S. thesis]: Eugene, University of Oregon, 136 p.

Lutz, A.T., Dorsey, R.J., Housen, B.A,, and Janecke, S.U., in press, Stratigraphic record of Pleistocene faulting and basin evolution in the Borrego Badlands,San Jacinto fault zone, southern California. Geological Society of America Bulletin.

Magistrale, H. and T. Rockwell, 1996. The central and southern Elsinore fault zone, southern California, Bull. Seism. Soc. Am. 86:1793-1803.

Merriam, R., and Bandy, O. L., 1965, Source of upper Cenozoic sediments in the Colorado delta region. Journal of Sedimentary Petrology, v. 35, p. 911-916.

Morley, E. R., 1963, Geology of the Borrego Mountain Quadrangle and the western portion of the Shell Reef Quadrangle, San Diego County, California, [MS Thesis]: University of Southern California, Los Angeles, 138 p.

Morton, D. M., and Matti, J. C., 1993, Extension and contraction in an evolving divergent strike-slip fault complex: the San Andreas and San Jacinto fault zones at their convergence in Southern California, *in* Powell, R. E., Weldon, R. J., and Matti, J. C., eds., The San Andreas fault system: displacement, palinspastic reconstruction, and geologic evolution: Geological Society of America Memoir, v. 178, p. 217-230.

Nicholson, C., Seeber, L., Williams, P., and Sykes, L.R., 1986, Seismic evidence for conjugate slip and block rotation in the San Andreas fault system, Southern California. Tectonics, v. 5, no. 4, p. 629-648.

Oskin, M., and Stock, J., 2003, Marine incursion synchronous with plate-boundary localization in the Gulf of California: Geology, v. 1, p. 23-26.

Reitz, D. T., 1977, Geology of the western and central San Felipe Hills, northwestern Imperial County, California, [MS Thesis]: University of Southern California, Los Angeles, 155 p.

Rockwell, T., Loughman, C., Merifield, P., 1990, Late Quaternary rate of slip along the San Jacinto fault zone near Anza, Southern California. Journal of Geophysical Research, v. 95, p. 8593-8605.

Rogers, T.H., 1965, Santa Ana sheet: California Division of Mines and Geology Geologic Map of California, scale, 1:250,000.

Schultejann, P.A., 1984, The Yaqui ridge antiform and detachment fault: Mid-Cenozoic extensional terrane west of the San Andreas fault. Tectonics, v. 3, no. 6, p. 677-691.

Sanders, C. O. 1989. Fault segmentation and earthquake occurrence in the strike-slip San Jacinto fault zone, California, *in* Schwartz, D. P., and Sibson, R. H., eds., Proceedings of Conference XLV; a workshop on Fault segmentation and controls of rupture initiation and termination, U. S. Geological Survey Open-File Report OF 89-0315, p. 324-349.

Sharp, I., Gawthorpe, R.L., Underhill, J., Gupta, S., 2000, Fault propagation folding inextensional settings; examples of structural style and synrift sedimentary response from the Suez Rift, Sinai, Egypt. Geological Society of America Bulletin, v. 146, no. 12, p. 1877-1899.

Sharp, R. V., 1967, San Jacinto fault zone in the Peninsular Ranges of southern California. Geological Society of America Bulletin, v. 78, p. 705-730.

Sharp, R.V., 1972, Tectonic Setting of the Salton Trough, *in* Sharp, R. V., ed., The Borrego Mountain Earthquake of April 9, 1968, USGS Professional Paper, p. 3-15.

Sharp, R.V., 1979, Some characteristics of the eastern Peninsular Ranges mylonite zone, *in* Proc. Conf. VIII: Analysis of actual fault zones in bedrock. United States Geological Survey Open File Report 79-1239, p. 258-267.

Silver, L.T., Taylor, H.P., and Chappell, B., 1979, Some petrological, geochemical and geochronological observations of the Peninsular Ranges Batholith near the international border of the U.S.A. and Mexico. *In:* Abbott, P., and Todd, V.R., *eds,* Mesozoic crystalline rocks; Peninsular Ranges Batholith and pegmatites; Point Sal Ophiolite. San Diego State University, San Diego, CA.

Simpson, C., 1984, Borrego Springs-Santa Rosa mylonite zone: A Late Cretaceous west-directed thrust in southern California. Geology, v. 12, p. 8-11.

Stinson, A. L., and Gastil, R. G., 1996, Mid- to Late-Tertiary detachment faulting in the Pinyon Mountains, San Diego County, California: A setting for long run-out landslides in the Split Mountain Gorge area, *in* Abbott, P. L., and Seymour, D. C., eds., Sturtzstrums and Detachment Faults, Anza-Borrego Desert State Park,

California, Santa Ana, California, South Coast Geological Society, p. 221-244.

Sylvester, A.G., 1988, Strike-slip faults. Geological Society of America Bulletin, v. 100, no. 11, p. 1666-1703.

Todd, V. R., Erskine, B. G., and Morton, D. M., 1988, Metamorphic and tectonic evolution of the northern Peninsular Ranges Batholith, southern California, *in* Ernst, W. G., ed., Metamorphism and Crustal Evolution of the Western United States; Rubey Volume VII, Englewood Cliffs, New Jersey, Prentice Hall, p. 894-937.

Wagner, D.L., 1996, Geologic map of the Tubb Canyon 7.5. quadrangle, San Diego County, California: California Division of Mines and Geology Open-File Report 96-06

Winker, C.D. 1987. Neogene stratigraphy of the Fish Creek - Vallecito section, southern California: implications for early history of the northern Gulf of California and Colorado delta. [Ph.D. dissertation]: Tucson, University of Arizona, 494 p.

Winker, C.D., and Kidwell, S.M., 1996, Stratigraphy of a marine rift basin: Neogene of the western Salton Trough, California, *in* Abbott, P.L., and Cooper, J.D., eds., Field conference guidebook and volume for the annual convention, San Diego, California, May, 1996, Bakersfield, California, Pacific Section. American Association of Petroleum Geologists, p. 295-336.

Winker, C. D., and Kidwell, S. M., 2002, Stratigraphic evidence for ages of different extensional styles in the Salton Trough, Southern California. Geological Society of America Abstracts with Programs, v. 34, no. 6, p. 83-84.

CHAPTER 4

SUMMARY AND CONCLUSIONS

We use geological mapping and structural and basin analyses to show that the West Salton detachment fault was active during the Pliocene in the western Salton Trough near Yaqui Ridge and may have initiated during the latest Miocene. Regionally the West Salton detachment fault strikes NNW, but at Yaqui Ridge it strikes anomolously NW to WNW. We show that crustal inheritance is important and that the West Salton detachment fault reactivates the late Cretaceous reverse-sense Eastern Peninsular Ranges mylonite zone at map-scale. Slickenlines are dispersed nearly 180° in the detachment fault plane when the fault on the SSW-dipping limb of the younger Yaqui Ridge anticline is restored to its original NE dip. This observation is best explained by: 1) dominantly east-directed extension during slip on the detachment fault with significant dispersion of data about this mean; followed by 2) flexural slip between the hanging wall and footwall of the detachment fault during folding of the Pleistocene Yaqui Ridge anticline. The east-directed extension during slip on the detachment fault at Yaqui Ridge shows that in that location the fault is actually a low-angle dextral oblique-slip fault. The 50° – 90° dispersion about an east-directed average may be characteristic of the West Salton detachment fault throughout its length.

Dominantly east-directed extension is not predicted by complete strain partitioning between the West Salton detachment fault and the contemporaneous San Andreas fault. However, east directed extension on north-striking normal faults is predicted by a 'wrench-style' model of structures along a NW-striking strike-slip fault (e.g. Christie-Blick and Biddle, 1985; Davis and Reynolds, 1996). We suggest that the West Salton detachment fault at Yaqui Ridge would have formed as a north-striking normal fault, but instead reactivated older, weaker fabrics with a NNW strike that still permitted east-directed extension. Although there are complex patterns of slickenlines

on the West Salton detachment fault, it is clearly not a simple detachment fault because its oblique slip produced an oblique hanging wall growth fold, its hanging wall is not internally extended by normal faults that sole into the detachment fault, and it co-evolved with the San Andreas fault to the east.

The Hawk Canyon formation is the basal deposit at Borrego Mountain and correlates with late Miocene-Pliocene marine deposits of the Imperial Group to the east near Squaw Peak and Shell Reef. The Pliocene West Butte conglomerate is a fluvial braid plain deposit that contains clasts of brittley to semi-brittley deformed and chloritically altered fault rocks that were eroded from the damage zone of the West Salton detachment fault to the south of Borrego Mountain. We correlate the West Butte conglomerate to 'L-suite' marine rocks of the Pliocene Imperial Group east of Borrego Mountain. The West Butte conglomerate is >300 m thick and ties basin-fill deposits to activity on the West Salton detachment fault. The distinctly younger Canebrake Conglomerate of the Palm Spring Group is strikingly similar to the West Butte conglomerate in clast composition, source area, and depositional environment, and records deeper exhumation of the footwall of the West Salton detachment fault. The associated Yaqui Ridge megabreccia is a long run-out rockslide interbedded in the Palm Spring Group, may be ~200 km^2 in extent, and is the largest recorded megabreccia deposit in the SW Salton Trough. The conglomeratic deposits and the megabreccia document activity on the West Salton detachment fault and the creation of steep topography in the footwall of the detachment fault.

The late Miocene to Pliocene basin-fill deposits contain progressive unconformities, significant thickness changes, and record the growth of a large hanging wall growth fold. The Borrego Mountain anticline formed as a result of slip on the detachment fault, trends ~N60°W, and has at least 420 m of structural relief. The anticline was active from deposition of the middle member of the Hawk Canyon formation through at least the Olla Formation of the Palm Spring Group. The crest of

the anticline remained fixed throughout deposition of these units and the northeast flank of the fold coincides with a narrow marine shoreline during deposition of the Pliocene Imperial Group. The Borrego Mountain anticline is not a simple roll-over monocline above a normal fault and nor can ramp-flat geometries along the West Salton detachment fault explain its existence. Although its formation is poorly understood it most likely formed as an E-W-tending wrench fold and has since been rotated to its current NW-trend.

Our new mapping and analyses record two structural and basin reorganizations in the SW Salton Trough in the Pleistocene. The older event likely started between ~1.1 - 1.3 Ma and records the abrupt (<1 m.y.) transition from activity on the West Salton detachment fault to cross-cutting dextral strike-slip faults of the San Felipe fault zone. The ~1.1 – 0.6 Ma coarse-grained Sunset conglomerate of the Ocotillo Formation was deposited during this transition. The younger event began ~0.6 Ma and records significant folding of the West Salton detachment fault, its crystalline footwall rocks, and the Sunset conglomerate. We suggest that this is a result of a change in the kinematics of the San Felipe fault zone, similar to the ~0.6 Ma onset of closely-spcaed folding along the San Jacinto fault zone (Kirby et al., in press; Lutz et al., in press).

The Sunset conglomerate consists of angular boulder conglomerate to conglomeratic coarse sandstone, was deposited by NE-directed alluvial fans, coarsens up and toward the bounding Sunset fault, and contains recycled sandstone clasts from older basin fill. The appearance of recycled clasts in the Ocotillo Formation throughout the SW Salton Trough records uplift and striping of older basin fill from the paleo-Vallecito and Fish Creek mountains. This uplift may have stripped up to 1.8 km of the Borrego Formation from these highlands before deposition of the Sunset conglomerate. The uplift may have been created by a fault-tip propagation fold during early stages of slip on the San Felipe fault zone. After the fault reached the surface, obliquity across the fault created accommodation space for the Sunset conglomerate and continued uplifting the

mountain ranges.

The San Felipe fault zone is a major dextral oblique fault zone in southern California that initiated in the early Pleistocene. It may have accumulated up to 5 km of right slip, and continues to be active. It strikes NW along most of its >160 km length and consists of relatively continuous fault strands. Near Yaqui Ridge the fault zone has an anomalous ~15 km long E-W-striking restraining bend and consists of the left-stepping, en-echelon, San Felipe, Sunset, and Fish Creek Mountains faults.

The San Felipe fault is divided into three structural segments south of Pinyon and Yaqui Ridges. The Grapevine Canyon segment is farthest west and strikes NW and appears to be a pure strike slip faults whereas the Pinyon Ridge and Mescal Bajada segments strike ~E-W and have significant reverse slip and north-south shortening. The boundary between the Pinyon Ridge and Mescal Bajada segments coincides with branch points of subsidiary normal and dextral faults and the SW tip of the basement-cored Yaqui Ridge anticline.

The oblique dextral Sunset fault is part of a complex, kinematically-linked left stepover between the San Felipe and Fish Creek Mountains faults, has less than ~2.5 km of slip, and was active during deposition of the ~1.1 Ma- 0.6 Ma Sunset conglomerate of the Ocotillo Formation. The San Felipe and Sunset faults cut the West Salton detachment fault near Yaqui Ridge. Kinematic analysis of slickenlines on the Sunset fault and West Salton detachment fault shows little to no overlap in slip vectors. The different populations of slip vectors and cross-cutting relationships show that the ~1.1 - 1.3 Ma initiation of the Sunset fault most likely dates the deactivation of the West Salton detachment fault. This transition occurred in <1 m.y., and may have occurred in as little as 0.2 – 0.4 m.y., although contemporaneous activity on both fault systems before ~0.6 Ma cannot be ruled out.

The West Salton detachment fault at Yaqui Ridge and the crystalline rocks in its footwall were folded in the stepover between the Mescal Bajada segment of the

San Felipe fault and the Sunset fault. The Quaternary Sunset conglomerate is folded between the Sunset fault and the NW segment of the Fish Creek Mountains fault. NE-side up components of slip on the reverse-dextral San Felipe fault, and NE-side down components of slip on the normal-dextral Fish Creek Mountains fault expose the two stepovers. Each domain records ~11-14% NE-SW shortening and has largely WNW-trending and fewer E-W and NE-trending folds. These are interpreted as WNW-trending strain-partitioned transpressional folds in the center of each stepover zone and E-W- to NE-trending wrench folds in more peripheral positions. These fold geometries are unlike those of most contractional stepovers and are likely a result of the obliquity of the bounding San Felipe fault zone. Folding in these stepovers probably began when their bounding faults initiated and mostly postdates the end of Sunset conglomerate deposition at ~0.6 Ma. Some folding may be recorded in syn-depositional folds, but current data are equivocal. Overall, this shows that the San Felipe fault zone experienced a significant period of activity after ~0.6 Ma similar to the San Jacinto fault zone (Kirby et al., in press; Lutz et al., in press).

The San Felipe Fault zone in the SW Salton Trough is a young fault zone as shown by its ~1.1 - 1.3 Ma initiation and continued deformation after ~0.6 Ma. Late Pleistocene or Holocene scarps on the main strands of the Pinyon Ridge segment, and on subsidiary faults of the Mescal Bajada segment suggest that the fault may be capable of generating future large earthquakes. The West Salton detachment fault was replaced as the major basin-bounding structure by this structure during a major region-wide reorganization of faults along the North American plate boundary.

REFERENCES

Kirby, S. M., Janecke, S. U., Dorsey, R. J., Housen, B. A., McDougall, K., and Steely, A. in press, Pleistocene Brawley and Ocotillo formations: Evidence for initial strike-slip deformation along the San Felipe and San Jacinto fault zones, California: Journal of Geology. 21 p. accepted July 2006.

Lutz, A.T., Dorsey, R.J., Housen, B.A,, and Janecke, S.U., in press, Stratigraphic record of Pleistocene faulting and basin evolution in the Borrego Badlands,San Jacinto fault zone, southern California. Geological Society of America Bulletin.

APPENDIXES

APPENDIX A

PERMISSION-TO-USE LETTERS

July 27, 2006
Alexander Steely
7854 Honeycomb Cir. #2
Salt Lake City, UT 84121

Dear Coauthor,

I am requesting your permission to include you as a coauthor for Chapter II of my thesis. A copy of the text is included with this letter. Please advise me of any changes you require.

Please indicate your approval of this request by signing in the space provided and attaching any other form or instruction necessary to confirm permission. If you have nay questions, please call me at (541) 556-9079.

Thank you for your cooperation,

I hereby acknowledge coauthorship of The West Salton detachment fault near Yaqui Ridge, SW Salton Trough: The tectonic evolution of its folded hanging wall, age, and kinematics, Chapter II of *The evolution from late Miocene West Salton detachment faulting to cross-cutting Pleistocene oblique strike-slip faults in the SW Salton Trough, southern California* [M.S. Thesis] 250 p., with the following authors; Alexander N. Steely, Susanne U. Janecke, Rebecca J. Dorsey, and Gary J. Axen.

Subject: Re: Permission to use letter2
From: Victoria E Langenheim <zulanger@usgs.gov>
Date: Mon, 04 Sep 2006 15:17:18 -0700
To: Alex Steely <asteely@cc.usu.edu>

September 4, 2006

I approve

Victoria E. Langenheim
U.S. Geological Survey MS 989
345 Middlefield Road
Menlo Park, CA 94025
(650) 329-5313 voice
(650) 329-5133 FAX

la vita puo' essere piu' facile senza capre gonfie

August 28, 2006
Alexander Steely
7854 Honeycomb Cir. #2
Salt Lake City, UT 84121

Dear Coauthor,
I am requesting your permission to include you as a coauthor for Chapter II of my thesis.

Please indicate your approval of this request by replying to this email with the words "I approve", and dating the e-mail.

Thank you for your cooperation,

I hereby acknowledge coauthorship of Plesitocene reorganization of plate-boundary fault
systems, SW Salton Trough, Chapter III of The evolution from late Miocene West Salton
detachment faulting to cross-cutting Pleistocene oblique strik- slip faults in the SW Salton
Trough, southern California [M.S. Thesis] 250 p., with the following authors; Alexander
N. Steely, Susanne U. Janecke, Gary J. Axen, Rebecca J. Dorsey, and Victoria
Langenheim

July 27, 2006
Alexander Steely
7854 Honeycomb Cir. #2
Salt Lake City, UT 84121

Dear Coauthor,

I am requesting your permission to include you as a coauthor for Chapter II of my thesis. A copy of the text is included with this letter. Please advise me of any changes you require.

Please indicate your approval of this request by signing in the space provided and attaching any other form or instruction necessary to confirm permission. If you have nay questions, please call me at (541) 556-9079.

Thank you for your cooperation,

I hereby acknowledge coauthorship of Plesitocene reorganization of plate-boundary fault systems, SW Salton Trough, Chapter III of *The evolution from late Miocene West Salton detachment faulting to cross-cutting Pleistocene oblique strik- slip faults in the SW Salton Trough, southern California* [M.S. Thesis] 250 p., with the following authors; Alexander N. Steely, Susanne U. Janecke, Gary J. Axen, Rebecca J. Dorsey, and Victoria Langenheim

APPENDIX B

DATA

A note on the data presented herein:

All the data presented in this appendix were collected by the author except where noted. All location data was collected in the field with a hand-held Garmin GPS unit. Many locations from the first field season do not have GPS coordinates. Locations are give in Universal Transverse Mercator coordinates. The projection for these coordinates is Zone 11 South (11S) of the North American Datum of 1983 (NAD83). Where a zero is the first number of the coordinate set it has been omitted. For example 0507899 is listed as 507899. The 'right hand rule' was used for planar data.

Clast counts in the West Butte conglomerate (Twb)

Station	Easting	Northing	Clast count	La Posta-type tonalite	Granite Mountain-type diorite	Fine-medium grained diorite/granodiorite/tonalite	Pegmatite	Mylonite	All metamorphics	All deformed and chloritically altered	Recycled Diablo Formation	Total
1184	578855	3669645	C1	19	5	2	7		5	12		50
1187	576403	3669630	C2	3	21	4	5		6	11		50
1188	576476	3671483	C3	8	5	17	4	1	7	9		51
1189	576326	3672413	C4	8	7	8	8		11	8		50
1190	573764	3673826	C5	3	5	14	8		11	10		51
1191	572672	3673341	C6	5	11	5	8		9	14		52
1192	572824	3673326	C7	5	5	8	6		17	10		51
1193	575017	3672165	C8	3	6	15	9		9	8		50
1194	573935	3671111	C9	1	19	9	3		12	9		53
1257	573871	3672223	C34	4	3	19			7	11		44
1259	573773	3672304	C35	3	9	9			12	9		42
1262	573622	3672229	C36	1	11	10		3	9	10		44
1265	573456	3672014	C37	7	4	7		1	15	11		45
1271	573251	3671774	C38	1	7	14		3	9	10		44
228	573967	3671816	x	5	21	25	8		8	30		97

Number of clasts	76	139	166	66	8	147	172		774
Percent of total clasts	9.8	18.0	21.4	8.5	1.0	19.0	22.2		

HEMATITIC ALTERATION OF CLASTS

Number of altered clasts	36	80	63	8	11	12	29		239
Percent of altered clasts	47.4	57.6	38.0	12.1	7.5	7.0	16.9		

UNBINNED METAMORPHIC LITHOLOGIES (Twb)

Station	Clast count	Metaplutonic	Quartzose metaseds	Biotite schist	Psamittic schist	Metasedimentary undifferentiated	Mixed metaseds and metaplutonic	Migmatite	Amphibolite	Gneiss
1184	C1	3		1	1					
1187	C2	1		2	3					
1188	C3	2		2	3					
1189	C4	1	5		3			2		
1190	C5		2	3	6					
1191	C6	1	3		5					
1192	C7	3	6	4	4					
1193	C8		3	3	3					
1194	C9	3	3	3	2			1		
1257	C34		3		3					1
1259	C35	4	3	1	3					1
1262	C36	2	1	1	3			1		1
1265	C37	4	4	1	2	2		1		1
1271	C38	3	3	1	1			2		
228	x			2		6				

	Metaplutonic, migmatite,	Quartzose metasedimentary	Schist (biotite+psamittic	Amphibolite	Others	Total
Number of metamorphic clasts	38	36	66		8	148
Percent of metamorphic clasts	25.7	24.3	44.6		5.41	

UNBINNED CHLORITIC ALTERATION FABRICS (Twb)

Station	Clast count	Brittle	Brittle-ductile	Ductile	Undistinguishable
1184	C1	5	2	1	4
1187	C2	5	2	1	3
1188	C3	6	1		2
1189	C4	3	3		2
1190	C5	3	1	1	5
1191	C6	9	1	1	3
1192	C7	3	2	2	4
1193	C8	7			1
1194	C9	6	3		
1257	C34	6	1		4
1259	C35	5			4
1262	C36	5	1	1	3
1265	C37	6		1	4
1271	C38	4	2	2	2
228	x	8		12	10

					Total
Number of altered clasts	81	19	22	51	173
Percent of altered clasts	46.8	11	12.7	29.5	

Clast counts in the Canebrake Formation (Tc)

Station	Easting	Northing	Clast count	La Posta-type tonalite	Granite Mountain-type diorite	Fine-medium grained diorite/granodiorite/tonalite	Pegmatite	Mylonite	All metamorphics	All deformed and chloritically altered	Recycled Diablo Formation	Total
1206	566022	3668638	C19	11		9	10	1				31
1207	565270	3668082	C20	5	2	14	7	4				32
1208	564463	3668599	C21	4		11	8	9				32
1209	563799	3669128	C22	4	3	12	7	5				31
1211	563233	3668758	C23	3	2	8	11	2				26
1229	560608	3669666	C27		3	5	11	20				39
1232	561954	3669389	C28		12	8	4	3				27
1233	560516	3671304	C29	2	7	13	7	6				35
1234	559967	3670099	C30	1	6	15	5	5				32
1235	559807	3671034	C31		11		4	21				36
1239	559236	3671168	C32		25		4	9				38
1241	559356	3671686	C33		28		3	8				39

Number of clasts	31	128	122	90	98	139	100		708
Percent of total clasts	4.4	18.1	17.2	12.7	13.8	19.6	14.1		

HEMATITIC ALTERATION OF CLASTS

Number of altered clasts	2	1	14						17
Percent of altered clasts	6.5	0.8	11.5						

UNBINNED METAMORPHIC LITHOLOGIES (Tc)

Station	Clast count	Metaplutonic	Quartzose metaseds	Biotite schist	Psamittic schist	Metasedimentary undifferentiated	Mixed metaseds and metaplutonic	Migmatite	Amphibolite	Gneiss
1206	C19	1	5	2	3			1	2	3
1207	C20	4	3	0	2				2	2
1208	C21	3	4	1	3		1	3	1	
1209	C22	4	6	0				2	2	1
1211	C23	8	6	1					2	1
1229	C27		0					4		
1232	C28	3	2	2					1	
1233	C29	3	3	2	2			1	1	
1234	C30	5	4	1	1			2	1	
1235	C31		1							
1239	C32		1							
1241	C33									

	Metaplutonic, migmatite,	Quartzose metasedimentary	Schist (biotite+psamittic	Amphibolite	Others	Total
Number of metamorphic clasts	60	35	31	12	1	139
Percent of metamorphic clasts	43.2	25.2	22.3	8.6	0.7	

UNBINNED CHLORITIC ALTERATION FABRICS (Tc)

Station	Clast count	Brittle	Brittle-ductile	Ductile	Undistinguishable
1206	C19	2	1	1	
1207	C20		2		3
1208	C21	1	1		
1209	C22		1	1	
1211	C23	1	1	3	2
1229	C27		2	4	
1232	C28	4	3	3	5
1233	C29			3	
1234	C30			1	3
1235	C31		2	11	
1239	C32			12	1
1241	C33	2		6	2

					Total
Number of altered clasts	10	13	45	16	84
Percent of altered clasts	5.8	7.5	26.0	9.2	

Clast counts in the Sunset conglomerate (Qo)

Station	Easting	Northing	Clast count	La Posta-type tonalite	Granite Mountain-type diorite	Fine-medium grained diorite/granodiorite/tonalite	Pegmatite	Mylonite	All metamorphics	All deformed and chloritically altered	Recycled Diablo Formation	Total
47	568226	3666428	C11	32			4	6	3			45
1195	568713	3667018	C10	41				5	2	1	1	50
1196	568189	3665909	C12	35			3	7	3	1	2	51
1197	568475	3665847	C13	31			1	9	2	3	4	50
1199	569159	3665386	C14	18			7	10	9	2	4	50
1200	569121	3665065	C15	43				8				51
1201	569211	3664785	C16	19			4	12	5	5	5	50
1202	570198	3664649	C17	19			7	14	9	2	1	52
1203	570333	3665197	C18	28			2	10	5	2	5	52
1212	566566	3666787	C24	40			1	4	3	2		50
1213	567522	3667099	C25	35			2	7	4	2		50
1214	567324	3666103	C26	44			1	5				50

Number of clasts	385		32	97		45	20	22	579
Percent of total clasts	64.1		5.3	16.1		7.5	3.3	3.7	

HEMATITIC ALTERATION OF CLASTS

Number of altered clasts									0
Percent of altered clasts									

UNBINNED METAMORPHIC LITHOLOGIES (Qo)

Station	Clast count	Metaplutonic	Quartzose metaseds	Biotite schist	Psamittic schist	Metasedimentary undifferentiated	Mixed metaseds and metaplutonic	Migmatite	Amphibolite	Gneiss
47	C11		1		1					
1195	C10		1	1	1					
1196	C12		1		1			1		
1197	C13		1		1					
1199	C14		2	4	1			2		
1200	C15		0							
1201	C16		1		2			2		
1202	C17		4	4	1					
1203	C18		1	2	2					
1212	C24	1	1							
1213	C25		1				1			
1214	C26		0							

	Metaplutonic, migmatite,	Quartzose metasedimentary	Schist (biotite+psamittic	Amphibolite	Others	Total
Number of metamorphic clasts	6	14	21		1	42
Percent of metamorphic clasts	14.3	33.3	50.0		2.4	

UNBINNED CHLORITIC ALTERATION FABRICS (Qo)

Station	Clast count	Brittle	Brittle-ductile	Ductile	Undistinguishable
47	C11				
1195	C10			1	
1196	C12	1			
1197	C13			1	2
1199	C14		2		
1200	C15				
1201	C16	3	1	1	
1202	C17	1			1
1203	C18		1		1
1212	C24	1		1	1
1213	C25	1	1	1	
1214	C26				

					Total
Number of altered clasts	7	5	5	5	22
Percent of altered clasts	31.8	22.7	22.7	22.7	

West Butte conglomerate clast imbrications

Station	Easting	Northing	Strike of bedding	Dip of Bedding	Strike of imbrication	Dip of imbrication	Trend of pole to imbrication	Plunge of pole to imbrication	Trend of back-rotated pole	Plunge of back rotated pole
222	?	?	225	20	155	52			48.3	42.1
222	?	?	225	20	190	36			72.5	67.7
222	?	?	225	20	174	62			72.8	39.1
222	?	?	225	20	196	76			104.5	41.9
222	?	?	225	20	195	56			121.3	59.2
222	578864	3669663	201	28	97	52			343	39.6
222	578864	3669663	201	28	95	33			322.6	52.5
222	578864	3669663	201	28	95	49			346.8	51.5
226	573376	3671892	172	29	125	44			22.1	64.1
226	573376	3671892	172	29	126	59			22.9	37.4
226	573376	3671892	172	29	108	64			16.7	12.5
226	573376	3671892	172	29	114	72			23	5
226	573376	3671892	172	29	121	50			26.7	27.5
227	573323	3671866	145	20	129	70			31	21.1
227	573323	3671866	145	20	118	62			17.6	24.6
227	573323	3671866	145	20	126	68			27.4	21.9
227	573323	3671866	145	20	106	75			8.9	36.8
227	573323	3671866	191	20	156	55			78.5	58.5
227	573323	3671866	191	20	129	68			33.7	36.2
227	573323	3671866	191	20	129	55			30.1	48.9
1151	573089	3673900	272	14	112	44			0.9	51.5
1151	573089	3673900	272	14	114	63			13.5	34.7
1151	573089	3673900	272	14	150	36			39	69.8
1151	573089	3673900	272	14	135	42			29.7	59.7
1151	573089	3673900	272	14	115	45			8.5	52.1
1151	573089	3673900	272	14	124	34			11.1	70.2
1192	572824	3673326	212	21	91	42			339.7	53.8
1192	572824	3673326	212	21	74	47			326.7	44.1
1192	572824	3673326	212	21	62	34			309.2	46.8
1192	572824	3673326	212	21	98	47			348.1	46.9
1192	572824	3673326	212	21	136	34			17.1	70.6
1194	573935	3671111	136	26	124	72			23.2	49.7
1194	573935	3671111	136	26	110	76			22.1	4.5
1194	573935	3671111	136	26	145	58			69.4	19.9
1194	573935	3671111	136	26	135	52			51.5	33.6
1194	573935	3671111	136	26	132	61			46.7	25.2
1257	573871	3672223	160	17	114	58			4.5	37.2
1257	573871	3672223	160	17	115	56			4	39.3
1257	573871	3672223	160	17	166	58			67	63.1
1257	573871	3672223	160	17	128	42			49.8	69

1259	573773	3672304	175	19	132	60			48.6	42
1259	573773	3672304	175	19	133	58			50.3	43.8
1259	573773	3672304	175	19	118	54			33.4	49.9
1259	573773	3672304	175	19	111	48			25.6	56.5
1259	573773	3672304	175	19	122	64			36.3	39.5
1262	573622	3672229	171	16	113	61			26.1	43.4
1262	573622	3672229	171	16	106	66			17.4	38.8
1262	573622	3672229	171	16	156	74			70.7	23.5
1262	573622	3672229	171	16	161	72			76.3	24.2
1262	573622	3672229	171	16	117	57			31.6	47
1265	573456	3672014	152	18	93	76			2.5	28.9
1265	573456	3672014	152	18	111	58			24.1	46.5
1265	573456	3672014	152	18	108	67			19.7	37.7
1265	573456	3672014	152	18	106	57			18	47.8
1265	573456	3672014	152	18	112	61			24.9	43.5
1271	573251	3671774	167	20	138	82			50.4	19.3
1271	573251	3671774	167	20	129	62			44.7	40.5
1271	573251	3671774	167	20	85	68			352.9	36.6
1271	573251	3671774	167	20	99	74			9.1	31
1271	573251	3671774	167	20	112	72			23.8	32.5
1271	573251	3671774	167	20	118	78			29.9	26
1271	573251	3671774	167	20	106	49			18.8	55.8
bq	?	?	145	35	70	44			329.2	58.6
bq	?	?	145	35	60	48			318.6	52.9
bs	?	?	345	16	78	38			337.3	65.6
bs	?	?	345	16	10	49			267.2	39.8
de	?	?	40	31	141	50			62.3	50
de	?	?	40	31	130	56			47.4	46.2
dj	?	?	22	10	124	24			64.8	77.7
dj	?	?	22	10	115	35			35.8	68.9
dj	?	?	22	10	85	54			351.4	50.5
fl'	?	?	184	28	120	45			38.5	58.5
fl'	?	?	184	28	110	59			22.8	45.6
fl'	?	?	184	28	160	64			77.7	32.2
fl'	?	?	184	28	154	68			70.3	29.7
fl'	?	?	184	28	160	75			74.5	21.6
gi	?	?	176	32	120	35			43.5	68.3
gi	?	?	176	32	130	42			52.9	59.8
hr	?	?	115	22	143	29			81	69
hr	?	?	115	22	136	36			64.7	64.3
kg	?	?	98	15	55	42			309.6	57.6
kg	?	?	98	15	81	65			348	39.2

West Butte conglomerate trough axes

Station	Easting	Northing	Strike of bedding	Dip of Bedding			Trend of trough axis		Trend of back-rotated axis	Plunge of back rotated axis
486	575828	3671586	140	18			20		18.7	
481	576308	3671247	73	15			345		164.5	
1151	573089	3673900	272	14			355		353.2	
1267	573325	3671864	152	24			11		8.5	
1267	573325	3671864	152	24			21		18.4	
1267	573325	3671864	152	24			36		34.9	
1267	573325	3671864	152	24			48		47.6	
226	573376	3671892	172	29			275		96.8	
227	573323	3671866	172	29			255		76.2	
227	573323	3671866	145	20			322		142.2	
227	573323	3671866	145	20			355		353.5	
222	?	?	225	20			352		350.6	

Canebrake Formation clast imbrications

Station	Easting	Northing	Strike of bedding	Dip of Bedding	Strike of imbrication	Dip of imbrication	Trend of pole to imbrication	Plunge of pole to imbrication	Trend of back-rotated pole	Plunge of back rotated pole
209	563129	3669140	190	32	108	55	18	35	355.7	33.2
209	563129	3669140	190	32	75	47	345	43	326.8	24.5
209	563129	3669140	190	32	105	50	15	40	349.6	35.5
209	563129	3669140	190	32	102	34	12	56	42.8	63.6
209	563129	3669140	190	32	124	50	34	40	50.7	42.6
209	563129	3669140	190	32	105	47	15	43	33.8	51.4
210	563338	3669012	50	19	91	56	1	34	13	47.1
210	563338	3669012	50	19	129	72	39	18	26	45.8
210	563338	3669012	50	19	85	37	355	53	310.9	49
210	563338	3669012	50	19	105	62	15	28	194.7	2
210	563338	3669012	50	19	78	55	348	35	352.4	7
210	563338	3669012	50	19	104	47	14	43	19	18.3
210	563338	3669012	50	19	72	44	342	46	356.2	27.6
210	563338	3669012	50	19	76	44	346	46	357.1	36.2
215	563239	3668756	159	34	114	30	24	60	23.1	44
215	563239	3668756	159	34	107	54	17	36	17.6	20
215	563239	3668756	159	34	110	54	20	36	20.1	20
232	565010	3668299	282	30	250	55	160	35	161.9	19.4
232	565010	3668299	282	30	246	55	156	35	158.4	19.7
232	565010	3668299	282	30	221	52	131	38	156.1	53.2
232	565010	3668299	282	30	235	60	145	30	163.9	40.1
232	565010	3668299	282	30	250	47	160	43	187.2	43.7
269	564462	3668875	305	26	40	55	310	35	301.6	13.6
269	564462	3668875	305	26	37	42	307	48	294.6	25
269	564462	3668875	305	26	70	50	340	40	322.2	28.3
270	564477	3668965	314	16	52	38	322	52	302.8	32.6
270	564477	3668965	314	16	39	36	309	54	293.5	31.1
270	564477	3668965	314	16	54	52	324	38	311.2	20.7
277	565972	3668724	291	16	172	48	82	42	78.5	69.9
277	565972	3668724	291	16	165	41	75	49	57.2	75.9
277	565972	3668724	291	16	180	54	90	36	94.2	63.8
277	565972	3668724	291	16	185	49	95	41	105.6	68.2
277	565972	3668724	291	16	162	60	72	30	64.1	56.9
476	558944	3672077	84	16	146	40	56	50	18.7	70.1
476	558944	3672077	84	16	160	60	70	30	61	56.5
476	558944	3672077	84	16	145	58	55	32	38.3	54.4
476	558944	3672077	84	16	175	57	85	33	85	61
318	569698	3670645	175	28	128	47	38	43	7.7	56.8
318	569698	3670645	175	28	135	39	45	51	3.5	65.9
318	569698	3670645	175	28	132	36	42	54	355	66.4

Canebrake Formation trough axes

Station	Easting	Northing	Strike of bedding	Dip of Bedding			Trend of trough axis		Trend of back-rotated axis	Plunge of back rotated axis
251	564008	3668944	305	34			45		37	
259	565205	3670602	345	16			57		246	

Olla and Diablo formation paleocurrents

ORIGINAL DATA ONLY

Station	Easting	Northing	Strike of bedding	Dip of Bedding	Clast imbrication (strike-dip)	Current lineation trend	Foreset bedding (strike dip)	Conglomerate trough axis	Trough cross bedding axis
ck	578907	3669484	184	25					90
cj	?	?	115	19					162
224	578775	3669709	162	38		320, 320, 325			280
225	578732	3669697	194	33					205
310	572359	3670261	130	12				105	
498	576809	3670598	338	35	89-33, 105-26, 87-32				45
498	576809	3670598	338	35	89-33, 105-26, 87-32				45
223	?	?	202	14	155-55, 142-52, 140-71, 152-80				85
223	?	?	202	14	155-55, 142-52, 140-71, 152-80				85
189	582383	3670360	294	30		290			
223	578785	3669664	211	13			228-32		

Ocotillo Formation clast imbrications

Station	Easting	Northing	Strike of bedding	Dip of Bedding	Strike of imbrication	Dip of imbrication	Trend of pole to imbrication	Plunge of pole to imbrication	Trend of back-rotated pole	Plunge of back-rotated pole
39	568638	3667074	78	16	149	49	59	41	73.6	44.3
39	568638	3667074	78	16	146	48	56	42	71.1	46
39	568638	3667074	78	16	143	60	53	30	48.1	8
39	568638	3667074	78	16	123	67	33	23	32.8	33
44	568493	3666664	288	26	115	50	25	40	23.1	49.8
44	568493	3666664	288	26	133	65	43	25	43.8	34.9
54	567527	3667097	125	10	115	64	25	26	20.7	47.3
54	567527	3667097	125	10	121	75	31	15	25.5	6.2
54	567527	3667097	125	10	126	65	36	25	24.5	17.2
54	567527	3667097	125	10	125	66	35	24	19.6	45
54	567527	3667097	125	10	124	55	34	35	27.7	30
54	567527	3667097	125	10	122	57	32	33	26.3	27.7
57	567443	3666774	128	22	142	52	52	38	46.6	37.3
57	567443	3666774	128	22	126	55	36	35	31.6	7
58	567700	3666508	225	30	175	50	85	40	66.9	26.4
58	567700	3666508	225	30	185	62	95	28	100.3	23.2
58	567700	3666508	225	30	224	43	134	47	139	36.3
80	569202	3666295	164	30	125	60	35	30	34.7	50
80	569202	3666295	164	30	127	67	37	23	37.3	43
93	568456	3666357	238	11	165	28	75	62	118.1	72.6
93	568456	3666357	238	11	150	47	60	43	43.3	47.4
93	568456	3666357	238	11	154	45	64	45	46	50.4
93	568456	3666357	238	11	145	52	55	38	67.7	48.7
106	569838	3665429	235	7	99	40	9	50	8.4	67
106	569838	3665429	235	7	87	42	357	48	337.6	34.9
1176	569028	3664720	282	30	200	61	110	29	111	54
1176	569028	3664720	282	30	228	65	138	25	148.4	45.6
1176	569028	3664720	282	30	226	47	136	43	147.5	15.2
1176	569028	3664720	282	30	205	62	115	28	125.1	9.5
1196	568189	3665909	74	12	175	47	85	43	113.6	35.9
1196	568189	3665909	74	12	156	46	66	44	101.9	46.6
1196	568189	3665909	74	12	171	42	81	48	115.7	41.4
1196	568189	3665909	74	12	166	39	76	51	115.9	45.8
1196	568189	3665909	74	12	171	46	81	44	111.9	38.7
1212	566566	3666787	126	20	107	55	17	35	37.7	65.3
1212	566566	3666787	126	20	99	60	9	30	19.2	62.9
1212	566566	3666787	126	20	111	61	21	29	38.8	58.4
1212	566566	3666787	126	20	113	58	23	32	44.4	60.4
1212	566566	3666787	126	20	119	55	29	35	56.2	60.2
1213	567522	3667099	217	17	134	47	44	43	83.7	58.2
1213	567522	3667099	217	17	150	53	60	37	90.1	45.1

1213	567522	3667099	217	17	160	74	70	16	82.2	23.2
1213	567522	3667099	217	17	122	55	32	35	60.1	58.8
1213	567522	3667099	217	17	135	61	45	29	68.7	47.3
1214	567324	3666103	100	17	118	54	28	36	56.1	61.5
1214	567324	3666103	100	17	98	52	8	38	22.6	70.8
1214	567324	3666103	100	17	98	57	8	33	19	66
1214	567324	3666103	100	17	109	68	19	22	31.2	52.6
1277	570520	3665030	198	25	144	42	54	48	98.8	55.6
1277	570520	3665030	198	25	124	61	34	29	56.5	52.9
1277	570520	3665030	198	25	155	44	65	46	103.5	48.4
1277	570520	3665030	198	25	141	69	51	21	68.4	37.7
1277	570520	3665030	198	25	143	54	53	36	83.2	48.3
196	584370	3669785	88	34	75	66	345	24	336.1	56.6
196	584370	3669785	88	34	71	75	341	15	333.5	47
196	584370	3669785	88	34	25	75	295	15	282.3	27.4
196	584370	3669785	88	34	45	63	315	27	293.2	47.8
196	584370	3669785	88	34	34	52	304	38	271.6	50.3

Ocotillo Formation trough axes

Station	Easting	Northing	Strike of bedding	Dip of Bedding			Trend of trough axis		Trend of back-rotated axis	Plunge of back rotated axis
1197	568475	3665847	178	15			38		37	5
1177	569773	3665106	288	14			65		246	5
1195	568713	3667018	215	18			85		84	5

WEST SALTON DETACHMENT FAULT

			Fault data		Slickenlines		
Station	Easting	Northing	Strike	Dip	Trend	Plunge	
27	566122	3666482	294	35	36	34	
27	566122	3666482	294	35	99	9	
27	566122	3666482	294	35	298	3	
29	566079	3666460	286	36	42	33	
29	566079	3666460	286	36	74	21	
29	566079	3666460	286	36	110	3	
29	566079	3666460	286	36	292	4	
32	566389	3666305	278	45	60	32	
33	566358	3666351	340	22			
73	566654	3666142	63	24			
140	561682	3669344	272	11			
148	560659	3669634	281	40	79	18	
154	559674	3670084	301	24			
159	558946	3671662	298	42			
160	558860	3670814	296	32			
197	561841	3669270	298	24	79	16	
201	562170	3669141	315	23			
203	562306	3669118	297	25			
206	562799	3668786	280	20			
207	562897	3668782	304	22			
213	563290	3668549	324	26			
214	563196	3668637	311	44			
216	562775	3668801	262	35			
219	566433	3666308	278	49	101	3	
219	566433	3666308	278	49	305	28	
230	565025	3667651	286	45			
234	564552	3667999	323	31	50	31	
239	564205	3668214	315	20			
242	563852	3668300	295	35	100	10	
247	563611	3668402	294	27			
248	563568	3668369	275	55			
280	566003	3667113	323	14	31	13	
280	566003	3667113	323	14	64	14	
280	566003	3667113	323	14	79	13	
280	566003	3667113	323	14	106	9	
282	565794	3667102	326	31			
286	565428	3666994	316	33	108	17	
295	565052	3667259	284	46			
299	565970	3666535	295	39			
305	566301	3666559	315	30			
475	558963	3671651	295	24			
503	558382	3671161	328	24			
1013	563544	3666578	24	39			
1032	563314	3668358	272	48	79	14	
1034	563230	3668591	327	21	75	20	
1034	563230	3668591	327	21	334	3	

Station	Easting	Northing	Strike	Dip	Trend	Plunge	
1035	563100	3668394	279	24			
1047	562971	3666988	134	26	298	8	
1048	562960	3667006	130	19			
1051	562996	3666948	136	21	195	18	
1052	562961	3667016	134	18	205	17	
1052	562961	3667016	134	18	321	2	
1055	562351	3666795	139	23	199	20	
1055	562351	3666795	139	23	220	23	
1058	562060	3666807	130	23	199	22	
1058	562060	3666807	130	23	235	22	
1075	562617	3668476	274	45			
1078	562384	3668466	281	41	50	34	
1133	565035	3665911	61	34	64	2	
1133	565035	3665911	61	34	90	18	
1133	565035	3665911	61	21			
1135	565114	3665783	80	10			
1210	563334	3668489	321	40			
1244	566369	3666303	294	38	77	25	
1244	566369	3666303	294	38	90	18	
1244	566369	3666303	294	38	104	8	
1246	566248	3666345	293	31	86	15	
1246	566248	3666345	293	31	95	11	
1250	566148	3666429	284	52	82	26	
1250	566148	3666429	284	52	100	5	
1250	566148	3666429	284	52	349	49	
1251	566117	3666469	308	34	105	15	
1253	565970	3666531	305	37	89	24	
1253	565970	3666531	305	37	112	10	
1289	558861	3670807	285	35	67	23	
1289	558861	3670807	285	35	92	9	
3001	566583	3665685	55	12	145	12	
3001	566583	3665685	55	12	160	12	
3001	566583	3665685	55	12	197	7	
3002	566630	3665663	31	14	35	1	
3003	566266	3665540	78	20	86	3	
3003	566266	3665540	78	20	204	16	
3004	566197	3665492	104	21			
3005	566252	3665497	86	25	101	7	
3006	565333	3665656	96	25	255	9	
3006	565333	3665656	96	25	287	5	
3007	566058	3665587	96	26			
3008	566293	3666586	317	27	78	24	
3008	566293	3666586	317	27	105	15	
3009	566238	3665493	96	28			
3010	565922	3665586	112	28			
3011	565180	3665970	141	28	224	28	
3011	565180	3665970	141	28	245	27	
3012	565750	3665641	111	34	194	34	
3013	566058	3666469	284	36			
3014	566096	3666465	281	37	68	22	

Station	Easting	Northing	Strike	Dip	Trend	Plunge	
3014	566096	3666465	281	37	284	2	
3015	565942	3665583	114	38	122	6	
3016	565713	3665645	125	46			
3017	565255	3665782	104	59			
3018	565117	3665797	102	64			
3019	565059	3665801	99	68			
3020	566742	3665814	352	16			
3022	565444	3665793	319	32			
4002	562763	3666807	124	18	229	17	

SUNSET FAULT

			Fault data		Slickenlines		
Station	Easting	Northing	Strike	Dip	Trend	Plunge	
62	567587	3666282	123	60			
63	567548	3666192	110	52			
66	567486	3665693	62	85			
74	566887	3666141	130	70			
77	566783	3666660	20	65			
102	568937	3664900	135	90			
116	569351	3664793	156	70			
118	569031	3664720	45	40			
118	569031	3664720	310	35			
217	569793	3664239	359	31			
218	571669	3665414	162	80	341	6	
1170	570827	3664325	132	56			
1171	569846	3664262	184	69	300	67	
1171	569846	3664262	184	69	196	28	
1171	569846	3664262	184	69	248	67	
1274	570671	3665051	264	70	76	21	
1281	567232	3665885	133	79	135	10	
1281	567232	3665885	133	79	146	49	
1281	567232	3665885	133	79	223	79	
1281	567232	3665885	350	64	4	27	
1282	567589	3665546	334	55	347	18	
1282	567589	3665546	334	55	340	8	
1284	567897	3665185	346	71	355	24	
1285	567959	3665161	135	65	141	14	
1285	567959	3665161	328	71	351	48	
1285	567959	3665161	328	71	344	39	
1285	567959	3665161	328	71	10	63	
1285	567959	3665161	344	78	162	10	
1285	567959	3665161	344	78	34	74	
1286	566871	3666152	119	71	121	7	

ALL OTHER FAULTS

			Fault data		Slickenlines		
Station	Easting	Northing	Strike	Dip	Trend	Plunge	Rake
4	571109	3665046	136	46			
26	556354	3666111	155	35			
135	569926	3666369	1	85			
204	562334	3669102	145	85			10SE
218.5	566433	3666308	278	49	305		
218.5	566433	3666308	278	49	101		
236	564470	3668209	310	72			
254	565540	3670806	185	80			
254	565540	3670806	195	75			
255	565512	3670891	195	75			15N to 15S
256	565418	3670987	168	76			
263	564916	3668993	150	72			
274	563960	3669413	155	75			
274	563960	3669413	147	70			
274	563960	3669413	327	70			
274	563960	3669413	160	75			
276	564551	3669692	145	90			
291	565400	3667219	306	70			
326	571221	3670755	172	85			
336	573980	3671102	20	80			
345	582575	3671224	55	60			70-90NE
398	574780	3671986	218	84			0
409	574311	3671709	145	90			25NW
410	574370	3671769	5	61			
420	574253	3671447	15	40			77 90
420	574253	3671447	5	60			
420	574253	3671447	2	65			
421	574301	3671598	221	90			65N
425	574748	3672220	250	80			
431	574897	3672218	45	59			
439	575070	3671807	235	70			
441	575334	3671856	25	52			
451	575603	3672636	200	30			
460	574899	3672044	20	78			0-10N 5S-10N 10S
460	574899	3672044	25	78			
460	574899	3672044	240	85			
462	576107	3672474	180	84			90
475	558963	3671651	295	24			
482	576232	3671196	170	80			
484	576052	3671412	15	62			70S
487	575671	3671585	228	54			40W

Station	Easting	Northing	Strike	Dip	Trend	Plunge	Rake
487	575671	3671585	224	47			
487	575671	3671585	235	40			
488	575679	3671451	230	70			
489	575540	3671301	22	42			
489	575540	3671301	235	11			
493	575323	3671500	176	61			90
493	575323	3671500	225	70			70s
493	575323	3671500	178	47			90
512	560539	3670763	305	75			
518	560834	3670427	168	52			
527	573067	3672078	325	75			
534	572759	3673242	342	64			17NW
534	572759	3673242	320	83			
536	572788	3673438	10	55			55-60N
1003	565424	3666620	202	45	210		
1009	565001	3666359	334	35			
1010	564991	3666461	15	54			
1027	563945	3667945	10	43			
1037	563156	3668262	28	67			
1037	563156	3668262	20	55			25-30 NE
1039	563096	3667980	6	39	32		
1087	561535	3667629	42	69			15SW
1088	561519	3667566	172	26			
1129	559484	3666987	301	70			
1132	564829	3665934	146	62			33S
1134	565068	3665792	113	66			
1136	565264	3665794	113	62			
1155	572897	3674071	199	62			32n
1159	574341	3673562	232	77			5s
1255	565565	3667148	131	79			48S
1255	565565	3667148	79	46			

Foliation and lineation data from the footwall of the West Salton detachment fault

Station	Easting	Northing	Strike of foliation	Dip of foliation	Trend of lineation	Plunge of lineation	Source
29	566079	3666460	276	60	70	5	Steely
30	566077	3666421	276	45	70	58	Steely
140	561682	3669344	199	23	246	17	Steely
143	561117	3669616	244	44	69	5	Steely
146	560737	3669590	274	76	70	37	Steely
149	560639	3669623	255	43	70	24	Steely
198	561987	3669115	244	31	55	5	Steely
202	562300	3669089	272	35	80	6	Steely
235	564416	3668081	285	24			Steely
241	563856	3668253	331	28	68	31	Steely
243	563775	3668278	285	43	72	27	Steely
248	563568	3668369	251	43	30	31	Steely
285	565534	3666864	336	41			Steely
287	565395	3666993	22	30	86	27	Steely
293	565078	3667198	300	30	75	16	Steely
294	565041	3667165	342	60	82	6	Steely
297	564816	3667571	325	47	70	12	Steely
298	565823	3666589	290	16	83	7	Steely
300	565997	3666409	310	40	85	39	Steely
302	566250	3666361	295	40	92	18	Steely
304	566364	3666331	335	34	100	0	Steely
501	558944	3671641	300	61			Steely
505	558636	3670675	300	30	60	27	Steely
521	565335	3666096	178	18	276	18	Steely
1001	565559	3666720	320	26			Steely
1002	565516	3666654	343	55			Steely
1003	565424	3666620	321	46			Steely
1004	565347	3666655	310	29			Steely
1005	565202	3666519	42	44			Steely
1006	565159	3666454	29	19			Steely
1007	565138	3666364	0	16			Steely
1008	565064	3666323	167	29			Steely
1009	565001	3666359	105	16			Steely
1010	564991	3666461	143	10			Steely
1011	564913	3666405	147	36			Steely
1013	563544	3666578	97	29			Steely
1014	563715	3666596	140	39			Steely
1015	563850	3666541	150	19	279	29	Steely
1016	564076	3666588	150	37	268	34	Steely
1017	564039	3666641	111	22			Steely
1018	564044	3666792	210	24	268	32	Steely
1019	564030	3667027	156	42	255	39	Steely
1020	564045	3667333	14	51			Steely
1021	564072	3667538	20	24			Steely

1022	564102	3667687	99	24			Steely
1023	564142	3667703	330	41			Steely
1024	564294	3667807	32	24			Steely
1025	564023	3667914	341	44			Steely
1026	563980	3667949	131	18	245	17	Steely
1027	563945	3667945	15	22			Steely
1028	563871	3668090	285	30			Steely
1029	563837	3668164	280	35	100	29	Steely
1030	563638	3668246	275	52	61	5	Steely
1031	563374	3668312	282	46			Steely
1033	563243	3668474	228	41			Steely
1036	563173	3668324	302	42	86	28	Steely
1038	563114	3668052	169	30			Steely
1040	563058	3667928	42	7			Steely
1041	562995	3667751	348	29			Steely
1042	563047	3667534	141	20			Steely
1043	563099	3667417	129	38	269	27	Steely
1044	563097	3667144	125	34			Steely
1045	562979	3667064	46	44			Steely
1046	562895	3667032	109	37			Steely
1050	563191	3666703	126	51	279	15	Steely
1053	562797	3666767	125	27			Steely
1054	562749	3666704	354	17			Steely
1056	562331	3666859	134	48			Steely
1057	562223	3666834	174	24	271	24	Steely
1059	561998	3666862	143	31	250	30	Steely
1060	561944	3666920	146	15	275	12	Steely
1061	562002	3666997	180	14			Steely
1062	562058	3667098	105	24			Steely
1064	562046	3667454	113	34			Steely
1065	562047	3667489	210	11			Steely
1066	562139	3667577	131	29			Steely
1067	562029	3667726	198	29			Steely
1069	562075	3667911	101	37	260	15	Steely
1070	562198	3667983	1	16	110	15	Steely
1071	562273	3668017	91	32	254	10	Steely
1072	562402	3668051	30	18			Steely
1073	562582	3668241	27	12			Steely
1074	562598	3668401	237	12			Steely
1076	562523	3668445	295	20			Steely
1077	562396	3668441	289	18	70	46	Steely
1079	562237	3668462	343	14	110	11	Steely
1080	562051	3668509	292	37			Steely
1081	561766	3668350	182	18			Steely
1082	561684	3668223	279	26			Steely
1083	561691	3668148	24	37			Steely
1084	561594	3667952	72	27	78	3	Steely
1085	561590	3667807	92	33	254	11	Steely
1086	561565	3667687	111	47	251	35	Steely
1088	561519	3667566	58	37			Steely
1089	561513	3667305	121	24	104	7	Steely

1090	561501	3666866	147	10			Steely
1092	561827	3666832	231	8	275	6	Steely
1093	561554	3669149	260	29	76	2	Steely
1094	561438	3669008	331	38	71	13	Steely
1095	561401	3668967	315	72			Steely
1096	561320	3668913	134	64	294	35	Steely
1097	561615	3668651	281	28	62	38	Steely
1098	561174	3668698	326	25			Steely
1099	561216	3668524	313	34			Steely
1100	561200	3668414	56	27	84	13	Steely
1101	561187	3668348	115	19	254	18	Steely
1102	561133	3668225	132	35			Steely
1103	561201	3667948	64	26			Steely
1104	561140	3667931	251	15	71	0	Steely
1105	561009	3667826	81	34	84	21	Steely
1106	560799	3667858	41	25			Steely
1107	560898	3667641	109	29	261	15	Steely
1108	560797	3667562	93	47			Steely
1109	560760	3667383	111	29	254	13	Steely
1110	560889	3667208	66	22	82	60	Steely
1111	561099	3667135	51	26			Steely
1112	561223	3666927	221	21	256	12	Steely
1113	561252	3666808	356	27	81	27	Steely
1114	560846	3666734	51	34	71	24	Steely
1115	560592	3666845	80	35	85	8	Steely
1116	560613	3667093	46	32			Steely
1117	560611	3667148	24	15			Steely
1118	560600	3667199	69	29	80	8	Steely
1119	560479	3667155	57	39	84	3	Steely
1120	560257	3666812	76	42	85	3	Steely
1121	560008	3666850	31	52			Steely
1122	559722	3666985	91	49			Steely
1123	559705	3667086	71	50			Steely
1124	559717	3667185	59	47	75	22	Steely
1125	559710	3667220	29	44	85	31	Steely
1126	559528	3667150	70	54	91	26	Steely
1127	559363	3667160	312	88			Steely
1130	559983	3667497	356	40	84	10	Steely
1132	564829	3665934	131	42	299	11	Steely
1138	566243	3665498	92	12			Steely
1139	566251	3665613	32	12	62	6	Steely
1140	565954	3665610	100	31			Steely
1141	565717	3665690	89	11			Steely
1142	565645	3665718	188	36			Steely
1143	565522	3665819	127	46	255	42	Steely
1144	565399	3665875	126	32			Steely
1145	565351	3665991	172	38	264	0	Steely
1146	565275	3665999	158	37	281	32	Steely
1147	565227	3665990	171	31			Steely
1216	561408	3669224	254	20	43	11	Steely
1217	561209	3669079	252	24	61	36	Steely

1218	561160	3669058	293	76			Steely
1219	560930	3668985	97	32			Steely
1220	560875	3669128	312	79			Steely
1221	560736	3669039	164	42	223	38	Steely
1222	560606	3668933	321	53	74	51	Steely
1223	560498	3668953	339	34	73	34	Steely
1224	560218	3668913	355	39	82	39	Steely
1225	560027	3668907	344	30	64	16	Steely
1226	560070	3669211	326	11	60	11	Steely
1227	560504	3669261	301	30	71	38	Steely
1228	560520	3669534	306	33	83	24	Steely
1231	560986	3669448	286	36	84	15	Steely
1245	566269	3666252	319	33	67	32	Steely
1247	566161	3666329	318	34	50	34	Steely
1249	566138	3666411	310	26	76	22	Steely
1252	565977	3666411	322	41	74	39	Steely
1254	565927	3666464	315	37	83	31	Steely
1288	558952	3671525	71	22			Steely
1289	558861	3670807	316	34			Steely
1290	558830	3670610	344	47	91	46	Steely
1291	558799	3670323	316	46	84	39	Steely
1292	558743	3670267	325	65	68	64	Steely
1293	558647	3670488	313	37	72	24	Steely
3026	566326	3665930	316	37	53	37	G. Axen
3027	566182	3665693	356	32	57	29	G. Axen
3028	565531	3666531	5	43	62	19	G. Axen
3029	565643	3666635	339	26	62	26	G. Axen
3030	566159	3665598	13	20	64	30	G. Axen
3031	566370	3666356	309	34	68	28	G. Axen
3032	565803	3666323	302	52	69	5	G. Axen
3033	565670	3665943	265	19	69	46	G. Axen
3034	566466	3666120	316	29	72	33	G. Axen
3035	566424	3665948	303	30	72	26	G. Axen
3036	566210	3665945	282	30	84	40	G. Axen
3037	566244	3665881	343	27	87	9	G. Axen
3038	565961	3665613	65	24	87	26	G. Axen
3039	565890	3666460	314	44	88	35	G. Axen
3040	565866	3666522	300	40	90	23	G. Axen
3041	566219	3665801	13	18	93	18	G. Axen
3042	565385	3666492	353	27	97	26	G. Axen
3043	565712	3665984	302	18	98	8	G. Axen
3044	565741	3666690	330	40	104	31	G. Axen
3045	565686	3665688	108	29	258	15	G. Axen
3046	565786	3665938	240	22	262	9	G. Axen
3047	565746	3666010	80	5	264	38	G. Axen
3048	565328	3665953	155	34	268	21	G. Axen
3049	565313	3665965	154	30	272	27	G. Axen
3050	565811	3666103	272	22	276	2	G. Axen
3051	565529	3665836	160	30	300	20	G. Axen
3052	565769	3666219	2	42			G. Axen
3053	565777	3666158	356	58			G. Axen

3054	565789	3666056	151	31			G. Axen
3055	565892	3665853	252	26			G. Axen
3056	566056	3665705	91	25			G. Axen
3057	566570	3665942	313	29			G. Axen
3058	565415	3665967	147	23			G. Axen
3059	565306	3666123	162	26			G. Axen
3060	565314	3666180	350	12			G. Axen
3061	565291	3666323	348	24			G. Axen
3062	565306	3666450	331	20			G. Axen
3063	566582	3666029	283	44			G. Axen
3064	566390	3666252	310	28			G. Axen
3065	564805	3665948	182	26			G. Axen
3066	564813	3665888	139	69			G. Axen
3067	564803	3665806	192	36			G. Axen
3068	565775	3665700	5	16			G. Axen

Foliation and lineation data from the hanging wall of the West Salton detachment fault at Squaw Peak

Station	Easting	Northing	Strike of foliation	Dip of foliation	Trend of lineation	Plunge of lineation	Source
348	582892	3671506	243	64	63	0	Steely
350	582668	3671308	228	38	42	5	Steely
342	582434	3671182	212	30	232	11	Steely
344	582517	3671203	165	36	210	27	Steely
345	582575	3671224	184	19			Steely
346	582821	3671353	40	22			Steely
362	581638	3671162	270	32			Steely
359	582165	3671191	267	39			Steely
361	581741	3671175	264	54			Steely
368	581306	3671105	241	59			Steely
358	581955	3671194	298	60			Steely
343	582451	3671171	115	61			Steely
357	582417	3671324	245	62			Steely
354	582654	3671496	230	63			Steely
353	582527	3671442	239	72			Steely
349	582835	3671460	232	80			Steely
352	582410	3671405	239	87			Steely

Strikes and dips of bedding

Station	Easting	Northing	Strike	Dip
1	571466	3665278	234	35
2	571450	3665264	206	20
3	571391	3665189	256	65
5	570954	3665150	272	28
7	570682	3665520	236	40
8	570010	3665274	5	8
9	570288	3665544	255	2
10	570356	3665431	157	16
11	570334	3665306	40	19
12	570320	3665350	36	3
13	570605	3665268	120	30
14	570341	3665553	287	15
15	570371	3665586	115	45
16	570314	3665584	290	31
17	565691	3669481	255	5
25	566186	3667794	190	5
33.5	570704	3665608	312	47
36	568130	3667161	105	14
37	568031	3666905	197	14
38	568316	3667071	145	7
39	568638	3667074	78	16
40	568724	3667074	92	10
41	568665	3666746	220	10
44	568493	3666664	288	26
45	568384	3666586	219	29
46	567991	3666174	296	6
47	568226	3666428	315	20
48	568702	3666881	18	9
49	577839	3671246	326	11
52	577815	3671244	331	26
53	567635	3667263	311	9
54	567527	3667097	125	10
55	567630	3667009	99	9
56	567523	3666762	144	19
57	567443	3666774	128	22
58	567700	3666508	225	30
59	567744	3666520	209	12
60	567771	3666522	325	7
61	567823	3666475	280	14
62	567587	3666282	200	22
64	567672	3666113	149	21
66	567486	3665693	324	66
67	567569	3665710	201	26
68	567513	3665627	284	32
69	567283	3666789	120	22
70	566415	3666822	130	32
71	566458	3666609	145	47
72	566420	3666481	349	4
74	566887	3666141	270	24
75	567361	3665840	256	17
76	567029	3666315	264	22
77	566783	3666660	185	32
79	569469	3666583	221	12
80	569202	3666295	164	30
81	569113	3666078	241	10
82	568150	3665640	142	32
83	568467	3665681	106	36
84	568460	3665863	149	16
85	568605	3665895	42	14
86	568725	3666013	290	15
87	568821	3665950	290	9
93	568456	3666357	238	11
94	568423	3666220	129	5
95	568146	3666130	234	26
96	568083	3665909	120	10
100	568721	3664843	170	20
101	568901	3664850	210	16
103	569274	3664949	250	22
105	569415	3665123	162	16
106	569838	3665429	235	7
107	569852	3665545	232	7
108	569529	3665434	155	12
110	569416	3665628	101	14
111	569436	3665691	148	18
113	570275	3664670	300	27
114	570103	3664633	313	24
115	569783	3664854	325	15
116	569351	3664793	311	16
118	569031	3664720	232	20
119	569139	3664734	295	52
120	569545	3664407	282	18
121	569653	3664216	182	22
122	569687	3664279	255	36
124	570450	3664627	256	31
125	570042	3664349	275	20
126	569976	3664295	224	20
127	569821	3664275	264	34
128	569838	3664267	258	13
130	570847	3664324	144	51
131	570531	3664564	252	39
132	571895	3664963	34	43
133	572065	3665544	229	11
134	569596	3666659	332	13
136	569911	3666205	316	16
137	570136	3666574	214	12
138	570921	3666902	250	9
142	561535	3669648	242	47

144	560937	3669760	245	27
147	560671	3669648	219	37
150	560398	3669829	208	40
152	559928	3669968	75	22
153	559961	3670049	70	28
156	559794	3671015	114	59
157	559694	3671587	335	44
158	558938	3672081	162	30
161	559161	3671469	145	27
162	559341	3671568	175	51
163	559349	3671591	261	25
164	559350	3671650	215	78
165	559567	3671495	324	20
166	559416	3671376	72	20
167	559304	3671201	90	36
168	559411	3671069	110	45
169	559511	3671122	62	30
170	559737	3670910	65	47
171	559859	3670755	190	18
172	560088	3670849	354	20
173	560111	3670879	72	50
174	560136	3670976	80	10
176	560120	3671526	195	48
177	560065	3671685	12	90
178	559925	3671725	205	44
179	559974	3671960	214	37
180	581589	3670500	124	47
181	581553	3670508	94	42
182	581561	3670405	144	36
183	581817	3670390	182	37
184	581891	3670501	222	14
185	581910	3670507	214	22
186	582060	3670548	260	24
187	582198	3670514	268	44
188	582296	3670343	115	20
189	582383	3670360	294	30
190	582398	3670314	198	12
191	582048	3670306	203	16
192	583470	3671239	131	8
193	584164	3669701	181	32
194	584282	3669824	155	32
195	584370	3669785	93	27
199	562205	3669343	5	34
200	562220	3669395	350	27
205	562638	3669056	234	36
208	563025	3668858	155	30
209	563129	3669140	190	32
210	563338	3669012	50	19
211	563379	3668756	169	22
215	563239	3668756	159	34

221	578879	3669640	229	17
222	578864	3669663	201	28
223	578785	3669664	211	13
224	578775	3669709	162	38
225	578732	3669697	194	33
226	573376	3671892	172	29
231	565079	3668204	301	22
232	565010	3668299	282	30
233	564760	3668300	226	25
236	564470	3668209	209	44
237	564406	3668226	240	39
249	563605	3668425	166	44
251	564008	3668944	305	34
252	564098	3669017	355	36
254	565540	3670806	75	20
257	565385	3670973	56	24
258	565202	3670726	22	15
259	565205	3670602	345	16
260	565637	3670552	322	5
261	565728	3669548	329	6
263	564916	3668993	294	14
264	564757	3668901	298	19
265	564819	3669065	350	31
266	564328	3668547	96	30
267	564470	3668602	285	6
268	564498	3668763	255	24
269	564462	3668875	305	26
270	564477	3668965	314	16
271	564529	3669141	311	22
272	564450	3669416	350	24
273	563883	3669221	9	44
274	563960	3669413	320	31
275	563979	3669461	265	10
277	565972	3668724	291	16
278	566220	3669218	36	14
279	566681	3669615	295	5
309	572403	3670365	118	16
310	572359	3670261	130	12
311	572337	3670124	334	8
317	569634	3670613	211	22
318	569698	3670645	175	28
319	569715	3670640	194	25
321	569924	3671063	126	26
322	570426	3670767	153	22
323	571967	3671023	149	27
324	571852	3671052	126	28
325	571799	3670964	151	15
327	571269	3671461	155	25
328	571614	3671578	127	22
329	571537	3671499	130	17

330	574337	3669285	139	25
331	574552	3669220	147	26
332	573727	3670994	52	26
333	573832	3671106	156	26
334	573924	3671024	75	30
335	573986	3671034	191	42
336	573980	3671102	165	20
337	574052	3671128	149	62
338	574035	3671171	25	82
339	574002	3671243	162	24
340	574310	3671275	174	29
341	574082	3670933	170	25
360	582125	3671243	51	9
365	581495	3671199	310	15
367	581367	3671162	289	20
369	581188	3670955	120	75
370	581238	3670939	90	43
371	581248	3670899	110	75
372	582520	3670493	88	21
373	582719	3670589	101	45
375	583992	3669739	141	26
376	583939	3669708	18	34
377	583897	3669561	217	31
378	584012	3669335	165	16
380	584261	3669068	265	14
381	584372	3669167	265	14
382	584448	3669412	24	9
383	584544	3669520	7	34
384	584600	3669597	60	24
385	584744	3668870	295	26
386	583977	3668907	111	64
387	584123	3668852	113	49
388	583306	3669173	204	37
389	583341	3669320	87	54
390	583390	3669294	221	22
391	583220	3669304	275	30
392	575290	3666569	171	17
393	575151	3666752	62	8
393	575151	3666752	165	27
394	574832	3666432	40	7
396	576127	3665945	174	16
397	576316	3667291	118	11
399	574705	3671934	175	16
401	574532	3672092	90	47
403	574493	3672015	81	17
404	574542	3672036	175	19
406	574382	3671852	352	55
411	574416	3671765	65	46
413	574510	3671774	185	20
414	574620	3671798	177	27

415	574583	3671663	202	21
416	574495	3671519	235	29
417	574397	3671405	200	34
418	574266	3671399	190	36
419	574243	3671420	30	27
422	574344	3671659	38	38
423	574436	3671672	99	20
424	574858	3672180	170	18
426	574646	3672212	115	11
427	574568	3672171	68	70
429	574583	3672343	345	37
430	574623	3672277	349	9
432	574873	3672354	112	14
433	574771	3672452	5	9
434	574927	3672474	20	11
435	575003	3672463	332	21
436	574741	3671420	215	25
437	574965	3671627	201	22
438	575159	3671347	112	8
439	575070	3671807	220	15
440	575131	3671836	292	7
441	575334	3671856	15	20
442	575477	3671936	346	14
443	575605	3672030	189	12
444	575685	3672291	336	18
445	575730	3672336	351	49
446	575750	3672367	351	68
447	575915	3672225	339	35
448	575974	3672453	25	24
449	575718	3672531	330	65
450	575597	3672467	329	51
451	575603	3672636	340	63
452	575462	3672543	321	50
453	575427	3672472	205	36
454	575376	3672352	340	14
455	575371	3672162	340	22
456	575179	3672064	337	21
457	575062	3672020	211	19
458	574972	3672082	162	25
461	574814	3671966	186	21
462	576107	3672474	180	19
462	575228	3672766	359	43
463	576107	3672474	282	21
464	576096	3672344	175	11
465	576120	3672201	172	11
466	576175	3672226	225	8
467	576179	3672292	210	4
468	576259	3672199	209	12
469	576347	3672273	180	18
470	576354	3672439	279	20

473	558818	3671485	157	40
476	558944	3672077	84	16
478	565279	3668078	328	64
480	576311	3671352	119	13
481	576308	3671247	73	15
482	576232	3671196	10	45
483	576206	3671145	207	15
484	576052	3671412	131	14
485	575981	3671551	138	16
486	575828	3671586	140	18
491	575558	3671479	19	20
492	575490	3671515	12	60
493	575323	3671500	202	37
495	570609	3665715	340	22
496	570471	3665874	332	51
498	576809	3670598	338	35
500	559018	3672400	219	21
502	558829	3671692	262	32
504	558657	3671464	75	29
506	559068	3670978	352	12
507	559141	3671024	50	27
508	559268	3671014	77	20
509	560358	3670542	205	22
510	560318	3670351	211	12
511	560551	3670668	260	32
513	560511	3671306	168	27
514	560281	3670929	159	8
515	559808	3671753	109	51
516	560889	3670174	188	19
517	560774	3670172	133	26
518	560834	3670427	252	24
519	560986	3670492	273	26
520	561199	3670439	315	49
522	572563	3672850	168	30
523	572530	3672008	175	29
524	572486	3672251	174	26
525	572775	3672163	141	22
526	573007	3672025	161	16
528	573138	3671995	164	16
529	573289	3672188	164	20
530	573109	3672397	163	18
531	572876	3672518	155	20
532	572816	3672785	145	25
533	572755	3673108	160	21
535	572830	3673344	150	18
537	572695	3673384	181	25
538	572555	3673245	162	17
539	572396	3672895	195	27
540	572675	3673709	309	20
1049	562941	3667024	196	12

1148	572687	3673796	264	8
1149	572931	3673792	352	11
1150	573023	3673827	256	10
1151	573089	3673900	272	14
1152	573226	3674174	261	19
1153	573069	3674211	282	22
1154	572960	3674106	266	22
1156	572887	3674346	254	26
1157	572721	3673953	274	17
1158	572651	3673899	242	7
1162	574683	3673226	349	27
1164	580678	3672755	311	12
1166	584243	3669013	184	17
1168	571390	3665189	266	61
1169	570518	3664703	193	42
1173	569576	3664355	237	35
1174	569559	3664389	295	22
1175	569704	3664363	267	31
1176	569028	3664720	282	30
1177	569773	3665106	288	14
1178	570553	3665766	318	22
1180	556872	3678497	36	52
1185	578675	3670371	133	26
1186	578646	3670435	173	31
1192	572824	3673326	212	21
1194	573935	3671111	136	26
1195	568713	3667018	215	18
1196	568189	3665909	74	12
1197	568475	3665847	178	15
1198	569260	3665724	51	17
1199	569159	3665386	134	16
1200	569121	3665065	134	16
1201	569211	3664785	293	38
1206	566022	3668638	313	14
1212	566566	3666787	126	20
1213	567522	3667099	217	17
1214	567324	3666103	100	17
1230	560818	3669729	220	32
1234	559967	3670099	113	24
1235	559807	3671034	124	54
1236	559815	3671165	121	46
1237	559669	3671354	133	23
1240	559117	3671264	74	41
1243	560264	3671996	201	26
1256	573926	3672228	175	25
1257	573871	3672223	160	17
1258	573851	3672235	160	19
1259	573773	3672304	175	19
1261	573694	3672279	165	17
1262	573622	3672229	171	16

1263	573531	3672129	147	19
1264	573526	3672050	166	25
1265	573456	3672014	152	18
1266	573400	3671927	155	22
1267	573325	3671864	152	24
1268	573299	3671796	167	20
1269	573243	3671778	171	26
1270	573206	3671775	154	19
1271	573251	3671774	167	20
1273	572753	3671732	172	24
1275	570597	3665082	114	74
1276	570552	3665101	276	44
1277	570520	3665030	198	25
1278	570645	3665629	288	24
1279	570338	3665591	68	7
1280	567217	3665900	301	17
1282	567589	3665546	326	34
1283	567822	3665316	303	52
1294	570540	3672251	168	22
1295	570701	3672139	143	23
1296	571359	3672046	201	26
1297	571544	3671616	157	25
1298	571136	3671705	133	25
1301	583601	3664566	115	31
1303	572636	3674159	343	10
1304	572539	3674193	301	17
1305	572486	3674322	57	32
1306	572472	3674423	284	17
1307	572353	3674185	239	17
1308	572147	3674249	237	21
1309	572151	3674096	184	21
1310	572087	3674032	272	6
1311	572069	3673842	107	26
1312	572076	3673508	176	14
1313	572165	3673334	34	4
1314	572472	3673281	174	18
1315	572420	3673623	166	12
1316	572392	3673801	47	7
1318	572699	3674034	259	17
1319	572645	3674665	314	23
1320	572737	3674778	78	26
2001	578924	3669442	164	14
2002	576411	3668828	165	21
2003	576617	3669206	170	20
2004	576543	3669399	185	14
2005	576615	3669410	162	5
2006	576693	3669279	85	25
2007	576773	3669327	90	37
2008	577238	3669470	35	10
2009	577094	3669431	50	10

2010	577029	3669472	90	26
2011	576921	3669481	115	35
2012	576879	3669470	129	41
2013	576726	3669570	22	10
2014	576773	3669687	32	20
2015	576500	3669726	105	14
2016	576982	3669739	40	31
2017	575816	3669104	155	18
2018	575747	3669104	149	16
2019	575717	3669158	164	25
2020	575754	3669388	194	15
2021	575830	3669648	170	20
2022	575973	3669748	183	18
2023	576022	3669739	150	21
2024	576038	3669863	30	16
2025	575662	3670034	193	25
2026	575808	3670011	165	21
2027	575817	3670102	175	25
2028	575866	3670201	175	6
2029	575983	3669999	171	4
2030	576055	3670041	125	9
2031	576127	3670034	35	16
2032	576213	3670021	149	16
2033	576656	3669932	68	20
2034	577103	3669813	15	27
2035	577188	3669833	10	37
2036	576637	3670041	80	5
2037	576537	3670030	194	20
2038	576329	3670141	181	15
2039	577038	3669984	345	28
2040	577008	3670054	10	22
2041	576953	3670162	335	18
2042	576797	3670165	345	17
2043	576955	3670305	330	50
2044	576762	3670314	298	12
2045	576686	3670271	10	15
2046	576613	3670282	324	19
2047	576259	3670273	100	18
2048	576326	3670403	30	12
2049	576107	3670349	126	8
2050	575901	3670353	140	22
2051	576031	3670524	115	9
2052	575856	3670553	79	8
2053	575945	3670605	155	22
2054	575565	3670746	168	21
2055	575675	3670839	151	17
2056	575654	3670971	171	21
2057	575812	3670928	174	32
2058	575829	3670984	155	22
2059	575881	3670778	178	19

2060	575940	3670698	182	20
2061	576062	3671021	141	19
2062	576014	3670935	189	25
2063	576205	3670913	90	12
2064	576255	3670809	140	15
2065	576237	3670583	186	10
2066	576250	3670529	215	11
2067	576381	3670442	165	11
2068	576439	3670537	345	11
2069	576545	3670646	17	0
2070	576441	3670713	15	45
2071	576469	3670705	20	65
2072	576721	3670414	25	16
2073	576667	3670451	338	18
2074	576695	3670549	257	20
2075	576819	3670486	330	24
2076	577001	3670692	155	15
2077	576849	3670989	130	8
2078	576771	3670995	145	17
2079	577972	3671013	315	14
2080	577924	3671022	320	28
2081	577920	3671269	302	7
2082	577776	3671402	345	8
2083	577581	3671328	5	24
2084	577753	3671451	334	30
2085	577646	3671606	293	20
2086	577527	3671681	152	15
2087	577356	3671900	78	5
2088	577345	3671992	242	21
2089	576956	3671994	294	24
2090	576846	3671920	210	19
2091	576733	3672293	282	40
2092	576618	3672055	233	14
2093	576588	3671970	215	16
2094	576713	3671991	212	27
2095	576280	3672311	275	35
2096	576418	3671638	200	10
2097	576605	3671632	198	17
2098	576555	3671464	175	16
2099	576731	3671503	198	19
2100	576789	3671312	165	14
2101	576410	3671143	80	9
2102	576293	3671128	105	11
2103	574891	3669332	173	22
2104	574934	3669416	180	25
2105	575040	3669470	90	32
2106	574805	3669527	199	45
2107	575082	3669675	20	25
2108	574736	3669725	245	35
2109	574726	3669774	179	28

2110	574805	3669784	200	36
2111	574533	3669935	180	23
2112	574679	3669923	217	21
2113	575082	3669910	114	32
2114	574728	3670383	197	25
2115	574869	3670022	170	9
2116	574929	3670014	205	19
2117	575154	3669989	338	24
2118	575173	3670086	5	25
2119	575042	3670143	125	19
2120	575065	3670017	207	13
2121	575151	3670284	215	10
2122	575042	3670440	170	15
2123	575023	3670536	213	24
2124	575319	3670536	215	22
2125	575243	3670566	200	15
2126	575196	3670623	175	11
2127	575243	3670761	87	5
2128	575198	3670712	196	14
2129	575413	3670944	169	19
2130	575423	3670860	132	15
2131	575324	3670865	175	30
2132	574689	3670793	203	21
2133	574508	3670937	360	22
2134	574315	3671033	100	85
2135	574597	3671137	155	20
2136	574570	3671246	210	29
2137	574227	3671460	171	32
2138	574266	3671358	160	26
2139	574127	3671270	160	17
2140	574144	3671640	165	30
2141	574812	3671528	201	29
2142	574151	3671259	161	26
2143	574151	3671224	160	20
2144	574201	3671196	170	20
2145	574200	3671235	158	22
2146	573305	3671590	163	23
2147	573888	3672443	161	8
2148	573918	3672415	165	15
2149	573982	3672304	161	20
2150	573999	3672142	145	16
2151	573986	3672001	158	19
2152	574014	3671981	180	38
2153	573992	3671953	152	15
2154	573999	3671775	135	15
2155	574062	3671797	160	20
2156	574073	3671829	162	32
2157	574046	3671875	145	25
2158	574008	3671866	151	12
2159	574929	3671888	145	20

2160	573795	3672335	130	25
2161	573730	3672402	166	14
2162	573684	3672436	60	48
2163	573650	3672495	155	26
2164	573597	3672499	169	25
2165	573574	3672595	175	28
2166	573231	3672664	172	32
2167	573335	3672814	179	30
2168	573478	3672923	199	31
2169	573361	3672946	179	23
2170	573411	3673014	184	28
2171	573320	3673109	191	33
2172	573465	3673211	175	18
2173	573450	3673252	180	21
2174	573448	3673307	255	20
2175	573528	3673293	231	33
2176	573643	3673382	310	24
2177	573331	3673410	216	19
2178	573461	3673541	260	38
2179	573532	3673565	290	11
2180	573546	3673512	220	65
2181	573676	3673641	270	25
2182	573782	3673634	265	35
2183	573960	3673614	224	16
2184	574480	3673884	343	20
2185	574559	3673719	6	24
2186	574684	3673610	349	26
2187	574489	3673335	303	34
2188	574530	3673198	285	36
2189	574502	3673157	315	58
2190	574912	3673437	322	29
2191	574875	3673398	11	12
2192	574953	3673378	291	6
2193	574958	3673296	229	7
2194	574723	3672994	0	28
2195	574832	3672946	8	37
2196	575010	3672922	1	44
2197	574921	3672907	25	15
2198	574654	3672838	242	20
2199	574702	3672870	340	12
2200	574895	3672840	290	14
2201	574947	3672860	331	22
2202	574919	3672695	329	24
2203	574971	3672712	354	26
2204	575049	3672705	344	33
2205	574827	3672562	325	17
2206	574713	3672525	350	4
2207	575235	3672530	329	38
2208	575350	3672458	353	62
2209	575179	3672397	326	30

2210	575237	3672350	339	26
2211	575186	3672252	10	16
2212	575127	3672257	335	27
2213	575077	3672189	345	10
2214	575047	3672105	36	14
2215	574862	3672315	275	15
2216	574877	3672382	185	40
2217	574840	3672400	310	10
2218	574938	3672454	302	7
2219	574966	3672532	345	18
2220	575014	3672556	345	16
2221	575049	3672564	342	45
2222	575671	3672200	315	15
2223	575698	3672068	36	11
2224	575639	3671968	165	15
2225	575480	3671853	302	16
2226	575400	3671790	217	6
2227	575240	3671638	265	3
2228	575244	3671528	305	10
2229	575819	3671684	61	12
2230	575767	3671768	196	9
2231	575608	3671673	0	17
2232	575528	3671629	350	17
2233	575507	3671399	15	33
2234	575663	3671514	65	25
2235	575739	3671501	70	18
2236	575806	3671525	73	23
2237	575901	3671525	148	9
2238	575852	3671411	22	6
2239	575969	3671367	192	13
2240	575875	3671226	130	14
2241	575080	3672034	75	4
2242	575080	3671976	155	22
2243	575022	3671970	175	16
2244	579030	3669448	262	2
2245	579005	3669439	194	22

ROCK SAMPLES

Station	Easting	Northing	Sample Number	Station	Easting	Northing	Sample Number
6	571000	3665191	102303-3	355	582643	3671316	120303-5
29	566079	3666460	102903-1 102903-2 102903-3 102903-4	356	582415	3671291	120303-6
37	568031	3666905	103003-1	358	581955	3671194	120303-7
51	577871	3671165	103103-1 103103-2	363	581640	3671216	120303-8
56	567523	3666762	110103-1	366	581446	3671148	120303-9
93	568456	3666357	110303-1 110303-2	403	574493	3672015	120603-1
97	567586	3665534	110303-3 110303-4	472	559136	3671384	120803-1
98	567970	3665175	110303-5	482	576232	3671196	120903-1
99	568175	3664984	110303-6	490	575405	3671209	120903-2
124	570450	3664627	110603-1	495	570609	3665715	121003-1
127	569821	3664275	110603-2	499	576790	3673839	121003-2
133	572065	3665544	110603-3	521	565335	3666096	121403-3
183	581817	3670390	111303-1	525	572775	3672163	121503-1
192	583470	3671239	111303-2	530	573109	3672397	121503-2
202	562300	3669089	111403-1	541	574013	3671803	121503-3
203	562306	3669118	111403-2	542	574018	3671798	121503-4
217	569793	3664239	111503-1	543	574007	3671812	121503-5
219	574048	3671901	111603-1	544	574134	3671408	121503-7
224	578775	3669709	111703-6	1026	563980	3667949	121604-2
226	573376	3671892	111703-7	1043	563099	3667417	121604-3
234	564552	3667999	112003-1 112003-2	1044	563097	3667144	121604-4
241	563856	3668253	112003-3	1060	561944	3666920	121704-1
247	563611	3668402	112003-5	1063	562115	3667262	121704-2
248	563568	3668369	112003-4	1068	562039	3667874	121704-3
281	565882	3667066	112203-1	1109	560760	3667383	122704-1
283	565807	3667002	112203-2	1129	559484	3666987	122704-2 122704-3
285	565534	3666864	112202-3	1131	564748	3666002	123034-1
286	565428	3666994	112203-4	1134	565068	3665792	123004-2 123004-3
287	565395	3666993	112203-5	1137	565854	3665618	123004-4
289	565412	3667024	112203-6	1138	566243	3665498	123004-5
290	565509	3667063	112203-7	1148	572687	3673796	123104-1
301	566068	3666403	112203-8	1151	573089	3673900	123104-2
303	566266	3666421	112203-9	1159	574341	3673562	123104-3
344	582517	3671203	120303-1	1163	580630	3672729	123104-4
349	582835	3671460	120303-2	1166	584243	3669013	123104-5
351	582410	3671429	120303-3	1167	584708	3668856	123104-6
353	582527	3671442	120303-4	1178	570553	3665766	10205-1

Station	Easting	Northing	Sample Number
1185	578675	3670371	10605-1
1233	560516	3671304	11005-1
1238	559402	3671371	11005-2
			11005-3
1239	559236	3671168	11005-4
1255	565565	3667148	11105-1
1257	573871	3672223	11205-1
1259	573773	3672304	11205-3
1265	573456	3672014	11305-1
1271	573251	3671774	11305-2
1297	571544	3671616	11905-1
			11905-2
1300	571789	3671225	12005-2
1302	553801	3664552	12105-1
	571944	3656204	121303-1
			121303-2
			121303-3
	565995	3661570	121403-1
	565065	3665554	121403-2

Plate 1. Geologic Map of portions of the 7.5' Borrego Mountain, Borrego Sink, Harper Canyon, Squaw Peak, Tubb Canyon, and Whale Peak quadrangles

Alexander N. Steely[1], Susanne U. Janecke[1], Gary J. Axen[2], Rebecca J. Dorsey[3]

[1] Department of Geology, Utah State University, Logan, UT 84322
[2] Department of Earth and Environmental Sciences, New Mexico Tech, Socorro, NM 87801
[3] Department of Geological Sciences, University of Oregon, Eugene, OR 97405

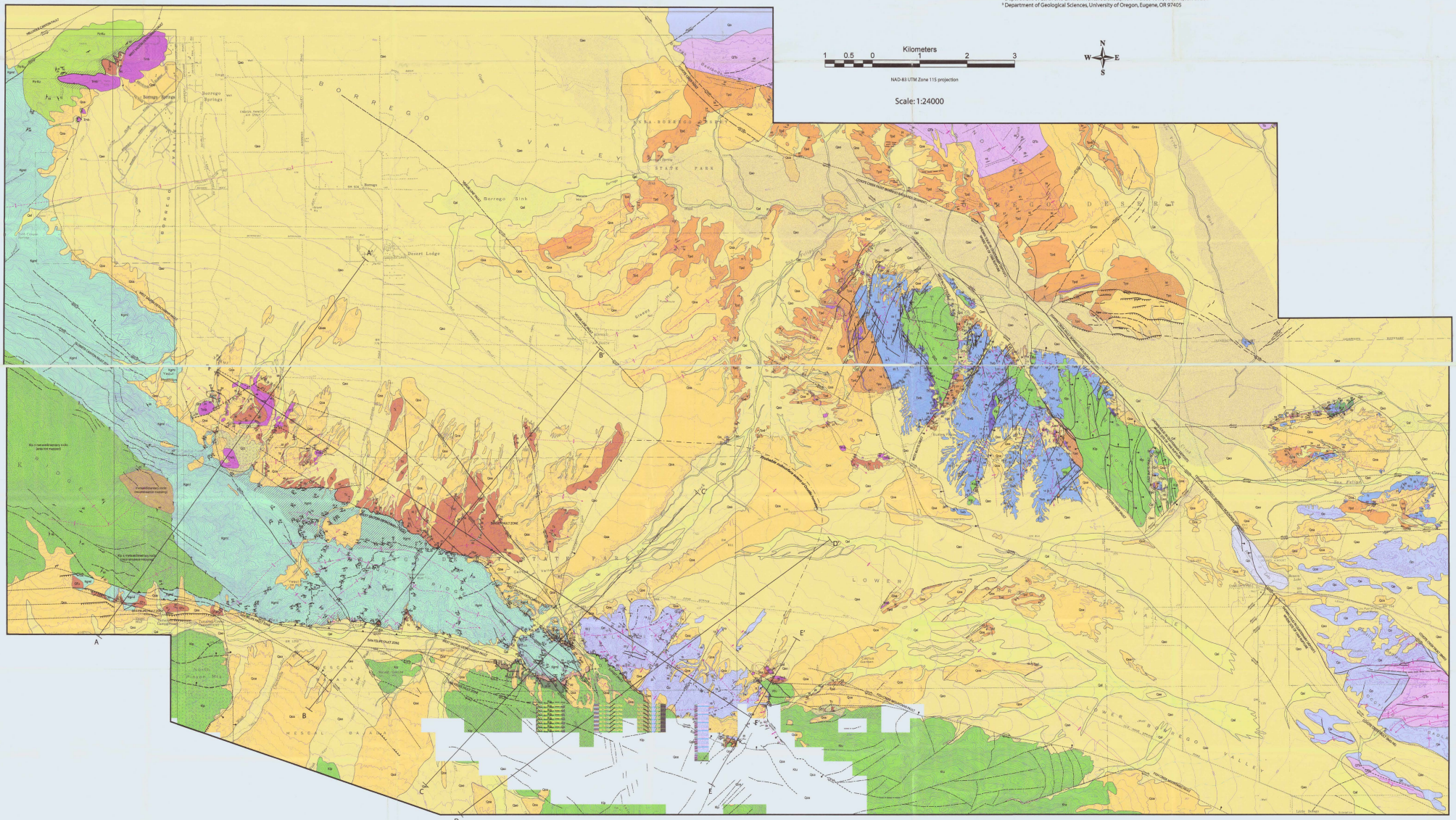

Plate 2. Legend and Unit Descriptions for the Geologic Map of portions of the 7.5' Borrego Mountain, Borrego Sink, Harper Canyon, Squaw Peak, Tubb Canyon, and Whale Peak quadrangles

Alexander Steely[1], Susanne Janecke[1], Gary Axen[2], Rebecca Dorsey[3]

QUATERNARY

Qal **Modern Alluvial deposits**— Gravelly to fine-grained sediment deposited in modern drainages and stream channels.

Qao **Alluvial Deposits, older**—Immobile gravelly to fine-grained sediment that modern sediments cut. Locally contain fault scarps along the Coyote Creek fault.

Qp **Playa Deposits**—Fine-grained sand to clay deposits localized in extensional fault stepovers of the Coyote Creek fault. Contained scarps along the trace of the 1968 rupture of the Coyote Creek fault (Sharp and Clark, 1972).

Qd **Dune Deposits**—Medium- to fine-grained sand form large (up to 30 m-tall) eolian sand dunes. Dunes are located on the east (leeward) side of cliffs and other topographic barriers such as in Borrego Mountain wash, and Blow Sand canyon.

Qc **Colluvium and Talus Deposits**— Very coarse- to fine-grained, angular to rounded rock debris and soil material.

Ql **Landslide Deposits**—Landslides and slumps that contain large boulders to fine-grained sand. Composition varies with parent material and may contain rotated blocks.

Qoa **Old Alluvium**—Poorly sorted boulder- to fine-grained deposits with gently sloping surfaces. These deposits cut the older Ocotillo Formation but are slightly to moderately dissected by younger alluvium. Near West Butte this deposit may correlate with the Font's Point sandstone of Ryter (2002) and Lutz (2005). Locally there are up to seven distinct levels of this deposit that reach elevations of over 1700' above the lowest deposits. These highest deposits are likely older than the lowest deposits, although region-wide correlation is difficult.

Qo **Ocotillo Formation (Sunset conglomerate)**—The Ocotillo Formation is a basin-wide unit of coarse-grained alluvial sandstone, conglomerate, and interbedded finer-grained lithologies (Bartholomew, 1968; Dibblee, 1984; Lutz et al., in review; Kirby, 2005). Its basal contact with the Borrego Formation changes laterally in the Borrego Badlands from a slight disconformity in the west to a conformable contact in the east (Lutz et al., in review). It is also a slight disconformity in the eastern San Felipe Hills but changes to an angular unconformity across the crest of the San Felipe anticline in the western San Felipe Hills (Dibblee, 1954; 1984; Kirby et al., in review). The Brawley Formation is the finer-grained, fluvial-deltaic lateral equivalent of the Ocotillo Formation (Kirby, 2005). The age of the Ocotillo and Brawley formations has been revised to ~1.1- to 0.5-0.6 Ma based on new magnetostratigraphy in the Borrego Badlands (Lutz, 2005; Lutz et al., in review) and San Felipe Hills (Kirby, 2005; Kirby et al., in review). Based on the similar stratigraphic position, thickness, basal contact, grain size, depositional environments, paleoflow, composition, and recycled Diablo sandstone clasts, we interpret the Sunset conglomerate as a proximal part of the Ocotillo Formation.

The Sunset conglomerate is exposed NE of the Sunset fault for 5.7 km from Harper Canyon in the east to Yaqui Narrows in the west, and up to 2.6 km NE of the Sunset fault (Fig. 3-5a). The Sunset conglomerate has been exhumed due to uplift in the San Felipe fault zone and is the only exposure of this unit near the fault zone. The Sunset conglomerate lies along slight angular unconformity on a thin belt of Canebrake, Olla, and Diablo formations of the Palm Spring Group near Harper Canyon where the intervening Borrego Formation was either never deposited or was eroded away before the Sunset conglomerate was deposited. At this location the Palm Spring Group dips 10°-15° more steeply north than the overlying Sunset conglomerate. Elsewhere, the base of the conglomerate is not exposed. The Sunset conglomerate is at least 600 m-thick based on map estimates and geological cross sections.

The Sunset conglomerate consists of light gray to gray-tan, moderately to poorly consolidated, poorly sorted coarse to pebbly sandstone, pebble-cobble conglomerate, and angular to sub-rounded boulder to cobble conglomerate. Overall the unit coarsens upsection from pebbly conglomeratic sandstone near the base to angular to rounded boulder conglomerate near the top. The unit also coarsens laterally SW toward the Sunset fault where grain size changes from coarse sandstone ~2 km NE of the fault to angular boulder conglomerate along the fault in the SW.

Imbricated clasts show overall NE paleotransport when corrected for bedding tilt. We interpret the coarse beds near the Sunset fault as debris-flow deposits. These beds fine laterally NE into beds that we interpret as dominantly gravelly sheet-flood deposits with some conglomerate-filled stream channels. The lateral continuity of these facies and the paleoflow indicators suggest deposition in the upper and middle part of a NE-flowing alluvial fan.

TERTIARY

Tb **Borrego Formation** (Pliocene-Pleistocene)—The lacustrine Borrego Formation overlies the Diablo Formation along a complexly interbedded and gradational contact in the San Felipe-Borrego sub-basin (Fig. 3-4) (Dibblee, 1954; 1984; Kirby, 2005). The Borrego Formation is ~1.6-1.8 km-thick in the San Felipe Hills and Borrego Badlands and consists of claystone, mudstone, and lesser sandstone (Dibblee, 1984; Kirby, 2005). Deposits in the Borrego Formation accumulated in a perennial freshwater to brackish lacustrine environment that experienced rare lake-level low stands (Kirby et al., in review). Coarse pebbly sandstone is rare in most exposures of the Borrego Formation but becomes common (up to ~ 50%) in the western Borrego Badlands where it is interbedded with lacustrine mudstone and claystone of the upper Borrego Formation. There, sandy pebble conglomerate in the upper ~95 meters of the Borrego Formation contains clasts of well cemented sandstone reworked from the underlying Diablo and Olla Formations.

PALM SPRING GROUP

Tc **Canebrake Conglomerate** (Pliocene-Pleistocene (?))—Regionally the Diablo and Olla formations pass laterally west and southwest into locally-derived coarse sandstone to cobble-boulder conglomerate of the Canebrake Conglomerate (Dibblee, 1954; 1984; Winker and Kidwell, 1996). The Canebrake Conglomerate is exposed in an 18 km-long outcrop belt along the northeast side of Yaqui Ridge where it is faulted against mylonitic plutonic rocks by the West Salton low-angle fault. Approximately 600 m of section is measured between the oldest exposed conglomerate and the Yaqui Ridge megabreccia northeast of Yaqui Ridge using cross sections constructed parallel and perpendicular to the West Salton detachment fault.

The Canebrake Conglomerate consists of gray to tan-colored, poorly to moderately cemented, moderately to well sorted, rounded pebble to boulder conglomerate and poorly to moderately sorted, sub-angular to rounded pebbly sandstone. Coarse conglomerate beds are clast-supported and grain sizes range from medium sand up to ~1 m boulders. Individual conglomerate beds range in thickness from ~50 cm to >3 m-thick and bedding is poorly defined. Planar bedding to low-angle cross stratification are the most common bedforms in all grain sizes, whereas trough cross bedding is rare throughout the unit. However, because most outcrops are only a few square meters many larger-scale bedforms may be present but not well exposed. Overall, the Canebrake Conglomerate is coarser and has a greater variability of grain sizes than the West Butte conglomerate.

Clast lithologies within the Canebrake Conglomerate are constrained by 14 counts of 50 clasts in the outcrop belt northeast of Yaqui Ridge. Clasts consists of ~4% La Posta-type tonalite, 18% Granite Mountain-type diorite and granodiorite, 17% fine-medium-grained undifferentiated plutonic rocks, 13% pegmatitic material, ~14% mylonitic plutonic rocks, 20% metamorphic rocks, and 14% chloritically altered plutonic rocks. Of the metamorphic rocks, ~51% are biotite and psamittic schist, 33% are quartzose, and 14% are undifferentiated metaplutonic, migmatite, and gneiss. The chloritically altered rocks are nearly evenly distributed between brittle, ductile, brittle ± ductile, and undifferentiated categories. Hematitic alteration is rare within clasts of the Canebrake Formation (<3% of all clasts) and is only developed in the plutonic rocks. Overall, mean paleotransport was NNE when measurements are corrected for bedding dip.

Tmb **Yaqui Ridge Megabreccia** (Pliocene)—Several locations in the study area expose a ~1-10 m-thick, sheet-like deposit of brecciated plutonic and metamorphic rocks interbedded within the Palm Spring Group. In all locations medium to fine-grained 'c-suite' sandstone of the Diablo Formation is closely associated with the megabreccia deposit. Using the four outcrops, a lateral pinch-out near West Butte, and the lack of this deposit on the northeast side of the Coyote Creek fault, a conservative estimate of ~200 km^2 can be made for the areal extent of the megabreccia deposit.

The megabreccia commonly consists of massively brecciated to highly fractured plutonic rock with little or no internal stratification. Grain sizes range from fine sand-sized to large boulders (up to ~6 m across) and individual grains are angular and fit together with a jigsaw fabric. Near Yaqui Meadows, severely fractured to brecciated outcrops up to ~100 square meters across locally contain continuous pegmatites that can be traced for several meters. These features suggest translation of large rock masses with little internal distortion.

The lithology of the megabreccia deposit is similar across the field area, generally consists of Granite Mountain-type plutonic rocks that show a range of deformational fabrics from undeformed to brittle to mylonitic, but locally have significant variations. Between ~20-70% of the lithologies at each locality consist of undeformed medium to large-grained Granite Mountain-type diorite. At Yaqui Ridge these lithologies are mixed with up to ~30% chloritically altered ultramylonite, mylonite, protomylonite, brittle shear zones, and pegmatite. At Church Ridge, the megabreccia is dominated by unaltered Granite Mountain-type diorite and contains <20% strained rocks. At Harper Canyon the megabreccia contains ~40% Granite Mountain-type diorite, ~30-50% fine-grained tonalite and diorite (not La Posta-type tonalite), and up to 10-20% pegmatite and spotted tonalite. The outcrop near West Butte displays the largest range of lithologies and consists of ~20-30% Granite Mountain-type diorite, ~20% chloritically altered brittle to ultramylonitic shear zones, ~20% chloritically altered to non altered protomylonite and mylonite, and ~20-30% 'spotted' tonalite, unaltered tonalite, minor gneiss, and schistose rocks.

We interpret the brecciation, coarse grain sizes, textures, and sudden change of provenance in this deposit relative to the Diablo Formation, as the result of a long-runout landslide. Textures and brecciation are similar to those of the upper and lower megabreccia deposits of the Fish Creek-Vallecito basin (Abbot and Rightmer, 1996; Winker and Kidwell, 1996), the 'Vallecito' megabreccia within the Palm Spring Group near Whale Peak (Hart, 1991), and the Blackhawk landslide along the northern San Bernadino Mountains (Shreve, 1994).

Td **Diablo Formation** (Pliocene)—The Diablo Formation crops out near Borrego Mountain where it overlies the Olla Formation and is at least ~550 m-thick (Dorsey et al., 2004). In Harper Canyon to the south and Yaqui Meadows to the southwest, a few tens of meters of Diablo Formation crop out where neither the base nor the top are exposed, but instead, the unit is interbedded with the Canebrake and Olla formations. The base of the Diablo Formation is placed where thick 'c-suite' cross-bedded sandstone and thick red mudstone beds overlie the thinner bedded 'l-suite' sandstone beds of the Olla Formation. The top of the Diablo Formation is not exposed in the study area, but to the north and east it consists of a complexly interbedded section of Diablo and Borrego formation lithologies (Kirby, 2005; Lutz, 2005).

Within the study area the Diablo Formation generally consists of interbedded tan to yellow 'c-suite' sandstone beds and red claystone to siltstone beds. Sandstone beds are generally fine-to medium-grained, well sorted, and medium to thick bedded. Locally, they pinch out into mudstone over tens to hundreds of meters and contain concretions from 1 to 30 cm in diameter. Trough cross bedding and planar bedding are the most common sedimentary textures and many well-cemented sandstone beds have current lineations. Mudstone beds are generally red-colored silty claystone to clayey siltstone, and may locally contain bentonitic clay (Morley, 1963). Beds are medium to thick bedded (up to ~8 m-thick), have broadly lenticular geometries, and are typically structureless to laminated.

To **Olla Formation** (Pliocene)—Around Borrego Mountain, the Olla Formation overlies the West Butte conglomerate along a gradational contact. The base of the unit is defined as being above the last thick conglomerate bed of the West Butte conglomerate and where sandstone is greater than 50%. The Olla Formation is up to 120 m-thick near the south of Borrego Mountain wash, but thins to ~38 m at the north end of the wash. This thickness change is also accompanied by a change from tan colored beds where the unit is thick, to red colored beds where the unit is thin. The Olla Formation is inferred to buttress out against basement tonalite north of Middle Butte.

In general, where the Olla Formation is thick it consists of 'l-suite' tan, red, and yellow fine to coarse grained sandstone, with rare interbeds of tan to red siltstone, mudstone, and pebble to granule sized conglomeratic sandstone. Sandstone grains are generally sub angular to sub rounded, moderately sorted, and composed of quartz, feldspar, lithics, and lesser amounts of biotite. Beds vary from ~1-3 cm- to 1-2 m-thick and commonly display parallel bedding. Low angle cross stratification is also common, but trough cross stratification is rare. Locally, conglomeratic beds have up to a 20 cm-deep erosional channel at their base. In locations where the Olla Formation is thin it consists of interbedded red arkosic sandstone, granule to pebble-sized conglomeratic sandstone, and red siltstone to mudstone beds.

Around Borrego Mountain and just northeast across the Coyote Creek fault, a 1-5 m thick prominent yellow-weathering sandstone bed crops out 10-15 m beneath the contact with the Diablo Formation. This bed is composed of both 'L-suite' and 'C-suite' coarse to fine sand grains, is generally planar-bedded but may contain up to 1 m trough cross-beds, has locally developed current lineations, weathers out small 1-2 cm diameter 'c-suite' concretions, and is well cemented. This lithology is unique to this bed making it an ideal structural and stratigraphic marker.

Tpu **Palm Spring Group, undivided** (Pliocene)—Unit used in cross sections only and may contain any formations of the Palm Spring Group.

IMPERIAL GROUP

Twb **West Butte conglomerate** (Pliocene)—The West Butte conglomerate crops out around Borrego Mountain where it varies from 0 to ~280 m thick. This unit overlies the Hawk Canyon formation along a progressive unconformity. Where the Hawk Canyon formation is not present the West Butte conglomerate lies depositionally on basement tonalite. Across Borrego Mountain the West Butte conglomerate fines upward into the overlying Olla Formation of the Palm Spring Group and the top of the unit is placed above the last persistent >10 cm-thick conglomerate bed or where sandy conglomerate becomes subordinate to coarse sandstone.

The West Butte conglomerate consists of buff, tan, and tan-red, moderately cemented, poorly to moderately-sorted, rounded, interbedded pebbly sandstone, sandy conglomerate, and pebble to boulder conglomerate. Overall, the average grain size throughout the unit is between coarse sand and pebbles and is relatively consistent. The upper ~1/4 of the unit slightly fines upward and shows more variation in grain size because the frequency of thick conglomerate beds decreases. Bedding is dominated by planar bedding, but low-angle cross stratification is also common. Individual beds are poorly to well defined by changes in grain size and vary in thickness from ~1 cm to >2 m. Channel troughs are rare in the lower 2/3 of the unit, but become more common near the top. Trough cross beds are typically <20 cm tall, but are rare throughout the unit.

Sandstone throughout the unit is composed of subangular to rounded, poorly to moderately sorted, medium to granule-sized grains that are dominated by quartz, feldspar, lithics, and lesser biotite. Sandstone beds vary from ~1 to 50 cm-thick but are usually less than 15 cm throughout most of the unit. The matrix of sandy conglomerate and conglomeratic sandstone beds is dominated by this lithology and these beds are also ~1 to 50 cm thick. In outcrops that are stained red or have significant hematitic alteration of larger clasts, individual biotite grains in the matrix appear fresh and unaltered.

Conglomerate beds are clast to matrix-supported, typically ~3 to 100 cm thick but can be as thick as 2 m, and vary from pebble- and granule-size through rare boulders up to 2 m in diameter. Clasts are mostly subrounded to rounded by vary from subangular to well rounded. Sedimentary structures are generally lacking within these conglomerate beds, but locally fining upward trends are observed. These beds usually have sharp, undulatory bottom contacts above coarse to pebbly sandstone beds. Locally, ~10 to 50 cm-deep channels are present at the base of these coarser beds. Clast lithologies in the West Butte conglomerate consist of plutonic, metamorphic, chloritically altered and deformed plutonic rocks, and hematitically altered rocks, but do not match the lithology of the underlying crystalline bedrock. Mylonite or proto-mylonite constitutes less than 1% of the total clast lithologies. Deformed and chloritically altered plutonic rocks account for 22% of the total clast lithologies in the West Butte conglomerate. All of these clasts preserve significant brittle deformation but also contain lesser but consistent incipient ductile deformation. The semi-brittle deformation mechanisms are consistent with deformation at ~200° C but below 300°-350° C (Scholz, 1988; White, 2001). Overall, we interpret these rocks as being derived from a major fault zone in the source area of the West Butte conglomerate.

All of the clast lithologies within the West Butte conglomerate also show some hematitic alteration. Clasts that have been affected by this alteration typically have much of their original biotite altered to hematite and have red matrix between grains. The alteration commonly permeates the entire clast, but some clasts only have a thin 0.5-2 cm rind of red to red-brown alteration. Some heavily altered clasts have both hematitic alteration and a less characterized yellow alteration that appears to affect feldspar and possibly quartz grains. Typically ~45% of plutonic lithologies are hematitically altered, whereas only ~10% of metamorphic or chloritically altered rocks have hematitic alteration

Overall, paleotransport was N26°E ± 7° when measurements are corrected for bedding dip. We interpret the moderately to poorly-sorted, planar bedded to low-angle cross stratified coarse sandstone to sandy pebble conglomerate as sheet-flood deposits. We interpret the deformed and chloritic clasts as derived from the damage zone of the West Salton detachment fault. The NNE-directed paleotransport direction shows that the source of these clasts was SSW of the Borrego Mountain area near Whale Peak, a corrugation in the West Salton detachment fault.

Th **Hawk Canyon formation, undivided** (Late Miocene-Pliocene)—The Hawk Canyon formation is 0-88 m-thick and consists of a lower, middle, and upper member that are exposed in five major outcrops around Borrego Mountain, including excellent exposures in Hawk Canyon and at the east end of East Butte. The formation is depositional on Cretaceous La Posta-type tonalite with up to 4 m of local relief and the entire formation buttresses out against basement rocks along strike. The top of the Hawk Canyon formation is placed beneath the first thick conglomerate bed of the West Butte conglomerate.

The lowest member of the Hawk Canyon formation is 0 to 7 m-thick, coarse to sub-rounded, moderately sorted, gray to gray-green, arkosic sandstone that lies nonconformably within slight depressions on basement tonalite. Locally, the unit has up to 2 m high buttress unconformities. Bedding is typically structureless but locally, medium to thick planar beds are poorly defined by slight grain-size segregations. Clast and grain lithologies are dominated by angular to subangular quartz and feldspar with lesser biotite. In Hawk Canyon, outsized boulders and cobbles of distinctive red and white banded pegmatites are embedded within the overlying sandstone less than 4 meters from their bedrock source and several pegmatite ridges protrude into the sandstone. The top of this unit is placed at a generally sharp contact between the relatively structureless sandstone of the lower member and well bedded to ripple cross bedded sandstone of the middle member. The lower member is exposed at most outcrops of the Hawk Canyon formation. A late Miocene faunal assemblage is documented in this member at Hawk Canyon (Jefferson, 1999)

The middle member of the Hawk Canyon formation is 0 to 55 m-thick, and generally fines upward from white to gray-green arkosic medium-grained sandstone into green and mottled green-red mudstone. It conformably overlies the lower member where present, but otherwise is depositional on basement tonalite and locally buttresses out against basement rocks. Pebbles and cobbles of basement pegmatite are present as outsized clasts where the unit is depositional on basement rocks. The base of the middle member is placed above the structureless sandstone of the lower member, and the top is placed above the highest green mudstone.

The base of the middle member consists of moderately planar bedded, moderately sorted, gray to gray-green, angular to sub-rounded arkosic sandstone overlain by a ~3.5 m-thick green mudstone to claystone. Thin 3-4 cm-thick conglomeratic sandstone beds with tonalite pebbles are interbedded near the base of the member. Finer grained sandstone and siltstone beds commonly contain significant back-filled vertical burrow tracks. The upper part of the sandy interval locally contains 25-30 cm-thick planar to low-angle cross stratified beds. Possible hummocky cross stratification is locally observed but rare. Locally, symmetrical ripples in fine to medium-grained sandstone beds are overlain by thin beds or laminae of siltstone and mudstone and display flaser bedding structures. These ripples have wavelengths of 5-7 cm and rare climbing ripples show propagation to the SSE when restored for local bedding tilt. Sandstone beds above these flaser-bedded intervals commonly show abundant bioturbation.

Green silty claystone to mud shale overlies the lower sandy interval along a sharp contact and contains 2-5 cm-thick interbeds of fine-grained gray-green arkosic sandstone every 10-40 cm. Mudstone and claystone beds are commonly fissile and locally contain gypsum partings. Several mudstone samples were collected in Hawk Canyon and show freshwater ostracodes and no marine diatoms (R. Dorsey, written comm., 2005). The abundance and thickness of sandstone beds increase up section to the top of this unit to become subequal to the mudstone. Most sandstone interbeds show significant burrow mottling and bioturbation.

Th **Hawk Canyon formation, continued**

The upper member of the Hawk Canyon formation is 0 to 30 m-thick and generally coarsens upward from interbedded red mudstone and subordinate red arkosic sandstone to dominantly sandstone and subordinate mudstone. It conformably overlies the middle member of the Hawk Canyon formation or is depositional on basement tonalite and locally buttresses out against basement. The base of the upper member is placed above the last green mudstone of the middle member. The top of the upper member is placed below the first thick conglomerate bed of the overlying West Butte conglomerate. This contact is sharp and undulating with scour-and-fill geometries and within Hawk Canyon a slight angular unconformity truncates strata of the Hawk Canyon formation to the north. The contact is also an angular unconformity along the east and northeast sides of East Butte but changes vergence and truncates strata to the south.

The base of the upper member typically consists of a 1-2 m-thick interval of dark red to mottled red and green, fissile, silty claystone or mud shale. Above this basal fine-grained interval begins a ~10-28 m-thick interbedded sandstone-mudstone interval that continues to the top of the unit. Sandstone beds increase thickness upsection from 5-20 cm-thick near the base to 200 cm-thick near the top and are laterally continuous for hundreds of meters, broadly lenticular in geometry, generally coarsen up, and locally contain 5 cm-thick granule or small pebble lags at their bases. Sandstone beds are mostly planar to weakly planar or massive bedded near the base and gradually become better defined and locally display trough cross bedding and low-angle cross stratification near the top. Pebble and granule composition is difficult to determine due to the small size of clasts, but a 20 cm-thick bed of rounded to sub-rounded pebble to small cobble conglomerate near the middle of the member shows tonalite, deformed and chloritically altered plutonic rocks, and assorted metamorphic clasts similar to the clast composition of the overlying West Butte conglomerate. Mudstone beds decrease thickness upsection from 20-200 cm-thick near the base to 1-15 cm-thick near the top.

Ti **Imperial Formation** (Late Miocene-Pliocene)—The Imperial Group is also exposed near Squaw Peak ~4 km east of Borrego Mountain, grades upward into the Palm Spring Group, and is at least several hundred meters thick, but estimates are hampered by many cross-cutting oblique strike-slip faults that separate the depositional base from the top of the unit (Morley, 1963; Reitz, 1977). Morley (1963) reports a maximum thickness of ~890 m, but based on our mapping this is a severe overestimate. The basal contact is a low-angle depositional to buttress nonconformity between 'l-suite' fossiliferous sandstone, pebbly sandstone, and the underlying basement rocks that has up to 4 m of paleorelief. The basement rocks were formerly named the Squaw Peak schist (Morley, 1963; Dibblee, 1984) although the majority of these rocks are not schist, but rather a complexly deformed group of mylonitic granodiorite, foliated tonalite, other metaplutonic rocks, and lesser calc-silicate and quartzose metasedimentary rocks.

The basal Imperial Group generally consists of gray 'l-suite', medium- to coarse-grained, fossiliferous sandstone, pebbly sandstone to sandy pebble conglomerate, and rare thin gray to blue sandy limestone beds with some vertical and horizontal cemented burrows, 2-3 m long and other fossils (Reitz, 1977). Fossiliferous sandstone beds are calcite-cemented, and commonly contain oyster casts, pelecypod shell fragments, and rare silicified wood fragments (Morley, 1963). Several 1-3 m-thick pebbly sandstone beds in the lower part of the section consist of calcite-cemented medium- to coarse-grained sandstone with granules to pebbles interbedded with tan, brown, and green siltstone to claystone and 0.5-3 m-thick oyster coquina beds. Clast lithologies in the conglomeratic beds dominantly consist of tonalite and other plutonic rocks, but locally contain up to ~25% chloritically altered plutonic rocks with brittle deformation fabrics. Although these clasts are generally small, they are nearly identical to chloritically-altered clasts observed in the West Butte conglomerate near Borrego Mountain.

The upper part of the Imperial Group exposed south of Squaw Peak consists of interbedded and variegated sandstone, siltstone and claystone, and oyster coquina beds. Sandstone beds are generally thin to thick bedded, fine- to coarse-grained, moderately sorted, subrounded, and have 'l-suite' compositions. Outcrops of 'c-suite' sandstone beds are rare but increase in abundance to the south of the outcrop belt. Claystone beds are typically gray to yellow and green, locally gypsiferous, contain variable amounts of silt and sand, and grade laterally and vertically into siltstone and fine-grained sandstone beds (Morley, 1963). Up to 3 m-thick, tan to dark gray oyster shell coquina beds are interbedded with sandstone and siltstone and grade upward into pelecypod-bearing fossiliferous sandstone beds. Locally, siltstone and fine-grained sandstone beds grade upward into coarse sandstone beneath the coquina beds and in one location a pebbly sandstone bed grades into planar bedded coarse sandstone beneath a sharp contact with the overlying coquina bed. Coquina beds locally have up to 2 m-high tabular cross stratification.

CRETACEOUS

Klp **La Posta-type tonalite** (Late Cretaceous)—These rocks are undeformed, commonly light-colored, have tonalitic composition, and are characterized by large euhedral quartz grains (<2 mm), rare biotite, and large feldspar grains. Euhedral 1-2 mm sphene crystals are also common. At Borrego Mountain up to 1.5 m-thick pegmatites are common, although elsewhere pegmatites are rare. Most of the plutonic rocks in the hanging wall of the West Salton detachment fault are part of the La Posta-type TTG (tonalite-trondhjemite-granodorite) suite (Grove et al., 2003). These plutons differ from other plutons in the area because they are voluminous (up to 1400 km^2 surface exposure), internally zoned from hornblende-biotite granodiorite in the outer zone to muscovite-biotite granodiorite in the core (Clinkenbeard and Walawender, 1989; Walawender et al, 1991), and emplaced over a relatively short time period of 96 ± 3 Ma (Grove et al., 2003). We use the term 'La Posta-type' plutons when referring to these relatively mafic-poor and undeformed tonalites which comprise the majority of the Vallecito and Fish Creek mountains.

Kgml **Granite Mountain-type and mixed Granite Mountain- and fine-grained La Posta-type plutonic rocks** (Late Cretaceous)—These rocks are typically deformed by the Eastern Peninsular Ranges Mylonite zone and are foliated to mylonitic, medium gray in color, and have a diorite to granodiorite composition. Biotite is common and typically forms large books 1-10 mm across. Quartz grains are usually <2 mm and much less common than in the La Posta tonalite. Pegmatites are common and are locally sheared along mylonitic foliation planes. We use the term 'Granite Mountain-type' to refer to these hornblende-biotite-to biotite-rich tonalite and quartz diorite plutons. These more mafic plutonic rocks crop out dominantly in the footwall of the West Salton low-angle fault where they either form the more mafic margins of La Posta-type plutons, or form distinct plutons (Grove et al., 2003; Kairouz, 2005). Locally along the trace of the Yaqui Ridge anticline these Granite-Mountain-type lithologies are intermixed with fine- to medium-grained tonalite and diorite and may be part of a mixing zone along a plutonic boundary. These rocks are generally older than the La Posta-type plutons and range from 105-89 Ma (Silver et al, 1979).

PALEOZOIC

Pzu **Metasedimentary rocks, undifferentiated** (Paleozoic)—This unit generally consist of mylonitic to foliated carbonate- and quartz-rich metasedimentary rocks. Locally, blue-gray marbles crop out near the tip of Yaqui Ridge, contain tan-colored silicic concretions, and are interleaved with mylonitic plutonic rocks. These rocks were pre-batholithic volcanic and sedimentary rocks of Paleozoic to mid-Cretaceous age (Gastil and Miller, 1984), and Jurassic to early-Cretaceous volcanic arc-related sedimentary rocks (Gastil et al, 1975; Silver et al, 1979; Todd et al, 1988).

Correlation of Map Units

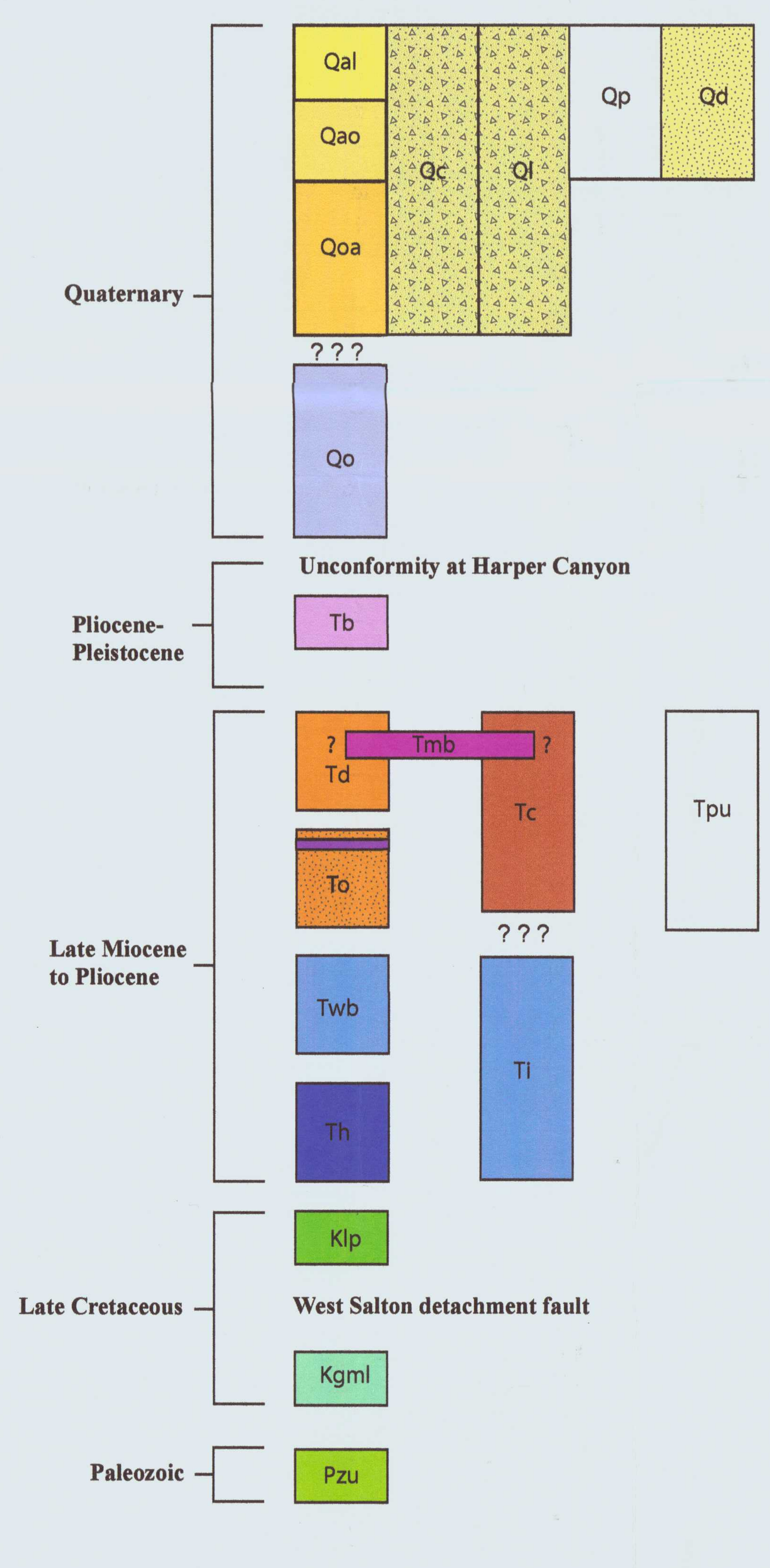

References

Clinkenbeard, J.P., and Walawender, M.J., 1989, Mineralology of the La Posta pluton: Implications for the origin of zoned plutons in the eastern Peninsular Ranges batholith, southern and Baja California. American Mineralogist, v. 74, p. 1258-1269.

Dibblee, T.W. Jr., 1954, Geology of the Imperial Valley Region, California, Geology of Southern California. California Division of Mines Bulletin 170, p. 21-28.

Dibblee, T.W. Jr., 1984, Stratigraphy and tectonics of the San Felipe Hills, Borrego Badlands, Superstition Hills, and vicinity. In: Rigsby, C.A., (ed.), 1984, The Imperial Basin-tectonics, sedimentation, and thermal aspects. Pacific Section S.E.P.M., p. 31-44.

Dorsey, R. J.; Janecke, S. U.; Kirby, S.; Axen, G.; and Steely, A. N. 2004. Pliocene Lacustrine Transgression in the Western Salton Trough, Southern California: Implications for Regional Tectonics and Evolution of the Colorado River Delta. Geological Society of America Abstracts with Programs 36:317.

Gastil, R.G., 1975, Plutonic zones in the Peninsular Ranges of southern California and northern Baja California: Geology, v. 3, p. 361-363.

Gastil, R.G., and Miller, R.H., 1984, Prebatholithic paleogeography of peninsular California and adjacent Mexico, in Frizzell, A., Jr., ed., Geology of Baja California peninsula: Los Angeles, California, Society of Economic Paleontologists and Mineralogists Pacific Section, v. 39, p. 9-16.

Grove, M., Lovera, O., and Harrison, M., 2003, Late Cretaceous cooling of the east-central Peninsular Ranges batholith (33N): Relationship to La Posta pluton emplacement, Laramide shallow subduction, and forearc sedimentation, in Scott, J.E., Scott, P.R., Fletcher, J.M., Girty, G.H., Kimbrough, D.L., and Martin-Barajas, A, (eds), Tectonic evolution of northwestern Mexico and Southwestern USA, Geological Society of America Special Paper 374, p. 355-379.

Hart, M.W., 1991, Landslides in the Peninsular Ranges, southern California. In: Walawender, M.J., and Hanan, B.B., (eds.), Geological excursions in southern California. Guidebook 1991 Annual Meeting Geological Society of America, San Diego, California, p. 297-312.

Herzig, C., Carrasco, A., Schar, T., Murray, G., Rightmer, D., Lawerence, J., Milton, Q., Wirths, T., 1995, Neogene stratigraphy of the Borrego Mountain area, Anza-Borrego Desert State Park, California, in Remeika, P., and Sturz, A., eds., Paleontology and geology of the western Salton Trough detachment, Anza-Borrego Desert State Park, California. Field trip guidebook and volume for the 1995 San Diego Assoc. of Geologist's field trip to Anza-Borrego Desert State Park. Volume 1, p. 133-136.

Jefferson, G.T., 1999, A late Miocene terrestrial vertebrate assemblage from Anza-Borrego Desert State Park. In: The 1999 Desert Research Symposium, edited by R.E. Reynolds, Abstracts of Papers Submitted to the Meetings, San Bernardino County Museum Association Quarterly v. 46, n. 3. p. 109-111.

Kairouz, M.E., 2005, Geology of the Whale Peak Region of the Vallecito Mountains: Emphasis on the Kinematics and Timing of the West Salton Detachment fault, Southern California [M.S. Thesis] University of California, Los Angeles. 156 p.

Kirby, S.M., 2005, The Quaternary tectonic and structural evolution of the San Felipe Hills, California. [M.S. Thesis]: Utah State University, 182 p.

Kirby, S.M., Janecke, S.U., Dorsey, R.J., Housen, B.A., Langenheim, V., McDougal, K., and Steely, A.N., in review, Timing and complexities of initial strike-slip deformation in the southwestern Salton Trough, California, constrained by the Pleistocene Brawley and Ocotillo Formations, submitted to: Journal of Geology.

Lutz, A.T., 2005, Tectonic controls on Pleistocene basin evolution in the central San Jacinto fault zone, southern California [M.S. thesis]: University of Oregon, 136 p.

Lutz, A.T., Dorsey, R.J., Housen, B.A,, and Janecke, S.U., in review, Stratigraphic record of Pleistocene faulting and basin evolution in the Borrego Badlands,San Jacinto fault zone, southern California. Submitted to GSA Bulletin.

Morley, E. R., 1963, Geology of the Borrego Mountain Quadrangle and the western portion of the Shell Reef Quadrangle, San Diego County, California. [M.S. Thesis] University of Southern California, Los Angeles, California, 138 p.

Reitz, D. T., 1977, Geology of the western and central San Felipe Hills, northwestern Imperial County, California. Master's thesis, University of Southern California, Los Angeles, California, 155 p.

Rightmer, D.A., and Abbott, P.L., 1996, The Pliocene Fish Creek sturzstrom, Anza-Borrego Desert State Park, southern California. In Abbott, P. L. and Seymour, D. C., (eds.), Sturzstroms and Detachment Faults, Anza-Borrego Desert State Park, California. South Coast Geological Society Annual Field Trip Guide Book, No. 24, p. 165-184.

Ryter, D.W., 2002, Late Pleistocene kinematics of the central San Jacinto fault zone, Southern California. [Ph.D. dissertation] University of Oregon, Eugene, OR. 137 p.

Scholz, C.H., 1988, The brittle-plastic transition and the depth of seismic faulting. International Journal of Earth Science, V. 77, n. 1, p. 319-328.

Sharp, R.V., and Clark, M.M., 1972, Geologic evidence of previous faulting near the 1968 rupture on the Coyote Creek fault. In: The Borrego Mountain Earthquake of April 9, 1968, U.S. Geological Survey Professional Paper, p. 131-140.

Shreve, R.L., 1994, The Blackhawk landslide, southwestern San Bernardino County, California. In: Murbach, D., and Baldwin, J., (eds.), Annual Field Trip Guidebook, South Coast Geological Society, v. 22, p. 432-438.

Silver, L.T., Taylor, H.P., and Chappell, B., 1979, Some petrological, geochemical, and geochronological observations of the Peninsular Ranges batholith near the international border of the U.S.A. and Mexico. In: Abbott, P.L., and Todd, V.R., eds., Mesozoic crystalliune rocks – Peninsular Ranges batholith and pegmatites, Point Sal Ophiolite. Guidebook of the Geological Society of America Annual Meeting, San Diego State University, San Diego, CA, p. 177-231

Todd, V. R., Erskine, B. G., and Morton, D. M., 1988, Metamorphic and tectonic evolution of the northern Peninsular Ranges Batholith, southern California. In: Ernst, W. G., ed., Metamorphism and Crustal Evolution of the Western United States; Rubey Volume VII, Englewood Cliffs, New Jersey, Prentice Hall, p. 894-937.

Walawender, M.J., Girty, G.H., Lombardi, M.R., Kimbrough, D., Girty, M.S., and Anderson, C., 1991, A synthesis of recent work in the Peninsular Ranges batholith. In: Walawender, M.J., and Hanan, B.B., (eds.), Geological excursions in southern California. Guidebook 1991 Annual Meeting Geological Society of America, San Diego, California, p. 297-312.

Winker, C.D., and Kidwell, S.M., 1996, Stratigraphy of a marine rift basin: Neogene of the western Salton Trough, California. In: Abbott, P.L., and Cooper, J.D., (eds.), Field conference guidebook and volume for the annual convention, San Diego, California, May, 1996, Bakersfield, California, Pacific Section. American Association of Petroleum Geologists, p. 295-336.

White, S., 2001, Textural and microstructural evidence for semi-brittle flow in natural fault rocks with varied mica contents. International Journal of Earth Sciences, v. 90, n. 1, p. 14-27.

Map Symbols

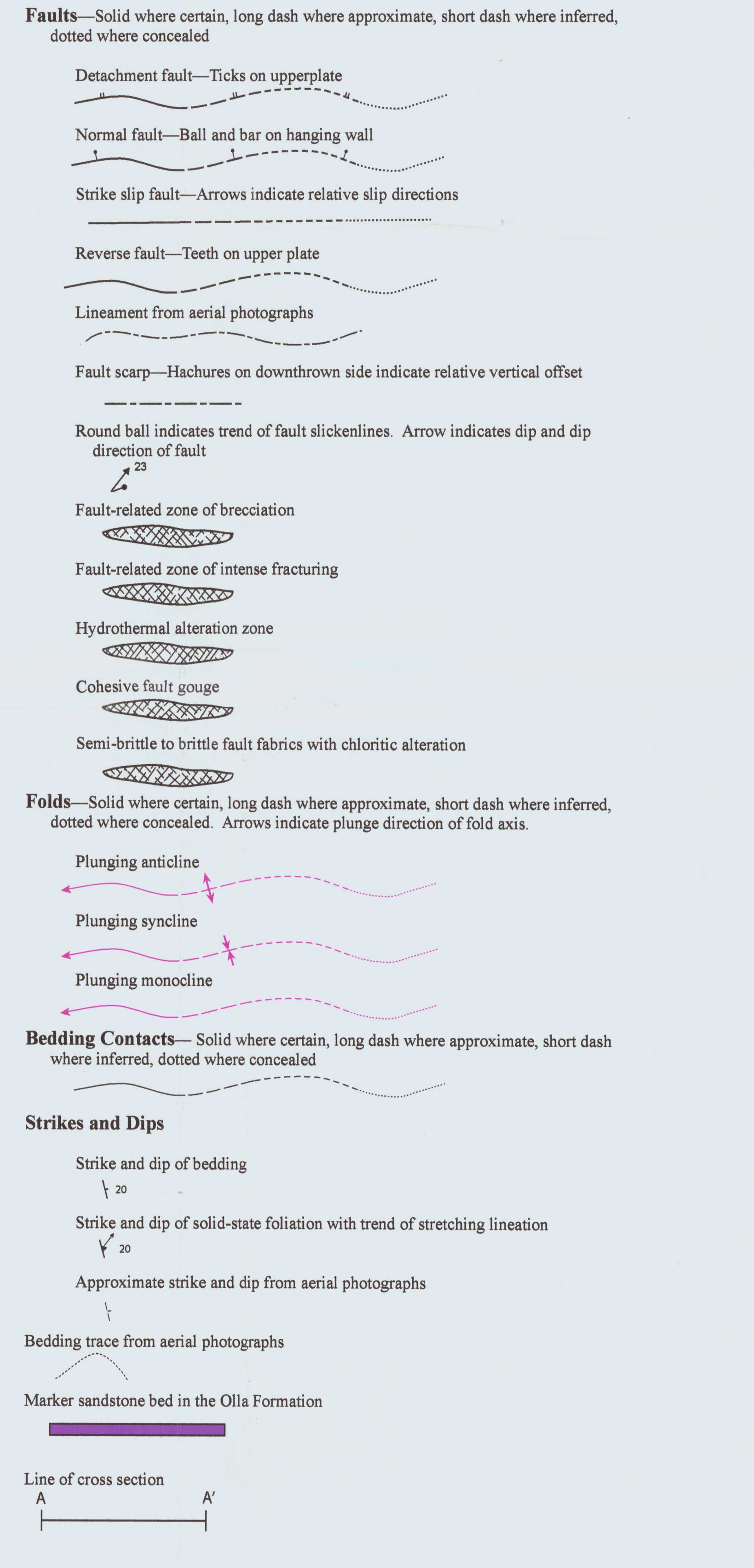

Plate 3. Cross sections for the Geologic Map of portions of the 7.5' Borrego Mountain, Borrego Sink, Harper Canyon, Squaw Peak, Tubb Canyon, and Whale Peak quadrangles

Alexander Steely[1], Susanne Janecke[1], Gary Axen[2], Rebecca Dorsey[3]

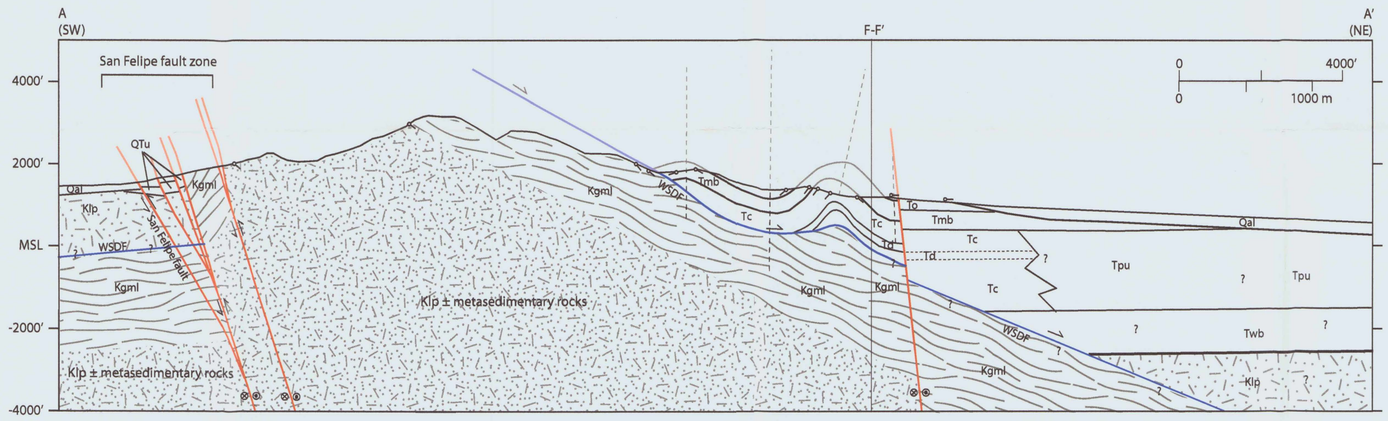

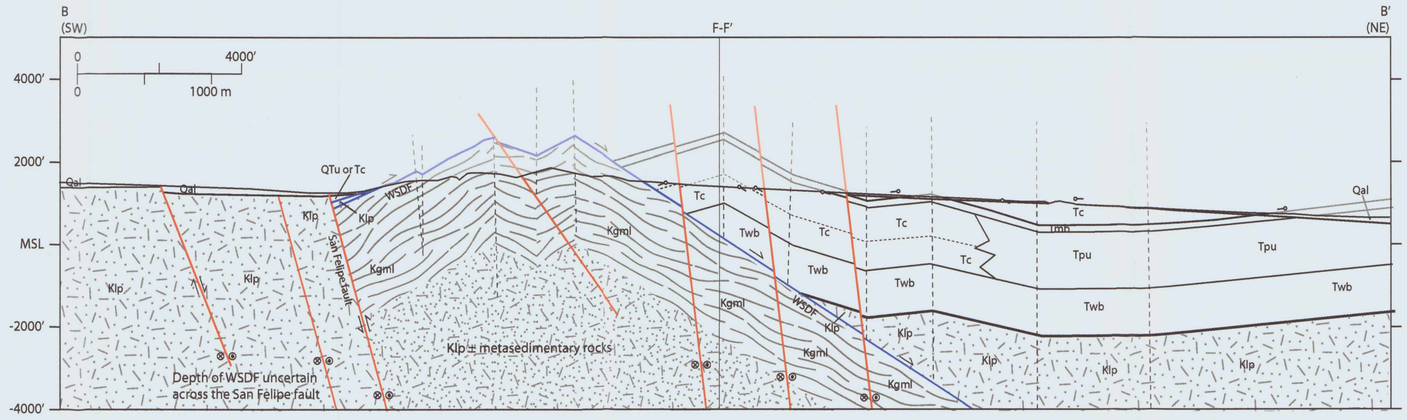

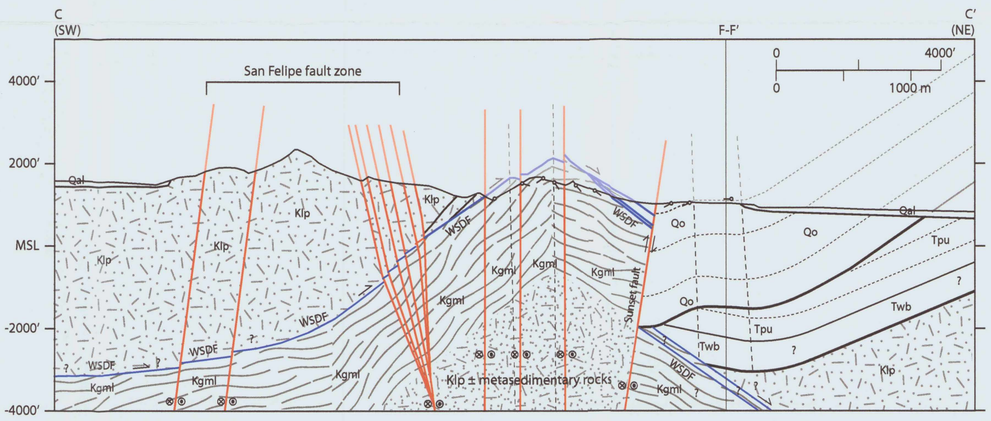

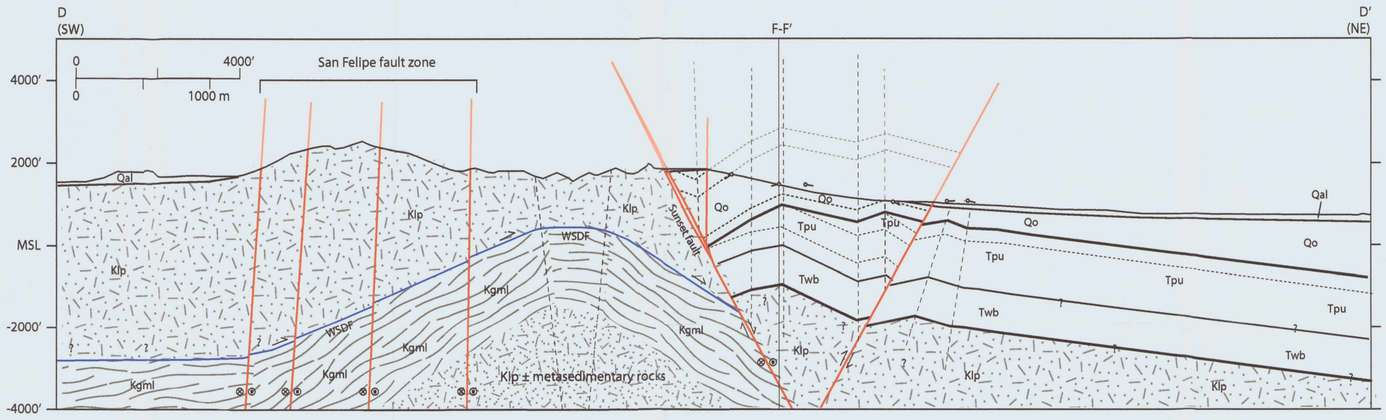

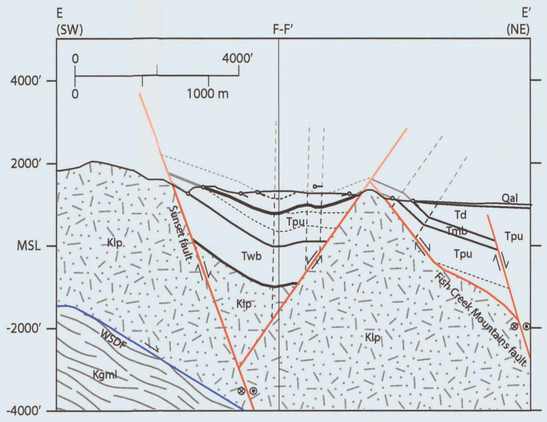

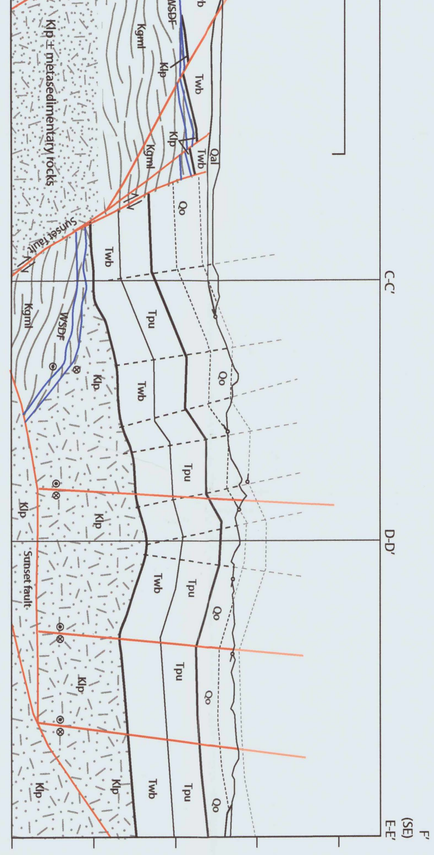

West Salton detachment fault

San Felipe fault zone

Fold axis

Unconformity

Form line

Dip tadpole showing projected dip from geological map

Direction of movement on faults

Plate 4. Measured sections of the West Butte conglomerate and Hawk Canyon formation

The West Butte conglomerate measured at its proposed type locality south of West Butte

The Hawk Canyon formation measured at two locations within Hawk Canyon near West Butte